



HAL
open science

Middle-Late Triassic metamorphism of the Guajira Arch-basement: Insights from zircon U–Pb and Lu–Hf systematics

Alejandro Piraquive, Andreas Kammer, Cristhian Gómez, Matthias Bernet, Jimmy Alejandro Muñoz-Rocha, Carlos Alberto Quintero, Oscar Laurent, Albrecht von Quadt, Mary Luz Peña-Urueña

► To cite this version:

Alejandro Piraquive, Andreas Kammer, Cristhian Gómez, Matthias Bernet, Jimmy Alejandro Muñoz-Rocha, et al.. Middle-Late Triassic metamorphism of the Guajira Arch-basement: Insights from zircon U–Pb and Lu–Hf systematics. *Journal of South American Earth Sciences*, 2021, 110, pp.103397. 10.1016/j.jsames.2021.103397 . hal-03436631

HAL Id: hal-03436631

<https://hal.science/hal-03436631>

Submitted on 23 Nov 2021

HAL is a multi-disciplinary open access archive for the deposit and dissemination of scientific research documents, whether they are published or not. The documents may come from teaching and research institutions in France or abroad, or from public or private research centers.

L'archive ouverte pluridisciplinaire **HAL**, est destinée au dépôt et à la diffusion de documents scientifiques de niveau recherche, publiés ou non, émanant des établissements d'enseignement et de recherche français ou étrangers, des laboratoires publics ou privés.

Journal Pre-proof

Middle-Late Triassic metamorphism of the Guajira Arch-basement: Insights from zircon U–Pb and Lu–Hf systematics

Alejandro Piraquive, Andreas Kammer, Cristhian Gómez, Matthias Bernet, Jimmy Alejandro Muñoz, Carlos Alberto Quintero, Oscar Laurent, Albrecht von Quadt, Mary Luz Peña-Urueña

PII: S0895-9811(21)00244-3

DOI: <https://doi.org/10.1016/j.jsames.2021.103397>

Reference: SAMES 103397

To appear in: *Journal of South American Earth Sciences*

Received Date: 5 November 2020

Revised Date: 22 May 2021

Accepted Date: 23 May 2021

Please cite this article as: Piraquive, A., Kammer, A., Gómez, C., Bernet, M., Muñoz, J.A., Quintero, C.A., Laurent, O., von Quadt, A., Peña-Urueña, M.L., Middle-Late Triassic metamorphism of the Guajira Arch-basement: Insights from zircon U–Pb and Lu–Hf systematics, *Journal of South American Earth Sciences* (2021), doi: <https://doi.org/10.1016/j.jsames.2021.103397>.

This is a PDF file of an article that has undergone enhancements after acceptance, such as the addition of a cover page and metadata, and formatting for readability, but it is not yet the definitive version of record. This version will undergo additional copyediting, typesetting and review before it is published in its final form, but we are providing this version to give early visibility of the article. Please note that, during the production process, errors may be discovered which could affect the content, and all legal disclaimers that apply to the journal pertain.

© 2021 Published by Elsevier Ltd.



Author statement

Alejandro Piraquive: Conceptualization, Methodology, Formal analysis, Investigation, Writing - Original Draft, Visualization, Funding acquisition.

Andreas Kammer: Conceptualization, Investigation, Writing - Review & Editing, Supervision, Funding acquisition.

Cristhian Gómez: Methodology, Formal analysis, Investigation, Writing - Review & Editing, Visualization.

Matthias Bernet: Investigation, Writing - Review & Editing, Supervision

Jimmy Muñoz: Data acquisition, Validation, Data Curation

Carlos Quintero: Methodology, Investigation

Oscar Laurent: Formal analysis, Investigation

Albrecht von Quadt: Formal analysis, Investigation, Resources.

Mary Peña-Urueña: Investigation, Supervision, Resources.

Middle-Late Triassic metamorphism of the Guajira Arch-basement: Insights from zircon U-Pb and Lu-Hf systematics

Alejandro Piraquive^{1,2,3†}, Andreas Kammer³, Cristhian Gómez³, Matthias Bernet², Jimmy Alejandro Muñoz¹, Carlos Alberto Quintero³, Oscar Laurent^{4,5}, Albrecht von Quadt⁴, Mary Luz Peña-Urueña¹

1. Grupo de Asuntos Nucleares, Dirección de Asuntos Nucleares, Servicio Geológico Colombiano, Carrera 50 No 26-20, 111321 Bogotá, Colombia

2. Institut des Sciences de la Terre, Université Grenoble Alpes, CNRS 1381, rue de la Piscine, 38058 Grenoble Cedex 9, France.

3. Grupo de Investigación en Geología Estructural y Fracturas, Universidad Nacional de Colombia. Apartado Aéreo, 14490 Bogotá, Colombia.

4. Department of Earth Sciences, Institute of Geochemistry and Petrology, ETH Zentrum, Clausiusstrasse 25, 8092 Zürich, Switzerland

5. CNRS, Observatoire Midi-Pyrénées, Géosciences Environnement Toulouse UMR5563-CNRS-UPS-IRD-CNES, 14 avenue Edouard Belin, F-31400 Toulouse, France

Abstract

The Guajira Arch is located in the northernmost portion of South America and holds the record of several stages of magmatism and metamorphism. We performed LA-ICP-MS U-Pb zircon geochronology coupled with Lu-Hf isotope geochemistry on 11 samples from a high-grade gneissic basement hosting interleaved complexes of younger meta-granitoids and meta-sediments to unravel its tectono-metamorphic evolution. The oldest rocks correspond to a Rodinia-type basement at ca. 1100-880 Ma, affected by mafic magmatism during the Permian at ca. 272 Ma, anatexis during the Carnian at ca. 230 Ma, updoming and the formation of an extensional detachment fault during the Norian at ca. 224 Ma concluding with Jurassic magmatism since ca. 190 Ma. Trace element geochemistry shows that Triassic zircons are depleted in HREE and yield lower Th/U ratios than Jurassic zircons enriched both in HREE, Yb, and Y. Hf systematics indicates a Triassic to Jurassic evolution towards more radiogenic compositions. The lithological associations, structural setting, U-Pb ages, and Hf isotope geochemistry of the Triassic-Jurassic rocks at the Guajira Arch characterize an active margin setting of a hot orogenic belt in NW-Gondwana, comprising the Central Cordillera of Colombia, the Santa Marta Massif, the Merida Andes, the Perijá Range, the Santander Massif and the para-autochthonous terranes south of the Ouachita-Marathon Suture (Oaxaquia, Acatlán, and Maya), and thus vindicate the existence of a conjugate margin with Laurentia until the Late Triassic, preceding the breakup of western Pangaea. The Triassic anatexites and Jurassic granitoids from the Guajira Arch yield Proterozoic Hf T_{DMi} ages which are indistinguishable from the autochthonous Proterozoic basement and thus render an allochthonous origin by terrane accretion highly improbable. Instead, these data point to melting of the continental crust by the incorporation of primitive material reflecting a two-stage process at the boundary of a large underlying mantle convection cell (i) Triassic slab steepening, subduction arrest, updoming anatexis at ca. 230-223 Ma and (ii) Early Jurassic arc-magmatism at ca. 190-165 Ma due renewed convergence. Furthermore, we propose that the structural setting, lithology, and isotope geochemistry of the Guajira Arch units, fit into the style of a cordilleran core-complex emplaced in a roll-back extensional setting preceding Pangaea break-up.

Keywords: *Guajira Arch, Geochronology, Peri-Gondwana terranes, amphibolite facies metamorphism, Pangaea.*

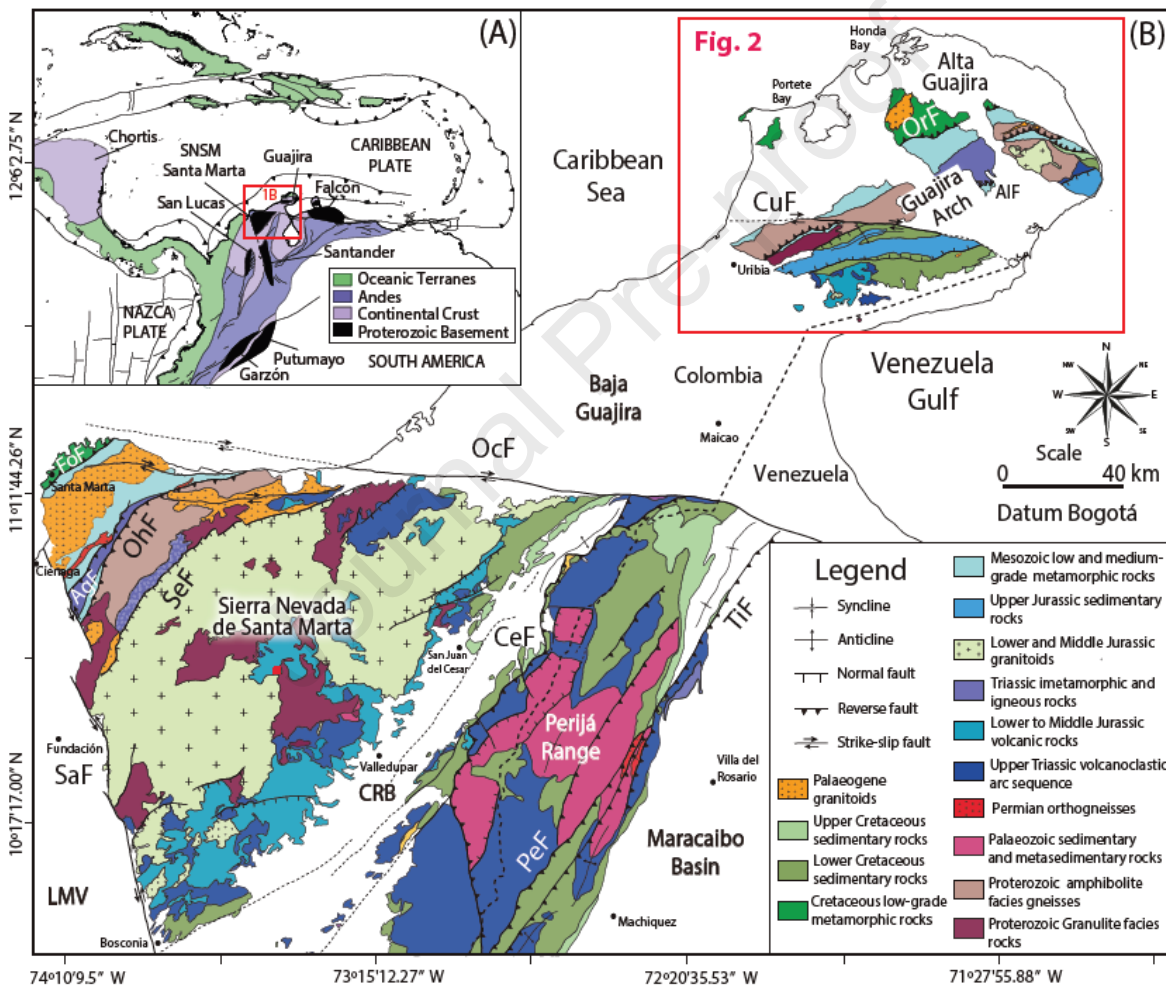
30 1. INTRODUCTION

31 The Late Paleozoic-Early Mesozoic evolution of western Pangaea continental margin was
32 governed by subduction geodynamics, typical of cordilleran orogenic systems (Collins and
33 Richards, 2008; Decelles et al., 2009; Collins et al., 2011). This evolution involves a plate setting
34 prompted by the reorganization of a far stress field, intermittent arc-magmatism, and
35 metamorphism linked to alternating periods of extension and compression, changes in slab
36 geometries and convergence rates, the accretion of para-autochthonous blocks, and their
37 corresponding feedbacks (Pindell, 1985; Murphy et al., 2004; Meert and Lieberman, 2008;
38 Pindell and Kennan, 2009; Nance et al., 2012; Spikings et al., 2015; van der Lelij et al., 2016b;
39 Cardona et al., 2016).

40 A prime challenge in such a geodynamic context consists of unravelling multiple
41 magmatic-arc building stages and associated metamorphic events (Zuluaga, 2015; Montes et al.,
42 2019; Zuluaga and Lopez, 2019). In this work, we focus on a regional Late Paleozoic - Early
43 Mesozoic first contractional and then extensional orogenic evolution that is widely documented
44 along the Northern Andean continental margin (Fig. 1A; Vinasco et al., 2006a; Cardona et al.,
45 2010b; Villagómez et al., 2011; Van Der Lelij, 2013; Cochrane et al., 2014a; Martens et al.,
46 2014; van der Lelij et al., 2016b; Zuluaga et al., 2017; Spikings and Paul, 2019; Tazzo-Rangel et
47 al., 2019).

48 During the Permian to Early-Triassic assembly of Pangaea, north-western Gondwana
49 basement inliers (i.e., Oaxaquia block, southern Chiapas massif, Acatlán and Xolapa complexes,
50 and the Tahamí terrane) were juxtaposed into a complex array and recorded, by their position at
51 the active continental margin, the Panthalassian subduction (Weber et al., 2007; van der Lelij et
52 al., 2016b; Riel et al., 2018), in addition to the far-reaching collisional events related to the
53 Alleghanian orogeny along the Ouachita-Marathon Suture (Pindell, 1985; Sacks and Secor,

54 1990; Weber et al., 2007; Murphy et al., 2010; Nance et al., 2012; van der Lelij et al., 2016b;
 55 Spikings and Paul, 2019; Coombs et al., 2020). The Late Paleozoic-Triassic tectono-
 56 metamorphic events during Pangaea assembly were followed by extensive magmatic arc build-
 57 up that culminated in rifting during Jurassic Pangaea break-up (Bayona et al., 2006; Pindell and
 58 Kennan, 2009; Cochrane et al., 2014a, 2014b; Zuluaga, 2015; Spikings et al., 2015; van der Lelij
 59 et al., 2016b, 2016a; Quandt et al., 2018).



60

61 **Figure 1. A) Plate tectonic overview of Northern South America, the Antilles, and Central America, showing**
 62 **in black the Proterozoic basement exposures of the Northern Andes and part of the Chortis block (adapted**
 63 **from Luzieux et al., 2006; Veloza et al., 2012; Weber et al., 2018; Vallejo et al., 2019; Tazzo-Rangel et al.,**
 64 **2019), black square encloses mapped area shown in B) Regional geology and new field mapping (this study) of**
 65 **the NW-Maracaibo block, the Guajira Peninsula, the Santa Marta Massif and the Perjá Range. LMV—**
 66 **Magdalena –valley, CRB—Cesar-Rancheria Basin, AgF—Aguja Fault, CeF—Cerrejón Fault, CuF—Cuisa**
 67 **Fault, FoF—Florín Fault, OcF—Oca Fault. OhF—Orihueca Fault, OrF—Ororio Fault, PeF—Perija Fault,**
 68 **SaF—Santa Marta Fault, SeF—Sevilla Fault, TiF—El Tigre Fault (compiled from Tschanz et al., 1969, 1974;**
 69 **Irving, 1972, 1975; Kellogg, 1984; Colmenares, 2007, and new mapping from this study).**

70 At the northernmost Andes, the Guajira Peninsula (Fig. 1B) consists of two well-defined
71 domains. The Baja Guajira southern lowlands expose a Cenozoic basin fill (Irving, 1975),
72 whereas the hilly/mountainous north-eastern part is subdivided among the Macuira, Jarara,
73 Simarua, and Cosinas ranges (Figs. 1-2). Along these four ranges, an ENE-WSW trending high-
74 grade basement inlier named the Guajira Arch is mantled by sedimentary rocks, low-to medium-
75 grade meta-pelites, intruded by several igneous and meta-igneous suites (Fig. 2; MacDonald,
76 1964; Lockwood, 1965; Alvares, 1967). The Macuira, Jarara, and Simarua ranges are separated
77 by localized basins infilled by Oligocene-Pliocene sedimentary rocks (Fig. 2). The latter most
78 likely originated by transtensional tectonics during Cenozoic transient stages of accretion of the
79 Caribbean plate (Kellogg, 1984; Gómez and Burke, 2001; Quintero, 2017).

80 The paleogeographic setting of the Guajira Arch concerning its position along the
81 continental margin of Gondwana has been questioned (Bayona et al., 2019), and different
82 hypotheses heralding an autochthonous (Bartok et al., 2015), para-autochthonous (Nova et al.,
83 2019), or allochthonous origin (Cediel et al., 2019; Colmenares et al., 2019) are discussed. These
84 divergent interpretations were based on stratigraphy (Bartok et al., 2015), detrital zircon
85 geochronology, and paleomagnetic data obtained from Mesozoic volcanic suites and platform
86 sedimentary rocks (MacDonald and Opdyke, 1972; Bayona et al., 2006; Nova et al., 2019).
87 However, isotopic data from this basement inlier to support such diverse models remains scarce,
88 making it difficult to discern the participation of primitive/juvenile crustal sources in magma
89 generation and its late detrital reworking. The collection of new geochemical-isotopic data is
90 crucial for establishing which of the invoked processes, as terrane migration or sediment
91 transferring were dominant during Early Mesozoic times. Furthermore, a unifying synthesis that
92 integrates deformation phases and metamorphic events based on radiometric ages of
93 crystallization and cooling events for basement and cover altogether has not been elaborated so

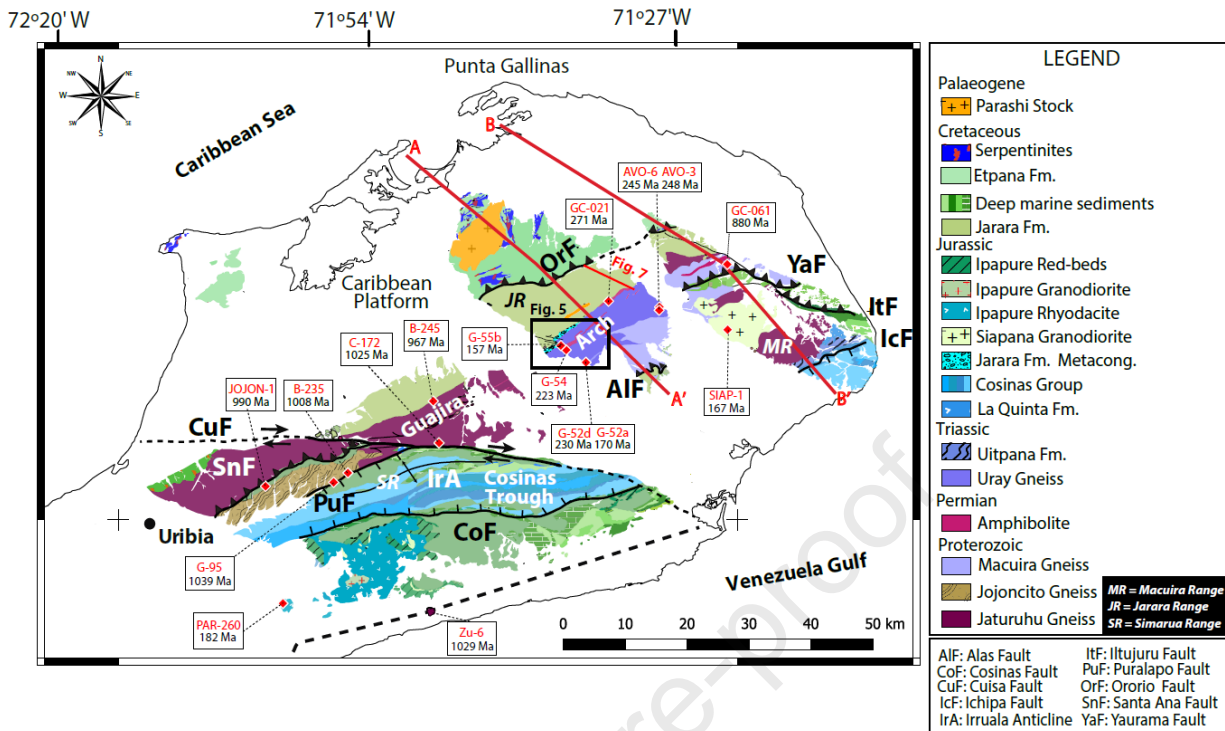
94 far (MacDonald, 1964; MacDonald and Opdyke, 1972; Cordani et al., 2005; Weber et al., 2009,
95 2010; Cardona et al., 2010a, 2014; López and Zuluaga, 2012).

96 In this contribution, we integrated field mapping with zircon U-Pb geochronology, Lu-Hf
97 isotopic, and trace element compositions on representative key samples of the various lithologies
98 from the Guajira Arch, in order to: 1) examine the possible distinction between a Proterozoic
99 high-grade metamorphic basement and overlying younger meta-sediments; 2) to discuss the
100 geochronological and isotopic affinity of the Guajira Arch basement concerning the Proterozoic
101 Gondwanan continental realm and other para-autochthonous terranes; 3) to highlight the
102 importance of a Late Paleozoic-Early Mesozoic tectono-metamorphic event, comprising the
103 structural evolution of the continental margin; and finally, 4) to elucidate the geodynamic
104 significance of the onset of Jurassic arc-magmatism.

105 Our results deliver new geochronological and isotopic constraints on the Proterozoic and
106 Permo-Jurassic tectono-metamorphic events that affected this part of the western Pangaea realm
107 and give insight into the evolution of this highly remobilized crustal section in a geodynamic
108 context.

109 110 **2. GEOLOGICAL SETTING**

111 The Guajira Peninsula is located at about 12°N and constitutes the northernmost
112 extension of the Andes (Figs 1-2). At the north-eastern part of the peninsula, a high-grade
113 basement inlier named the Guajira Arch (Fig. 2) is covered at its NW-SE flanks by low-to-
114 medium grade metasediments and sedimentary rocks of Jurassic to Late Cretaceous age (Renz,
115 1960; Alvares, 1967). Towards the south, the Cosinas Trough (Fig. 2) sedimentary units are
116 juxtaposed to granodiorites, rhyodacites, and overlying volcanoclastic deposits remnants of a
117 Jurassic magmatic arc (Rollins, 1965; Alvares, 1967; Zuluaga et al., 2015).



118

119 **Figure 2. Detailed geological map of the Guajira Arch (SNSM) with cross-sections A-A' Jarara range and B-**
 120 **B' Macuira range (Fig. 3). Including sampling sites and U-Pb ages obtained in this study, modified from**
 121 **Irving, (1972) and new data (this study). Uray Gneiss samples (AVO-3, AVO-6), Jojoncito Gneiss sample**
 122 **(JOJON-1), Siapana Granodiorite (SIAP-1), Atuschón gneiss sample (Zu-6), and Ipapure Rhyodacite sample**
 123 **(PAR-260) compiled from Cardona et al. (2006); Zuluaga et al. (2015); Baquero et al. (2015), and Weber et al.**
 124 **(2010). A detailed map of the Uray gneiss and Jarara Formation contact is framed in figure 5. A stratigraphic**
 125 **section in figure 7 is indicated.**
 126

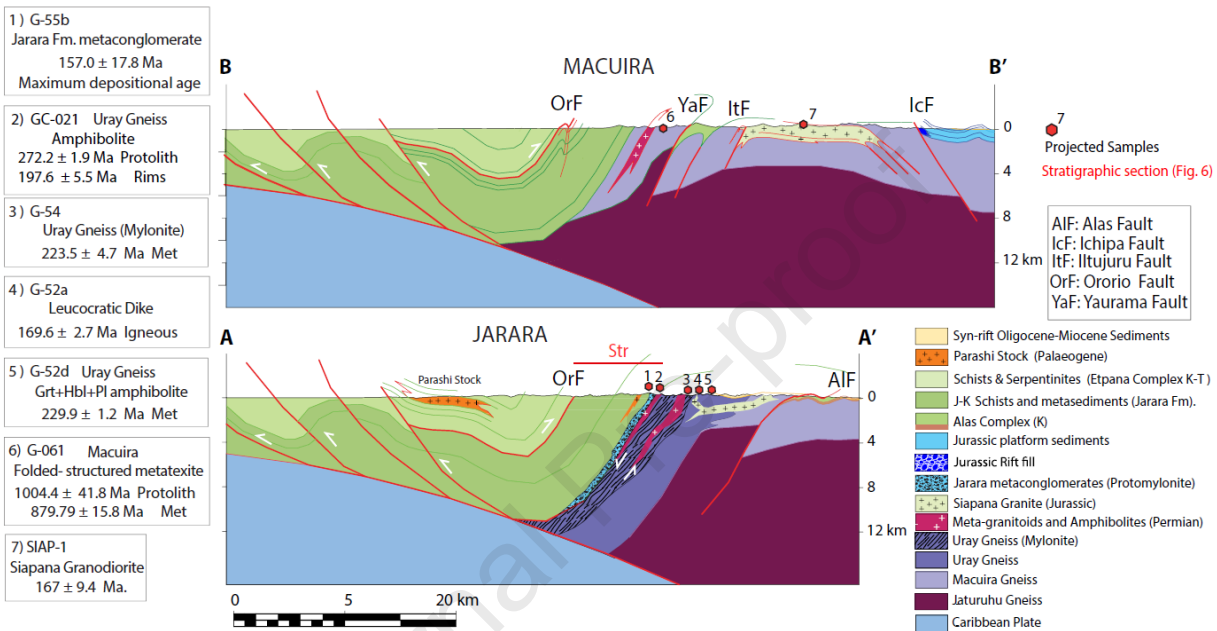
127 The Meso-Neoproterozoic basement of high-grade amphibolite to granulite facies units
 128 comprises the Macuira schists, Jaturuhu, Atuschón, and Jojoncito gneisses (Fig. 2; Radelli, 1962;
 129 MacDonald, 1964; Lockwood, 1965; Alvares, 1967; Irving, 1972; Cordani et al., 2005). The
 130 Atuschón and Jojoncito granitic gneisses yield zircon inherited core ages of 1550-1200 Ma.
 131 Metamorphism is dated at ca. 1028.7 Ma for the Atuschón Gneiss, whereas the Jojoncito Gneiss
 132 discloses a rim recrystallization age of ca. 916 Ma (Cordani et al., 2005; Baquero et al., 2015),
 133 bracketing a Late Mesoproterozoic-Early Neoproterozoic event. Currently, there are not
 134 available zircon U-Pb ages from the Macuira schists, yet an Sm/Nd model age (T_{DM}) of =1.45 Ga
 135 obtained from a muscovite schist hint to a Mesoproterozoic crustal source (Cardona et al., 2006).

136 In contrast, available Ar-Ar ages in amphibole may indicate a Mesozoic thermal event at ca. 200-
137 100 Ma; however, these ages are highly discordant and should be treated carefully as they could
138 also reflect alteration, partial resetting, slow cooling, Ar excess, recoil, or recrystallization
139 (MacDonald, 1964; MacDonald and Opdyke, 1972; Cardona et al., 2006). The Meso-Proterozoic
140 granulite facies basement exposures are mantled by Late Paleozoic-Triassic amphibolite facies
141 mylonitic meta-granitoids, amphibolites, and paraschists named Uray Gneiss (Fig. 5; Lockwood,
142 1965; Alvares, 1967; Weber et al., 2010). Leucocratic units from the latter yield a Middle
143 Triassic age (ca. 245 Ma; AVO-3, AVO-6 Fig. 3; Weber et al., 2010).

144 At the Jarara Range, the amphibolite facies mylonites from the Uray Gneiss are overlain
145 in a tectonic contact at the NW by the greenschists facies meta-sediments of the Jarara Formation
146 (Figs. 2-3). The Jarara Formation sets in with a basal meta-conglomerate level superseded by
147 muddy to siliciclastic meta-sediments, with sporadic marble seams. At its middle part, bryozoans
148 indicate an Upper Cretaceous age. These marine sedimentary rocks are superseded by mafic
149 meta-volcanic rocks and felsic to intermediate meta-tuffs (Lockwood, 1965). At its top, the
150 Jarara Formation is thrust by the Epana Complex by the N-dipping Ororio fault (Figs. 2-3).
151 This suite contains blocks of strongly serpentinized meta-ultramafic and meta-mafic rocks,
152 embedded in a meta-pelitic matrix containing submarine lava flows and mafic meta-tuffs,
153 glaucophane schists, and eclogite blocks, interpreted as a subduction channel (Medina
154 Avellaneda, 2009). Paleogene conglomerates fringing the Jarara range contain blocks of
155 eclogites derived from the Epana Complex (Weber et al., 2010).

156 The Siapana granodiorite (Figs. 2 & 3) intruded the Macuira schists at ca. 167 Ma in a
157 continental arc setting, and magma genesis entailed significant crustal contribution considering
158 the Sm/Nd model age (T_{DM}) of = 1.47 Ga (Cardona et al., 2006, 2014). Jurassic arc build-up led
159 to thermal metamorphism and, ultimately, to basement exhumation before the deposition of the

160 Cretaceous successions as evidenced by zircon provenance and fission-track data from the
 161 Cosinas Group, indicating sourcing from Jurassic plutons and Proterozoic basement ca. 154 Ma
 162 (Radelli, 1962b; MacDonald, 1964; García-Gonzales et al., 2010; Nova et al., 2019), implying
 163 that some of the Jurassic plutons had to be exposed at the time of deposition of these units.



164 **Figure 3. Cross-sections A-A' and B-B' from the Jarara and Macuira ranges, in which a Late Cretaceous**
 165 **accretionary prism obducts the metamorphic Proterozoic-Triassic core. Mylonites separate the high-grade**
 166 **Triassic anatectites from a low-grade metasedimentary cover. Sub-vertical thrusts at the metamorphic core**
 167 **separate metasedimentary imbrications from the Proterozoic basement and maybe equivalent to crystalline**
 168 **nappes that overlay the Alas Complex metasediments. See cross-section location in Figure 2. AIF: Alas fault,**
 169 **IcF: Ichipa fault, ItF: Itujuru fault, OrF: Ororio fault, YaF: Yaurama fault.**

171

172 During the Late Cretaceous-Paleogene, associated platform sequences of the Jarara
 173 Formation and the Etpana Complex were partially obducted onto the continental margin as the
 174 convergence between the Caribbean plate and continental South America was increased
 175 (Lockwood, 1971; Weber et al., 2010, 2011). By Eocene times, the subduction gradually ceased
 176 as the convergence of the Caribbean plate against the continental margin of NW South America
 177 became oblique (Fig. 3; Lockwood, 1971; García-Casco et al., 2008; Cardona et al., 2011, 2014;
 178 Montes et al., 2019; Bustamante et al., 2021). The emplacement of the Parashi stock has

179 occurred under a transtensional regime that affected the upper plate, causing syn-kinematic
180 deformation of the Jarara Formation, Etpana complex, and Parashi stock (Bustamante et al.,
181 2021).

182 The east-trending right-lateral Cuisa fault activity (Fig. 2), which dissects the Guajira
183 Arch, is recorded at least since the Oligocene by the Siamana Formation deposits (Renz, 1960;
184 Gómez and Burke, 2001; Vence, 2008; García-Gonzales et al., 2010; Zapata et al., 2010;
185 Quintero, 2017). Dextral transtensional structures as the Cuisa and Oca faults (Figs. 1-2)
186 remained active during the Neogene, coeval to exhumation and relief building (Gómez and
187 Burke, 2001; Cardona et al., 2011; Bustamante et al., 2021 Figs. 1-2). The strain was transferred
188 from the Caribbean plate to the continental margin through clockwise block rotation (MacDonald
189 and Opdyke, 1972; Bayona et al., 2006, 2011, 2013; Montes et al., 2010; Zapata et al., 2014;
190 Cardona et al., 2018).

191 This process disrupted the otherwise continuous continental margin into Proterozoic
192 inliers separated by pull-apart basins, for instance, the Santa Marta Massif and Guajira Arch
193 separated by the Baja Guajira basin (Alvares, 1967; Irving, 1975; Macellari, 1995; Montes et al.,
194 2010, 2019; Zapata et al., 2014; Londono et al., 2015; Piraquive et al., 2018).

195

196 **3. METHODS**

197 Samples were crushed and zircons extracted following the standard procedures (e.g.,
198 Mange and Maurer 1992) at the Colombian Geological Survey (SGC) and Universidad Nacional
199 de Colombia facilities. Lithium polytungstate (2.89 g/cm^3) and Methylene iodide ($d = 3.32$
200 g/cm^3) were used for density separation out of the sieved 400-63 μm fraction. Zircon grains from
201 the heavy mineral concentrates were randomly selected by pipette and then hand-picked. After
202 mounting in epoxy, grains were abraded to a sub-equatorial section and polished. Zircon

203 cathodoluminescence (CL) imaging was carried out using a Vega ©Tescan MV2300VP SEM at
204 the Institute of Geochemistry and Petrology of the (ETHZ) at Zurich, Switzerland, and at the
205 Colombian Geological Survey (SGC) using the JEOL JSM-IT300LV SEM, with a MiniCL
206 Gatan to observe the internal structures of the crystals.

207 U–Pb geochronology and *in-situ* trace element composition of zircons were performed
208 through laser ablation inductively coupled mass spectrometry (LA-ICP-MS) at both the ETHZ
209 and SGC facilities. Zircon Lu-Hf isotopic compositions were measured by laser ablation, multi-
210 collector inductively coupled plasma mass spectrometry (LA-MC-ICP-MS) at ETHZ. Lu-Hf
211 results were plotted using the visual and statistical approach described by Andersen et al. (2018).
212 The detailed analytical parameters and specifications of the methods and procedures are
213 described in Appendix 1.

214

215 **4. RESULTS**

216 Sample location and lithology are shown in Table 1 and figures 2-7. Zircons detailed CL
217 morphology, Th/U ratio, and Y content are presented in Table 2. Cathodoluminescence imagery,
218 Concordia plots, and trace element geochemistry are plotted in figures 8-14. The complete
219 datasets of U-Pb geochronological results are compiled in Table A1, trace element compositions
220 in table A2, and Lu-Hf isotopic data in table A3.

221

222 **4.1 Sample description, field relationships, and petrography**

223 This section describes our new findings regarding the geological mapping of the units
224 that compose the Guajira Arch, emphasizing the field relations and petrography of the Uray
225 Gneiss and Jarara Formation at the Jarara Range. Our results highlight the stratigraphic and
226 structural relations of a gneissic dome mantled by meta-sediments. Moreover, we briefly discuss

227 the high-amphibolite to granulite-facies Proterozoic inliers of the Guajira Arch cropping out in
228 the Simarua and Macuira ranges, respectively analyzed in this study.

229 *Proterozoic high-grade basement*

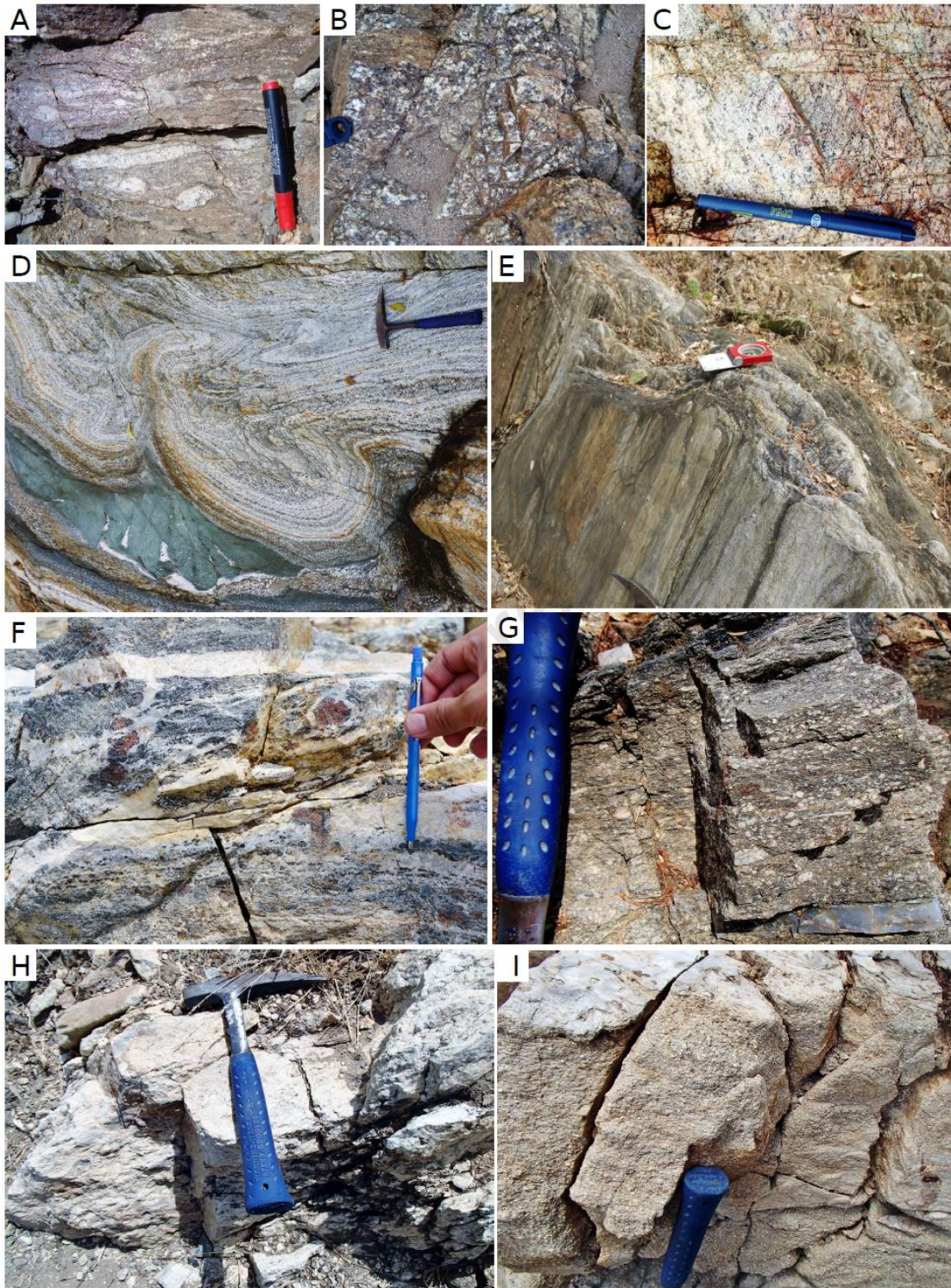
230 The Guajira Arch backbone comprises high-amphibolite-to granulite facies units that
231 form gneiss domes. Multiple lithological varieties have been recognized, and several units have
232 been named as the Jojoncito Gneiss, Jaturuhu Gneiss, Macuira Schists, showing rather complex
233 structural and stratigraphic relationships. It has recently been proposed to unify the Guajira Arch
234 metamorphic units under the Macuira Gneiss definition (Lopez et al., 2014). However, in this
235 work, we based our cartographic synthesis and followed the nomenclature originally proposed by
236 Radelli (1962b), MacDonald (1964), Lockwood (1965), Alvares (1967), and Irving (1972). As
237 will be discussed further in section 4.2, the division of the Proterozoic units of the Guajira Arch
238 is also supported by new geochronological data.

239

240 *Jaturuhu gneiss*

241 In the Simarua range, we followed the Jaturuhu Gneiss definition posed by Alvares
242 (1967), which corresponds with the description of heterogeneous migmatites given by Radelli
243 (1962b). The Jaturuhu gneiss displays stromatic migmatitic segregations composed of feldspar
244 with mesoperthite intergrowths, microcline, and quartz neosome, whereas the melanosome is
245 composed of hornblende garnet and biotite.

246 From this unit, we collected two samples consisting of a mylonitic quartz-feldspathic
247 augen-gneiss rich in biotite, muscovite, and garnet located close to the contact with the overlying
248 Jarara Formation (sample B-245; Fig. 3, 4A) and an amphibolite melanosome in the vicinity of
249 the Cuisa fault (sample C-172).



250

251 **Figure 4. Field photographs of samples from the Guajira Arch metamorphic units analyzed in this study** A)
 252 **Quartz-feldspathic gneiss with augen texture (B-245, Jaturuhu Gneiss); B) Quartz-feldspathic gneiss with**
 253 **granoblastic texture (B-235, Jojoncito Gneiss); C) Felsic granulite (G-95, Jojoncito Gneiss); D) Folded**
 254 **structured metatexite (GC-061, Macuira Schists); E) Amphibole-epidote mylonitic schist (GC-021, Ug1; Uray**
 255 **Gneiss); F) Uray Garnet-amphibolite gneiss, (G-52D, Ug2; Uray Gneiss); G) Staurolite-biotite-garnet**
 256 **mylonite (G-54, Ug3; Uray Gneiss); H) Leucocratic dike Qtz+Pl+Ms (G-52A, Siapana Granodiorite); I)**
 257 **Quartz-muscovite protomylonitic meta-conglomerate (G-55B, Jf1; Jarara Formation).**

258 **Jojoncito gneiss**

259 The Jojoncito gneiss is an elongated NE trending body in the eastern part of the Simarua
260 range (Radelli, 1962a; Alvares, 1967; Cordani et al., 2005). Two samples were collected from; a
261 granulite-facies quartz-feldspathic gneiss (sample B-235; Fig. 4B) and a felsic granulite (sample
262 G-95; Fig. 4C). This body is hosted within the Jaturuhu gneiss, seemingly intrusive with the
263 surrounding schists and gneisses from the Jaturuhu gneiss (Alvares, 1967). Its aspect is typically
264 a massive white pinkish to cream color granitic gneiss, with textures that vary from strongly
265 foliated to locally granoblastic, characterized by elongated and stretched, purplish-bluish, or
266 smoky quartz within a K-feldspar and plagioclase matrix.

267

268 **Macuira schists**

269 We followed the definition of Macuira Schists by MacDonald (1964) for a suite of schists
270 and migmatites outcropping in the Macuira and Jarara Ranges (Fig. 2-3), named by Radelli
271 (1962b) as homogeneous migmatites or Macuira Series, characterized by folded metatexites,
272 fine-grained biotite-muscovite, quartz-feldspathic schists, hornblende schists that mantle a core
273 of diatexitic migmatites, defining a migmatitic dome structure around the Siapana pluton
274 (Radelli, 1962b; MacDonald, 1964). These folded migmatites differ from the typically stromatic
275 metatexites that characterize the Jaturuhu gneiss (Fig. 4A & D).

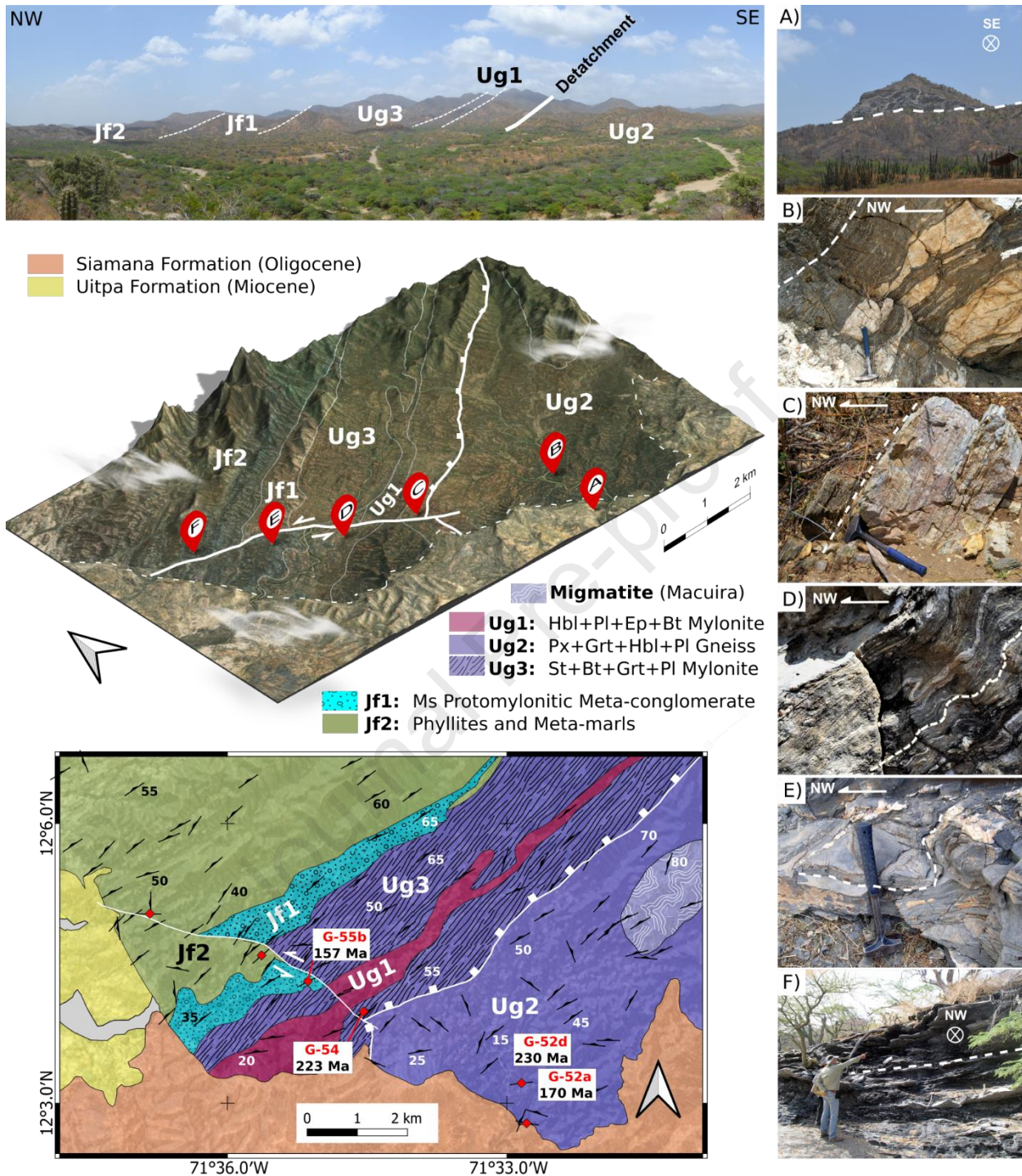
276 Folded-structured metatexites typically display granitic leucosomes of quartz-feldspathic
277 compositions (sample GC-061; Fig. 4D), whereas hornblende composes of the melanosome.
278 Banding ranges from cm-scale to several meters in thickness. The unit reached the upper-
279 amphibolite facies, as determined by hornblende-almandine paragenesis (MacDonald, 1964).
280 Towards the Macuira Range northwest, the Macuira Schists are overlain by the Jarara Formation
281 (Figs. 2 & 3).

282 ***Permian-Triassic high-to medium grade basement (Uray gneiss)***

283 In the southern Jarara Range, the Uray Gneiss can be differentiated into three main
284 lithotypes i.e., Ug1, Ug2, Ug3 (Fig. 4E-G). The metamorphic units of this complex were lately
285 intruded by muscovite-rich leucocratic dikes (Fig. 4H). Detailed structural mapping (Fig. 5)
286 reveals a high contrast between the Uray Gneiss high-amphibolite facies rocks and the
287 greenschist-facies overlying Jarara Formation, that at its base can be differentiated between two
288 sub-units (Jf1 and Jf2; Fig. 5), with a decreasing metamorphic grade from high-amphibolite-
289 facies (Ug1) to greenschist facies (Jf2) towards the NW (Fig. 5).

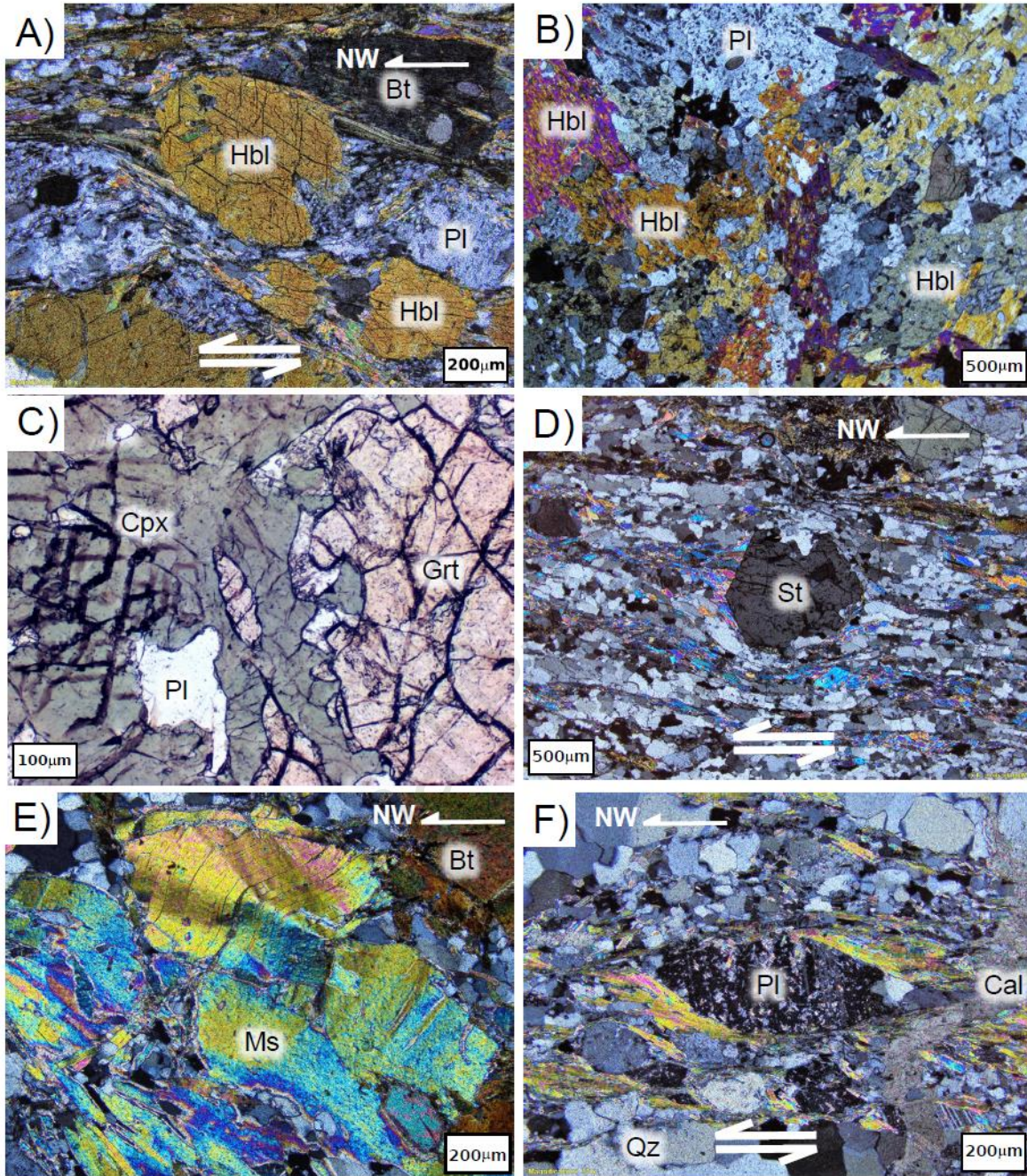
290 **Uray gneiss**

291 In the Jarara Range, the Uray Gneiss is unconformably overlain by the Oligocene
292 deposits of the Siamana Formation (Fig. 5A). Internally, the Uray Gneiss units are arranged in a
293 high-grade core mantled by medium-to low-grade meta-pelites with a regional NW foliation dip
294 direction (Fig. 5). Three lithotypes are differentiated within the Uray Gneiss: amphibole
295 mylonitic schist (Ug1, sample GC-021; Figs. 4E-5) composed by
296 hornblende+biotite+epidote+plagioclase+quartz (Fig. 6A). High-amphibolite facies anatectic
297 gneiss displays mostly granoblastic textures, locally foliated with leucosomatic segregations
298 (Ug2; sample G-52d; Fig. 4F-5B) bearing pyroxene+garnet+hornblende+plagioclase (Fig. 6B-
299 C), in which garnet crystals at the cm-scale are embedded in a pyroxene+hornblende matrix (Fig
300 6C), alternated with plagioclase bands. A detachment fault separates the gneissic core (Ug2)
301 from a unit composed of strongly foliated mylonitic schists (Ug3, Fig. 4G-5C) bearing
302 staurolite+biotite+garnet (sample G-54; Fig. 6D). The Uray gneissic core is intruded by
303 leucocratic dikes (sample G-52A; Fig. 4H) composed of quartz, K-feldspar, and muscovite (Fig.
304 6E). Sigma porphyroclasts and s-c shear bands from the Uray mylonites indicate sinistral top to
305 NW shear sense (Fig. 6).



306
307
308
309
310
311
312
313
314
315
316

Figure 5 Composite topographic relief and geology of the south western Jarara range. Top: panoramic view of the Jarara range taken from point C. Center: relief map of the Jarara range showing main structures and sites A-F. Bottom: detailed geological map of the Jarara range dip data compiled from (Lockwood, 1965). Left Panel A) Angular unconformity of the Oligocene sediments of the Siamana Formation over the Uray gneiss anatectic core B) Uray gneiss with foliation parallel leucosome segregations in a Px+Grt+Hbl groundmass (Ug2), dashed lines indicate foliation C) Uray gneiss alternate of St+Grt+Bt mylonitic schists (Ug3) D) Jarara Formation fine banded quartz-muscovite protomylonites with recumbent cascading or spruce-tree folds (Jf1) E) Jarara Formation phyllites and meta-marls with steeply plunging cascading or spruce-tree folds (Jf2) F) Jarara Formation slates gently dipping towards the NW. Dashed lines indicate unconformity in A, and foliation B-F, photo insets are oriented as indicated.



317
 318
 319
 320
 321
 322
 323
 324
 325
 326
 327
 328
 329
 330

Figure 6 Optical images of low- to high-grade metamorphic rocks from the Jarara range. A) Subhedral hornblende δ porphyroblast and plagioclase porphyroblasts surrounded by biotite and quartz aggregates, biotite strain shadows indicate top to NW sinistral shear sense. Sample GC-021 (Ug1), cross-polarized light. B) Poikilitic hornblende and plagioclase crystals, showing a granoblastic texture. Sample GC-52D (Ug2), cross-polarized light. C) Anhedral clinopyroxene (augite) surrounding subhedral garnet (pyrope) crystals. Sample G-52D (Ug2), transmitted light. D) Subhedral staurolite σ -porphyroblast surrounded by alternating quartz-plagioclase and biotite-muscovite strain shadows indicate top to NW sinistral shear sense. Sample G-54 (Ug3), cross-polarized light. E) Large muscovite crystals showing kink bands. Sample G-52A, cross-polarized light. F) Sericitized plagioclase σ -porphyroblast mantled by muscovite strain shadows indicate top to NW sinistral shear sense and quartz-orthoclase crystals with polygonal texture. Sample G-55B (Jf1), cross-polarized light. Abbreviations: Bt, biotite; Cal, calcite; Cpx, Clinopyroxene; Grt, garnet; Hbl, hornblende; Ms, muscovite; Pl, plagioclase; Qz, quartz; St, staurolite.

331 ***Mesozoic metasedimentary cover***

332 Over the high-amphibolite facies Uray Gneiss, the Jarara Formation greenschist facies
333 meta-sedimentary rocks rest unconformably. This sedimentary cover gradually decreases in
334 metamorphic grade towards the NW. This section describes the basal part of the Jarara
335 Formation a basal meta-conglomerate level (Jf1), which marks the contact between the two units.

336 **Jarara Formation**

337 The greenschist facies meta-conglomerate (Jf1; Fig. 4H; Fig. 5) is followed by alternating
338 meta-pelites, meta-marls, and marble (Jf2). The latter frequently shows cascading folds with
339 foliation strike parallel axes (Fig. 5 insets D, E, F).

340 The muscovite-rich meta-conglomerate (Jf1) displays a protomylonitic fabric (G-55b;
341 Fig. 4I). Muscovite is the dominant index mineral that mantles feldspar, orthoclase, and quartz
342 porphyroclasts (Fig. 6F). Along with zircon, apatite is present as an accessory, and also sporadic
343 calcite veins cut through the foliation. The protomylonitic fabric is also defined by sinistral s-c
344 structures (Fig. 6F) that commonly display sigmoidal plagioclase porphyroclasts with muscovite
345 pressure shadows (Fig. 6F), indicating a top to NW sinistral displacement. The basal meta-
346 conglomerate varies into muscovite-rich quartzites, muscovite schists, phyllites, slates, and a
347 marble level. These are overlain by a second meta-conglomerate level in which muscovite is
348 absent, superseded by black phyllites and slates interbedded with marbles and siliciclastic beds
349 that are internally graded and show sporadic carbonate olistostromes. The sequence is
350 superseded by greenschist facies mafic meta-volcanic flows and meta-tuffs, characterized by
351 actinolite-chlorite phyllites (Fig. 7).

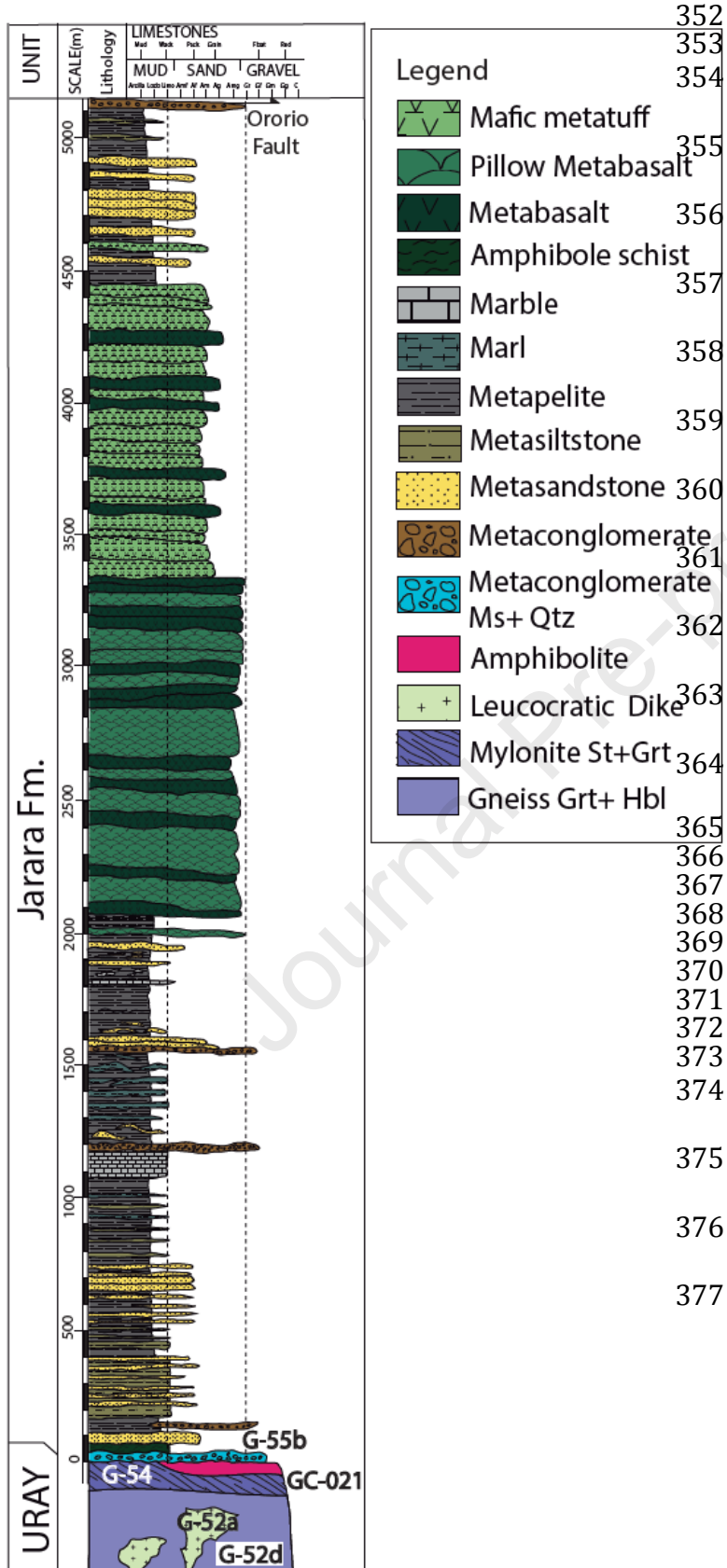


Figure 7. Semi-detailed Stratigraphic column of the Jarara Formation at the Jarara Range, Samples analyzed in this study are indicated within the Uray Gneiss and at the basal metaconglomerate (Jf1) of the Jarara Formation. The section is located in Figs. 2-3.

TABLE 1. LOCATION, DESCRIPTION, OF SAMPLES ANALYSED BY U-Pb and Lu-Hf LA-ICP-MS

| Sample Code | Coordinates | | Lithology | Stratigraphic division | Unit | Intrepreted protolith | U-Pb Age | 2s | MSWD | $^{176}\text{Hf}/^{177}\text{Hf}$ | ϵHf_t^e | $T_{dm}(\text{Ga})$ | Type |
|----------------|-------------|-----------|-----------------------------|------------------------|--------------------------|-----------------------|-------------|-------------|------------|-----------------------------------|-------------------------|---------------------|----------------------------------|
| | Lat (°N) | Long (°W) | | | | | | | | | | | |
| B-245 | 11.993 | -71.774 | Pl+Hbl+Grt+Qtz gneiss | Proterozoic | Jaturuhu Gneiss | volcanoclastic | 967 | 4.2 | 0.2 | - | - | - | Metamorphic rims |
| C-172 | 11.932 | -71.766 | Hbl lense | Proterozoic | Jaturuhu Gneiss | mafic rock | 1026 | 5.4 | 1.3 | - | - | - | Metamorphic Concordia Age |
| B-235 | 11.889 | -71.902 | Pl+Kfs+Qtz Gneiss | Proterozoic | Jojoncito Gneiss | pelite | 1009 | 3.8 | 0.8 | - | - | - | Metamorphic Weighted Average Age |
| G-95 | 11.876 | -71.923 | Kfs+Pl+Qtz | Proterozoic | Jojoncito Gneiss | granitoid | 1039 | 14.5 | 1.8 | - | - | - | Metamorphic Weighted Average Age |
| | | | | | | | 238 | 30 | 2.7 | - | - | - | Lower intercept |
| GC-061 | 12.194 | -71.351 | Pl+Hbl+Bt+Qtz | Proterozoic | Macuira Schists | mica schist | 880 | 4.2 | 0.8 | - | - | - | Metamorphic rims |
| GC-021 | 12.136 | -71.513 | Hbl+Ep+Pl+Qtz | Permian | Uray Gneiss | mafic rock | 272 | 1.1 | 0.6 | - | - | - | Core ages |
| | | | | | | | 198 | 4 | 0.1 | - | - | - | Metamorphic rims |
| G-52D | 12.047 | -71.547 | Px+Grt+Hbl+Pl gneiss | Triassic | Uray Gneiss | mafic rock | 230 | 0.5 | 0.9 | 0.282165-0.282886 | (-2.4-8.7) | 0.7-1.3 | Metamorphic Concordia Age |
| G-54 | 12.065 | -71.577 | St++Bt+Grt+Pl+Qtz mylonite | Triassic | Uray Gneiss | pelite | 223 | 0.6 | 1.3 | 0.281706-0.282778 | (-32-10) | 1.2-3.5 | Metamorphic Concordia Age |
| G-52A | 12.047 | -71.547 | Pl+Ms+Qtz leucocratic dike | Jurassic | Jurassic Intrusive suite | granitoid | 170 | 2.2 | 0.1 | 0.282638-0.282883 | (-1.5-6.9) | 0.9-1.2 | Magmatic Concordia age |
| G-55B | 12.072 | -71.584 | Qtz+Pl+Ms meta-conglomerate | Jurassic | Jarara Formation | pelite | 157 | 3.4 | 1.5 | 0.280791-0.282903 | (-27.8-7.8) | 0.9-3.1 | Maximum depositional Age |
| JOJON-1 | 11.871 | -72.024 | Granitic Gneiss | Proterozoic | Jojoncito Gneiss | granitoid | 916 | 19 | 0.5 | - | - | - | Metamorphic rims |
| AVO-3 | 12.122 | -71.438 | Ms+Bt+Qtz+Pl schist | Triassic | Uray Gneiss | pelite | 248 | 4.1 | 0.4 | - | - | - | Metamorphic weighted average age |
| AVO-6 | 12.127 | -71.438 | Ms+Bt+Qtz+Pl schist | Triassic | Uray Gneiss | pelite | 246 | 3.9 | 0.5 | - | - | - | Metamorphic weighted average age |

Mineral abbreviations used in the text, figures, and tables: **Bt**: Biotite, **Ep**: Epidote, **Grt**: Garnet, **Hbl**: Hornblende, **Ksp**: Potassium feldspar, **Ms**: Muscovite, **Pl**: Plagioclase, **Px**: Pyroxene **Qtz**: Quartz, **St**: Staurolite

Samples in italic belong to previous works (Weber et al., 2009, Cardona et al., 2006)

MSWD of equivalence, uncertainties are propagated at 2s level

378 **4.2 Zircon U-Pb geochronology and trace element geochemistry**

379 *Proterozoic high-grade metamorphic basement*

380 Geochronological results reveal that the Proterozoic units of the Guajira Arch outcrop in
381 the Simarua and Macuira ranges. The units described in this section yield distinctive zircon age
382 spectra and morphological traits presented in the following paragraphs and summarized in Tables
383 1 and 2 and Figures 8-10A.

384 *Jaturuhu Gneiss*

385 The Jaturuhu Gneiss zircon spectra (sample B-245) comprises Paleoproterozoic inherited
386 cores in some cases with twinned grains mantled by bright rims (Fig. 8A), in arrays of complex
387 zoning patterns, showing intragrain crystallographic misorientation, and truncating geometries
388 (Table 2), with ages spanning between 2005-1630 Ma, mantled by Meso-Neoproterozoic rims
389 with ages spanning 1400-950 Ma. Discordant ages yield an upper intercept ca. 1837 ± 89 Ma and
390 a Neoproterozoic lower intercept ca. 1041 ± 40 Ma (Table. 1), pointing to metamorphic
391 recrystallization (Fig. 8A). The youngest four rims cluster around a Concordia age of 967 ± 26
392 Ma (MSWD= 2.6; Fig. 9A). The Paleo-Neoproterozoic growth zones can be observed in several
393 crystals (Fig. 8A). Five crystals were recovered from an amphibolite melanosome within the
394 Jaturuhu Gneiss (sample C-172; Fig. 8B), out of which four yield a Concordia age of 1026 ± 31
395 Ma (MSWD = 2.4; Fig. 9B). One of the crystals exhibits an inherited core of 1151 Ma, mantled
396 by thick bright rims (Fig. 8B).

397 *Jojoncito gneiss*

398 The Jojoncito Gneiss samples (B-235, G-95) yield ages between 1300-1000 Ma. Both
399 analyzed samples lack Paleoproterozoic inherited cores (Fig. 8C-D). Quartz-feldspathic gneiss
400 (sample B-235) attests for partial recrystallization at 1008 ± 7.2 Ma (MSWD=0.85; Fig. 9C),
401 with cores mantled by brighter rims that display slightly misoriented cores.

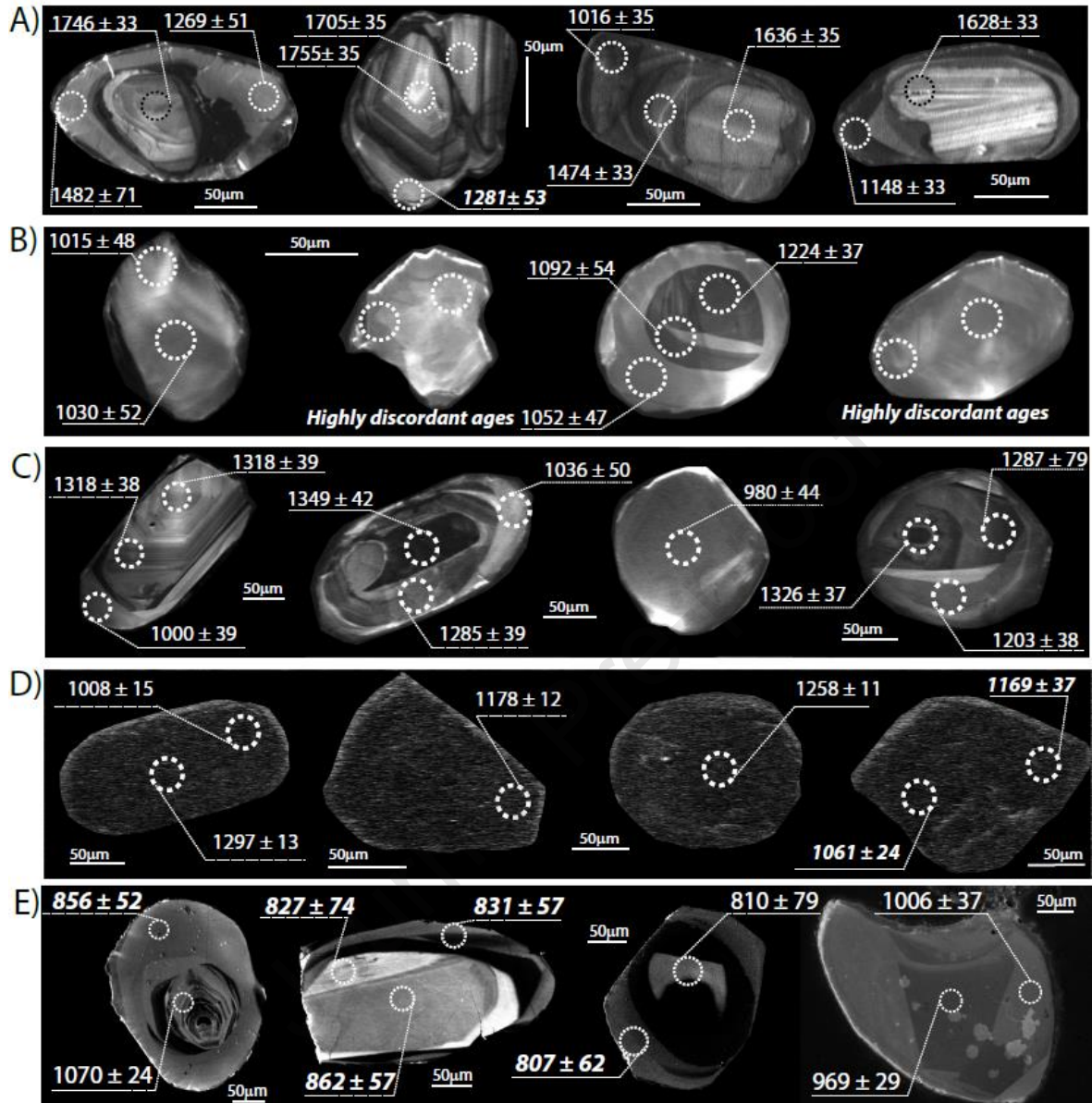
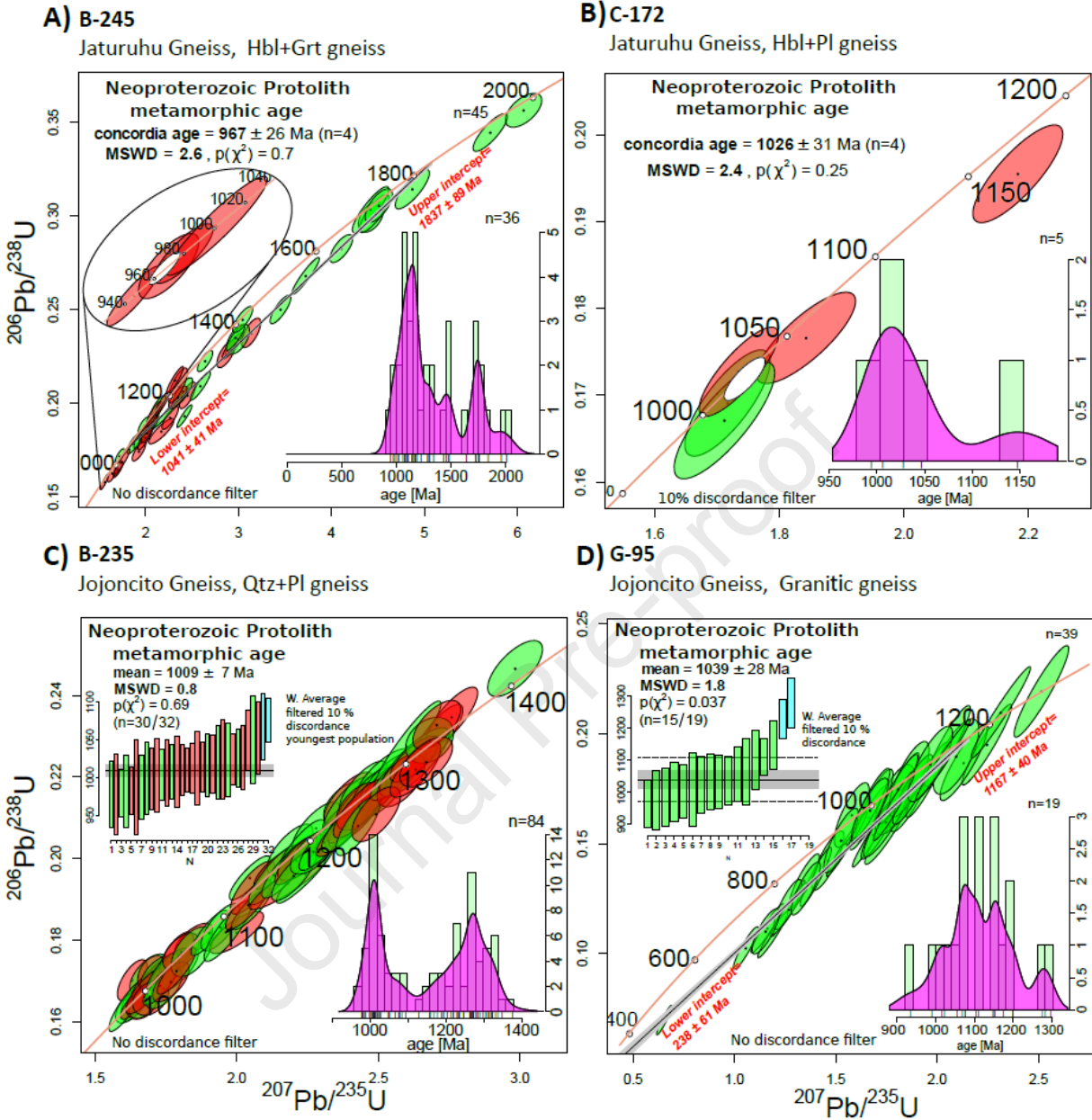


Figure 8. Panchromatic cathodoluminescence imagery of zircons from the Proterozoic units of the Guajira Arch analyzed in this study: A) Quartz-feldspathic gneiss with augen texture (B-245, Jaturuhu Gneiss); B) Amphibolite melanosome (C-172, Jaturuhu Gneiss); C) Quartz-feldspathic gneiss with granoblastic texture (B-235, Jojoncito Gneiss); D) Felsic granulite (G-95, Jojoncito Gneiss); E) Folded structured metatexite (GC-061, Macuira Schists). U-Pb ages are indicated in cores and rims, values in italics correspond to discordant data. Dashed circles ablation size diameter 25 μm except for sample G-95 that was analyzed with a spot of 30 μm .

Zircons retrieved from a granoblastic felsic gneiss (sample G-95) show a low CL response with homogenized crystals and a weighted average age of 1039 ± 28 Ma (MSWD= 1.77; Figs. 8D & 9D). The whole dataset, including discordant ages, describes a Triassic lower intercept at ca. 238 ± 61 Ma (MSWD= 2.7; Fig. 9D).

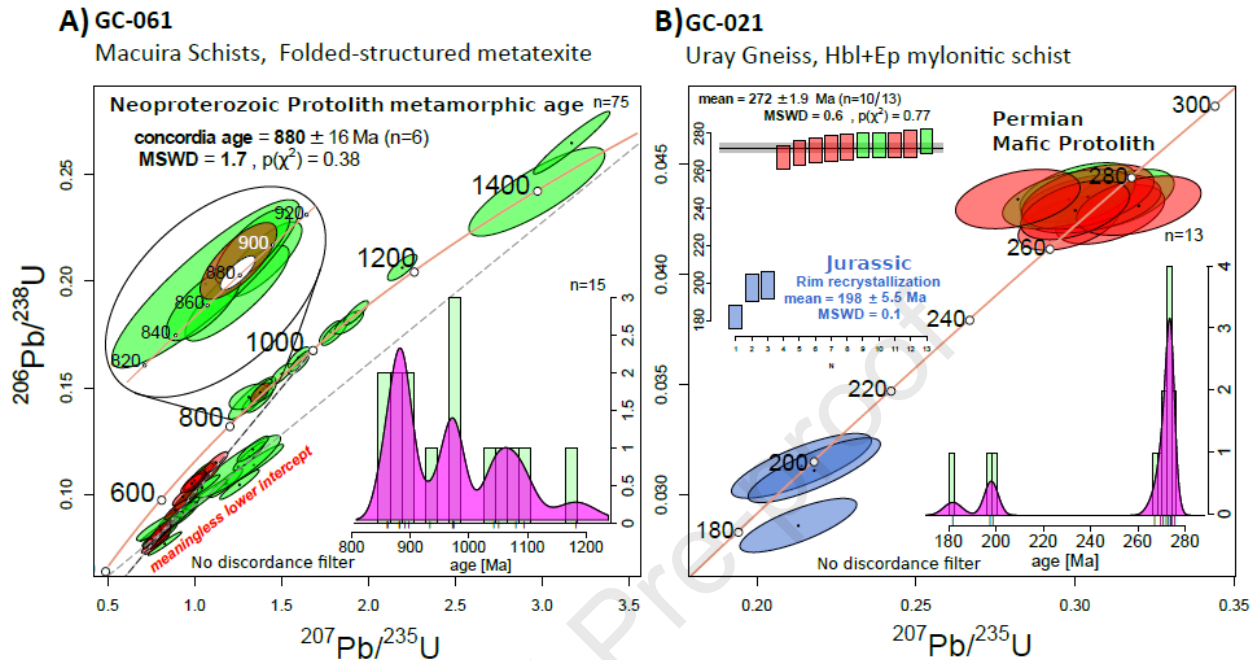


415
416 **Figure 9. Composite plot of zircon U-Pb LA-ICP-MS geochronological data from the Jaturuhu (A-B) and**
417 **Jojoncito gneisses (C-D) at the Simarua range. Metamorphic ages are calculated from rim recrystallization,**
418 **lower intercepts, and weighted average values. Green ellipses represent cores, and red ellipses represent rims.**
419

420 Macuira schists

421
422 Zircons from a folded metatexite of the Macuira Schists (sample GC-61) are subhedral
423 and display intensely resorbed rims, with inherited cores with internal crystallographic
424 misorientation (Fig.8E). Analyzed crystals resulted in 75 % of discordant ages that rendered
425 meaningless lower and upper intercepts (Fig. 11A). The remaining concordant data includes

426 Mesoproterozoic grains of 1400-1000 Ma from inherited cores. A younger age cluster of 6
 427 Neoproterozoic crystals yields a concordant age of 880 ± 16 Ma (MSWD= 1.7; Fig. 10A).

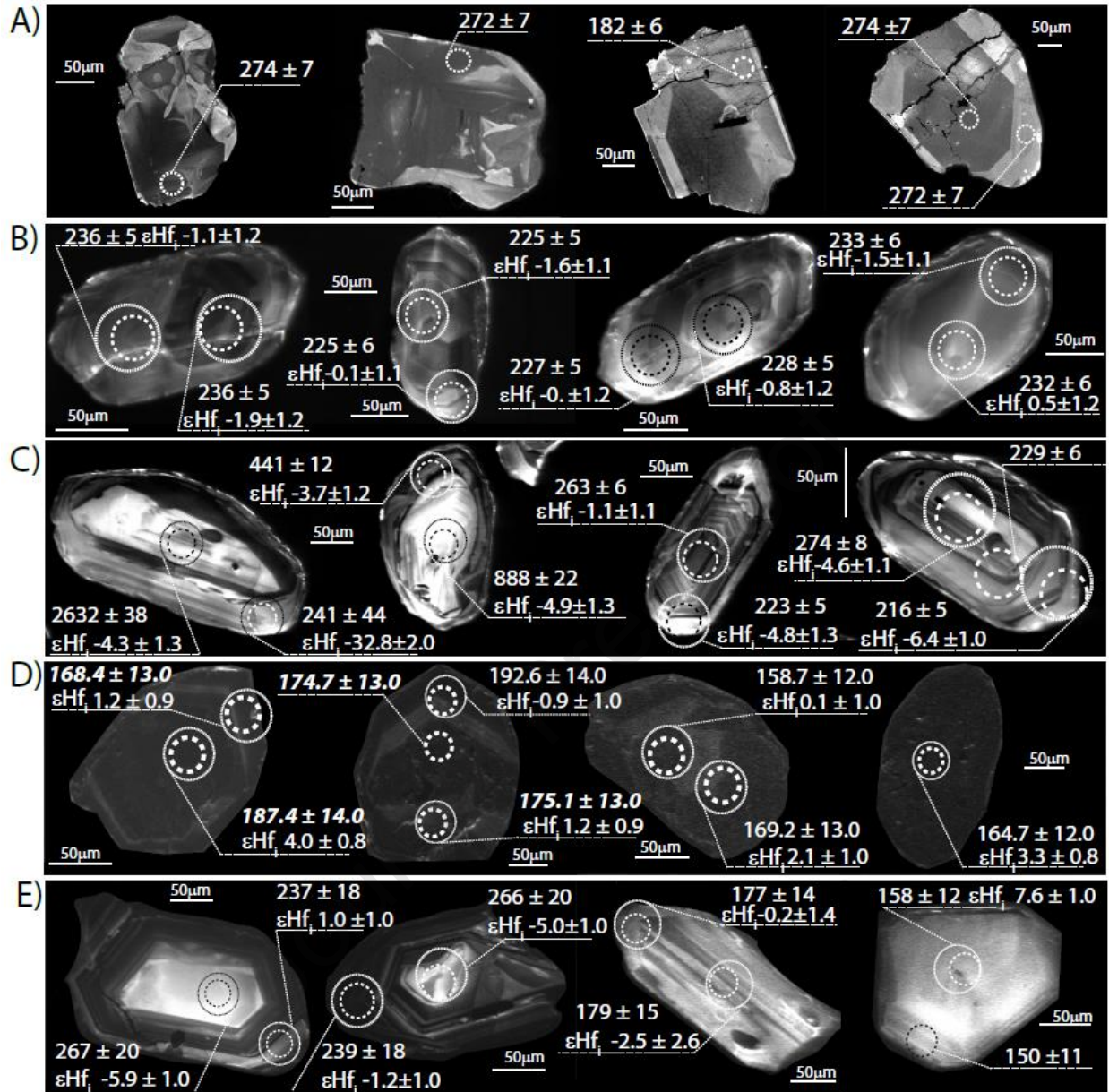


428
 429 **Figure 10. Composite plot of zircon U-Pb LA-ICP-MS geochronological data from the A) Folded structured**
 430 **metatexite from Macuira Schists (sample GC-061) and B) amphibole-epidote mylonitic schist (Ug1, sample**
 431 **GC-021). Intercept ages were calculated without filtering 10% of discordance. Metamorphic ages are**
 432 **calculated from Concordia age of youngest age peak. Green ellipses represent cores, and red-blue ellipses**
 433 **represent rims.**
 434

435 *Permian-Triassic high-to medium-grade basement (Uray gneiss)*

436 *Amphibole+epidote mylonitic schists (Ug1)*

437 Thirteen zircon crystals were recovered from a hornblende+epidote+plagioclase+quartz
 438 mylonitic schist (sample GC-21). Age data indicate a Permian Concordia age at ca. 272 ± 1.9 Ma
 439 (MSWD=0.64) with three Jurassic growth sectors of ca. 198 ± 5.5 Ma (MSWD=0.10; Fig. 10B)
 440 in rims. Zircons display complex growth zoning, local intermediate resorption, sector to patchy
 441 zoning, and subhedral shapes (Fig. 11A; Table 2).



442

443 Figure 11. Panchromatic cathodoluminescence imagery of zircons from the Permian-Jurassic units of the
 444 Guajira Arch analyzed in this study, with U-Pb age and ϵHf_i : A) Amphibole+epidote mylonitic schist (GC-
 445 021, Ug1; Uray Gneiss); B) Pyroxene+garnet+hornblende gneiss, (G-52D, Ug2; Uray Gneiss); C)
 446 Staurolite+biotite+garnet mylonite (G-54, Ug3; Uray Gneiss); D) Leucocratic dike muscovite+plagioclase (G-
 447 52A, Siapana Granodiorite suite); E) Quartz-muscovite protomylonitic meta-conglomerate (G-55B, Jf1;
 448 Jarara Formation). Dashed circles ablation size diameter for U-Pb analyses 30 μm and 50 μm for Lu-Hf
 449 analyses.

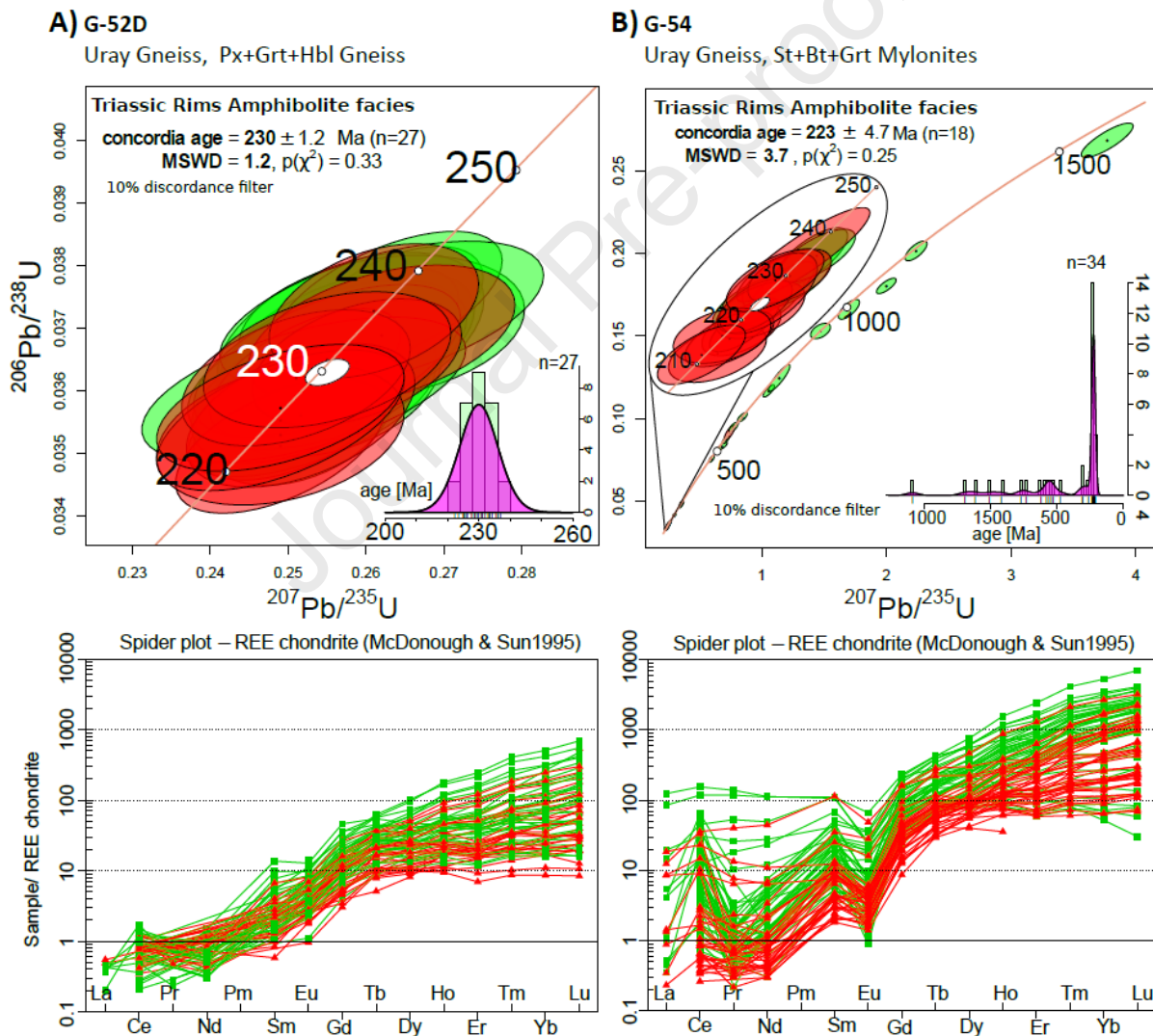
450

451

452

453 ***Pyroxene+ Garnet+Hornblende gneiss (Ug2)***

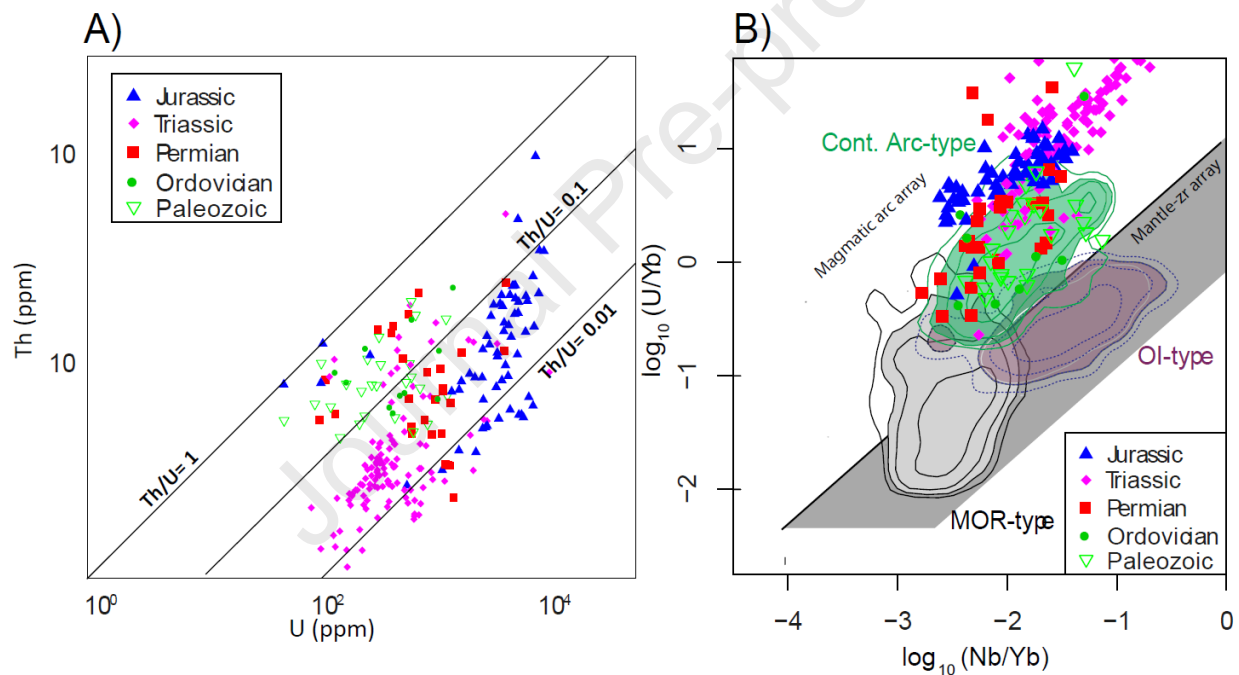
454 The obtained crystals from this garnet-rich anatectic gneiss (sample G-52D) show regular
 455 polygonal, oscillatory, or sector, generally weak zoning (Fig. 11B), and define a Carnian
 456 Concordia age of 230 ± 1.2 Ma (MSWD=1.2; Fig. 12A). All analyzed spots either in cores or
 457 rims are within this age range, and there are no inherited cores preserved (Fig. 11B). All crystals
 458 are strongly depleted in HREE, with average values below 900 ppm and a high U/Yb ratio (Figs.
 459 12A and 13).



460
 461 **Figure 12. Composite plot of zircon U-Pb LA-ICP-MS geochronological data from the A) Uray gneiss**
 462 **Px+Grt+Hbl gneiss (Ug2, sample G-52D) and B) Uray gneiss St+Bt+Grt mylonite (Ug3, sample G-54). Below,**
 463 **Primitive chondrite-normalized REE patterns (McDonough and Sun, 1995). Green ellipses represent cores,**
 464 **and red ellipses represent rims.**

465 ***Staurolite+Biotite+Garnet mylonitic schists (Ug3)***

466 Zircons recovered from these mylonites (G-54) yield inherited cores differentiated from
 467 highly resorbed rims by truncating geometries (Fig. 11C; Table 2). Age spectra are defined by
 468 inherited cores that range between 1500-500 Ma (Fig. 12B). Rims, in contrast, are restricted to
 469 the Norian, with a Concordia metamorphic age of 223 ± 4.7 Ma (MSWD= 3.7; Fig. 12B). Cores
 470 are enriched in HREE in comparison with rims, and concentrations are below 1000 ppm. Triassic
 471 rims are constantly below 500 ppm. Accordingly, Triassic crystals display low Yb and Y
 472 contents and high U/Yb ratios (Fig. 12B and 13).

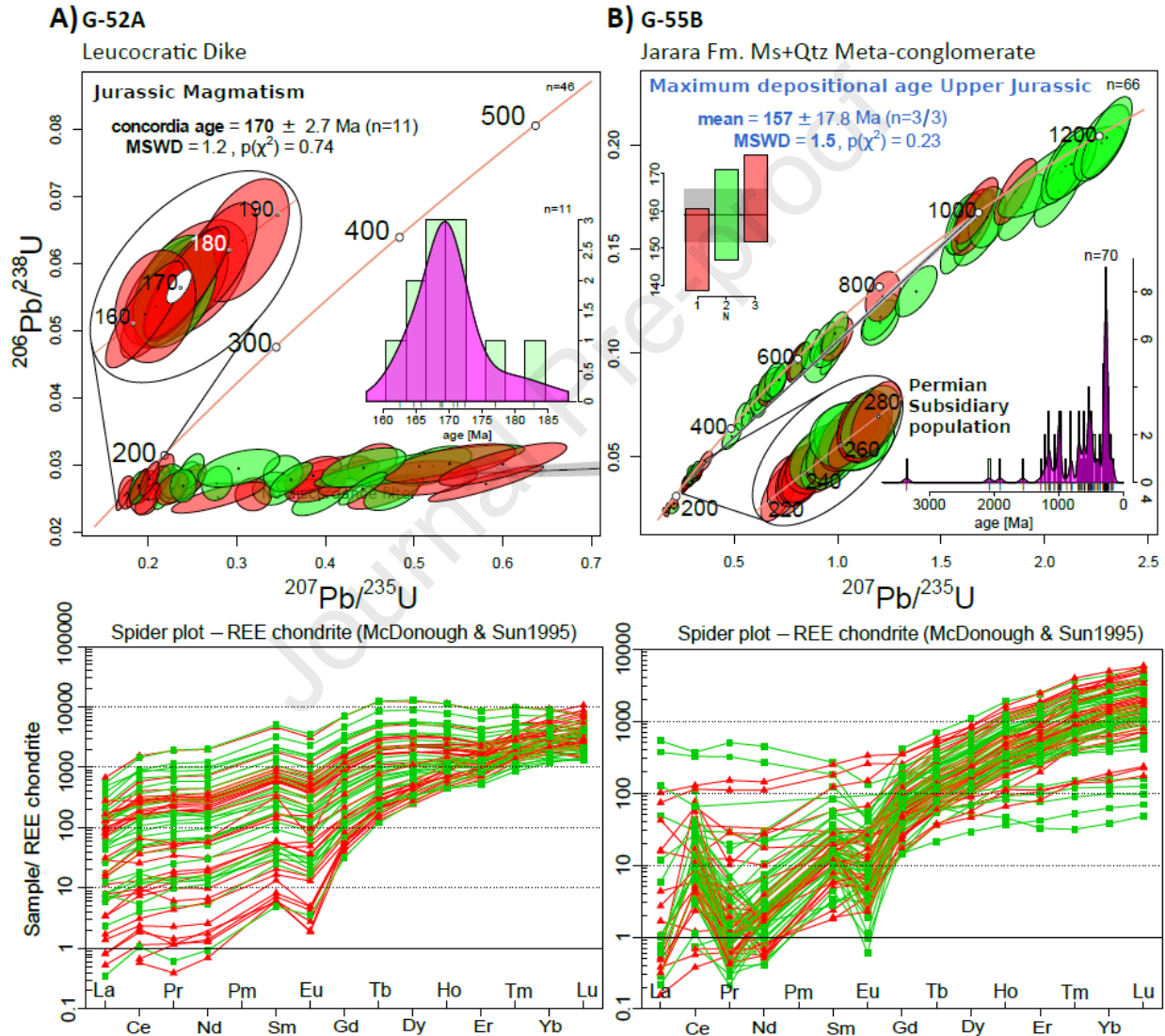


473
 474 **Figure 13. Uray Gneiss, Jarara meta-conglomerate and leucocratic dike zircon trace element geochemistry**
 475 **(including Phanerozoic inherited cores) bivariate plot. A) Th vs. U plot and B) U-Nb-Yb-based zircon**
 476 **discrimination plot and density distribution based on geochemical proxies or tectono-magmatic setting, after**
 477 **Grimes et al., (2015). The shaded fields are overlapping two-dimensional kernel density distributions for**
 478 **compiled datasets of the mid-ocean ridge (MOR-type), plume-influenced settings of Iceland & Hawaii (ocean-**
 479 **island (OI)-type), and continental arc (Cont. arc-type) zircon.**

480
 481 ***Leucocratic Dike***

482 A plagioclase+muscovite+quartz pegmatitic dike (sample G-52A) intruding the
 483 pyroxene+garnet++hornblende Uray Gneiss (Ug1) yields zircons with a low CL response,

484 internal morphology is barely discernible with weak oscillatory zoning (Fig. 11D). Ages are
 485 mainly discordant, evidencing extensive common Pb incorporation. Data obtained from cores are
 486 highly discordant, and only 11 concordant ages in rims indicate a Middle Jurassic (Bajocian) age
 487 of crystallization at ca. 170 ± 2.7 Ma (MSWD=1.2; Fig. 14A). The HREE concentrations are
 488 extremely high, up to 10000 ppm with high U/Yb ratios (Fig. 13).



489

490 **Figure 14. Composite plot of zircon U-Pb LA-ICP-MS geochronological data from the A) leucocratic dike**
 491 **intruding Ug2 (sample G-52A) and B) Jarara Formation basal meta-conglomerate Ms+Pl+Qtz (sample G-**
 492 **55B). Below, Primitive chondrite normalized REE patterns (McDonough and Sun, 1995). Green ellipses**
 493 **represent cores, and red ellipses represent rims.**

494

495

496 *Mesozoic metasedimentary cover*

497 **Jarara Formation Protomylonitic meta-conglomerate (Jf1)**

498 Zircon retrieved from the basal meta-conglomerate of the Jarara Formation (sample G-
499 55b) display a wide morphological and age range, commonly with inherited cores, differentiated
500 from highly resorbed rims by truncating geometries or separated subrounded and unzoned cores.
501 Several crystals show regular polygonal, oscillatory, or sector zoning and are mainly concordant
502 (Fig. 11E).

503 This sample zircon age range includes two Paleoproterozoic crystals and a single
504 Paleoproterozoic concordant crystal at 3432 ± 22 Ma. The remaining analyzed crystals from this
505 sample comprises four coherent populations, as follows: (i) The 1200-1000 Ma inherited cores
506 may or not be mantled by recrystallized rims; (ii) Ediacaran - Devonian (770-400 Ma); (iii) a
507 Permian-Triassic population between 280 and 218 Ma (Fig. 14B); and (iv) the youngest
508 population composed of four Jurassic ages corresponding to two grains containing two consistent
509 analyses each, which constrain a maximum depositional age for the meta-conglomerate at ca.
510 157 ± 17.8 Ma (MSWD=1.5; Fig. 14B). Distinctively, most Triassic ages are found as rims that
511 mantle Paleozoic or older cores (Fig. 11E). Most cores and rims are enriched in HREE with
512 values between 900 and 7000 ppm, and variable Yb contents oscillating between 30-7000 ppm
513 (Figs. 13-14B).

514

515 **4.3 Zircon Hf isotope geochemistry**

516 We conducted Lu-Hf isotopic analyses on three samples from the Uray Gneiss suite and
517 one sample from the Jarara Formation (G-52D, G-54, G-55B, G-52A). These were previously
518 analyzed by U-Pb dating with spots of different sizes but in the same growth zones (Fig. 11).

519 The results are summarized in Table 1. In Figure 15, the initial $^{176}\text{Hf}/^{177}\text{Hf}$ is calculated using
520 individual apparent $^{206}\text{Pb}/^{238}\text{U}$ ages of laser spots measured on the same zircon growth zones.

521 Samples yield a broad range of ϵHf_i values of +10 to -30 (Fig. 15; Table 1), evidencing
522 both crustal recycling and the addition of new crust (e.g., Collins et al., 2011). Inherited zircon
523 cores (~275 Ma to ~1.2 Ga) within the sampled meta-sediments plot on the CHUR array (Fig.
524 15) and represent the range of meta-sedimentary protoliths that underwent crustal anatexis.

525 *Uray gneiss*

526 *Pyroxene+Garnet+Hornblende gneiss (Ug2)*

527 Triassic crystals of sample G-52D yield $^{176}\text{Hf}/^{177}\text{Hf}$ values ranging from 0.282165 to
528 0.282886 (ϵHf_i from -2.4 to +8.7; Figs 11B & 15), making this sample the most juvenile in
529 composition. A single Devonian core yields ϵHf_i -13.7. Thus, the ϵHf spectrum is dominated by
530 juvenile compositions with the mixing of older crustal unradiogenic sources. The crustal $T_{\text{DM}(\text{Hf}_i)}$
531 model ages range from ~0.7 to ~1.3 Ga for all Triassic crystals (~230 Ma; Fig. 15) and ca. 2.17
532 Ga for the Devonian core.

533 *Staurolite+Biotite+Garnet mylonitic schists (Ug3)*

534 Triassic rims from sample G-54 yield $^{176}\text{Hf}/^{177}\text{Hf}$ ranging from 0.281706 to 0.282778
535 (ϵHf_i -32 to +0.86). Ordovician to Permian inherited cores yield $^{176}\text{Hf}/^{177}\text{Hf}$ of 0.281960 to
536 0.282911 and displayed dominantly negative values (ϵHf_i from -23.3 to +0.7; Figs. 11C and 14)
537 that hint at the reworking of older crustal unradiogenic sources.

538 $^{176}\text{Hf}/^{177}\text{Hf}$ values from Proterozoic cores fluctuate between 0.280864 to 0.282353 (ϵHf_i
539 from -7.5 to +7.4; Figs. 11C & 15). The crustal $T_{\text{DM}(\text{Hf}_i)}$ model ages for all Triassic rims ranges
540 from ~1.2 to ~3.2 Ga (Fig. 15, Table A3), with dominant Paleo-Mesoproterozoic ages,

TABLE 2. MORPHOLOGICAL TRAITS AND TRACE ELEMENT GEOCHEMISTRY OF ZIRCONS ANALYSED BY U-Pb LA-ICP-MS

| Sample Code | Lithology | Unit | Zircon Morphology | CL Zoning | Process | Th/U | Y |
|---------------|---|--------------------------|---|--|--|-------------------------------|------------|
| B-245 | Qtz+Kfs+Pl and Cpx+Hbl+Bt+Grt gneiss | Jaturuhu Gneiss | Subrounded subhedral translucent | Complex zoning as intragrain crystallographic misorientation, the formation of twinned grains and subgrains. Inherited cores mantled by rims with truncating geometries separated subrounded, oscillatory zoned, chaotically zoned cores | Crystallization from a melt or precipitation from a fluid evidencing several stages of deep resorption | 0.04- 1.0 cores 0.03-0.4 rims | - |
| C-172 | Amphibolite lens | Jaturuhu Gneiss | Subrounded subhedral translucent | High CL response crystals display weak oscillatory zoning tending to homogeneous, subrounded shapes and homogeneous texture indicates high resorption | Crystallization from a melt or precipitation from a fluid evidencing several stages of deep resorption | 0.05-0.3 | - |
| B-235 | Quartzfeldspathic Gneiss | Jojoncito Gneiss | Subrounded subhedral translucent | Dark inherited cores mantled by brighter rims, complex zoning patterns intragrain crystallographic misorientation, the formation of subgrains, truncating geometries, or separated subrounded, homogeneous, or chaotically zoned cores with rutile inclusions. | Crystallization from a melt or precipitation from a fluid evidencing several stages of deep resorption | 0.1-0.6 cores, 0.06-0.3 rims | - |
| G-95 | Kfs+Pl+Qtz | Jojoncito Gneiss | Subrounded, subhedral, Translucent, fractured | Crystals appear completely dark and homogeneous, with a rugged surface of porosity and inclusions | Homogenization process, hydrothermal alteration reprecipitation | 0.05-0.4 | 1000-5300 |
| GC-061 | Pl+Hbl+Qtz folded structured metatexite | Macuira Schists | Translucent to slightly yellowish color, and are characterized by sub-rounded sub-anhedral shapes | Highly resorbed rims subhedral and xenocrystic cores with the sub-grain formation and internal crystallographic misorientation, sometimes show patchy zoning and homogenization | Crystallization from a melt or precipitation from a fluid, migmatization, in -situ anatectic recrystallization | 0.4-1.3 | - |
| GC-021 | Amphibolite | Uray Gneiss (Ug1) | Subhedral dipyrmidal translucent | Complex growth zoning, local intermediate resorption, sector to patchy zoning, and subhedral shapes, rims display patchy and convoluted zoning | Metamictization, fluid alteration, initial stages of replacement | 0.8-1.65 | - |
| G-52D | Px+Grt+Hbl+Pl gneiss | Uray Gneiss /(Ug2) | Translucent, subangular, euhedral, dipyrmidal prismatic | Regular polygonal, oscillatory, or sector, generally weak zoning | Anatexis | 0.05 | 20-250 |
| G-54 | St+Bt+Grt+Pl mylonite | Uray Gneiss (Ug3) | Translucent and subangular dipyrmidal prismatic. | Inherited cores, differentiated from highly resorbed rims by truncating geometries, | High strain rates and mylonitization | 0.3 rims, 1.1 cores | 150-2400 |
| G-52A | Pl+Ms+Qtz leucocratic dike | Jurassic Intrusive suite | Euhedral dipyrmidal prismatic with a prism-pyramid ratio of 2:1 | Low CL response and crystals appear dark, internal morphology is barely discernible. Weak Oscillatory zoning. Cores appear with patchy and mosaic zoning, some inclusions | Metamictization, fluid alteration, or hydrothermal conditions | 0.2-0.01 | 1000-15000 |
| G-55B | Qtz+Pl+Ms meta-conglomerate | Jarara Fm. (Jf1) | Translucent and subangular euhedral, dipyrmidal and elongated prismatic. | Inherited cores, differentiated from highly resorbed rims by truncating geometries or separated subrounded, and unzoned cores. Crystals show regular polygonal, oscillatory, or sector zoning | Detrital zircon derived from igneous/metamorphic sources | 1.5-0.02 cores, 0.6-0.02 rims | 90-3000 |

Th-U ratios are reported as an average of cores and rims or a single value if constant, Y content is reported in ppm, morphology described according to Murali et al., 1983; Vavra et al., 1999; Rubatto, 2017, Harley et al., 2007, Schaltegger et al., 1999

541 and a single Neoproterozoic $T_{DM(Hf)}$ age ~ 0.9 . Similar tendencies are disclosed for Permian to
542 Ordovician inherited cores with $T_{DM(Hf)}$ age values between ~ 1.2 to ~ 3.0 Ga. Proterozoic cores
543 disclose exclusively Paleoproterozoic and older $T_{DM(Hf)}$ age values ~ 1.5 to ~ 3.5 Ga. Overall
544 dominant-negative ϵHf values hint at the reworking of older crustal unradiogenic sources (Fig.
545 15).

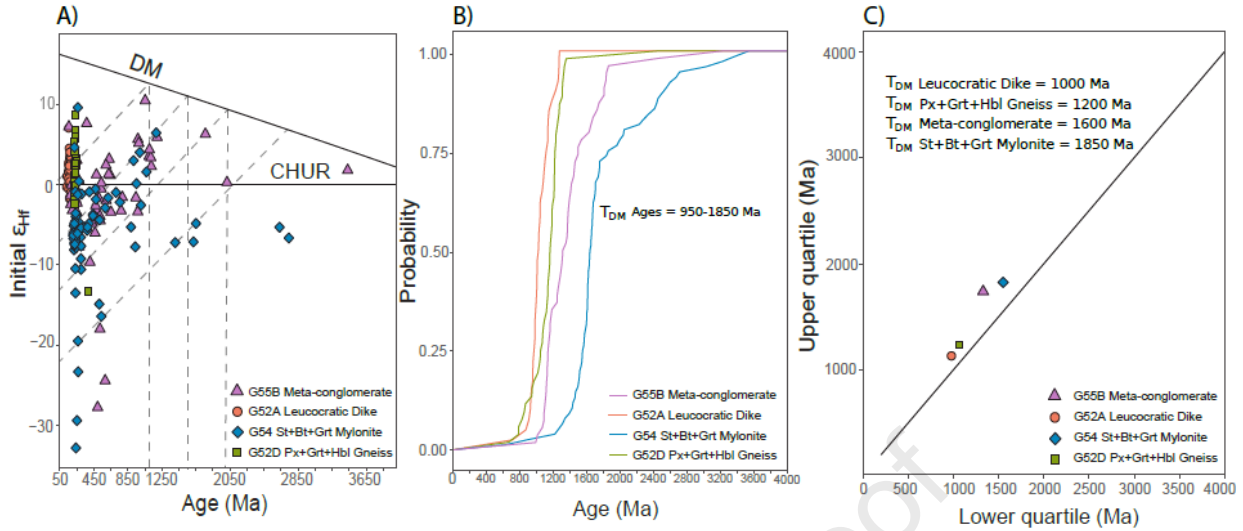
546 **Leucocratic Dike**

547 Jurassic crystals of sample G-52d yield $^{176}Hf/^{177}Hf$ ranging from 0.282638 to 0.282883
548 (ϵHf_i from -1.5 to +6.9; Figs. 11D & 15), with a narrow compositional spectrum that clusters
549 toward the CHUR array. It indicates the input of primitive sources and slightly depleted juvenile
550 compositions. The crustal $T_{DM(Hf)}$ model ages range from ~ 0.9 to ~ 1.2 Ga for all Jurassic crystals
551 (~ 170 Ma; Fig. 15).

552 **Jarara Formation Protomylonitic meta-conglomerate (Jf1)**

553 Jurassic crystals from sample G-55b yield $^{176}Hf/^{177}Hf$ ranging from 0.282583 to 0.282903
554 (ϵHf_i from -2.8 to +0.31; Figs. 11E & 15). Triassic crystals yield $^{176}Hf/^{177}Hf$ ranging from
555 0.282481 to 0.282740 (ϵHf_i from -5.1 to +3.6), whereas Permian to Ordovician crystals yields
556 $^{176}Hf/^{177}Hf$ ranging from 0.281688 to 0.282773 (ϵHf -27.8 – +7.8). The latter compares to
557 Proterozoic inherited cores that yield $^{176}Hf/^{177}Hf$ ranging from 0.280791 to 0.282489 (ϵHf_i from -
558 24.2 to +7.3).

559 The crustal $T_{DM(Hf)}$ model ages vary from ~ 0.9 to ~ 1.5 Ga for all Mesozoic crystals,
560 whereas for Paleozoic crystals $T_{DM(Hf)}$ model ages are older (~ 1.2 to ~ 3.1 Ga; Fig. 15). Younger
561 crystals plot closer to the CHUR array and are representative of the range of meta-sedimentary
562 protoliths that underwent crustal anatexis.



563
 564 **Figure 15.** $^{176}\text{Hf}/^{177}\text{Hf}$ versus time diagrams for samples from the Jarara Range showing depleted mantle and
 565 chondritic uniform reservoir (CHUR) evolution trends after Bouvier et al. (2008). (A) Initial ϵ_{Hf_i} versus
 566 $^{206}\text{Pb}/^{238}\text{U}$ apparent ages of individual zircon grains, every single analysis represented by a point. Crustal
 567 evolution models for different $T_{\text{DM(Hf)}}$ ages for zircons assume that it crystallized from a system with a time-
 568 integrated $^{176}\text{Lu}/^{177}\text{Hf}$ ratio of 0.015 (Griffin et al., 2002). (B) Empirical cumulative distribution curves for
 569 model ages of the data from samples analyzed in this study. Compiled T_{DM} ages range between 900-1750 Ma,
 570 note meta-sediments yield older components with mostly negative ϵ_{Hf_i} crustal values, whereas anatectites and
 571 dikes indicate T_{DM} ages around 900-1200 Ma and juvenile positive ϵ_{Hf_i} values. (C) Lower vs. upper quartile
 572 Hf model age plot for the samples of Triassic metamorphic rocks of the Uray gneiss, and late leucocratic dike.
 573 Model ages have been calculated relative to a commonly accepted depleted mantle model and plotted using
 574 the detzrc CRAN package for R (Andersen et al., 2018).
 575
 576

577 5. DISCUSSION

578 The basement of the northern Andes has been investigated (Macdonald and Hurley, 1969;
 579 Cordani et al., 2005; Cardona et al., 2006, 2010a), revealing the presence of Proterozoic inliers
 580 that compose the northernmost portion of the Guajira peninsula denominated as the Guajira
 581 Arch.

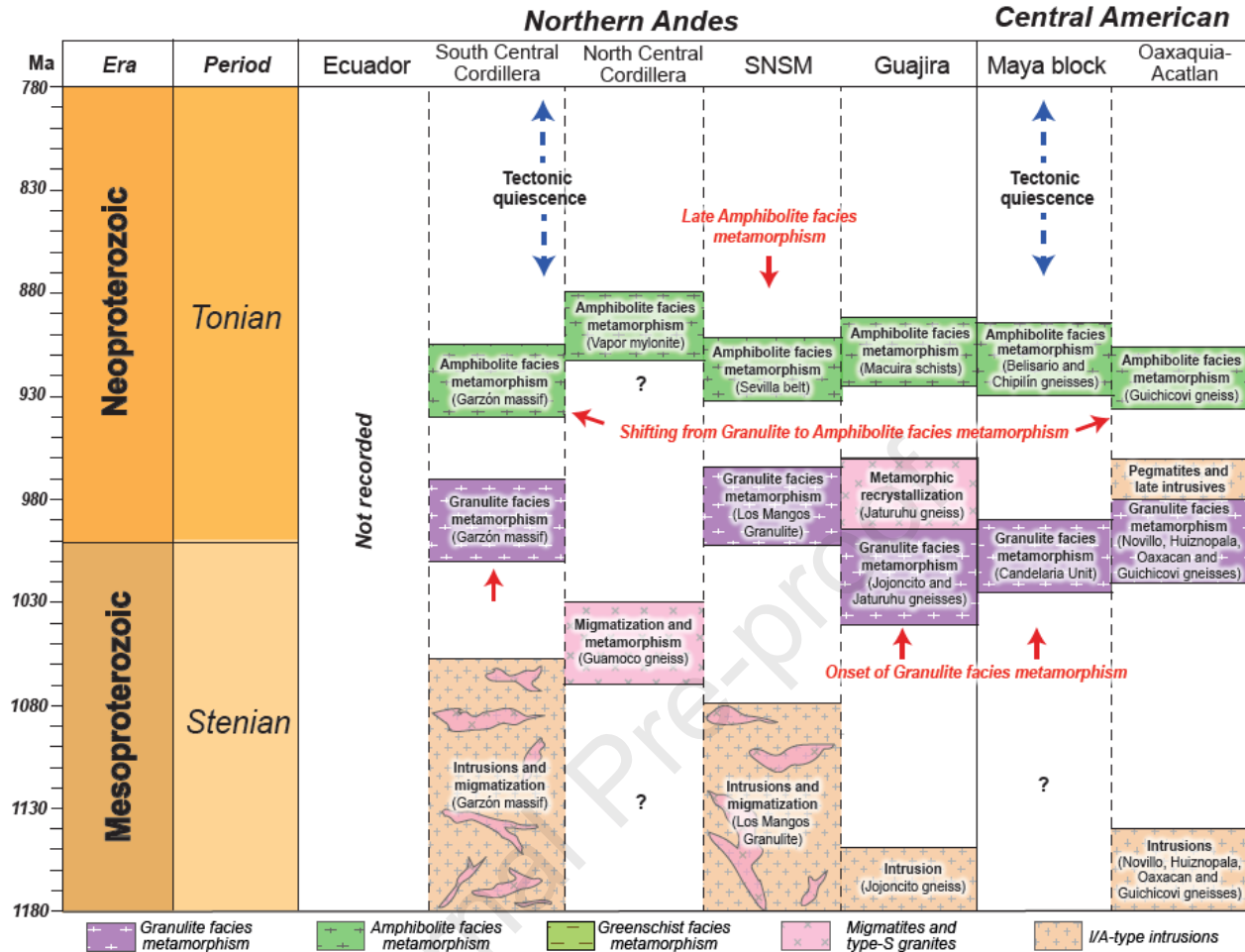
582 Regarding an Early Mesozoic evolution of the Guajira Arch, there is an ongoing
 583 discussion if this basement inlier currently disconnected from the main Andean trunk system is
 584 autochthonous or para-autochthonous to north-western Gondwana (MacDonald and Opdyke,
 585 1972; Bartok et al., 2015; Nova et al., 2019). In the following paragraphs, we will discuss the

586 geochronological and isotopic characteristics of the Guajira Arch Proterozoic basement and its
587 reworking during a Triassic tectono-thermal event.

588 **Meso-Neoproterozoic metamorphism**

589 The Guajira Arch Proterozoic basement holds evidence of at least two metamorphic
590 recrystallization episodes during the Late Mesoproterozoic and the Early Neoproterozoic
591 (Lockwood, 1965). The Jaturuhu Gneiss yields distinctive 2.0 – 1.7 Ga Paleoproterozoic
592 inherited cores, which underwent recrystallization by the end of the Mesoproterozoic at ca. 1041
593 \pm 40 Ma, as indicated by the Discordia lower intercept (Fig. 9A). The examined amphibolite
594 melanosome discloses similar age trends ca. 1026 \pm 31 Ma (Fig. 9B), suggesting an age range
595 (1050-1020 Ma) for the stromatic banding event (Radelli, 1962b), affecting a Paleoproterozoic
596 basement. Paleoproterozoic U-Pb ages are comparable to the ages of migmatites and
597 orthogneisses in Oaxaquia and the southern Chiapas Massif (Fig. 16), which underwent a
598 granulite facies metamorphism at ca. 990 Ma (Weber and Schulze, 2014; Ortega-Gutiérrez et al.,
599 2018; Solari et al., 2018). The latter is close to rim recrystallization ca. 967 \pm 26 Ma ages of the
600 Jaturuhu gneiss (Figs. 9A and 16).

601 The Jojoncito Gneiss granulite facies metamorphism led to anatexis at temperatures >
602 700°C (Zuluaga et al., 2009). The ages for the Jojoncito Gneiss reveal inheritance from
603 Mesoproterozoic magmatic sources between 1.4 -1.0 Ga. The timing of this episode is
604 constrained to 1039 \pm 28 M, and 1009 \pm 7 Ma, which broadly correlates to the migmatization age
605 of the Jaturuhu Gneiss and closely precedes a metamorphic event at ca. 990 Ma, corresponding
606 to the climax of the Putumayo orogeny of western Amazonia (Cordani et al., 2005; Cardona et
607 al., 2006; Ibañez-Mejía, 2020). The Jojoncito gneiss ages are indistinguishable from the
608 Atuschón gneiss metamorphic ages ca.1028 \pm 34 Ma, with rim ages ca. 967 \pm 5.8 Ma (Baquero
609 et al., 2015).



610

611

612 **Figure 16. Stratigraphic summary sketch of the Guajira Arch, Sierra Nevada de Santa Marta massif, North**
 613 **Central Cordillera, South Central Cordillera, Ecuador (Northern Andes), Oaxaquia-Acatlán, and Maya**
 614 **block (Central American - Mexican) from the Mesoproterozoic to Neoproterozoic. Major tectono-**
 615 **metamorphic events are indicated, references are disclosed in the discussion.**

616

617 Interestingly, although Jaturuhu and Jojoncito gneisses share similar metamorphic ages,

618 our data reveal a missing Paleoproterozoic inheritance in the Jojoncito Gneiss (Fig. 9C-D), while

619 the Jaturuhu Gneiss lacks a Mesoproterozoic inheritance between 1.25 -1.6 Ma (Fig. 9A-B). This

620 indicates that the two gneissic complexes were derived from different protoliths. Besides, the

621 zircon morphology in both complexes varies significantly with dark homogenized crystals from

622 the Jojoncito gneiss contrasting with the typical metamorphic crystals with inherited cores of the

623 Jaturuhu gneiss (Fig. 8).

624 Paleoproterozoic cores yield high Th/U ratios between 1.0-0.4, whereas rims with
625 Mesoproterozoic U/Pb ages show Th/U values decreasing from 0.3 to 0.05, and younger rims
626 with Neoproterozoic U/Pb ages have the lowest Th/U ratios between 0.2-0.06. This evidence a
627 decrease in the Th/U ratio towards younger ages, thus stressing the importance of an Early-
628 Neoproterozoic metamorphic event.

629 In synthesis, the Proterozoic basement of the Guajira Arch was affected by
630 metamorphism during the Putumayo orogeny of western Amazonia at the final stages of Rodinia
631 amalgamation (Ibañez-Mejia, 2020). Therefore, the Guajira Arch Proterozoic basement shares a
632 common tectono-magmatic history with central-American Oaxaquia and Maya blocks, in
633 agreement with other localities of the Northern Andes (Santa Marta Massif, Garzón Massif,
634 Santander Massif, Central Cordillera, and the Falcon basin; Kroonenberg, 1982; Ruiz et al.,
635 1999; Ordóñez, 1999; Cordani et al., 2005; Cardona et al., 2010a; Ibanez-Mejia et al., 2011;
636 Baquero et al., 2015; Cediel et al., 2019; Fig. 16).

637 Furthermore, the geochronological age spectrum of the Jojoncito Gneiss is similar to ages
638 documented at the southern Chiapas Massif, affected by an age-equivalent Meso-Neoproterozoic
639 metamorphic event (Weber and Schulze, 2014; Weber et al., 2018; Fig. 16), comprising inherited
640 cores of age ca. 1005 ± 7 Ma, with rim recrystallization by 950 ± 8 Ma. On the other hand, the
641 Macuira Schists record a younger Neoproterozoic event at ca. 880 ± 16 Ma (Fig. 10A) through
642 extensive zircon recrystallization, similar to the youngest metamorphic ages of the southern
643 Chiapas Massif (Belisario Dominguéz and Chipilín gneisses; Weber et al., 2018; Fig. 16), which
644 are strikingly younger than the widespread 990-960 Ma event.

645 **Permian magmatism**

646 Our data reveal that hornblende+epidote mylonitic schists (Ug1) from the Uray Gneiss
647 suite yield a Permian age, with a crystallization age of ca. 272 ± 1.9 Ma and high Th/U ratios

648 between 0.8 and 1.67 lacking inherited cores (Fig. 11A). Elevated Th/U ratios in Permian
649 amphibole schists from the Guajira Arch may indicate they are derived from an igneous
650 protolith, most likely of mafic composition evidencing igneous activity by this period.

651 Widespread Permian continental arc-magmatism, bracketed between 288 and 255 Ma is
652 documented in Northern Mexico (Arvizu et al., 2009), the southern Chiapas massif and Acatlán
653 complex (Weber et al., 2007; Ortega-Obregón et al., 2014), the Maya block (Ratschbacher et al.,
654 2009), the Paraguaná Peninsula (van der Lelij et al., 2016b) the Santa Marta Massif (Cardona et
655 al., 2010b; Piraquive, 2017), the Central Cordillera (Vinasco et al., 2006b; Cochrane et al.,
656 2014a; Bustamante et al., 2017; Shaw et al., 2019), and the Ecuadorian Andes (Paul et al., 2018),
657 evidencing subduction-related diachronic magmatism along with western Gondwana (Riel et al.,
658 2018; Spikings and Paul, 2019; Figs. 17-18B)

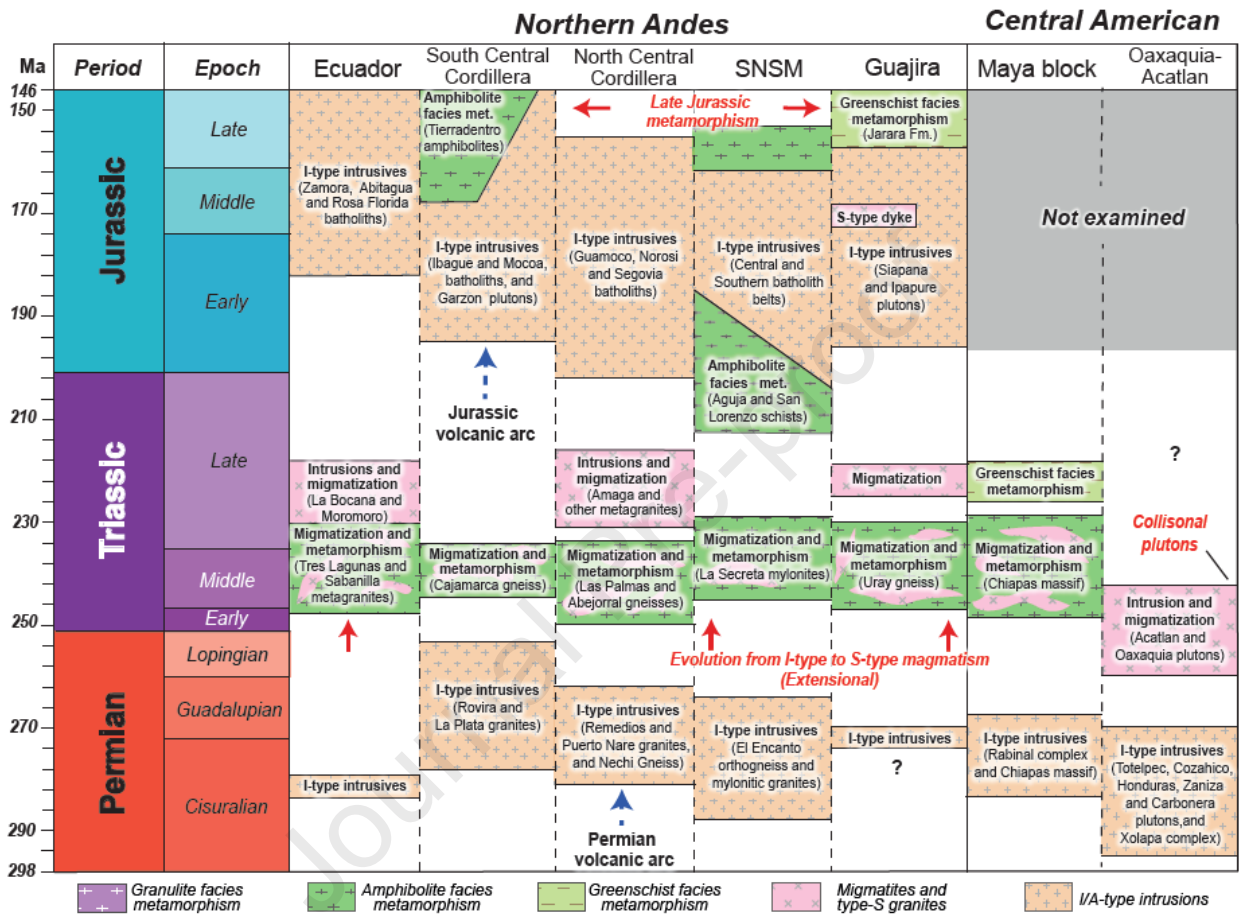
659

660 **Triassic metamorphism**

661 In the Guajira Arch, previous works documented Early Triassic mylonites at the Uray
662 Gneiss, with an age ca. 246 ± 3.9 Ma (Weber et al., 2010; Fig. 2). New data at the Jarara Range
663 evidence Triassic metamorphism spanning ca. 230-223 Ma (Fig. 12), with ϵ_{Hf_i} (from -2.4 to 8.7)
664 that hints at the incorporation of juvenile material (Fig. 15) with Model T_{DM} ages of ~0.8 to ~1.3
665 Ga (Fig. 15) may indicate *in-situ* anatexis of the Macuira Schists by incorporation of juvenile
666 material.

667 Middle-Late Triassic ages of 245-223 Ma for the anatectic core emplacement and
668 mylonitization, were rapidly followed by cooling as evidenced by $^{40}\text{Ar}/^{39}\text{Ar}$ and K-Ar ages from
669 the Macuira Schists spanning 220-160 Ma (MacDonald, 1964; Cardona et al., 2006). Triassic
670 metamorphism is widely recognized along the Andes and is characterized by crustal attenuation
671 and anatexis. It has been described in La Secreta mylonites at the Santa Marta Massif (Piraquive,

672 2017), the Central Cordillera (Vinasco et al., 2006a; Cochrane et al., 2014a), and in El Oro
 673 Complex at the Ecuadorian Andes (Riel et al., 2013), sharing a similar age span, lithological
 674 varieties, and Hf isotopic signature (Fig. 17).



675
 676
 677 **Figure 17. Stratigraphic summary sketch of the Guajira Arch, Sierra Nevada de Santa Marta massif, North**
 678 **Central Cordillera, South Central Cordillera, Ecuador (Northern Andes), Oaxaquia-Acatlán, and Maya**
 679 **block (Central American-Mexican) from the Permian to Jurassic. Major tectono-metamorphic events are**
 680 **indicated, references are disclosed in the discussion.**
 681

682 Late Permian magmatism and Early Triassic anatexis are documented at ca. 263-243 Ma
 683 in the Marathon-Sonora section of the Pangaea collision zone in the western Gulf of Mexico
 684 (Coombs et al., 2020), whereas localized exposures of igneous rocks in the Maya Block range
 685 between 249–226 Ma (Spikings and Paul, 2019, and references therein; Fig. 17) Triassic

686 anatexites are also documented at Oaxaquia, southern Chiapas Massif, Acatlán and Xolapa
687 complexes (Fig. 17; Helbig et al., 2012).

688 The Triassic metamorphic record in the Central American-Mexican terranes and North
689 America indicates that orogenic metamorphism was terminated by extension and followed by
690 rifting during Pangaea break-up (Estrada-Carmona et al., 2009). The overlap between Central
691 American- Mexican terranes and South America would correspond to the Acatlán, Xolapa
692 complexes, and southern Chiapas Massif, juxtaposed against the Central Cordillera, Santa Marta
693 Massif, and Guajira Arch, in which Oaxaquia may constitute the oldest crust of the conjugate
694 margin.

695 Late Triassic metamorphism during extension is recorded at the Maya block and Chuacús
696 complex as rim recrystallization ages in detrital rocks (Spikings and Paul, 2019, and references
697 therein). At the Guajira Arch, anatexis at ca. 230 Ma was in part a delayed thermal response from
698 a back-arc extension, causing U-Pb resetting of Proterozoic zircons. In this scenario, back-arc
699 extension and increased geothermal gradients due to ascending sub-lithospheric continental
700 mantle may have given rise to a gneissic dome formation *sensu* Whitney et al. (2004; Fig. 18A).

701 The processes involved in the formation of the Guajira Arch Triassic core complex (Fig.
702 18C) can be thus related to roll-back extension and rifting at the initial stages of western Pangaea
703 break-up between 235 and 216 Ma (Cochrane et al., 2014a; Spikings and Paul, 2019), which is
704 also documented at the Santa Marta Massif, where rift sequences of Carnian age attest for
705 extension during this epoch (Gómez et al., 2021). Furthermore, extensional mechanisms driving
706 anatexis by crustal extension at the Guajira Arch are evidenced by a top-to NW sinistral shear
707 sense observed in the mylonitic units of the Uray Gneiss (Ug1, Ug3; Fig. 6), that also decrease in
708 metamorphic grade towards the NW, in contrast to an anatectic core mostly granoblastic (Ug2,
709 Fig. 6), indicating a ductile to brittle-ductile shear zone.

710 In synthesis, for the interval 245-220 Ma, the formation of a mylonitic lower grade
711 detachment (Ug3) assisted the emplacement of the anatectic core (Ug2) at upper crustal levels.

712 Although the schematic representation of a gneissic dome (Fig. 18A) provides insight
713 into the relationships between the metamorphic complexes described for the Guajira Arch,
714 further detail to establish a more precise structural context is still pending task. However, so far
715 the combined field, petrographic, structural observations, and the new geochronological and
716 isotopic datasets presented in this work may be conceptualized as the architectural elements of a
717 cordilleran metamorphic core complex (Fig. 18A; Whitney et al., 2004, 2013). In this scenario,
718 upper plate extension may have been caused by decreasing convergence and slab steepening
719 during the Late Triassic, in which rejuvenation of the lower crust in a back-arc setting was
720 prompted by the incorporation of juvenile material from the asthenosphere (Costa and Rey,
721 1995; Chapman et al., 2017).

722 Analogous structural configurations involving anatexis, mafic underplating, and
723 isothermal decompression are bracketed within the same timespan 230-220 Ma at the Ecuadorian
724 Andes in El Oro Metamorphic Complex (Riel et al., 2013). Thus, it implies a large-scale thermal
725 anomaly occurring at the western Gondwana margin during the Late Triassic.

726

727 **Jurassic arc build-up**

728 Jurassic magmatism is well documented at the northern Andes and Central-American and
729 Mexican terranes (McHone, 2000; Pérez-Gutiérrez et al., 2009; Stanek et al., 2009; Villagómez
730 and Spikings, 2013; Spikings et al., 2015; Bustamante et al., 2016; Centeno-García, 2017;
731 Rodríguez et al., 2018; Shaw et al., 2019). At the Guajira Arch, Jurassic magmatism is evidenced
732 by the two-stage evolution of a magmatic arc, comprising the Siapana Granodiorite and
733 associated granitoids, and the syn-tectonic volcanoclastic deposits of the Cosinas through, south

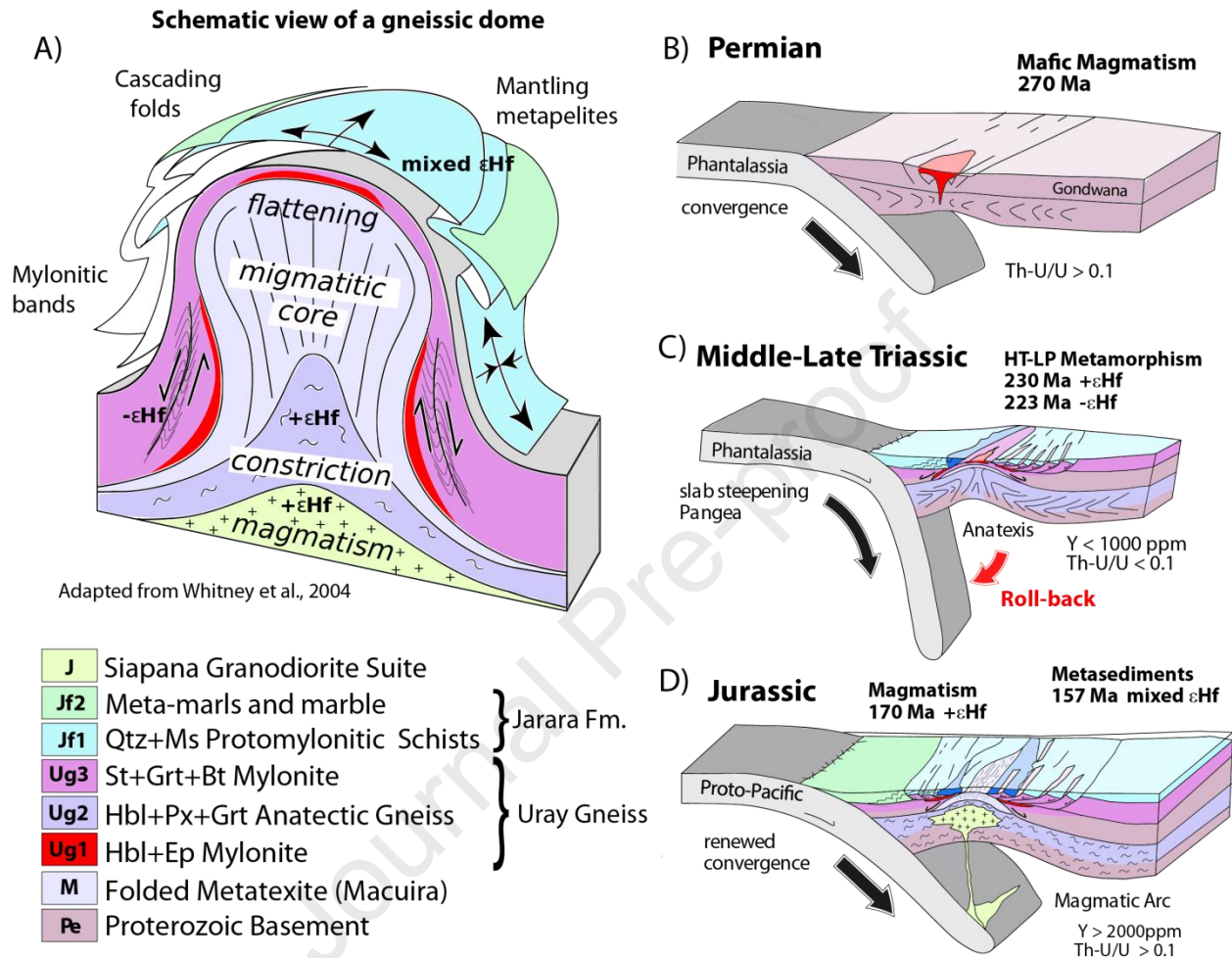
734 of the Cuisa fault (Rollins, 1965; Zuluaga et al., 2015). Protracted emplacement of the Siapana
735 granodiorite at the upper plate at ca. 195 ± 8 Ma, 167 ± 9.4 Ma and 158 ± 0.6 Ma (Cardona et al.,
736 2006; Rodríguez–García et al., 2020) is evidenced by zircon inheritance, negative ϵNd_i -5.90,
737 and a model T_{DM} age of = 1.45 Ma, highly similar to the hosting Macuira schists T_{DM} Sm-Nd
738 model age of 1.47 Ga (Cardona et al., 2006).

739 The emplacement of magmas derived from crustal sources was coeval to volcanic
740 activity. Besides, calc-alkaline signature, light rare earth element enrichment, Nb-Ta depletion,
741 and Eu negative anomaly attests for a subduction-related affinity in a converging tectonic-
742 setting (Zuluaga et al., 2015). Magmatic arc build-up was coeval to the development of a
743 continental back-arc basin built in a low-lying magmatic arc (Fig. 18D), as evidenced by the
744 silicic volcanism of the Ipapure rhyodacite by 184 ± 0.7 Ma (Zuluaga et al., 2015). In this
745 scenario, a newly formed basin at the Cosinas trough was filled by sediments mixed from
746 volcanic sources and the Guajira Arch exposed basement (Nova et al., 2019).

747 Recrystallized sectors of Jurassic age in Permian amphibole mylonitic schists evidence
748 the thermal overprint of magmatism at ca. 180 Ma. At the Jarara range, Jurassic dikes related to
749 the Siapana Granodiorite suite intruded the Uray gneiss anatexic core (Ug2) at ca. 170 ± 2.7 Ma.
750 Trends of near CHUR to positive ϵHf_i values of these dikes (Figs. 15 & 18) indicate mixing of
751 primitive sources and slightly depleted compositions. In the setting of a low-lying magmatic arc
752 (Zuluaga et al., 2015), crustal attenuation would lead to melts originating in the upper mantle and
753 closest to the trench, resulting in an isotopically juvenile material with asthenospheric
754 contributions (Chapman et al., 2017).

755 This may indicate that Triassic crustal attenuation, anatexis, and possibly doming, was
756 followed by slab advance during Early-Middle Jurassic (Fig. 18C-D). Jurassic magmatic activity
757 preceded the expansion of local depocenters, in which the cessation of volcanism is defined by

758 the development of a mixed siliciclastic-carbonate marine platform since the Callovian ca. 166
 759 Ma (Renz, 1960; Rollins, 1965; Quintero, 2017; Nova et al., 2019).



760
 761 **Figure 18. A) Schematic view of a gneissic dome adapted from Whitney et al. (2004). Schematic multi-stage**
 762 **evolution proposed for the emplacement of melts at the Guajira Arch during Pangea assembly and break-up**
 763 **since B) Late Permian C) Middle-Late Triassic D) Jurassic. Late Triassic anatexis may be a response of roll-**
 764 **back extension and crustal attenuation in the upper plate. Significant U-Pb ages, εHf, and variations in**
 765 **HREE and Y contributions are indicated in ppm and discussed in the text and Table 2.**

766
 767 Exhumation of the Guajira Arch since Middle Jurassic times is evidenced by fission track
 768 data collected from the Cosinas group and the mixed provenance signal characterized by
 769 Proterozoic, Permo-Triassic, and Jurassic zircons (García-Gonzales et al., 2010; Quintero, 2017;
 770 Nova et al., 2019).

771 At the fore-arc position northwest of the Guajira Arch, the low-grade basal
772 protomylonitic meta-conglomerates of the Jarara Formation (Jf1) yield an age spectrum
773 characterized by Jurassic, Triassic (Carnian), Paleozoic (including Devonian and Ordovician),
774 and Proterozoic inheritance, with a maximum depositional age 157 ± 17.8 Ma. It is
775 indistinguishable from the Sr-isotope and U-Pb maximum depositional ages recovered from the
776 Cosinas group (at ca. 161-157 Ma, Nova, et al., 2019). Furthermore, Carnian (230-220Ma)
777 zircons in Jurassic meta-conglomerates (Jf1) are clear evidence that the anatectic core and
778 intruding granitic suites of the Guajira Arch had to be already exhumed during its protolith
779 deposition as there are not known volcanic sources of ca. 230 Ma nearby (Solari et al., 2011;
780 Spikings and Paul, 2019; López-Isaza and Zuluaga, 2020).

781 Greenschist facies metamorphism at ca. 157 Ma of the Jarara basal meta-conglomerates
782 may be interpreted as a product of continued extension (Fig. 18D) to judge from top to NW
783 sinistral shear kinematic markers, also observed at the underlying high-amphibolite facies
784 Triassic mylonites (Ug1, Ug3; Fig. 6). Similar Late Jurassic meta-sediments are documented at
785 the Cajamarca complex at the Central Cordillera, consisting of schists and amphibolites (Blanco-
786 Quintero et al., 2014; Rodríguez–García et al., 2020), although their structural relations remain
787 unknown.

788 During the Late Jurassic, a waning magmatic arc along western Gondwana is evidenced
789 by post-rift plutons. At the Guajira Arch, their ages comprise the youngest ages of the Siapana
790 Granodiorite ca. 158 ± 0.6 Ma (Rodríguez–García et al., 2020); evidencing contemporaneous
791 magmatism exhumation and sedimentation in north-western Gondwana, coeval with the drifting
792 between Gondwana to the south and Chortis-Mexico block in North and Central America
793 (Pindell and Kennan, 2009; Cochrane et al., 2014a).

794

795 6. CONCLUSIONS

796 1) The Guajira Arch Proterozoic basement shows a geochronological and isotopic affinity
797 with Proterozoic inliers of the northern Andes and the Proterozoic basement of the southern
798 Chiapas massif and Oaxaquia, sustaining a scenario of a conjugate margin during Rodinia
799 assembly.

800 2) During Permian times, the Proterozoic basement was affected by mafic intrusions ca.
801 270 Ma, correlative in age to meta-granitoids and mafic intrusions documented at the Santa
802 Marta massif, Central Cordillera of Colombia, and the southern Chiapas Massif, evidencing a
803 continuous magmatic arc through western Pangaea.

804 3) Triassic metamorphism at ca. 230 Ma occurred due to anatexis under an extensional
805 regime as evidenced by Hf_i T_{DM} ages that indicate reworking of the Proterozoic lower crust by
806 incorporation of juvenile material sourced from the asthenospheric mantle. Depletion in LILE,
807 HREE, and low Th/U ratios indicates that contributions from water-light and incompatible
808 elements from a subducting lithosphere were negligible during Triassic, fitting to a diminished
809 convergence and slab steepening during the first stages of Pangaea breakup.

810 4) Metamorphism at high amphibolite facies and anatexis that originated the migmatites,
811 and afterward, the amphibolites and mylonites found at the Guajira Arch may correspond to the
812 emplacement of a cordilleran core-complex during roll-back extension of the upper plate.
813 Rejuvenated Triassic crust at the core is flanked by mylonitic detachments defining a dome
814 structure.

815 5) Given the $T_{DM(Hf)}$ ages of the Triassic metamorphic rocks indicating melting of a
816 Proterozoic Gondwanan crust, assembly of allochthonous or para-autochthonous terranes is thus
817 no longer necessary to explain the structural setting of the metamorphic complex of the Guajira
818 Arch that is instead explained as *in-situ* anatexis of the lower crust.

819 6) Renewed convergence between the proto-Pacific plate and NW Gondwana during the
820 Jurassic is evidenced by the emplacement of large volumes of magma enriched in LILE, HREE,
821 U, and Th, along with a juvenile ϵ Hf composition. An attenuated crust in a near trench position
822 reflects compositional variations due to mixing from subducted sediment, remelting of oceanic
823 crust, lower arc crust, slab-derived fluids, and isotopically juvenile asthenospheric mantle during
824 the establishment of a continental low-lying magmatic arc setting after western Pangaea break-
825 up.

826 **Acknowledgments**

827 The authors want to thank the Journal of South American Earth Sciences editors and the
828 reviewers for their constructive comments, which greatly improved this paper. This work was
829 financially supported by COLCIENCIAS in the framework of the project “Evolución Tectónica
830 del Margen Caribeño Colombiano grant number 110166044454,” and also supported by a Bonus
831 Qualité Recherche (BQR) Sud grant from ISTERre, Université Grenoble Alpes, also we express
832 our gratitude to the staff of the U-Pb geochronology and SEM laboratories at the Colombian
833 Geological Survey and the direction de Asuntos Nucleares (DAN) who supported the
834 development of this research; at ETH Zürich Marcel Guillong carefully explained
835 geochronological U-Pb data reduction procedures, we want to acknowledge also Vladimir Zapata
836 in the year 2013, who explored with us the different outcrops of the Guajira peninsula. Finally,
837 last but not least, we want to express our gratitude to the inhabitants of the Porshina rancheria
838 and the Pushaina leader Luz Esther Gonzales, Professor Juana Perez, and Machin Gonzales, and
839 also from the Cachinapa rancheria leader Mrs. Margarita Uriana, finally we dedicate this work to
840 the Wayuú communities ancestral inhabitants of the Guajira peninsula.

841 **8. REFERENCES**

842 Alvares, W., 1967, Geology of the Simarua and Carpintero areas, Guajira Peninsula, Colombia: University of Princeton, 164 p.

- 843 Andersen, T., Kristoffersen, M., and Elburg, M.A., 2018, Visualizing, interpreting and comparing detrital zircon age and Hf
844 isotope data in basin analysis - a graphical approach: *Basin Research*, v. 30, p. 132–147, doi:10.1111/bre.12245.
- 845 Arvizu, H.E., Iriondo, A., Izaguirre, A., Chávez-Cabello, G., Kamenov, G.D., Solís-Pichardo, G., Foster, D.A., and Cruz, R.L.S.,
846 2009, Rocas graníticas pérmicas en la Sierra Pinta, NW de Sonora, México: Magmatismo de subducción asociado al inicio
847 del margen continental activo del SW de Norteamérica: *Revista Mexicana de Ciencias Geológicas*, v. 26, p. 709–728,
848 http://www.scielo.org.mx/scielo.php?script=sci_arttext&pid=S1026-87742009000300013 (accessed May 2020).
- 849 Baquero, M., Grande, S., Urbani, F., Cordani, U., Hall, C., and Armstrong, R., 2015, Chapter 4: New Evidence for Putumayo
850 Crust in the Basement of the Falcon Basin and Guajira Peninsula, Northwestern Venezuela: , p. 103–136,
851 http://archives.datapages.com/data/specpubs/memoir108/data/103_aapg-sp1970103.htm.
- 852 Bartok, P., Mejia-Hernandez, M.C., and Ismael, M., 2015, Paleogeographic Constraints on Middle- to Late-Jurassic Tectonic
853 Reconstruction of the Maya Block of Southern Mexico and Equivalent Strata of Northwestern South America, *in* *Memoir*
854 108: *Petroleum Geology and Potential of the Colombian Caribbean Margin*, AAPG, doi:10.1306/13531937m1082953.
- 855 Bayona, G. et al., 2013, Onset of fault reactivation in the Eastern Cordillera of Colombia and proximal Llanos Basin: response to
856 Caribbean–South American convergence in early Palaeogene time: *Geological Society London Special Publications*, v.
857 377, doi:10.1144/SP377.5.
- 858 Bayona, G., Bustamante, C., Nova, G., and Salazar-Franco, A.M., 2019, Jurassic Evolution of the Northwestern Corner of
859 Gondwana: Present Knowledge and Future Challenges in Studying Colombian Jurassic Rocks, *in* *The Geology of*
860 *Colombia*, v. 2, p. 37, doi:10.32685/pub.esp.36.2019.05.
- 861 Bayona, G., Montes, C., Cardona, A., Jaramillo, C., Ojeda, G., Valencia, V., and Ayala-Calvo, C., 2011, Intraplate subsidence
862 and basin filling adjacent to an oceanic arc–continent collision: a case from the southern Caribbean–South America plate
863 margin: *Basin Research*, v. 23, p. 403–422, doi:10.1111/j.1365-2117.2010.00495.x.
- 864 Bayona, G., Rapalini, A.E., and Costanzo-Alvarez, V., 2006, Paleomagnetism in Mesozoic rocks of the Northern Andes and its
865 Implications in Mesozoic Tectonics of Northwestern South America: *Earth, Planets and Space*, v. 58, p. 1255–1272,
866 doi:10.1186/BF03352621.
- 867 Blanco-Quintero, I.F., García-Casco, A., Toro, L.M., Moreno, M., Ruiz, E.C., Vinasco, C.J., Cardona, A., Lázaro, C., and
868 Morata, D., 2014, Late Jurassic terrane collision in the northwestern margin of Gondwana (Cajamarca Complex, eastern
869 flank of the Central Cordillera, Colombia): *International Geology Review*, v. 56, p. 1852–1872,
870 doi:10.1080/00206814.2014.963710.
- 871 Bouvier, A., Vervoort, J.D., and Patchett, P.J., 2008, The Lu-Hf and Sm-Nd isotopic composition of CHUR: Constraints from
872 unequilibrated chondrites and implications for the bulk composition of terrestrial planets: *Earth and Planetary Science*
873 *Letters*, v. 273, p. 48–57, doi:10.1016/j.epsl.2008.06.010.
- 874 Bustamante, C., Archanjo, C.J., Cardona, A., Bustamante, A., and Valencia, V.A., 2017, U-pb ages and hf isotopes in zircons
875 from parautochthonous mesozoic terranes in the Western margin of Pangea: Implications for the terrane configurations in
876 the northern andes: *Journal of Geology*, v. 125, p. 487–500, doi:10.1086/693014.
- 877 Bustamante, C., Archanjo, C.J., Cardona, A., and Restrepo, M., 2021, Magnetic fabric of the Parashi stock and related dyke
878 swarm, Alta Guajira (Colombia): The Caribbean–South American plates oblique convergence:,
879 doi:10.5027/ANDGEOV48N2-3332.
- 880 Bustamante, C., Archanjo, C.J., Cardona, A., and Vervoort, J.D., 2016, Late Jurassic to Early Cretaceous plutonism in the
881 Colombian Andes: A record of long-term arc maturity: *Geological Society of America Bulletin*, p. B31307.1,
882 doi:10.1130/B31307.1.
- 883 Cardona, A., Chew, D., Valencia, V.A., Bayona, G., Mišković, A., and Ibañez-Mejía, M., 2010a, Grenvillian remnants in the
884 Northern Andes: Rodinian and Phanerozoic paleogeographic perspectives: *Journal of South American Earth Sciences*, v.
885 29, p. 92–104, doi:10.1016/j.jsames.2009.07.011.
- 886 Cardona, A., Cordani, U.G., MacDonald, W.D., Cardona, A., Cordani, U.G., and MacDonald, W.D., 2006, Tectonic correlations
887 of pre-Mesozoic crust from the northern termination of the Colombian Andes, Caribbean region: *Journal of South*
888 *American Earth Sciences*, v. 21, p. 337–354, doi:10.1016/j.jsames.2006.07.009.
- 889 Cardona, A., León, S., Jaramillo, J.S., Montes, C., Valencia, V., Vanegas, J., Bustamante, C., and Echeverri, S., 2018, The
890 Paleogene arcs of the northern Andes of Colombia and Panama: Insights on plate kinematic implications from new and
891 existing geochemical, geochronological and isotopic data: *Tectonophysics*, v. 749, p. 88–103,
892 doi:10.1016/j.tecto.2018.10.032.
- 893 Cardona, A., Valencia, V., Garzón, A., Montes, C., Ojeda, G., Ruiz, J., and Weber, M., 2010b, Permian to Triassic I to S-type
894 magmatic switch in the northeast Sierra Nevada de Santa Marta and adjacent regions, Colombian Caribbean: Tectonic
895 setting and implications within Pangea paleogeography: *Journal of South American Earth Sciences*, v. 29, p. 772–783,
896 doi:10.1016/j.jsames.2009.12.005.
- 897 Cardona, A., Valencia, V.A., Lotero, A., Villafañez, Y., and Bayona, G., 2016, Provenance of middle to late Palaeozoic
898 sediments in the northeastern Colombian Andes: implications for Pangea reconstruction: *International Geology Review*, v.
899 58, p. 1914–1939, doi:10.1080/00206814.2016.1190948.
- 900 Cardona, A., Valencia, V.A., Weber, M., Duque, J., Montes, C., Ojeda, G., Reiners, P., Domanik, K., Nicolescu, S., and
901 Villagomez, D., 2011, Transient Cenozoic tectonic stages in the southern margin of the Caribbean plate: U-Th/He
902 thermochronological constraints from Eocene plutonic rocks in the Santa Marta massif and Serranía de Jarara, northern
903 Colombia: *Geologica Acta*, v. 9, p. 445–469, doi:10.1344/105.000001739.
- 904 Cardona, A., Weber, M., Valencia, V., Bustamante, C., Montes, C., Cordani, U., and Muñoz, C.M., 2014, Geochronology and
905 geochemistry of the Parashi granitoid, NE Colombia: Tectonic implication of short-lived Early Eocene plutonism along the

- 906 SE Caribbean margin: *Journal of South American Earth Sciences*, v. 50, p. 75–92, doi:10.1016/j.jsames.2013.12.006.
- 907 Cediell, F., Shaw, R., A. R.-P.P., Kroonenberg, S., Zuluaga, C.A., Lopez, J.A., and Leal-mejía, H., 2019, *Geology and Tectonics*
- 908 *of Northwestern South America The Pacific-Caribbean-Andean Junction*: 1,1001 p., doi:10.1007/978-3-319-76132-9.
- 909 Centeno-García, E., 2017, Mesozoic tectono-magmatic evolution of Mexico: An overview: *Ore Geology Reviews*, v. 81, p.
- 910 1035–1052, doi:10.1016/j.oregeorev.2016.10.010.
- 911 Chapman, J.B., Ducea, M.N., Kapp, P., Gehrels, G.E., and DeCelles, P.G., 2017, Spatial and temporal radiogenic isotopic trends
- 912 of magmatism in Cordilleran orogens: *Gondwana Research*, v. 48, p. 189–204, doi:10.1016/j.gr.2017.04.019.
- 913 Cochrane, R., Spikings, R., Gerdes, A., Ulianov, A., Mora, A., Villagómez, D., Putlitz, B., and Chiaradia, M., 2014a, Permo-
- 914 Triassic anatexis, continental rifting and the disassembly of western Pangaea: *Lithos*, v. 190–191, p. 383–402,
- 915 doi:10.1016/j.lithos.2013.12.020.
- 916 Cochrane, R., Spikings, R., Gerdes, A., Winkler, W., Ulianov, A., Mora, A., and Chiaradia, M., 2014b, Distinguishing between
- 917 in-situ and accretionary growth of continents along active margins: *Lithos*, v. 202–203, p. 382–394,
- 918 doi:10.1016/j.lithos.2014.05.031.
- 919 Collins, W.J., Belousova, E.A., Kemp, A.I.S., and Murphy, J.B., 2011, Two contrasting Phanerozoic orogenic systems revealed
- 920 by hafnium isotope data: *Nature Geoscience*, v. 4, p. 333–337, doi:10.1038/ngeo1127.
- 921 Collins, W.J., and Richards, S.W., 2008, Geodynamic significance of S-type granites in circum-Pacific orogens: *Geology*, v. 36,
- 922 p. 559–562, doi:10.1130/G24658A.1.
- 923 Colmenares, F., Román García, L., Sánchez, J.M., and Ramirez, J.C., 2019, Diagnostic structural features of NW South America:
- 924 Structural cross sections based upon detailed field transects: *Frontiers in Earth Sciences*, p. 651–672, doi:10.1007/978-3-
- 925 319-76132-9_9.
- 926 Coombs, H.E., Kerr, A.C., Pindell, J., Buchs, D., Weber, B., and Solari, L., 2020, Petrogenesis of the crystalline basement along
- 927 the western Gulf of Mexico: Postcollisional magmatism during the formation of Pangea, *in* Southern and Central Mexico:
- 928 Basement Framework, Tectonic Evolution, and Provenance of Mesozoic–Cenozoic Basins, Geological Society of
- 929 America, doi:10.1130/2020.2546(02).
- 930 Cordani, U.G., Cardona, A., Jimenez, D.M., Liu, D., and Nutman, A.P., 2005, Geochronology of Proterozoic basement inliers in
- 931 the Colombian Andes: Tectonic history of remnants of a fragmented Grenville belt: *Geological Society Special*
- 932 *Publication*, v. 246, p. 329–346, doi:10.1144/GSL.SP.2005.246.01.13.
- 933 Costa, S., and Rey, P., 1995, Lower crustal rejuvenation and growth during post-thickening collapse: insights from a crustal cross
- 934 section through a Variscan metamorphic core complex: *Geology*, v. 23, p. 905–908, doi:10.1130/0091-
- 935 7613(1995)023<0905:LCRAGD>2.3.CO;2.
- 936 Decelles, P.G., Ducea, M.N., Kapp, P., and Zandt, G., 2009, Cyclicity in Cordilleran orogenic systems: *Nature Geoscience*, v. 2,
- 937 p. 251–257, doi:10.1038/ngeo469.
- 938 Estrada-Carmona, J., Weber, B., Hecht, L., and Martens, U., 2009, P-T-t trajectory of metamorphic rocks from the central
- 939 Chiapas Massif Complex: The Custepec Unit, Chiapas, Mexico: *Revista Mexicana de Ciencias Geológicas*, v. 26, p. 243–
- 940 259.
- 941 García-Casco, A., Iturralue-Vinent, M.A., and Pindell, J., 2008, Latest Cretaceous collision/accretion between the Caribbean
- 942 plate and Caribeana: Origin of metamorphic terranes in the greater antilles: *International Geology Review*, v. 50, p. 781–
- 943 809, doi:10.2747/0020-6814.50.9.781.
- 944 García-Gonzales, M., Mier-Umaña, R., and Cruz-Guevara, L.E., 2010, PALEOTHERMAL HISTORY RECONSTRUCTION OF
- 945 THE BAJA GUAJIRA SUB-BASIN, COLOMBIA: *Boletín de Geología*, v. 32, p. 55–71,
- 946 <https://revistas.uis.edu.co/index.php/revistaboletindegologia/article/view/2065/2486> (accessed March 2020).
- 947 Gómez, I., and Burke, K., 2001, Structural style and evolution of the Cuisa fault system, Guajira, Colombia: *Geosciences*, p. 147,
- 948 <http://search.epnet.com/login.aspx?direct=true&db=geh&an=2004-057439>.
- 949 Gómez, C., Kammer, A., Bernet, M., Piraquive, A., and von Quadt, A., 2021, Late Triassic rift tectonics at the northernmost
- 950 Andean margin (Sierra Nevada de Santa Marta): *Journal of South American Earth Sciences*, v. 105,
- 951 doi:10.1016/j.jsames.2020.102953.
- 952 Griffin, W.L., Wang, X., Jackson, S.E., Pearson, N.J., O'Reilly, S.Y., Xu, X., and Zhou, X., 2002, Zircon chemistry and magma
- 953 mixing, SE China: In-situ analysis of Hf isotopes, Tonglu and Pingtan igneous complexes: *Lithos*, v. 61, p. 237–269,
- 954 doi:10.1016/S0024-4937(02)00082-8.
- 955 Grimes, C.B., Wooden, J.L., Cheadle, M.J., and John, B.E., 2015, “Fingerprinting” tectono-magmatic provenance using trace
- 956 elements in igneous zircon: *Contributions to Mineralogy and Petrology*, v. 170, p. 1–26, doi:10.1007/s00410-015-1199-3.
- 957 Helbig, M., Keppie, J.D., Murphy, J.B., and Solari, L.A., 2012, U-Pb geochronological constraints on the Triassic-Jurassic Ayú
- 958 Complex, southern Mexico: Derivation from the western margin of Pangea-A: *Gondwana Research*, v. 22, p. 910–927,
- 959 doi:10.1016/j.gr.2012.03.004.
- 960 Ibañez-Mejía, M., 2020, The Putumayo Orogen of Amazonia: A Synthesis, *in* The Geology of Colombia, Volume 1 Proterozoic –
- 961 Paleozoic, Bogotá, v. 1, p. 101–131, doi:10.32685/pub.esp.35.2019.06.
- 962 Ibañez-Mejía, M., 2020, The Putumayo Orogen of Amazonia: A Synthesis (in press): *Publicaciones Geológicas Especiales*, v. 1,
- 963 p. 101–131, doi:10.32685/pub.esp.35.2019.06.
- 964 Ibañez-Mejía, M., Ruiz, J., Valencia, V.A., Cardona, A., Gehrels, G.E., and Mora, A.R., 2011, The Putumayo Orogen of
- 965 Amazonia and its implications for Rodinia reconstructions: New U-Pb geochronological insights into the Proterozoic
- 966 tectonic evolution of northwestern South America: *Precambrian Research*, v. 191, p. 58–77,
- 967 doi:10.1016/j.precamres.2011.09.005.
- 968 Irving, E.M., 1972, Mapa Geológico de la península e la Guajira (Compilacion). Escala 1:100.000.:

- 969 Irving, E., 1975, Structural Evolution of the Northernmost Andes , Colombia Structural Evolution of the Northernmost Andes ,
970 Colombia: Geological Survey Professional, v. 846.
- 971 Kellogg, J.N., 1984, Cenozoic tectonic history of the Sierra de Perijá, Venezuela-Colombia, and adjacent basins: Memoir of the
972 Geological Society of America, v. 162, p. 239–261, doi:10.1130/MEM162-p239.
- 973 Kroonenberg, S.B., 1982, A Grenvillian granulite belt in the Colombian Andes and its relation to the Guiana Shield.: *Geologie en*
974 *Mijnbouw*, v. 61, p. 325–333, [https://research.wur.nl/en/publications/a-grenvillian-granulite-belt-in-the-colombian-andes-](https://research.wur.nl/en/publications/a-grenvillian-granulite-belt-in-the-colombian-andes-and-its-relat)
975 [and-its-relat](https://research.wur.nl/en/publications/a-grenvillian-granulite-belt-in-the-colombian-andes-and-its-relat) (accessed March 2020).
- 976 Van Der Lelij, R., 2013, Reconstructing north-western Gondwana with implications for the evolution of the Iapetus and Rheic
977 Oceans: a geochronological, thermochronological and geochemical study: University of Geneva, [https://archive-](https://archive-ouverte.unige.ch/unige:31653)
978 [ouverte.unige.ch/unige:31653](https://archive-ouverte.unige.ch/unige:31653).
- 979 van der Lelij, R., Spikings, R., and Mora, A., 2016a, Thermochronology and tectonics of the Mérida Andes and the Santander
980 Massif, NW South America: *Lithos*, v. 248–251, p. 220–239, doi:10.1016/j.lithos.2016.01.006.
- 981 van der Lelij, R., Spikings, R., Ulianov, A., Chiaradia, M., and Mora, A., 2016b, Palaeozoic to Early Jurassic history of the
982 northwestern corner of Gondwana, and implications for the evolution of the Iapetus, Rheic and Pacific Oceans: *Gondwana*
983 *Research*, v. 31, p. 271–294, doi:10.1016/j.gr.2015.01.011.
- 984 Lockwood, J.P., 1971, Detrital serpentinite from the Guajira peninsula, Colombia: Memoir of the Geological Society of America,
985 v. 130, p. 55–75, doi:10.1130/MEM130-p55.
- 986 Lockwood, J.P., 1965, Geology of the Serranía de Jarara area Guajira peninsula, Colombia: University of Princeton, 250 p.,
987 [https://books.google.com.co/books/about/Geology_Of_the_Serrania_de_Jarara_Area_G.html?id=JhgeNAAACAAJ&redir](https://books.google.com.co/books/about/Geology_Of_the_Serrania_de_Jarara_Area_G.html?id=JhgeNAAACAAJ&redir_esc=y)
988 [_esc=y](https://books.google.com.co/books/about/Geology_Of_the_Serrania_de_Jarara_Area_G.html?id=JhgeNAAACAAJ&redir_esc=y).
- 989 Londono, J., Schiek, C., and Biegert, E., 2015, Basement architecture of the Southern Caribbean Basin, Guajira Offshore,
990 Colombia, *in* AAPG Memoir, American Association of Petroleum Geologists, v. 108, p. 85–102,
991 doi:10.1306/13531932M1083639.
- 992 López-Isaza, J.A., and Zuluaga, C.A., 2020, Late Triassic to Jurassic Magmatism in Colombia: Implications for the Evolution of
993 the Northern Margin of South America., doi:10.32685/pub.esp.36.2019.03.
- 994 López, I.J.A., and Zuluaga, C.C.A., 2012, Macuira gneiss: Tectonic evolution of the paleozoic metamorphic rocks, alta guajira -
995 colombia: *Boletín de Geología*, v. 34, p. 15–36.
- 996 Lopez, I., Zuluaga, C., Lopez, J., and Zuluaga, C., 2014, Neis de Macuira: evolución tectónica de las rocas metamórficas
997 paleozoicas de la Alta Guajira, Colombia: *BOLETÍN DE GEOLOGÍA*, v. 34,
998 <http://revistas.uis.edu.co/index.php/revistaboletindegologia/article/view/3095>.
- 999 MacDonal, W., 1964, Geology of the Serranía de Macuira area Guajira peninsula, colombia.:
- 1000 Macdonald, W.D., and Hurley, P.M., 1969, Precambrian Gneisses from Northern Colombia, South America: Geological Society
1001 of America Bulletin, v. 80, p. 1867, doi:10.1130/0016-7606(1969)80[1867:PGFNCS]2.0.CO;2.
- 1002 MacDonal, W.D., and Opdyke, N.D., 1972, Tectonic rotations suggested by paleomagnetic results from northern Colombia,
1003 South America: *Journal of Geophysical Research*, v. 77, p. 5720–5730, doi:10.1029/JB077i029p05720.
- 1004 Macellari, C.E., 1995, Cenozoic Sedimentation and Tectonics of the Southwestern Caribbean Pull-Apart Basin, Venezuela and
1005 Colombia: , p. 757–780, <http://archives.datapages.com/data/specpubs/memoir62/41macell/0757.htm>.
- 1006 Martens, U., Restrepo, J.J., Ordóñez-Carmona, O., and Correa-Martínez, A.M., 2014, The Tahamí and Anacona Terranes of the
1007 Colombian Andes: Missing Links between the South American and Mexican Gondwana Margins: *The Journal of Geology*,
1008 v. 122, p. 507–530, doi:10.1086/677177.
- 1009 McDonough, W.F., and Sun, S. -s., 1995, The composition of the Earth: *Chemical Geology*, v. 120, p. 223–253,
1010 doi:10.1016/0009-2541(94)00140-4.
- 1011 McHone, J.G., 2000, Non-plume magmatism and rifting during the opening of the central Atlantic Ocean: *Tectonophysics*, v.
1012 316, p. 287–296, doi:10.1016/S0040-1951(99)00260-7.
- 1013 Medina Avellaneda, P.A., 2009, PETROLOGIA DEL CONJUNTO METAMORFICO DE ETPANA Y SU CORRELACION
1014 CON OTRAS UNIDADES METAMORFICAS CRETACICAS DE LA ALTA GUAJIRA COLOMBIANA: Universidad
1015 Nacional de Colombia, 129 p.
- 1016 Meert, J.G., and Lieberman, B.S., 2008, The Neoproterozoic assembly of Gondwana and its relationship to the Ediacaran-
1017 Cambrian radiation: *Gondwana Research*, v. 14, p. 5–21, doi:10.1016/j.gr.2007.06.007.
- 1018 Montes, C., Guzman, G., Bayona, G., Cardona, A., Valencia, V., and Jaramillo, C., 2010, Clockwise rotation of the Santa Marta
1019 massif and simultaneous Paleogene to Neogene deformation of the Plato-San Jorge and Cesar-Ranchería basins: *Journal of*
1020 *South American Earth Sciences*, v. 29, p. 832–848, doi:10.1016/j.jsames.2009.07.010.
- 1021 Montes, C., Rodríguez-Corcho, A.F., Bayona, G., Hoyos, N., Zapata, S., and Cardona, A., 2019, Continental margin response to
1022 multiple arc-continent collisions: The northern Andes-Caribbean margin: *Earth-Science Reviews*, v. 198, p. 102903,
1023 doi:10.1016/j.earscirev.2019.102903.
- 1024 Murphy, J.B., Keppie, J.D., Nance, R.D., and Dostal, J., 2010, Comparative evolution of the Iapetus and Rheic Oceans: A North
1025 America perspective: *Gondwana Research*, v. 17, p. 482–499, doi:10.1016/j.gr.2009.08.009.
- 1026 Murphy, J.B., Pisarevsky, S.A., Nance, R.D., and Keppie, J.D., 2004, Neoproterozoic? Early Paleozoic evolution of peri-
1027 Gondwanan terranes: implications for Laurentia-Gondwana connections: *International Journal of Earth Sciences*, v. 93, p.
1028 659–682, doi:10.1007/s00531-004-0412-9.
- 1029 Nance, R.D., Gutiérrez-Alonso, G., Keppie, J.D., Linnemann, U., Murphy, J.B., Quesada, C., Strachan, R.A., and Woodcock,
1030 N.H., 2012, A brief history of the Rheic Ocean: *Geoscience Frontiers*, v. 3, p. 125–135, doi:10.1016/j.gsf.2011.11.008.
- 1031 Nova, G. et al., 2019, Jurassic break-up of the Peri-Gondwanan margin in northern Colombia: Basin formation and implications

- 1032 for terrane transfer: *Journal of South American Earth Sciences*, v. 89, p. 92–117, doi:10.1016/j.jsames.2018.11.014.
- 1033 Ordóñez, O., 1999, ROCAS GRENVILLIANAS EN LA REGIÓN DE PUERTO BERRIO - ANTIOQUIA;
1034 [https://www.researchgate.net/publication/260871363_ROCAS_GRENVILLIANAS_EN_LA_REGION_DE_PUERTO_B](https://www.researchgate.net/publication/260871363_ROCAS_GRENVILLIANAS_EN_LA_REGION_DE_PUERTO_BERRIO_-_ANTIOQUIA)
1035 [ERRIO_-_ANTIOQUIA](https://www.researchgate.net/publication/260871363_ROCAS_GRENVILLIANAS_EN_LA_REGION_DE_PUERTO_BERRIO_-_ANTIOQUIA).
- 1036 Ortega-Gutiérrez, F., Elías-Herrera, M., Morán-Zenteno, D.J., Solari, L., Weber, B., and Luna-González, L., 2018, The pre-
1037 Mesozoic metamorphic basement of Mexico, 1.5 billion years of crustal evolution: *Earth-Science Reviews*, v. 183, p. 2–
1038 37, doi:10.1016/j.earscirev.2018.03.006.
- 1039 Ortega-Obregón, C., Solari, L., Gómez-Tuena, A., Elías-Herrera, M., Ortega-Gutiérrez, F., and Macías-Romo, C., 2014,
1040 Permian–Carboniferous arc magmatism in southern Mexico: U–Pb dating, trace element and Hf isotopic evidence on
1041 zircons of earliest subduction beneath the western margin of Gondwana: *International Journal of Earth Sciences*, v. 103, p.
1042 1287–1300, doi:10.1007/s00531-013-0933-1.
- 1043 Paul, A.N., Spikings, R.A., Ulianov, A., and Ovtcharova, M., 2018, High temperature (>350 °C) thermal histories of the long
1044 lived (>500 Ma) active margin of Ecuador and Colombia: Apatite, titanite and rutile U–Pb thermochronology: *Geochimica*
1045 *et Cosmochimica Acta*, v. 228, p. 275–300, doi:10.1016/j.gca.2018.02.033.
- 1046 Pérez-Gutiérrez, R., Solari, L.A., Gómez-Tuena, A., and Martens, U., 2009, Mesozoic geologic evolution of the Xolapa
1047 migmatitic complex north of Acapulco, southern Mexico: implications for paleogeographic reconstructions: *Revista*
1048 *Mexicana de Ciencias Geológicas*, v. 26, p. 201–221.
- 1049 Pindell, J.L., 1985, Alleghenian reconstruction and subsequent evolution of the Gulf of Mexico, Bahamas, and Proto-Caribbean:
1050 *Tectonics*, v. 4, p. 1–39, doi:10.1029/TC004i001p00001.
- 1051 Pindell, J.L., and Kennan, L., 2009, Tectonic evolution of the Gulf of Mexico, Caribbean and northern South America in the
1052 mantle reference frame: An update: *Geological Society Special Publication*, v. 328, p. 1–55, doi:10.1144/SP328.1.
- 1053 Piraquive, A., 2017, Cadre structurel, déformations et exhumation des Schistes du Santa Marta : accumulation , et histoire de
1054 déformation d’ un terrain Caraïbe au nord de la Sierra Nevada de Santa Marta Marco estructural deformaciones y
1055 exhumación de los Esquistos de Santa: 234 p.
- 1056 Piraquive, A., Pinzón, E., Kammer, A., Bernet, M., and von Quadt, A., 2018, Early Neogene unroofing of the Sierra Nevada de
1057 Santa Marta, as determined from detrital geothermochronology and the petrology of clastic basin sediments: *Bulletin of*
1058 *the Geological Society of America*, v. 130, p. 355–380, doi:10.1130/B31676.1.
- 1059 Quandt, D. et al., 2018, The geochemistry and geochronology of Early Jurassic igneous rocks from the Sierra Nevada de Santa
1060 Marta, NW Colombia, and tectono-magmatic implications: *Journal of South American Earth Sciences*, v. 86, p. 216–230,
1061 doi:10.1016/j.jsames.2018.06.019.
- 1062 Quintero, C.A., 2017, TECTÓNICA TRANSPRESIVA EN EL MARGEN SEPTENTRIONAL DE LA SERRANÍA DE
1063 COSINAS EN LA ALTA GUAJIRA (COLOMBIA): Universidad Nacional de Colombia, sede Bogotá, 124 p.,
1064 <https://repositorio.unal.edu.co/handle/unal/61032>.
- 1065 Radelli, L., 1962a, Acerca de la geología de la Serranía de Perijá entre Codazzi y Villanueva (Magdalena-Guajira, Colombia):
1066 *Geología Colombiana*, v. 1, p. 23–42, <http://www.revistas.unal.edu.co/index.php/geocol/article/view/30322>.
- 1067 Radelli, L., 1962b, Las dos granitizaciones de la Península de la Guajira (Norte de Colombia): *Geología Colombiana*, v. 1, p. 5–
1068 20, <https://revistas.unal.edu.co/index.php/geocol/article/view/30321> (accessed March 2020).
- 1069 Ratschbacher, L. et al., 2009, The North American-Caribbean Plate boundary in Mexico-Guatemala-Honduras: *Geological*
1070 *Society Special Publication*, v. 328, p. 219–293, doi:10.1144/SP328.11.
- 1071 Renz, O., 1960, Geología de la parte sureste de la península de la Guajira (Republica de Colombia): *Boletín Geológico de*
1072 *Venezuela*, v. 1, p. 317–349.
- 1073 Riel, N. et al., 2013, Metamorphic and geochronological study of the Triassic El Oro metamorphic complex, Ecuador: Implications
1074 for high-temperature metamorphism in a forearc zone: *Lithos*, v. 156–159, p. 41–68, doi:10.1016/j.lithos.2012.10.005.
- 1075 Riel, N., Jaillard, E., Martelat, J.E., Guillot, S., and Braun, J., 2018, Permian-Triassic Tethyan realm reorganization: Implications
1076 for the outward Pangea margin: *Journal of South American Earth Sciences*, v. 81, p. 78–86,
1077 doi:10.1016/j.jsames.2017.11.007.
- 1078 Rodríguez, G., Arango, M.I., Zapata, G., and Bermúdez, J.G., 2018, Petrotectonic characteristics, geochemistry, and U–Pb
1079 geochronology of Jurassic plutons in the Upper Magdalena Valley-Colombia: Implications on the evolution of magmatic
1080 arcs in the NW Andes: *Journal of South American Earth Sciences*, v. 81, p. 10–30, doi:10.1016/j.jsames.2017.10.012.
- 1081 Rodríguez, G., Correa-Martínez, A.M., Zapata-García, G., Arango-Mejía, M.I., Obando-Erazo, Gloria, Zapata-Villada, J.P., and
1082 Bermudez, J.G., 2020, Diverse Jurassic magmatic arcs of the Colombian Andes: Constraints from petrography,
1083 geochronology, and geochemistry, *in* *The Geology of Colombia*, v. 2 Mesozoic, p. 54, doi:10.32685/pub.esp.36.2019.04.
- 1084 Rollins, J.F., 1965, Stratigraphy and structure of the Goajira Peninsula, northwestern Venezuela and northeastern Colombia:
1085 *University of Nebraska studies*, 1–103 p.
- 1086 Ruiz, J., Tosdal, R.M., Restrepo, P.A., and Murillo-Muñetón, G., 1999, Pb isotope evidence for Colombia-southern México
1087 connections in the Proterozoic: *Special Paper of the Geological Society of America*, v. 336, p. 183–197, doi:10.1130/0-
1088 8137-2336-1.183.
- 1089 Sacks, P.E., and Secor, D.T., 1990, Kinematics of Late Paleozoic Continental Collision Between Laurentia and Gondwana:
1090 *Science*, v. 250, p. 1702–1705, doi:10.1126/science.250.4988.1702.
- 1091 Shaw, R.P., Leal-Mejía, H., and Melgarejo i Draper, J.C., 2019, Phanerozoic metallogeny in the Colombian Andes: A tectono-
1092 magmatic analysis in space and time: 411–549 p., doi:10.1007/978-3-319-76132-9_6.
- 1093 Solari, L.A., Gómez-Tuena, A., Ortega-Gutiérrez, F., and Ortega-Obregón, C., 2011, The chuacús metamorphic complex, central
1094 Guatemala: Geochronological and geochemical constraints on its paleozoic-mesozoic evolution: *Geologica Acta*, v. 9, p.

- 1095 329–350, doi:10.1344/105.000001695.
- 1096 Solari, L.A., González-León, C.M., Ortega-Obregón, C., Valencia-Moreno, M., and Rascón-Heimpel, M.A., 2018, The
- 1097 Proterozoic of NW Mexico revisited: U–Pb geochronology and Hf isotopes of Sonoran rocks and their tectonic
- 1098 implications: *International Journal of Earth Sciences*, v. 107, p. 845–861, doi:10.1007/s00531-017-1517-2.
- 1099 Spikings, R., Cochrane, R., Villagomez, D., Van der Lelij, R., Vallejo, C., Winkler, W., and Beate, B., 2015, The geological
- 1100 history of northwestern South America: from Pangaea to the early collision of the Caribbean Large Igneous Province
- 1101 (290–75 Ma): *Gondwana Research*, v. 27, p. 95–139, doi:10.1016/j.gr.2014.06.004.
- 1102 Spikings, R., and Paul, A.N., 2019, The Permian – Triassic History of Magmatic Rocks of the Northern Andes (Colombia and
- 1103 Ecuador): Supercontinent Assembly and Disassembly, *in* *The Geology of Colombia, Volume 2 Mesozoic.*, v. 2 Mesozoic,
- 1104 p. 42, doi:10.32685/pub.esp.36.2019.01.
- 1105 Stanek, K.P., Maresch, W. V., and Pindell, J.L., 2009, The geotectonic story of the northwestern branch of the Caribbean Arc:
- 1106 Implications from structural and geochronological data of Cuba: *Geological Society Special Publication*, v. 328, p. 361–
- 1107 398, doi:10.1144/SP328.15.
- 1108 Tazzo-Rangel, M.D., Weber, B., González-Guzmán, R., Valencia, V.A., Frei, D., Schaaf, P., and Solari, L.A., 2019, Multiple
- 1109 metamorphic events in the Palaeozoic Mérida Andes basement, Venezuela: insights from U–Pb geochronology and Hf–Nd
- 1110 isotope systematics: *International Geology Review*, v. 61, p. 1557–1593, doi:10.1080/00206814.2018.1522520.
- 1111 Vence, E.M., 2008, Subsurface structure, stratigraphy, and regional tectonic controls of the Guajira margin of northern Colombia:
- 1112 University of Texas at Austin.
- 1113 Villagómez, D., and Spikings, R., 2013, Thermochronology and tectonics of the Central and Western Cordilleras of Colombia:
- 1114 Early Cretaceous-Tertiary evolution of the Northern Andes: *Lithos*, v. 160–161, p. 228–249,
- 1115 doi:10.1016/j.lithos.2012.12.008.
- 1116 Villagómez, D., Spikings, R., Magna, T., Kammer, A., Winkler, W., and Beltrán, A., 2011, Geochronology, geochemistry and
- 1117 tectonic evolution of the Western and Central cordilleras of Colombia: *Lithos*, v. 125, p. 875–896,
- 1118 doi:10.1016/j.lithos.2011.05.003.
- 1119 Vinasco, C.J.J., Cordani, U.G.G., González, H., Weber, M., and Pelaez, C., 2006a, Geochronological, isotopic, and geochemical
- 1120 data from Permo-Triassic granitic gneisses and granitoids of the Colombian Central Andes: *Journal of South American*
- 1121 *Earth Sciences*, v. 21, p. 355–371, doi:10.1016/j.jsames.2006.07.007.
- 1122 Vinasco, C.J., Cordani, U.G., González, H., Weber, M., and Pelaez, C., 2006b, Geochronological, isotopic, and geochemical data
- 1123 from Permo-Triassic granitic gneisses and granitoids of the Colombian Central Andes: *Journal of South American Earth*
- 1124 *Sciences*, v. 21, p. 355–371, doi:10.1016/j.jsames.2006.07.007.
- 1125 Weber, M.B.I., Cardona, A., Paniagua, F., Cordani, U., Sepúlveda, L., and Wilson, R., 2009, The Cabo de la Vela Mafic-
- 1126 Ultramafic Complex, Northeastern Colombian Caribbean region: A record of multistage evolution of a Late Cretaceous
- 1127 intra-oceanic arc: *Geological Society Special Publication*, v. 328, p. 549–568, doi:10.1144/SP328.22.
- 1128 Weber, M., Cardona, A., Valencia, V., Altenberger, U., López-Martínez, M., Tobón, M., Zapata, S., Zapata, G., and Concha,
- 1129 A.E., 2011, Geochemistry and geochronology of the guajira eclogites, northern Colombia: Evidence of a metamorphosed
- 1130 primitive cretaceous caribbean Island-arc: *Geologica Acta*, v. 9, p. 425–443, doi:10.1344/105.000001740.
- 1131 Weber, M., Cardona, A., Valencia, V., García-Casco, A., Tobón, M., and Zapata, S., 2010, U/Pb detrital zircon provenance from
- 1132 late cretaceous metamorphic units of the Guajira Peninsula, Colombia: Tectonic implications on the collision between the
- 1133 Caribbean arc and the South American margin: *Journal of South American Earth Sciences*, v. 29, p. 805–816,
- 1134 doi:10.1016/j.jsames.2009.10.004.
- 1135 Weber, B., González-Guzmán, R., Manjarrez-Juárez, R., Cisneros de León, A., Martens, U., Solari, L., Hecht, L., and Valencia,
- 1136 V., 2018, Late Mesoproterozoic to Early Paleozoic history of metamorphic basement from the southeastern Chiapas
- 1137 Massif Complex, Mexico, and implications for the evolution of NW Gondwana: *Lithos*, v. 300–301, p. 177–199,
- 1138 doi:10.1016/j.lithos.2017.12.009.
- 1139 Weber, B., Iriando, A., Premo, W.R., Hecht, L., and Schaaf, P., 2007, New insights into the history and origin of the southern
- 1140 Maya block, SE México: U–Pb–SHRIMP zircon geochronology from metamorphic rocks of the Chiapas massif:
- 1141 *International Journal of Earth Sciences*, v. 96, p. 253–269, doi:10.1007/s00531-006-0093-7.
- 1142 Weber, B., and Schulze, C.H., 2014, Early Mesoproterozoic (>1.4 Ga) ages from granulite basement inliers of SE Mexico and
- 1143 their implications on the Oaxaquia concept - Evidence from U-Pb and Lu-Hf isotopes on zircon: *Revista Mexicana de*
- 1144 *Ciencias Geológicas*, v. 31, p. 377–394, www.rmccg.unam.mx (accessed May 2020).
- 1145 Whitney, D.L., Teyssier, C., Rey, P., and Buck, W.R., 2013, Continental and oceanic core complexes: *Geological Society of*
- 1146 *America Bulletin*, v. 125, p. 273–298, doi:10.1130/B30754.1.
- 1147 Whitney, D.L., Teyssier, C., and Vanderhaeghe, O., 2004, Gneiss domes and crustal flow: *Special Paper of the Geological*
- 1148 *Society of America*, v. 380, p. 15–33, doi:10.1130/0-8137-2380-9.15.
- 1149 Zapata, S., Cardona, A., Montes, C., Valencia, V., Vervoort, J., and Reiners, P., 2014, Provenance of the Eocene Soeibi Blanco
- 1150 formation, Bonaire, Leeward Antilles: Correlations with post-Eocene tectonic evolution of northern South America:
- 1151 *Journal of South American Earth Sciences*, v. 52, p. 179–193, doi:10.1016/j.jsames.2014.02.009.
- 1152 Zapata, S., Weber, M., Cardona, A., Valencia, V., Guzmán, G., and Tobón, M., 2010, Provenance of Oligocene conglomerates
- 1153 and associated sandstones from the Siamaná Formation, Serranía de Jarara, Guajira, Colombia: Implication on Oligocene
- 1154 Caribbean-South America tectonics: *Boletín Ciencias la Tierra*, v. 27, p. 7–24,
- 1155 [https://www.scopus.com/record/display.uri?eid=2-s2.0-](https://www.scopus.com/record/display.uri?eid=2-s2.0-80054002689&origin=inward&txGid=D0A2AE110429A9E33A40D769CC98E63B.wsnAw8kcdt7IPYLO0V48gA%3A1)
- 1156 [80054002689&origin=inward&txGid=D0A2AE110429A9E33A40D769CC98E63B.wsnAw8kcdt7IPYLO0V48gA%3A1.](https://www.scopus.com/record/display.uri?eid=2-s2.0-80054002689&origin=inward&txGid=D0A2AE110429A9E33A40D769CC98E63B.wsnAw8kcdt7IPYLO0V48gA%3A1)
- 1157 Zuluaga, C., 2015, Jurassic Silicic Volcanism and Associated Continental-arc Basin in Northwestern Colombia (Southern

- 1158 Boundary of the Caribbean Plate): , p. 137–160, doi:10.1306/13531934M1083640.
1159 Zuluaga, C. et al., 2009, Memoria de las planchas 2, 3, 5 y 6 (con parte de las planchas 4, 10 y 10Bis). Proyecto de investigación
1160 “Cartografía e historia geológica de la Alta Guajira, implicaciones en la búsqueda de recursos minerales”, Acuerdo
1161 Específico No. 030 de 2006: [s.n.].
1162 Zuluaga, C.A., Amaya, S., Urueña, C., and Bernet, M., 2017, Migmatization and low-pressure overprinting metamorphism as
1163 record of two pre-Cretaceous tectonic episodes in the Santander Massif of the Andean basement in northern Colombia
1164 (NW South America): *Lithos*, v. 274–275, p. 123–146, doi:10.1016/j.lithos.2016.12.036.
1165 Zuluaga, C.A., and Lopez, J.A., 2019, Ordovician orogeny and Jurassic low-lying Orogen in the Santander Massif, Northern
1166 Andes (Colombia), *in* *Frontiers in Earth Sciences*, Springer Verlag, p. 195–250, doi:10.1007/978-3-319-76132-9_4.
1167 Zuluaga, C.A., Pinilla, A., and Mann, P., 2015, Jurassic Silicic Volcanism and Associated Continental-arc Basin in Northwestern
1168 Colombia (Southern Boundary of the Caribbean Plate): *Memoir 108: Petroleum Geology and Potential of the Colombian*
1169 *Caribbean Margin*, p. 137–160, doi:10.1306/13531934M1083640.
1170
1171

Journal Pre-proof

Appendix 1. Methods

U-Pb Geochronology dating by Laser ablation inductively coupled plasma mass spectrometry on zircons (LA-ICP-MS)

We obtained U-Pb ages from 11 samples (Table 1), zircon crystals were extracted using standard mineral separation techniques, including rock crushing, sieving (430-60 μm fraction), and mineral concentration by means of magnetic and heavy liquids separation. About 50 to 200 clean, crack- and inclusion-free zircon grains per sample were mounted with epoxy, polished, and coated with graphite.

Cathodoluminescence imagery for samples (B-235, B-245, C-172, G-52a, G-52d, G-54, G-55b, G-95) was acquired using a Gatan MiniCl mounted on a JEOL JSM IT-300-LV scanning electron microscope at the Colombian Geological Survey in Bogotá.

For samples (GC-021, GC-061) Panchromatic cathodoluminescence imagery was performed at the ETHZ, using a Vega ©Tescan MV2300VP SEM in order to create a detailed set of images which served to define laser ablation spots both in grain cores and rims.

We performed zircon U-Pb geochronology and in-situ trace element analyses for 7 of the samples at the ETH Zürich (GC-021, GC-061, G-52a, G-52d, G-54, G-55b, G-95). Zircon U-Pb geochronology was performed by laser ablation inductively coupled plasma mass spectrometry (LA-ICP-MS) using an ASI RESolution S-155 193 nm ArF excimer laser ablation system coupled to a Thermo Scientific Element XR sector-field ICP-MS (Guillong et al., 2014; Von Quadt et al., 2016).

We used a laser output energy of ca. 2 J/cm², repetition rate of 5 Hz and spot diameter of 30 μm . The ablation was performed in the dual-volume, Laurin Technic S-155

ablation cell under a Helium flow of 0.7 L/min. Argon (ca. 1 L/min) was admixed to the aerosol within the funnel of the ablation cell to transport the ablated material to the ICP for ionization. The ICP-MS instrument was optimized for maximum sensitivity on the high mass range and minimum oxide generation ($\text{ThO}^+/\text{Th}^+ < 0.3\%$). A typical analysis consisted of 30 s baseline acquisition followed by 30 seconds of ablation. Trace element and U-Th-Pb isotopes were acquired within a single mass cycle on peak hopping mode, using short dwell times of 5 ms for most trace elements except for ^{49}Ti (20 ms), and longer dwell times for ^{206}Pb (30 ms), ^{207}Pb (30 ms), ^{235}U (20 ms), ^{232}Th (20 ms) and ^{238}U (20 ms) ensuring better counting statistics for dating.

Data were processed offline with the IGOR-based Iolite v.2.5 software (Paton et al., 2011), using the built-in data reduction scheme for trace elements and VizualAge (Petrus and Kamber, 2012) for U-Pb dating. Both data were obtained on the same signal integration intervals, ensuring that reported U-Pb dates and trace element concentrations correspond to the same zircon volume. Data from spots with anomalously elevated Al, P, Ca, Mn or Fe intensities were discarded as these values indicate the presence of mineral (e.g. apatite, feldspar) or melt inclusions. For trace elements, the stoichiometric Si concentration of 15.2 wt.% of zircon was used as an internal standard; quantification and instrumental drift correction were performed by normalization to the NIST SRM610 glass (Jochum et al., 2011) measured twice every 25 zircon analyses. For U-Pb dating, background-subtracted intensities were used to calculate isotope ratios, which were corrected for laser-induced Pb/U fractionation (Paton et al., 2010), instrumental mass discrimination, and drift by conventional standard-sample bracketing, against the primary zircon reference material GJ-1 (Jackson et al., 2004). The accuracy of the corrections was controlled by repeated measurements of secondary reference zircons 91500 (Wiedenbeck et al., 1995), Temora

(Black et al., 2003), Plešovice (Sláma et al., 2008), AusZ7.5 (Von Quadt et al., 2016) and SA2 (A. von Quadt, personal communication). All reference materials yield ages that agree within uncertainties to the reference values (see Supplementary Data, Table A1).

The remaining samples (B-235, B-245, C-172) were analyzed at the Colombian Geological Survey U-Pb geochronology laboratory selecting 60 to 80 zircons per sample. Radiometric dating was carried out following the protocols of the geochronology laboratory of the Colombian Geological Survey (Peña Urueña et al., 2018) using the Laser Ablation – Inductively Coupled Plasma Mass Spectrometry (LA-ICP-MS) method with a Thermo Scientific Element II single-collector ICP-MS coupled to a 193 nm Photon machine laser ablation system. The analytical conditions of the system were: maximum value of laser output energy 95%, the energy of 7.00 mJ, 8 Hz pulse repetition rate was used. and 126 shots per analysis, the ablation with a 25 μm spot was performed under helium flows of 0.100 L/min and 0.200 L/min, taking a total time of 1 min 5s, during which for 30 s run a target and then acquiring the masses ^{202}Hg , ^{204}Hg , ^{206}Pb , ^{207}Pb , ^{208}Pb , ^{232}Th , ^{235}U , and ^{238}U ; The reference materials are NIST610 glass to maximize the signal of Th and U by optimizing ICP-MS and Laser parameters, oxide generation was optimized at $\text{ThO}^+/\text{Th}^+ < 0.5\%$. The Plesovice zircon as the primary standard for the correction of isotopic ratios of 337.13 ± 0.37 Ma (Sláma et al., 2008), and each one of the secondary zircon standards of 91500 CA-ID-TIMS $^{207}\text{Pb}/^{206}\text{Pb}$ age 1062.4 ± 0.8 Ma (Wiedenbeck et al., 1995) and Mount Dromedary 99.12 ± 0.14 Ma (Renne et al., 1998).

Data reduction was performed with the IGOR-based Iolite v2.5 (Paton et al., 2011) and Vizual Age (Petrus and Kamber, 2012). Obtained isotope ratios and dates were corrected for mass bias, instrumental drift, and downhole fractionation using primary reference material. To carry out the manual integrations, the isotopes of ^{238}U , ^{206}Pb , and

^{204}Pb were used. Finally, the Concordia diagrams and data analysis presented are made only with data that have a percentage of discordance <10% for the systems $^{206}\text{Pb}/^{238}\text{U}$ vs. $^{207}\text{Pb}/^{206}\text{Pb}$, for crystals older than 200 Ma whereas for crystals younger than 200 Ma we used the $^{206}\text{Pb}/^{238}\text{U}$ vs. $^{207}\text{Pb}/^{235}\text{U}$ ratios.

Discordant ages arise from common Pb contamination either from inclusions or cracks, recent Pb-loss, or measuring different age domains in the grain leading to mixed ages. Isotopic ratio uncertainties reported in supplementary Table A1 have propagated uncertainties at the 95% confidence level. The total external error on pooled analyses used to calculate dates, estimated to be ~ 2 % for $^{206}\text{Pb}/^{238}\text{U}$ dates, is composed of the systematic uncertainties resulting from (1) uncertainty of the decay constants of ^{238}U and ^{235}U (0.05% and 0.07% respectively; Jaffey et al., 1971) (2) the uncertainty on the $^{206}\text{Pb}/^{238}\text{U}$ ratio of the primary standard (GJ-1 and Plesovice respectively), (3) uncertainty on the $^{238}\text{U}/^{235}\text{U}$ ratio (0.033%; Heiss et al., 2012) and (4) the long-term excess scatter of validation reference materials. Crystallization ages were calculated with 95% confidence and total uncertainties are given, including quadratically propagated external error as suggested in Horstwood et al. (2016). The external error-corrected ages are reported in supplementary Table A1, in which all uncertainties are reported at the 2s level. Statistical analyses of zircon data Concordia and KDE plots were performed using IsoplotR (Vermeesch, 2018). All discordant (> 10%) results of magmatic zircons were discarded.

Zircon Lu-Hf analyses by Laser ablation multi-collection inductively coupled plasma mass spectrometry (LA-MC-ICP-MS)

Zircon Lu-Hf isotopic analyses were carried out by LA-MC-ICP-MS at ETHZ using an ASI RESOLUTION S-155 193 nm ArF excimer laser ablation system attached to a Nu Instruments Nu Plasma 2 multi-collector sector-field mass spectrometer. We used a laser

spot diameter of 50 μm , a repetition rate of 5 Hz, and an energy density of $\sim 4 \text{ J/cm}^2$. The carrier gas consisted of high-purity helium ($\sim 0.35 \text{ L/min}$) and argon ($\sim 1.0 \text{ L/min}$). The integration time was set to 0.5 s and the detector array set to collect intensities for the following isotopes: ^{171}Yb (L4), ^{173}Yb (L2), ^{175}Lu (C), ^{176}Hf (H1), ^{177}Hf (H2), ^{178}Hf (H3), ^{179}Hf (H4), ^{180}Hf (H5) and ^{181}Ta (H6). The data were processed offline with the Igor Pro-based Iolite v2.5 software using an in-house data reduction scheme. Instrumental mass bias for Yb and Hf isotopes were corrected to the natural abundance ratios $^{173}\text{Yb}/^{171}\text{Yb}$ and $^{179}\text{Hf}/^{177}\text{Hf}$ from (Chu et al., 2002). The isobaric interferences of ^{176}Yb and ^{176}Lu on ^{176}Hf were corrected using the natural abundance ratios of $^{176}\text{Yb}/^{173}\text{Yb} = 0.79502$ and $^{176}\text{Lu}/^{175}\text{Lu} = 0.02656$. Accuracy and external reproducibility of the method was controlled by repeated analyses of reference zircon standards GJ-1 (Morel et al., 2008), Plešovice (Sláma et al., 2008), MudTank and Temora (Woodhead and Hergt, 2005). The $^{176}\text{Hf}/^{177}\text{Hf}$ ratios obtained on all reference materials are within 2s uncertainties identical to the recommended values. Calculations of initial $^{176}\text{Hf}/^{177}\text{Hf}$ ratios, ϵHf_i and depleted mantle Hf model ages (T_{DM}) were performed using a ^{176}Lu decay constant of 1.867×10^{-11} (Scherer et al., 2001) with $^{176}\text{Hf}/^{177}\text{Hf} = 0.0336$ and $^{176}\text{Lu}/^{177}\text{Hf} = 0.282785$ values for the chondritic uniform reservoir (CHUR) recommended by (Bouvier et al., 2008). Depleted mantle reservoir values were estimated according to $^{176}\text{Hf}/^{177}\text{Hf}_{\text{DM}}(0) = 0.28325$ (Salters and Stracke, 2004) and $^{176}\text{Lu}/^{177}\text{Hf}_{\text{DM}}(0) = 0.0388$ (Griffin et al., 2000). The T_{DM2} was calculated from the initial Hf composition of the zircons using an average crustal $^{176}\text{Lu}/^{177}\text{Hf}_{\text{crust, today}} = 0.015$ (Griffin et al., 2002). Measured $^{176}\text{Lu}/^{177}\text{Hf}$ was corrected by multiplying the measured value by the ratio of the natural abundance of both isotopes.

References

- Black, L.P., Kamo, S.L., Allen, C.M., Aleinikoff, J.N., Davis, D.W., Korsch, R.J., and Foudoulis, C., 2003, TEMORA 1: a new zircon standard for Phanerozoic U–Pb geochronology: *Chemical Geology*, v. 200, p. 155–170, doi:10.1016/S0009-2541(03)00165-7.
- Bouvier, A., Vervoort, J.D., and Patchett, P.J., 2008, The Lu–Hf and Sm–Nd isotopic composition of CHUR: Constraints from unequilibrated chondrites and implications for the bulk composition of terrestrial planets: *Earth and Planetary Science Letters*, v. 273, p. 48–57, doi:10.1016/j.epsl.2008.06.010.
- Chu, N.C., Taylor, R.N., Chavagnac, V., Nesbitt, R.W., Boella, R.M., Milton, J.A., German, C.R., Bayon, G., and Burton, K., 2002, Hf isotope ratio analysis using multi-collector inductively coupled plasma mass spectrometry: An evaluation of isobaric interference corrections: *Journal of Analytical Atomic Spectrometry*, v. 17, p. 1567–1574, doi:10.1039/b206707b.
- Griffin, W.L., Pearson, N.J., Belousova, E., Jackson, S.E., Van Achenbergh, E., O’Reilly, S.Y., and Shee, S.R., 2000, The Hf isotope composition of cratonic mantle: LAM–MC–ICPMS analysis of zircon megacrysts in kimberlites: *Geochimica et Cosmochimica Acta*, v. 64, p. 133–147, doi:10.1016/S0016-7037(99)00343-9.
- Griffin, W.L., Wang, X., Jackson, S.E., Pearson, N.J., O’Reilly, S.Y., Xu, X., and Zhou, X., 2002, Zircon chemistry and magma mixing, SE China: In-situ analysis of Hf isotopes, Tonglu and Pingtan igneous complexes: *Lithos*, v. 61, p. 237–269, doi:10.1016/S0024-4937(02)00082-8.
- Guillong, M., Von Quadt, A., Sakata, S., Peytcheva, I., and Bachmann, O., 2014, LA–ICP–MS Pb–U dating of young zircons from the Kos–Nisyros volcanic centre, SE Aegean arc, *in* *Journal of Analytical Atomic Spectrometry*, Royal Society of Chemistry, v. 29, p. 963–970, doi:10.1039/c4ja00009a.
- Hies, J., Condon, D.J., McLean, N., and Noble, S.R., 2012, 238U/235U systematics in terrestrial uranium-bearing minerals: *Science*, v. 335, p. 1610–1614, doi:10.1126/science.1215507.
- Horstwood, M.S.A. et al., 2016, Community-Derived Standards for LA–ICP–MS U–(Th–)Pb Geochronology–Uncertainty Propagation, Age Interpretation and Data Reporting:, doi:10.1111/j.1751-908X.2016.00379.x.
- Jackson, S.E., Pearson, N.J., Griffin, W.L., and Belousova, E.A., 2004, The application of laser ablation–inductively coupled plasma–mass spectrometry to in situ U–Pb zircon geochronology: *Chemical Geology*, v. 211, p. 47–69, doi:10.1016/j.chemgeo.2004.06.017.
- Jaffey, A.H., Flynn, K.F., Glendenin, L.E., Bentley, W.C., and Essling, A.M., 1971, Precision measurement of half-lives and specific activities of U235 and U238: *Physical Review C*, v. 4, p. 1889–1906, doi:10.1103/PhysRevC.4.1889.
- Jochum, K.P. et al., 2011, Determination of reference values for NIST SRM 610–617 glasses following ISO guidelines: *Geostandards and Geoanalytical Research*, v. 35, p. 397–429, doi:10.1111/j.1751-908X.2011.00120.x.
- Morel, M.L.A., Nebel, O., Nebel-Jacobsen, Y.J., Miller, J.S., and Vroon, P.Z., 2008, Hafnium isotope characterization of the GJ-1 zircon reference material by solution and laser-ablation MC–ICPMS: *Chemical Geology*, v. 255, p. 231–235, doi:10.1016/j.chemgeo.2008.06.040.
- Paton, C., Hellstrom, J., Paul, B., Woodhead, J., and Hergt, J., 2011, Iolite: Free ware for the visualisation and processing of mass spectrometric data: *Journal of Analytical Atomic Spectrometry*, v. 26, p. 2508–2518, doi:10.1039/c1ja10172b.
- Paton, C., Woodhead, J.D., Hellstrom, J.C., Hergt, J.M., Greig, A., and Maas, R., 2010, Improved laser ablation U–Pb zircon geochronology through robust downhole fractionation correction: IMPROVED LASER ABLATION U–Pb GEOCHRONOLOGY: *Geochemistry, Geophysics, Geosystems*, v. 11, p. n/a–n/a, doi:10.1029/2009GC002618.
- Peña Uruña, M.L., Muñoz Rocha, J.A., and Uruña, C.L., 2018, Laboratorio de Geocronología en el Servicio Geológico Colombiano: avances sobre datación U–Pb en circones mediante la técnica LA–ICP–MS: *Boletín Geológico*, v. 44, p. 39–56, doi:10.32685/0120-1425/boletingeo.44.2018.7.
- Petrus, J.A., and Kamber, B.S., 2012, VizualAge: A Novel Approach to Laser Ablation ICP–MS U–Pb Geochronology Data Reduction: *Geostandards and Geoanalytical Research*, v. 36, p. 247–270, doi:10.1111/j.1751-908X.2012.00158.x.
- Von Quadt, A., Wotzlaw, J.F., Buret, Y., Large, S.J.E., Peytcheva, I., and Trinquier, A., 2016, High-precision zircon U/Pb geochronology by ID–TIMS using new 1013 ohm resistors: *Journal of Analytical Atomic Spectrometry*, v. 31, p. 658–665, doi:10.1039/c5ja00457h.

- Renne, P.R., Swisher, C.C., Deino, A.L., Karner, D.B., Owens, T.L., and DePaolo, D.J., 1998, Intercalibration of standards, absolute ages and uncertainties in $^{40}\text{Ar}/^{39}\text{Ar}$ dating: *Chemical Geology*, v. 145, p. 117–152, doi:10.1016/S0009-2541(97)00159-9.
- Salters, V.J.M., and Stracke, A., 2004, Composition of the depleted mantle: *Geochemistry, Geophysics, Geosystems*, v. 5, doi:10.1029/2003GC000597.
- Scherer, E., Münker, C., and Mezger, K., 2001, Calibration of the lutetium-hafnium clock: *Science*, v. 293, p. 683–687, doi:10.1126/science.1061372.
- Sláma, J. et al., 2008, Plešovice zircon — A new natural reference material for U–Pb and Hf isotopic microanalysis: *Chemical Geology*, v. 249, p. 1–35, doi:10.1016/j.chemgeo.2007.11.005.
- Vermeesch, P., 2018, IsoplotR: A free and open toolbox for geochronology: *Geoscience Frontiers*, v. 9, p. 1479–1493, doi:10.1016/j.gsf.2018.04.001.
- Wiedenbeck, M., Allé, P., Corfu, F., Griffin, W.L., Meier, M., Oberli, F., Quadt, A. VON, Roddick, J.C., and Spiegel, W., 1995, Three Natural Zircon Standards for U- Th- Pb, Lu- Hf, Trace Element and Ree Analyses: *Geostandards Newsletter*, v. 19, p. 1–23, doi:10.1111/j.1751-908X.1995.tb00147.x.
- Woodhead, J.D., and Hergt, J.M., 2005, A Preliminary Appraisal of Seven Natural Zircon Reference Materials for In Situ Hf Isotope Determination: *Geostandards and Geoanalytical Research*, v. 29, p. 183–195, doi:10.1111/j.1751-908x.2005.tb00891.x.

TABLE A1. U, Pb AND Th ISOTOPIC DATA OBTAINED USING THE LA-ICP-MS METHOD

| I.D. | Target | Th (ppm) | U (ppm) | Th/U | Isotopic Ratios | | | | | | Rho 206/238-207/235 | Isotopic Ages | | | | | | Concordance % | | | |
|----------|--------|----------|---------|------|-------------------------------------|--------------------|----------------------|-------------------------------------|--------------------|----------------------|------------------------|--------------------------------------|--------------------|----------------------|-------------------------------------|--------------------|--------------------------------------|---------------|--------------------|-----|-------|
| | | | | | ²⁰⁷ Pb/ ²³⁵ U | ±2σ _{sys} | ±2σ _{sys} % | ²⁰⁶ Pb/ ²³⁸ U | ±2σ _{sys} | ±2σ _{sys} % | | Pb ²⁰⁷ /Pb ²⁰⁶ | ±2σ _{sys} | ±2σ _{sys} % | ²⁰⁶ Pb/ ²³⁸ U | ±2σ _{sys} | Pb ²⁰⁷ /Pb ²⁰⁶ | | ±2σ _{sys} | | |
| G-52a-60 | 0 | 11100 | 6440 | 1.80 | 0.9200 | 0.1400 | 15.22 | 0.0252 | 0.0021 | 8.33 | 0.2610 | 0.0260 | 9.96 | 0.98 | 646 | 71 | 160.1 | 13 | 3200 | 150 | 24.78 |
| G-52a-48 | 1 | 681 | 3610 | 0.20 | 1.7200 | 0.1600 | 9.30 | 0.0412 | 0.0035 | 8.50 | 0.3010 | 0.0150 | 4.98 | 0.86 | 1005 | 62 | 260 | 22 | 3459 | 76 | 25.87 |
| G-52a-6 | 0 | 3100 | 3590 | 0.28 | 1.1100 | 0.1100 | 9.91 | 0.0342 | 0.0029 | 8.48 | 0.2390 | 0.0220 | 9.21 | 0.33 | 751 | 54 | 217 | 18 | 3070 | 160 | 28.89 |
| G-52a-51 | 0 | 1368 | 7600 | 0.20 | 0.6920 | 0.0690 | 9.97 | 0.0244 | 0.0019 | 7.80 | 0.2050 | 0.0190 | 9.27 | 0.19 | 530 | 40 | 155.2 | 12 | 2830 | 150 | 29.28 |
| G-52a-7 | 1 | 927 | 8380 | 0.13 | 0.5480 | 0.0280 | 5.11 | 0.0210 | 0.0017 | 8.11 | 0.1888 | 0.0019 | 1.01 | 0.93 | 443 | 19 | 133.6 | 10 | 2731 | 17 | 30.16 |
| G-52a-41 | 1 | 233 | 3470 | 0.08 | 0.9680 | 0.0790 | 8.16 | 0.0329 | 0.0026 | 7.89 | 0.2090 | 0.0100 | 4.78 | 0.92 | 684 | 42 | 208.9 | 17 | 2880 | 86 | 30.54 |
| G-52a-30 | 0 | 2770 | 4570 | 0.60 | 0.8660 | 0.0810 | 9.35 | 0.0303 | 0.0023 | 7.60 | 0.2020 | 0.0140 | 6.93 | 0.67 | 628 | 43 | 192.2 | 14 | 2810 | 110 | 30.61 |
| G-52a-55 | 0 | 33.5 | 2330 | 0.02 | 0.9900 | 0.1400 | 14.14 | 0.0344 | 0.0029 | 8.43 | 0.2050 | 0.0220 | 10.73 | 0.95 | 687 | 77 | 218.1 | 18 | 2800 | 200 | 31.75 |
| G-52a-8 | 0 | 506 | 5340 | 0.11 | 0.6780 | 0.0520 | 7.67 | 0.0298 | 0.0023 | 7.73 | 0.1630 | 0.0082 | 5.03 | 0.80 | 523 | 31 | 189.1 | 15 | 2467 | 89 | 36.16 |
| G-52a-29 | 1 | 637 | 4200 | 0.17 | 0.5810 | 0.0530 | 9.12 | 0.0272 | 0.0022 | 8.08 | 0.1503 | 0.0078 | 5.19 | 0.91 | 463 | 34 | 173.1 | 14 | 2334 | 91 | 37.39 |
| G-52a-13 | 0 | 134 | 3060 | 0.05 | 0.6760 | 0.0700 | 10.36 | 0.0306 | 0.0024 | 7.83 | 0.1570 | 0.0120 | 7.64 | 0.76 | 520 | 44 | 194.6 | 15 | 2390 | 150 | 37.42 |
| G-52a-16 | 0 | 2070 | 8580 | 0.27 | 0.4050 | 0.0260 | 6.42 | 0.0203 | 0.0016 | 7.89 | 0.1419 | 0.0062 | 4.37 | 0.28 | 344 | 19 | 129.5 | 10 | 2238 | 72 | 37.65 |
| G-52a-56 | 1 | 519 | 3910 | 0.15 | 0.6000 | 0.0590 | 9.83 | 0.0301 | 0.0026 | 8.64 | 0.1432 | 0.0091 | 6.35 | 0.79 | 473 | 38 | 191.3 | 16 | 2230 | 130 | 40.44 |
| G-52a-23 | 0 | 1386 | 6960 | 0.22 | 0.4740 | 0.0250 | 5.27 | 0.0257 | 0.0020 | 7.79 | 0.1305 | 0.0035 | 2.68 | 0.48 | 394 | 17 | 163.3 | 13 | 2099 | 47 | 41.45 |
| G-52a-9 | 1 | 641 | 4340 | 0.17 | 0.4680 | 0.0350 | 7.48 | 0.0260 | 0.0021 | 8.09 | 0.1301 | 0.0051 | 3.92 | 0.70 | 389 | 24 | 165.2 | 13 | 2091 | 68 | 42.47 |
| G-52a-33 | 1 | 230 | 5300 | 0.05 | 0.5100 | 0.0500 | 9.80 | 0.0280 | 0.0021 | 7.49 | 0.1310 | 0.0130 | 9.92 | 0.26 | 415 | 33 | 178.3 | 13 | 2030 | 160 | 42.96 |
| G-52a-57 | 0 | 156 | 2300 | 0.07 | 0.4600 | 0.1200 | 26.09 | 0.0278 | 0.0024 | 8.63 | 0.1350 | 0.0340 | 25.19 | 0.97 | 403 | 93 | 176.8 | 15 | 1910 | 290 | 43.87 |
| G-52a-42 | 1 | 266 | 3810 | 0.08 | 0.5400 | 0.0610 | 11.30 | 0.0302 | 0.0024 | 7.95 | 0.1280 | 0.0120 | 9.38 | 0.64 | 435 | 40 | 191.8 | 15 | 2020 | 170 | 44.09 |
| G-52a-11 | 0 | 446 | 4630 | 0.11 | 0.5210 | 0.0360 | 6.91 | 0.0299 | 0.0024 | 8.04 | 0.1235 | 0.0057 | 4.62 | 0.50 | 424 | 24 | 189.7 | 15 | 1991 | 80 | 44.74 |
| G-52a-50 | 0 | 454 | 5500 | 0.09 | 0.4420 | 0.0220 | 4.98 | 0.0265 | 0.0020 | 7.55 | 0.1208 | 0.0017 | 1.41 | 0.87 | 371.5 | 15 | 168.4 | 13 | 1967 | 26 | 45.33 |
| G-52a-40 | 0 | 349 | 4590 | 0.08 | 0.5060 | 0.0970 | 19.17 | 0.0298 | 0.0026 | 8.72 | 0.1180 | 0.0190 | 16.10 | 0.81 | 405 | 62 | 189.1 | 16 | 1800 | 260 | 46.69 |
| G-52a-10 | 0 | 787 | 6140 | 0.14 | 0.3930 | 0.0250 | 6.36 | 0.0249 | 0.0020 | 8.04 | 0.1127 | 0.0037 | 3.28 | 0.64 | 336 | 18 | 158.5 | 12 | 1836 | 59 | 47.17 |
| G-52a-22 | 1 | 631 | 4100 | 0.18 | 0.4260 | 0.0280 | 6.57 | 0.0281 | 0.0022 | 7.84 | 0.1066 | 0.0040 | 3.75 | 0.65 | 359 | 20 | 178.4 | 14 | 1732 | 67 | 49.69 |
| G-52a-47 | 0 | 342 | 4290 | 0.09 | 0.4430 | 0.0390 | 8.80 | 0.0296 | 0.0024 | 8.11 | 0.1082 | 0.0065 | 6.01 | 0.54 | 371 | 27 | 188 | 15 | 1750 | 100 | 50.67 |
| G-52a-38 | 1 | 77.2 | 1513 | 0.06 | 0.4530 | 0.0230 | 5.08 | 0.0303 | 0.0023 | 7.58 | 0.1077 | 0.0026 | 2.41 | 0.34 | 379.4 | 16 | 192.6 | 14 | 1757 | 43 | 50.76 |
| G-52a-15 | 1 | 481 | 4350 | 0.12 | 0.3890 | 0.0280 | 7.20 | 0.0269 | 0.0020 | 7.44 | 0.1030 | 0.0053 | 5.15 | 0.46 | 333 | 20 | 170.9 | 13 | 1654 | 95 | 51.32 |
| G-52a-21 | 1 | 206 | 4000 | 0.06 | 0.3970 | 0.0430 | 10.83 | 0.0287 | 0.0022 | 7.68 | 0.0977 | 0.0080 | 8.19 | 0.68 | 336 | 31 | 182.1 | 14 | 1520 | 150 | 54.20 |
| G-52a-34 | 1 | 428 | 3220 | 0.13 | 0.3860 | 0.0260 | 6.74 | 0.0284 | 0.0023 | 8.09 | 0.0957 | 0.0041 | 4.28 | 0.51 | 330 | 19 | 180.7 | 14 | 1539 | 83 | 54.76 |
| G-52a-1 | 0 | 517 | 3315 | 0.15 | 0.3410 | 0.0190 | 5.57 | 0.0265 | 0.0020 | 7.56 | 0.0948 | 0.0038 | 4.01 | 0.11 | 297.9 | 14 | 168.4 | 13 | 1511 | 72 | 56.53 |
| G-52a-52 | 0 | 281 | 3490 | 0.09 | 0.3610 | 0.0200 | 5.54 | 0.0278 | 0.0021 | 7.55 | 0.0937 | 0.0023 | 2.45 | 0.75 | 312 | 15 | 176.9 | 13 | 1497 | 48 | 56.70 |
| G-52a-17 | 1 | 540 | 6870 | 0.09 | 0.3188 | 0.0170 | 5.33 | 0.0256 | 0.0020 | 7.81 | 0.0882 | 0.0030 | 3.40 | 0.03 | 280.7 | 13 | 162.3 | 12 | 1377 | 62 | 58.07 |
| G-52a-44 | 0 | 417 | 2840 | 0.16 | 0.3520 | 0.0180 | 5.11 | 0.0287 | 0.0022 | 7.67 | 0.0879 | 0.0027 | 3.07 | 0.11 | 305.8 | 13 | 183.4 | 14 | 1372 | 57 | 59.65 |
| G-52a-4 | 1 | 9000 | 44300 | 0.15 | 0.1098 | 0.0110 | 10.02 | 0.0102 | 0.0012 | 11.75 | 0.0803 | 0.0024 | 2.99 | 0.91 | 105.6 | 9.7 | 65.5 | 7.6 | 1197 | 59 | 62.03 |
| G-52a-18 | 1 | 61.6 | 1250 | 0.06 | 0.2790 | 0.0430 | 15.41 | 0.0251 | 0.0019 | 7.56 | 0.0772 | 0.0098 | 12.69 | 0.80 | 246 | 33 | 160.1 | 12 | 1020 | 220 | 65.08 |
| G-52a-39 | 0 | 210 | 2490 | 0.07 | 0.2776 | 0.0140 | 5.04 | 0.0273 | 0.0021 | 7.70 | 0.0723 | 0.0023 | 3.18 | 0.17 | 248.6 | 11 | 173.3 | 13 | 981 | 62 | 69.71 |
| G-52a-49 | 0 | 54.4 | 5650 | 0.01 | 0.3020 | 0.0380 | 12.58 | 0.0295 | 0.0023 | 7.80 | 0.0739 | 0.0089 | 12.04 | 0.48 | 265 | 29 | 187.4 | 14 | 920 | 230 | 70.72 |
| G-52a-37 | 1 | 86.6 | 3770 | 0.03 | 0.2470 | 0.0150 | 6.07 | 0.0275 | 0.0021 | 7.64 | 0.0637 | 0.0023 | 3.61 | 0.62 | 224.1 | 12 | 174.7 | 13 | 719 | 76 | 77.96 |
| G-52a-59 | 0 | 110 | 3580 | 0.03 | 0.2395 | 0.0120 | 5.01 | 0.0269 | 0.0020 | 7.44 | 0.0642 | 0.0020 | 3.12 | 0.05 | 217.9 | 9.9 | 171 | 13 | 755 | 69 | 78.48 |
| G-52a-14 | 0 | 174 | 2620 | 0.06 | 0.2380 | 0.0210 | 8.82 | 0.0269 | 0.0020 | 7.45 | 0.0631 | 0.0040 | 6.34 | 0.57 | 216 | 17 | 170.9 | 13 | 670 | 130 | 79.12 |
| G-52a-35 | 0 | 91 | 1776 | 0.04 | 0.2441 | 0.0120 | 4.92 | 0.0279 | 0.0021 | 7.52 | 0.0623 | 0.0012 | 1.93 | 0.43 | 221.6 | 9.6 | 177.5 | 13 | 679 | 41 | 80.10 |
| G-52a-58 | 1 | 145 | 3050 | 0.05 | 0.2270 | 0.0150 | 6.61 | 0.0265 | 0.0020 | 7.56 | 0.0626 | 0.0025 | 3.99 | 0.47 | 207.6 | 12 | 168.4 | 13 | 678 | 87 | 81.12 |
| G-52a-27 | 0 | 78.8 | 3340 | 0.03 | 0.2194 | 0.0110 | 5.01 | 0.0258 | 0.0020 | 7.75 | 0.0599 | 0.0011 | 1.84 | 0.72 | 201.3 | 9 | 164.2 | 12 | 595 | 38 | 81.57 |
| G-52a-28 | 0 | 83.9 | 2270 | 0.04 | 0.2279 | 0.0130 | 5.70 | 0.0268 | 0.0020 | 7.47 | 0.0602 | 0.0022 | 3.65 | 0.18 | 208.3 | 11 | 170.2 | 13 | 597 | 79 | 81.71 |
| G-52a-43 | 0 | 407 | 3380 | 0.14 | 0.2483 | 0.0120 | 4.83 | 0.0283 | 0.0022 | 7.59 | 0.0612 | 0.0013 | 2.12 | 0.54 | 225.1 | 10 | 184.2 | 14 | 643 | 46 | 81.83 |
| G-52a-36 | 0 | 64 | 1446 | 0.03 | 0.2268 | 0.0130 | 5.73 | 0.0275 | 0.0021 | 7.63 | 0.0585 | 0.0024 | 4.10 | 0.00 | 207.3 | 11 | 175.1 | 13 | 530 | 94 | 84.47 |
| G-52a-45 | 1 | 259 | 6270 | 0.04 | 0.1998 | 0.0120 | 6.01 | 0.0249 | 0.0019 | 7.62 | 0.0576 | 0.0020 | 3.47 | 0.63 | 184.8 | 9.9 | 158.7 | 12 | 502 | 74 | 85.88 |
| G-52a-3 | 0 | 139.3 | 4520 | 0.03 | 0.2184 | 0.0100 | 4.58 | 0.0272 | 0.0021 | 7.73 | 0.0605 | 0.0005 | 0.88 | 0.84 | 200.5 | 8.4 | 172.7 | 13 | 621 | 19 | 86.13 |
| G-52a-20 | 1 | 68 | 2990 | 0.02 | 0.1950 | 0.0130 | 6.67 | 0.0249 | 0.0019 | 7.63 | 0.0543 | 0.0024 | 4.42 | 0.06 | 180.7 | 11 | 158.5 | 12 | 400 | 100 | 87.71 |
| G-52a-32 | 1 | 28 | 2431 | 0.01 | 0.2096 | 0.0120 | 5.73 | 0.0273 | 0.0021 | 7.69 | 0.0545 | 0.0015 | 2.75 | 0.59 | 193.1 | 9.7 | 173.7 | 13 | 382 | 61 | 89.95 |
| G-52a-26 | 1 | 51.4 | 2320 | 0.03 | 0.2169 | 0.0100 | 4.61 | 0.0289 | 0.0022 | 7.60 | 0.0529 | 0.0010 | 1.80 | 0.59 | 199.3 | 8.5 | 183.8 | 14 | 321 | 41 | 92.22 |
| G-52a-24 | 1 | 36.8 | 4650 | 0.01 | 0.1962 | 0.0110 | 5.61 | 0.0267 | 0.0020 | 7.49 | 0.0517 | 0.0016 | 3.09 | 0.61 | 181.8 | 9.1 | 169.8 | 13 | 264 | 70 | 93.40 |
| G-52a-54 | 1 | 16.16 | 2008 | 0.01 | 0.2014 | 0.0090 | 4.47 | 0.0279 | 0.0021 | 7.52 | 0.0526 | 0.0007 | 1.39 | 0.72 | 186.3 | 7.6 | 177.6 | 13 | 315 | 35 | 95.33 |
| G-52a-31 | 1 | 34.8 | 5090 | 0.01 | 0.1909 | 0.0084 | 4.40 | 0.0266 | 0.0020 | 7.52 | 0.0510 | 0.0005 | 1.00 | 0.67 | 177.4 | 7.2 | 169.2 | 13 | 239 | 23 | 95.38 |
| G-52a-25 | 1 | 36.8 | 4900 | 0.01 | 0.1857 | 0.0084 | 4.52 | 0.0261 | 0.0020 | 7.66 | 0.0503 | 0.0005 | 1.01 | 0.79 | 172.9 | 7.2 | 166.2 | 13 | 208 | 23 | 96.12 |
| G-52a-46 | 0 | 27.2 | 2290 | 0.01 | 0.1885 | 0.0085 | 4.51 | 0.0266 | 0.0020 | 7.52 | 0.0509 | 0.0008 | 1.63 | 0.45 | 175.3 | 7.2 | 169.2 | 13 | 231 | 38 | 96.52 |
| G-52a-12 | 1 | 41.2 | 3920 | 0.01 | 0.1892 | 0.0084 | 4.44 | 0.0269 | 0.0020 | 7.44 | 0.0505 | 0.0005 | 0.99 | 0.79 | 175.9 | 7.2 | 171 | 13 | 216 | 23 | 97.21 |
| G-52a-53 | 1 | 33.9 | 3140 | 0.01 | 0.1892 | 0.0087 | 4.60 | | | | | | | | | | | | | | |

| | | | | | | | | | | | | | | | | | | | | | |
|------------|---|-------|-------|------|---------|--------|-------|--------|--------|------|--------|--------|-------|------|--------|-----|-------|-----|------|-----|-------|
| G-55b - 1 | 0 | 288 | 1228 | 0.27 | 0.9760 | 0.0480 | 4.92 | 0.0987 | 0.0074 | 7.50 | 0.0723 | 0.0012 | 1.66 | 0.84 | 691 | 25 | 606.7 | 44 | 993 | 34 | 61.10 |
| G-55b - 52 | 0 | 44 | 117.2 | 0.42 | 0.4900 | 0.0390 | 7.96 | 0.0600 | 0.0051 | 8.50 | 0.0603 | 0.0032 | 5.31 | 0.63 | 404 | 27 | 376 | 31 | 600 | 120 | 62.67 |
| G-55b - 6 | 0 | 14.56 | 53.1 | 0.31 | 1.2060 | 0.0750 | 6.22 | 0.1147 | 0.0089 | 7.76 | 0.0774 | 0.0027 | 3.49 | 0.47 | 806 | 32 | 700 | 51 | 1114 | 72 | 62.84 |
| G-55b - 75 | 1 | 94.8 | 771 | 0.13 | 0.3240 | 0.0190 | 5.86 | 0.0422 | 0.0032 | 7.58 | 0.0556 | 0.0018 | 3.24 | 0.51 | 284.6 | 14 | 266.5 | 20 | 423 | 70 | 63.00 |
| G-55b - 22 | 0 | 110 | 69.4 | 1.79 | 0.9020 | 0.0560 | 6.21 | 0.0948 | 0.0073 | 7.70 | 0.0698 | 0.0027 | 3.87 | 0.24 | 650 | 30 | 584 | 43 | 906 | 79 | 64.46 |
| G-55b - 56 | 0 | 133.6 | 461 | 0.33 | 1.2080 | 0.0710 | 5.88 | 0.1173 | 0.0091 | 7.76 | 0.0758 | 0.0030 | 3.96 | 0.63 | 803 | 32 | 715 | 53 | 1081 | 75 | 66.14 |
| G-55b - 71 | 1 | 12.07 | 1177 | 0.01 | 0.3288 | 0.0150 | 4.56 | 0.0433 | 0.0033 | 7.62 | 0.0550 | 0.0012 | 2.18 | 0.32 | 288.6 | 12 | 273.2 | 21 | 406 | 51 | 67.29 |
| G-55b - 38 | 1 | 342 | 538 | 0.72 | 0.3285 | 0.0160 | 4.87 | 0.0434 | 0.0033 | 7.60 | 0.0548 | 0.0011 | 2.01 | 0.45 | 288.3 | 12 | 273.9 | 20 | 400 | 46 | 68.48 |
| G-55b - 25 | 0 | 51.1 | 83.4 | 0.69 | 2.5200 | 0.1700 | 6.75 | 0.1859 | 0.0150 | 8.07 | 0.0987 | 0.0043 | 4.36 | 0.50 | 1273 | 49 | 1099 | 79 | 1586 | 80 | 69.29 |
| G-55b - 36 | 0 | 146.6 | 1523 | 0.11 | 0.2955 | 0.0140 | 4.74 | 0.0398 | 0.0030 | 7.53 | 0.0537 | 0.0009 | 1.60 | 0.60 | 262.8 | 11 | 251.8 | 19 | 354 | 36 | 71.13 |
| G-55b - 54 | 1 | 84 | 1970 | 0.05 | 0.3132 | 0.0160 | 5.11 | 0.0314 | 0.0024 | 7.64 | 0.0724 | 0.0022 | 3.04 | 0.19 | 276.5 | 12 | 199.3 | 15 | 988 | 60 | 72.08 |
| G-55b - 55 | 0 | 73.8 | 137.9 | 0.60 | 1.3800 | 0.0820 | 5.94 | 0.1297 | 0.0100 | 7.71 | 0.0757 | 0.0021 | 2.77 | 0.66 | 878 | 34 | 786 | 59 | 1079 | 53 | 72.85 |
| G-55b - 32 | 1 | 325 | 2696 | 0.13 | 0.2882 | 0.0150 | 5.20 | 0.0296 | 0.0023 | 7.78 | 0.0708 | 0.0024 | 3.39 | 0.16 | 256.9 | 12 | 187.8 | 14 | 937 | 68 | 73.10 |
| G-55b - 24 | 1 | 22.3 | 140.8 | 0.18 | 0.6430 | 0.0440 | 6.84 | 0.0586 | 0.0046 | 7.85 | 0.0790 | 0.0038 | 4.81 | 0.17 | 502 | 27 | 367.2 | 28 | 1150 | 95 | 73.15 |
| G-55b - 72 | 0 | 85.9 | 140.5 | 0.69 | 6.7100 | 0.3200 | 4.77 | 0.3142 | 0.0250 | 7.96 | 0.1524 | 0.0018 | 1.12 | 0.89 | 2073 | 43 | 1761 | 120 | 2380 | 23 | 73.99 |
| G-55b - 5 | 1 | 20.4 | 70.6 | 0.33 | 0.9960 | 0.0640 | 6.43 | 0.1066 | 0.0085 | 7.97 | 0.0688 | 0.0027 | 3.92 | 0.57 | 700 | 32 | 653 | 49 | 880 | 82 | 74.20 |
| G-55b - 48 | 0 | 16.8 | 74.3 | 0.25 | 0.9640 | 0.0660 | 6.85 | 0.1028 | 0.0080 | 7.78 | 0.0678 | 0.0032 | 4.72 | 0.62 | 684 | 34 | 631 | 47 | 849 | 93 | 74.32 |
| G-55b - 68 | 1 | 177 | 3040 | 0.07 | 0.2600 | 0.0110 | 4.23 | 0.0358 | 0.0027 | 7.55 | 0.0522 | 0.0005 | 1.03 | 0.68 | 234.6 | 9.3 | 226.6 | 17 | 294 | 24 | 77.07 |
| G-55b - 30 | 1 | 62 | 214 | 0.33 | 0.3620 | 0.0270 | 7.46 | 0.0270 | 0.0039 | 8.11 | 0.0549 | 0.0005 | 4.92 | 0.63 | 313 | 20 | 302.7 | 24 | 390 | 110 | 77.62 |
| G-55b - 66 | 1 | 124.9 | 125.8 | 1.10 | 0.2900 | 0.0190 | 6.55 | 0.0393 | 0.0030 | 7.63 | 0.0533 | 0.0024 | 4.50 | 0.40 | 258 | 15 | 248.6 | 19 | 320 | 96 | 77.69 |
| G-55b - 27 | 0 | 71.8 | 46.8 | 1.68 | 0.2630 | 0.0710 | 27.00 | 0.0282 | 0.0024 | 8.51 | 0.0670 | 0.0170 | 25.37 | 0.18 | 228 | 51 | 179.5 | 15 | 510 | 390 | 78.73 |
| G-55b - 34 | 0 | 273.6 | 265.2 | 1.17 | 2.0680 | 0.0970 | 4.69 | 0.1778 | 0.0140 | 7.87 | 0.0846 | 0.0012 | 1.42 | 0.74 | 1137 | 32 | 1054 | 75 | 1304 | 27 | 80.83 |
| G-55b - 80 | 1 | 64.7 | 214 | 0.34 | 1.2180 | 0.0680 | 5.58 | 0.1272 | 0.0098 | 7.70 | 0.0709 | 0.0024 | 3.39 | 0.36 | 808 | 31 | 772 | 56 | 948 | 70 | 81.43 |
| G-55b - 69 | 0 | 158 | 229.1 | 0.76 | 0.6220 | 0.0330 | 5.31 | 0.0761 | 0.0057 | 7.49 | 0.0596 | 0.0017 | 2.85 | 0.22 | 490 | 21 | 472.5 | 34 | 578 | 63 | 81.75 |
| G-55b - 21 | 0 | 106 | 350 | 0.34 | 0.9870 | 0.0520 | 5.27 | 0.1095 | 0.0084 | 7.67 | 0.0662 | 0.0017 | 2.57 | 0.62 | 697 | 26 | 670 | 49 | 806 | 52 | 83.13 |
| G-55b - 61 | 0 | 45 | 152.4 | 0.33 | 1.8890 | 0.0930 | 4.92 | 0.1701 | 0.0130 | 7.64 | 0.0807 | 0.0016 | 1.98 | 0.72 | 1076 | 33 | 1012 | 72 | 1212 | 39 | 83.50 |
| G-55b - 82 | 1 | 101.7 | 1001 | 0.11 | 0.2928 | 0.0140 | 4.78 | 0.0403 | 0.0031 | 7.69 | 0.0526 | 0.0012 | 2.28 | 0.51 | 260.6 | 11 | 254.7 | 19 | 304 | 49 | 83.78 |
| G-55b - 13 | 0 | 74.4 | 96.8 | 0.88 | 0.2100 | 0.0190 | 9.05 | 0.0253 | 0.0020 | 7.90 | 0.0587 | 0.0039 | 6.64 | 0.47 | 192 | 16 | 161.1 | 12 | 550 | 160 | 83.91 |
| G-55b - 76 | 0 | 24.7 | 64.4 | 0.43 | 1.6850 | 0.1000 | 5.93 | 0.1579 | 0.0130 | 8.23 | 0.0774 | 0.0025 | 3.23 | 0.70 | 1000 | 39 | 945 | 70 | 1121 | 64 | 84.30 |
| G-55b - 83 | 0 | 32.8 | 738 | 0.05 | 0.2932 | 0.0150 | 5.12 | 0.0405 | 0.0030 | 7.41 | 0.0526 | 0.0014 | 2.66 | 0.42 | 260.9 | 11 | 255.8 | 19 | 302 | 59 | 84.70 |
| G-55b - 15 | 0 | 85.7 | 1248 | 0.08 | 1.5810 | 0.0690 | 4.36 | 0.1527 | 0.0120 | 7.86 | 0.0750 | 0.0008 | 1.04 | 0.71 | 962.6 | 27 | 916 | 65 | 1068 | 21 | 85.77 |
| G-55b - 41 | 1 | 281 | 918 | 0.34 | 0.2617 | 0.0120 | 4.59 | 0.0366 | 0.0028 | 7.65 | 0.0517 | 0.0009 | 1.82 | 0.32 | 235.9 | 9.5 | 231.6 | 17 | 269 | 41 | 86.10 |
| G-55b - 65 | 0 | 85.3 | 114.5 | 0.82 | 0.2900 | 0.0200 | 6.90 | 0.0398 | 0.0031 | 7.79 | 0.0526 | 0.0028 | 5.32 | 0.37 | 258 | 16 | 251.7 | 19 | 290 | 110 | 86.79 |
| G-55b - 59 | 0 | 301 | 569 | 0.60 | 0.5690 | 0.0260 | 4.57 | 0.0714 | 0.0054 | 7.56 | 0.0577 | 0.0010 | 1.73 | 0.54 | 457.3 | 17 | 444.5 | 32 | 512 | 38 | 86.82 |
| G-55b - 20 | 0 | 143.3 | 362 | 0.45 | 0.9280 | 0.0490 | 5.28 | 0.1052 | 0.0081 | 7.70 | 0.0640 | 0.0014 | 2.19 | 0.73 | 665 | 26 | 645 | 47 | 737 | 44 | 87.52 |
| G-55b - 42 | 0 | 114.8 | 97.6 | 1.34 | 0.7000 | 0.0390 | 5.57 | 0.0846 | 0.0065 | 7.68 | 0.0603 | 0.0022 | 3.65 | 0.49 | 541 | 26 | 523 | 39 | 597 | 79 | 87.60 |
| G-55b - 84 | 0 | 126 | 162 | 0.88 | 5.5160 | 0.2500 | 4.53 | 0.3212 | 0.0250 | 7.78 | 0.1241 | 0.0016 | 1.29 | 0.83 | 1902 | 39 | 1795 | 120 | 2015 | 22 | 89.08 |
| G-55b - 43 | 0 | 305 | 1120 | 0.30 | 0.6960 | 0.0380 | 5.46 | 0.0846 | 0.0069 | 8.16 | 0.0595 | 0.0008 | 1.28 | 0.93 | 535 | 23 | 523 | 41 | 582 | 28 | 89.86 |
| G-55b - 62 | 0 | 67.8 | 15.6 | 4.88 | 2.0800 | 0.2500 | 12.02 | 0.1870 | 0.0180 | 9.63 | 0.0811 | 0.0097 | 11.96 | 0.83 | 1127 | 91 | 1104 | 98 | 1220 | 210 | 90.49 |
| G-55b - 35 | 1 | 111 | 559 | 0.22 | 0.2719 | 0.0140 | 5.15 | 0.0381 | 0.0029 | 7.61 | 0.0516 | 0.0011 | 2.13 | 0.53 | 244 | 11 | 241.2 | 18 | 264 | 49 | 91.36 |
| G-55b - 16 | 0 | 36.9 | 104.2 | 0.40 | 2.1290 | 0.1000 | 4.70 | 0.1909 | 0.0140 | 7.33 | 0.0815 | 0.0017 | 2.09 | 0.64 | 1157 | 33 | 1126 | 78 | 1229 | 42 | 91.62 |
| G-55b - 45 | 1 | 25.5 | 202 | 0.14 | 0.8060 | 0.0410 | 5.09 | 0.0950 | 0.0073 | 7.68 | 0.0612 | 0.0014 | 2.29 | 0.60 | 599 | 23 | 585 | 43 | 638 | 52 | 91.69 |
| G-55b - 81 | 0 | 84.6 | 225.3 | 0.42 | 1.7220 | 0.0750 | 4.36 | 0.1653 | 0.0120 | 7.26 | 0.0753 | 0.0011 | 1.46 | 0.34 | 1016.6 | 28 | 986 | 69 | 1074 | 29 | 91.81 |
| G-55b - 67 | 0 | 167.9 | 492 | 0.39 | 0.8170 | 0.0400 | 4.90 | 0.0964 | 0.0073 | 7.57 | 0.0613 | 0.0011 | 1.79 | 0.72 | 606 | 22 | 593.3 | 43 | 646 | 37 | 91.84 |
| G-55b - 26 | 1 | 177.2 | 100.4 | 1.99 | 0.2100 | 0.0150 | 7.14 | 0.0279 | 0.0022 | 7.88 | 0.0543 | 0.0032 | 5.89 | 0.03 | 193 | 13 | 177.5 | 14 | 360 | 130 | 91.97 |
| G-55b - 57 | 1 | 5.9 | 1301 | 0.00 | 0.3073 | 0.0150 | 4.88 | 0.0424 | 0.0032 | 7.55 | 0.0522 | 0.0008 | 1.53 | 0.71 | 271.9 | 11 | 267.5 | 20 | 290 | 35 | 92.24 |
| G-55b - 17 | 1 | 12.37 | 1111 | 0.01 | 0.3460 | 0.0190 | 5.49 | 0.0442 | 0.0034 | 7.70 | 0.0572 | 0.0013 | 2.27 | 0.89 | 301.6 | 14 | 278.5 | 21 | 492 | 50 | 92.34 |
| G-55b - 31 | 0 | 93.3 | 126.8 | 0.81 | 0.5440 | 0.0310 | 5.70 | 0.0695 | 0.0054 | 7.77 | 0.0568 | 0.0021 | 3.70 | 0.39 | 440 | 20 | 433.4 | 33 | 467 | 85 | 92.81 |
| G-55b - 29 | 0 | 155.1 | 317 | 0.55 | 2.1000 | 0.0960 | 4.57 | 0.1899 | 0.0150 | 7.90 | 0.0805 | 0.0012 | 1.49 | 0.69 | 1148 | 31 | 1121 | 79 | 1207 | 29 | 92.87 |
| G-55b - 46 | 0 | 30.2 | 206 | 0.17 | 0.7180 | 0.0390 | 5.43 | 0.0872 | 0.0069 | 7.91 | 0.0595 | 0.0014 | 2.35 | 0.70 | 549 | 23 | 539 | 41 | 576 | 52 | 93.58 |
| G-55b - 4 | 0 | 231 | 299 | 0.87 | 26.0600 | 1.4000 | 5.37 | 0.6490 | 0.0500 | 7.70 | 0.2930 | 0.0042 | 1.43 | 0.85 | 3344 | 52 | 3221 | 200 | 3432 | 22 | 93.85 |
| G-55b - 7 | 1 | 85 | 151.8 | 0.63 | 1.6510 | 0.0840 | 5.09 | 0.1629 | 0.0130 | 7.98 | 0.0740 | 0.0017 | 2.30 | 0.58 | 989 | 32 | 973 | 70 | 1036 | 45 | 93.92 |
| G-55b - 9 | 0 | 25 | 630 | 0.04 | 1.6660 | 0.0730 | 4.38 | 0.1639 | 0.0120 | 7.32 | 0.0741 | 0.0007 | 0.93 | 0.82 | 995.3 | 28 | 979 | 69 | 1042 | 19 | 93.95 |
| G-55b - 23 | 1 | 61.8 | 1050 | 0.06 | 0.3150 | 0.0170 | 5.40 | 0.0414 | 0.0033 | 7.97 | 0.0549 | 0.0014 | 2.55 | 0.73 | 277.7 | 13 | 261.5 | 21 | 400 | 58 | 94.17 |
| G-55b - 14 | 1 | 137 | 253 | 0.62 | 0.1705 | 0.0110 | 6.45 | 0.0236 | 0.0018 | 7.63 | 0.0525 | 0.0025 | 4.76 | 0.36 | 159.6 | 9.1 | 150.3 | 11 | 280 | 100 | 94.17 |
| G-55b - 47 | 1 | 43.8 | 195.9 | 0.25 | 0.8090 | 0.0460 | 5.69 | 0.0961 | 0.0075 | 7.80 | 0.0609 | 0.0017 | 2.79 | 0.66 | 601 | 26 | 592 | 44 | 627 | 60 | 94.42 |
| G-55b - 37 | 0 | 240 | 294 | 0.92 | 0.3160 | 0.0170 | 5.38 | 0.0438 | 0.0034 | 7.77 | 0.0524 | 0.0016 | 3.05 | 0.45 | 278.7 | 13 | 276.2 | 21 | 291 | 71 | 94.91 |
| G-55b - 3 | 0 | 52.2 | 950 | 0.06 | 0.6340 | 0.0290 | 4.57 | 0.0800 | 0.0061 | 7.63 | 0.0578 | 0.0008 | 1.38 | 0.66 | 498.4 | 18 | 496 | 36 | 521 | 30 | 95.20 |
| G-55b - 39 | 0 | 58.3 | 777 | 0.08 | 0.8710 | 0.0390 | 4.48 | 0.1019 | 0.0077 | 7.56 | 0.0616 | 0. | | | | | | | | | |

| | | | | | | | | | | | | | | | | | | | | | |
|------------|---|---------|-------|-------|--------|--------|-------|--------|--------|-------|--------|--------|-------|------|--------|-----|-------|-----|--------|-----|--------|
| G-55b - 79 | 1 | 95.2 | 275 | 0.39 | 1.6690 | 0.0860 | 5.15 | 0.1684 | 0.0130 | 7.72 | 0.0716 | 0.0012 | 1.68 | 0.75 | 996 | 32 | 1003 | 73 | 973 | 33 | 103.08 |
| G-55b - 33 | 0 | 46.7 | 86 | 0.56 | 0.7000 | 0.0410 | 5.86 | 0.0870 | 0.0068 | 7.82 | 0.0580 | 0.0025 | 4.31 | 0.24 | 538 | 25 | 538 | 40 | 507 | 93 | 106.11 |
| G-55b - 53 | 0 | 32.5 | 47.1 | 0.78 | 0.6820 | 0.0560 | 8.21 | 0.0851 | 0.0067 | 7.87 | 0.0577 | 0.0036 | 6.24 | 0.44 | 525 | 33 | 526 | 40 | 480 | 130 | 109.58 |
| G-95 - 30 | | 533 | 4130 | 0.14 | 0.6540 | 0.0310 | 4.74 | 0.0698 | 0.0055 | 7.88 | 0.0693 | 0.0005 | 0.78 | 0.94 | 510.4 | 19 | 435 | 33 | 908 | 16 | 47.91 |
| G-95 - 6 | | 1205000 | 56500 | 23.86 | 1.5210 | 0.0670 | 4.40 | 0.1210 | 0.0092 | 7.60 | 0.0898 | 0.0009 | 0.99 | 0.82 | 938.4 | 27 | 737 | 53 | 1421 | 19 | 51.86 |
| G-95 - 29 | | 846 | 3400 | 0.28 | 1.0560 | 0.0500 | 4.73 | 0.1025 | 0.0079 | 7.71 | 0.0767 | 0.0006 | 0.74 | 0.92 | 732 | 24 | 629 | 46 | 1113 | 15 | 56.51 |
| G-95 - 3 | | 694 | 4160 | 0.19 | 1.1900 | 0.0610 | 5.13 | 0.1086 | 0.0086 | 7.92 | 0.0783 | 0.0005 | 0.66 | 0.96 | 795 | 28 | 664 | 50 | 1154 | 13 | 57.54 |
| G-95 - 33 | | 398 | 2843 | 0.15 | 1.1540 | 0.0550 | 4.77 | 0.1101 | 0.0084 | 7.63 | 0.0766 | 0.0012 | 1.57 | 0.81 | 778 | 26 | 673 | 49 | 1109 | 32 | 60.69 |
| G-95 - 24 | | 284 | 2740 | 0.12 | 1.2680 | 0.0740 | 5.84 | 0.1200 | 0.0100 | 8.33 | 0.0780 | 0.0008 | 1.05 | 0.96 | 830 | 33 | 730 | 58 | 1146 | 21 | 63.70 |
| G-95 - 15 | | 307 | 3060 | 0.11 | 1.1630 | 0.0660 | 5.67 | 0.1115 | 0.0091 | 8.16 | 0.0747 | 0.0009 | 1.18 | 0.95 | 782 | 31 | 681 | 53 | 1061 | 24 | 64.18 |
| G-95 - 21 | | 292.4 | 2514 | 0.13 | 1.2640 | 0.0560 | 4.43 | 0.1223 | 0.0093 | 7.60 | 0.0745 | 0.0006 | 0.75 | 0.83 | 829.6 | 25 | 743 | 53 | 1054 | 15 | 70.49 |
| G-95 - 28 | | 674 | 2702 | 0.28 | 1.3520 | 0.0590 | 4.36 | 0.1296 | 0.0098 | 7.56 | 0.0764 | 0.0005 | 0.64 | 0.84 | 868.1 | 26 | 785.4 | 56 | 1105 | 13 | 71.08 |
| G-95 - 35 | | 150 | 2490 | 0.07 | 1.3440 | 0.0610 | 4.54 | 0.1331 | 0.0100 | 7.51 | 0.0744 | 0.0006 | 0.81 | 0.89 | 864 | 27 | 805 | 59 | 1052 | 16 | 76.52 |
| G-95 - 2 | | 571 | 2124 | 0.29 | 1.7510 | 0.0870 | 4.97 | 0.1553 | 0.0120 | 7.73 | 0.0803 | 0.0008 | 1.01 | 0.93 | 1026 | 32 | 931 | 67 | 1204 | 20 | 77.33 |
| G-95 - 17 | | 287 | 2590 | 0.12 | 1.4020 | 0.0630 | 4.49 | 0.1349 | 0.0110 | 8.15 | 0.0742 | 0.0006 | 0.74 | 0.94 | 890 | 27 | 815 | 60 | 1045 | 15 | 77.99 |
| G-95 - 8 | | 745 | 3325 | 0.25 | 1.6840 | 0.0830 | 4.93 | 0.1540 | 0.0120 | 7.79 | 0.0793 | 0.0005 | 0.58 | 0.97 | 1002 | 32 | 923 | 66 | 1178 | 12 | 78.35 |
| G-95 - 9 | | 685 | 2410 | 0.32 | 1.7220 | 0.0790 | 4.59 | 0.1577 | 0.0120 | 7.61 | 0.0788 | 0.0008 | 1.04 | 0.92 | 1016 | 30 | 944 | 67 | 1165 | 21 | 81.03 |
| G-95 - 14 | | 245 | 2478 | 0.10 | 1.7480 | 0.0900 | 5.15 | 0.1598 | 0.0130 | 8.14 | 0.0790 | 0.0015 | 1.90 | 0.89 | 1025 | 34 | 955 | 72 | 1169 | 37 | 81.69 |
| G-95 - 34 | | 148 | 2950 | 0.05 | 1.5550 | 0.0820 | 5.27 | 0.1498 | 0.0120 | 8.01 | 0.0759 | 0.0005 | 0.70 | 0.98 | 952 | 33 | 900 | 69 | 1092 | 14 | 82.42 |
| G-95 - 5 | | 1285000 | 56800 | 25.25 | 1.4610 | 0.0650 | 4.45 | 0.1423 | 0.0110 | 7.73 | 0.0739 | 0.0004 | 0.57 | 0.82 | 914 | 27 | 857 | 61 | 1039 | 11 | 82.48 |
| G-95 - 39 | | 152 | 1690 | 0.09 | 1.7880 | 0.0830 | 4.64 | 0.1672 | 0.0130 | 7.78 | 0.0794 | 0.0005 | 0.63 | 0.97 | 1040 | 30 | 996 | 73 | 1181 | 12 | 84.34 |
| G-95 - 40 | | 240 | 1976 | 0.14 | 1.5260 | 0.0700 | 4.59 | 0.1514 | 0.0120 | 7.93 | 0.0751 | 0.0007 | 0.87 | 0.84 | 940 | 28 | 909 | 65 | 1072 | 17 | 84.79 |
| G-95 - 4 | | 298 | 2399 | 0.10 | 1.8720 | 0.0820 | 4.38 | 0.1713 | 0.0130 | 7.59 | 0.0783 | 0.0005 | 0.64 | 0.88 | 1070.7 | 29 | 1019 | 71 | 1155 | 13 | 88.23 |
| G-95 - 16 | | 252 | 1854 | 0.14 | 2.1310 | 0.0950 | 4.46 | 0.1867 | 0.0140 | 7.50 | 0.0815 | 0.0006 | 0.75 | 0.88 | 1159 | 31 | 1103 | 77 | 1233 | 15 | 89.46 |
| G-95 - 25 | | 127.1 | 2794 | 0.05 | 1.8790 | 0.0800 | 4.26 | 0.1746 | 0.0130 | 7.45 | 0.0782 | 0.0005 | 0.59 | 0.89 | 1073.5 | 28 | 1037 | 72 | 1150 | 12 | 90.17 |
| G-95 - 1 | | 83.3 | 2091 | 0.04 | 1.8630 | 0.0830 | 4.46 | 0.1730 | 0.0130 | 7.51 | 0.0777 | 0.0005 | 0.58 | 0.88 | 1067 | 30 | 1028 | 72 | 1138 | 11 | 90.33 |
| G-95 - 7 | | 1321 | 3066 | 0.48 | 2.2460 | 0.1000 | 4.45 | 0.1950 | 0.0150 | 7.69 | 0.0826 | 0.0005 | 0.55 | 0.95 | 1195 | 32 | 1148 | 82 | 1258 | 11 | 91.26 |
| G-95 - 12 | | 100.7 | 1785 | 0.06 | 1.7900 | 0.0790 | 4.41 | 0.1700 | 0.0130 | 7.65 | 0.0764 | 0.0006 | 0.80 | 0.70 | 1041.6 | 29 | 1012 | 71 | 1106 | 16 | 91.50 |
| G-95 - 13 | | 51.4 | 2528 | 0.02 | 1.9520 | 0.0850 | 4.35 | 0.1790 | 0.0140 | 7.82 | 0.0778 | 0.0003 | 0.44 | 0.93 | 1098.7 | 29 | 1061 | 74 | 1142.1 | 8.8 | 92.90 |
| G-95 - 37 | | 286 | 1610 | 0.11 | 2.0290 | 0.1100 | 5.42 | 0.1881 | 0.0150 | 7.97 | 0.0798 | 0.0009 | 1.15 | 0.98 | 1123 | 35 | 1110 | 81 | 1190 | 22 | 93.28 |
| G-95 - 11 | | 304 | 551 | 0.61 | 2.0940 | 0.0920 | 4.39 | 0.1896 | 0.0140 | 7.38 | 0.0799 | 0.0007 | 0.86 | 0.71 | 1146.5 | 30 | 1119 | 77 | 1195 | 17 | 93.64 |
| G-95 - 18 | | 119.4 | 1042 | 0.13 | 1.6640 | 0.0760 | 4.57 | 0.1619 | 0.0120 | 7.41 | 0.0735 | 0.0005 | 0.68 | 0.93 | 995 | 29 | 968 | 69 | 1026 | 14 | 94.35 |
| G-95 - 27 | | 213 | 2296 | 0.09 | 1.8070 | 0.0810 | 4.48 | 0.1747 | 0.0130 | 7.44 | 0.0761 | 0.0006 | 0.76 | 0.92 | 1048 | 30 | 1038 | 73 | 1097 | 15 | 94.62 |
| G-95 - 26 | | 89 | 1387 | 0.07 | 1.8620 | 0.0810 | 4.35 | 0.1793 | 0.0140 | 7.81 | 0.0762 | 0.0006 | 0.79 | 0.77 | 1067.6 | 29 | 1063 | 74 | 1101 | 16 | 96.55 |
| G-95 - 20 | | 107.4 | 827 | 0.14 | 1.6690 | 0.0740 | 4.43 | 0.1651 | 0.0120 | 7.27 | 0.0728 | 0.0005 | 0.74 | 0.82 | 996.5 | 28 | 985 | 69 | 1008 | 15 | 97.72 |
| G-95 - 32 | | 109.4 | 1474 | 0.08 | 1.6750 | 0.0750 | 4.48 | 0.1683 | 0.0130 | 7.72 | 0.0734 | 0.0005 | 0.63 | 0.90 | 999 | 28 | 1003 | 71 | 1025 | 13 | 97.85 |
| G-95 - 10 | | 99.4 | 800 | 0.14 | 1.8080 | 0.0840 | 4.65 | 0.1742 | 0.0140 | 8.04 | 0.0744 | 0.0006 | 0.78 | 0.93 | 1048 | 30 | 1035 | 75 | 1056 | 14 | 98.01 |
| G-95 - 23 | | 63.8 | 1758 | 0.04 | 1.9660 | 0.0900 | 4.58 | 0.1862 | 0.0140 | 7.52 | 0.0771 | 0.0006 | 0.79 | 0.81 | 1103 | 31 | 1101 | 77 | 1123 | 16 | 98.04 |
| G-95 - 19 | | 183 | 1220 | 0.16 | 2.5150 | 0.1100 | 4.37 | 0.2192 | 0.0170 | 7.76 | 0.0842 | 0.0006 | 0.68 | 0.93 | 1276 | 33 | 1278 | 88 | 1297 | 13 | 98.54 |
| G-95 - 36 | | 92.6 | 715 | 0.14 | 1.5790 | 0.0700 | 4.43 | 0.1630 | 0.0120 | 7.36 | 0.0721 | 0.0006 | 0.85 | 0.78 | 961.7 | 28 | 973.5 | 68 | 987 | 17 | 98.63 |
| G-95 - 22 | | 99.7 | 1265 | 0.09 | 1.6920 | 0.0740 | 4.37 | 0.1679 | 0.0130 | 7.74 | 0.0730 | 0.0005 | 0.74 | 0.86 | 1005 | 28 | 1000 | 70 | 1012 | 15 | 98.81 |
| G-95 - 38 | | 875 | 2274 | 0.42 | 2.3140 | 0.1200 | 5.19 | 0.2096 | 0.0170 | 8.11 | 0.0817 | 0.0006 | 0.67 | 0.97 | 1214 | 36 | 1226 | 89 | 1237 | 13 | 99.11 |
| G-95 - 31 | | 78.6 | 1456 | 0.06 | 2.0510 | 0.0920 | 4.49 | 0.1944 | 0.0150 | 7.72 | 0.0776 | 0.0005 | 0.66 | 0.93 | 1132 | 31 | 1145 | 81 | 1137 | 13 | 100.70 |
| G-54 - 6 | 0 | 28.1 | 571 | 0.05 | 0.3470 | 0.0130 | 3.75 | 0.0421 | 0.0010 | 2.38 | 0.0598 | 0.0016 | 2.68 | 0.70 | 302.3 | 9.9 | 265.5 | 6.3 | 591 | 60 | 44.92 |
| G-54 - 70 | 1 | 24.2 | 574 | 0.05 | 0.4000 | 0.0200 | 5.00 | 0.0477 | 0.0014 | 2.94 | 0.0608 | 0.0020 | 3.29 | 0.78 | 341 | 15 | 300.1 | 8.9 | 625 | 77 | 48.02 |
| G-54 - 31 | 0 | 23.7 | 849 | 0.03 | 0.3435 | 0.0140 | 4.08 | 0.0424 | 0.0012 | 2.83 | 0.0587 | 0.0016 | 2.73 | 0.75 | 299.7 | 11 | 267.9 | 7.5 | 551 | 59 | 48.62 |
| G-54 - 5 | 0 | 38.1 | 395 | 0.11 | 0.7390 | 0.0550 | 7.44 | 0.0768 | 0.0044 | 5.73 | 0.0698 | 0.0026 | 3.72 | 0.87 | 561 | 37 | 477 | 27 | 918 | 94 | 51.96 |
| G-54 - 18 | 0 | 56.4 | 1146 | 0.05 | 0.3920 | 0.1700 | 43.37 | 0.0479 | 0.0150 | 31.32 | 0.0593 | 0.0025 | 4.22 | 0.95 | 335 | 88 | 301 | 89 | 575 | 80 | 52.35 |
| G-54 - 69 | 1 | 25.3 | 592 | 0.05 | 0.4030 | 0.0190 | 4.71 | 0.0495 | 0.0018 | 3.64 | 0.0592 | 0.0017 | 2.87 | 0.79 | 344 | 15 | 311.3 | 11 | 566 | 58 | 55.00 |
| G-54 - 1 | 0 | 53 | 542 | 0.11 | 0.3780 | 0.0220 | 5.82 | 0.0470 | 0.0018 | 3.83 | 0.0582 | 0.0019 | 3.26 | 0.85 | 325 | 16 | 296.2 | 11 | 526 | 74 | 56.31 |
| G-54 - 88 | 1 | 43.1 | 369 | 0.13 | 0.6290 | 0.0270 | 4.29 | 0.0709 | 0.0021 | 2.96 | 0.0644 | 0.0018 | 2.80 | 0.76 | 495 | 17 | 441.3 | 12 | 750 | 61 | 58.84 |
| G-54 - 2 | 0 | 79.8 | 105.3 | 0.86 | 0.3340 | 0.0210 | 6.29 | 0.0434 | 0.0013 | 3.00 | 0.0569 | 0.0035 | 6.15 | 0.28 | 296 | 16 | 274 | 8.1 | 450 | 130 | 60.89 |
| G-54 - 90 | 1 | 12.43 | 387 | 0.04 | 0.2870 | 0.1900 | 66.20 | 0.0381 | 0.0073 | 19.16 | 0.0548 | 0.0110 | 20.07 | 0.64 | 256 | 100 | 241.2 | 44 | 388 | 250 | 62.16 |
| G-54 - 73 | 1 | 11.83</ | | | | | | | | | | | | | | | | | | | |

| | | | | | | | | | | | | | | | | | | | | | |
|-----------|---|-----------|-------|------|---------|--------|-------|--------|--------|------|--------|--------|------|------|-------|-----|--------|-----|------|-----|--------|
| G-54 - 28 | 0 | 80.1 | 543 | 0.16 | 1.9180 | 0.0610 | 3.18 | 0.1687 | 0.0039 | 2.31 | 0.0825 | 0.0017 | 2.06 | 0.76 | 1086 | 21 | 1005 | 22 | 1255 | 39 | 80.08 |
| G-54 - 89 | 0 | 86.4 | 161.2 | 0.60 | 9.4800 | 0.3400 | 3.59 | 0.3877 | 0.0110 | 2.84 | 0.1779 | 0.0040 | 2.25 | 0.78 | 2384 | 35 | 2112 | 50 | 2632 | 38 | 80.24 |
| G-54 - 20 | 0 | 35.9 | 228 | 0.18 | 0.4130 | 0.0220 | 5.33 | 0.0538 | 0.0016 | 2.97 | 0.0557 | 0.0023 | 4.13 | 0.64 | 350 | 15 | 337.8 | 9.5 | 420 | 86 | 80.43 |
| G-54 - 66 | 1 | 24.2 | 1030 | 0.03 | 0.3260 | 0.0390 | 11.96 | 0.0444 | 0.0041 | 9.23 | 0.0535 | 0.0015 | 2.80 | 0.70 | 286 | 27 | 280.1 | 25 | 348 | 57 | 80.49 |
| G-54 - 14 | 0 | 260 | 397 | 0.62 | 0.3050 | 0.0150 | 4.92 | 0.0417 | 0.0010 | 2.40 | 0.0532 | 0.0021 | 3.95 | 0.61 | 270.4 | 12 | 263.5 | 6.4 | 321 | 86 | 82.09 |
| G-54 - 65 | 1 | 7.39 | 715 | 0.01 | 0.2584 | 0.0094 | 3.64 | 0.0361 | 0.0009 | 2.58 | 0.0520 | 0.0015 | 2.88 | 0.62 | 233.2 | 7.5 | 228.6 | 5.8 | 278 | 66 | 82.23 |
| G-54 - 21 | 0 | 96.8 | 261 | 0.41 | 10.9700 | 0.3200 | 2.92 | 0.4193 | 0.0094 | 2.24 | 0.1899 | 0.0035 | 1.84 | 0.78 | 252.0 | 28 | 225.7 | 43 | 2741 | 30 | 82.34 |
| G-54 - 62 | 1 | 69 | 585 | 0.11 | 0.2696 | 0.0100 | 3.71 | 0.0375 | 0.0009 | 2.27 | 0.0522 | 0.0017 | 3.26 | 0.49 | 242.2 | 8.4 | 237.4 | 5.3 | 287 | 74 | 82.72 |
| G-54 - 46 | 0 | 103.1 | 430 | 0.27 | 0.2521 | 0.0100 | 3.97 | 0.0353 | 0.0008 | 2.27 | 0.0519 | 0.0017 | 3.28 | 0.56 | 228.1 | 8.3 | 223.4 | 5 | 270 | 73 | 82.74 |
| G-54 - 67 | 0 | 66.5 | 673 | 0.11 | 0.4600 | 0.0150 | 3.26 | 0.0596 | 0.0013 | 2.18 | 0.0561 | 0.0014 | 2.50 | 0.64 | 384.1 | 11 | 372.9 | 8.1 | 450 | 55 | 82.87 |
| G-54 - 13 | 1 | 153 | 431 | 0.32 | 0.2852 | 0.0120 | 4.21 | 0.0395 | 0.0010 | 2.53 | 0.0525 | 0.0018 | 3.43 | 0.58 | 254.6 | 9.2 | 249.4 | 6.3 | 298 | 75 | 83.69 |
| G-54 - 74 | 0 | 58.9 | 185.2 | 0.36 | 1.7020 | 0.0620 | 3.64 | 0.1592 | 0.0041 | 2.58 | 0.0777 | 0.0020 | 2.57 | 0.71 | 1008 | 23 | 952 | 23 | 1133 | 51 | 84.02 |
| G-54 - 64 | 0 | 70.3 | 288 | 0.27 | 0.4960 | 0.0210 | 4.23 | 0.0639 | 0.0016 | 2.50 | 0.0563 | 0.0019 | 3.37 | 0.60 | 408 | 14 | 399 | 9.8 | 473 | 66 | 84.36 |
| G-54 - 82 | 1 | 8.52 | 1089 | 0.01 | 0.2464 | 0.0087 | 3.53 | 0.0348 | 0.0008 | 2.42 | 0.0515 | 0.0013 | 2.52 | 0.70 | 223.6 | 7 | 220.2 | 5.3 | 258 | 58 | 85.35 |
| G-54 - 47 | 1 | 71.6 | 327 | 0.24 | 0.2461 | 0.0120 | 4.88 | 0.0346 | 0.0010 | 2.89 | 0.0517 | 0.0022 | 4.26 | 0.50 | 223.1 | 9.7 | 219.5 | 6.4 | 256 | 91 | 85.74 |
| G-54 - 16 | 0 | 413 | 553 | 0.83 | 0.2806 | 0.0096 | 3.42 | 0.0390 | 0.0010 | 2.43 | 0.0522 | 0.0014 | 2.68 | 0.63 | 251 | 7.6 | 246.8 | 5.9 | 287 | 61 | 85.99 |
| G-54 - 77 | 0 | 95.4 | 89 | 1.20 | 1.6320 | 0.1400 | 8.58 | 0.1566 | 0.0120 | 7.66 | 0.0757 | 0.0024 | 3.17 | 0.93 | 981 | 65 | 938 | 67 | 1080 | 68 | 86.85 |
| G-54 - 43 | 1 | 11.62 | 401 | 0.03 | 0.2640 | 0.0110 | 4.17 | 0.0370 | 0.0010 | 2.70 | 0.0518 | 0.0017 | 3.28 | 0.62 | 237.4 | 8.9 | 234.1 | 6.5 | 269 | 72 | 87.03 |
| G-54 - 11 | 1 | 7.37 | 294 | 0.03 | 0.2458 | 0.0110 | 4.48 | 0.0346 | 0.0010 | 2.89 | 0.0515 | 0.0019 | 3.69 | 0.57 | 222.9 | 9.3 | 219.5 | 6.3 | 252 | 80 | 87.10 |
| G-54 - 91 | 0 | 53.5 | 240 | 0.25 | 7.0300 | 0.2900 | 4.13 | 0.3581 | 0.0110 | 3.07 | 0.1424 | 0.0028 | 1.97 | 0.89 | 2113 | 35 | 1972 | 52 | 2256 | 34 | 87.41 |
| G-54 - 40 | 1 | 10.4 | 289 | 0.04 | 0.2530 | 0.0120 | 4.74 | 0.0357 | 0.0009 | 2.38 | 0.0516 | 0.0023 | 4.46 | 0.37 | 228.7 | 9.9 | 225.9 | 5.3 | 258 | 98 | 87.56 |
| G-54 - 25 | 0 | 55.5 | 820 | 0.08 | 0.2707 | 0.0100 | 3.69 | 0.0379 | 0.0010 | 2.61 | 0.0519 | 0.0014 | 2.70 | 0.68 | 243 | 8.1 | 239.6 | 6.1 | 273 | 61 | 87.77 |
| G-54 - 79 | 1 | 150 | 3500 | 0.04 | 0.2930 | 0.0093 | 3.17 | 0.0410 | 0.0011 | 2.68 | 0.0523 | 0.0011 | 2.11 | 0.75 | 260.8 | 7.4 | 258.8 | 7 | 294 | 46 | 88.03 |
| G-54 - 60 | 0 | 56 | 452 | 0.14 | 0.5650 | 0.0260 | 4.60 | 0.0713 | 0.0023 | 3.23 | 0.0575 | 0.0015 | 2.61 | 0.83 | 454 | 16 | 443.8 | 14 | 504 | 55 | 88.06 |
| G-54 - 86 | 1 | 30 | 780 | 0.04 | 0.4085 | 0.0140 | 3.43 | 0.0545 | 0.0012 | 2.20 | 0.0545 | 0.0013 | 2.39 | 0.72 | 347.6 | 9.9 | 342 | 7.4 | 386 | 55 | 88.60 |
| G-54 - 71 | 0 | 158.4 | 361 | 0.49 | 1.9990 | 0.0640 | 3.20 | 0.1804 | 0.0038 | 2.11 | 0.0802 | 0.0017 | 2.12 | 0.76 | 1114 | 22 | 1069.3 | 21 | 1201 | 43 | 89.03 |
| G-54 - 93 | 1 | 5.18 | 681 | 0.01 | 0.2420 | 0.0089 | 3.68 | 0.0344 | 0.0008 | 2.27 | 0.0513 | 0.0016 | 3.12 | 0.54 | 219.9 | 7.3 | 217.7 | 4.9 | 244 | 71 | 89.22 |
| G-54 - 23 | 0 | 205 | 302 | 0.76 | 0.6810 | 0.0340 | 4.99 | 0.0832 | 0.0020 | 2.40 | 0.0594 | 0.0020 | 3.37 | 0.81 | 527 | 20 | 514.9 | 12 | 576 | 75 | 89.39 |
| G-54 - 42 | 0 | 71.3 | 262 | 0.28 | 0.3540 | 0.0150 | 4.24 | 0.0480 | 0.0016 | 3.33 | 0.0534 | 0.0015 | 2.81 | 0.75 | 307 | 11 | 302.2 | 9.7 | 338 | 66 | 89.41 |
| G-54 - 17 | 0 | 86.5 | 381 | 0.25 | 1.0560 | 0.0370 | 3.50 | 0.1168 | 0.0030 | 2.57 | 0.0657 | 0.0014 | 2.13 | 0.80 | 731 | 18 | 712 | 18 | 793 | 46 | 89.79 |
| G-54 - 80 | 0 | 94 | 8430 | 0.01 | 0.2533 | 0.0073 | 2.88 | 0.0359 | 0.0008 | 2.12 | 0.0513 | 0.0010 | 1.87 | 0.76 | 229.2 | 6 | 227.2 | 4.7 | 252 | 43 | 90.16 |
| G-54 - 33 | 0 | 12.18 | 1200 | 0.01 | 0.2627 | 0.0087 | 3.31 | 0.0370 | 0.0008 | 2.13 | 0.0515 | 0.0012 | 2.33 | 0.71 | 236.7 | 7 | 234.4 | 4.9 | 259 | 55 | 90.50 |
| G-54 - 26 | 1 | 13.86 | 428 | 0.03 | 0.2354 | 0.0110 | 4.67 | 0.0335 | 0.0009 | 2.57 | 0.0511 | 0.0021 | 4.11 | 0.48 | 214.5 | 8.7 | 212.3 | 5.4 | 234 | 86 | 90.73 |
| G-54 - 9 | 1 | 10.79 | 1908 | 0.01 | 0.2428 | 0.0078 | 3.21 | 0.0345 | 0.0008 | 2.32 | 0.0511 | 0.0011 | 2.15 | 0.74 | 220.6 | 6.4 | 218.8 | 5 | 240 | 51 | 91.17 |
| G-54 - 35 | 1 | 34 | 486 | 0.08 | 0.2472 | 0.0100 | 4.05 | 0.0351 | 0.0009 | 2.42 | 0.0513 | 0.0018 | 3.51 | 0.51 | 224.1 | 8.1 | 222.1 | 5.3 | 242 | 76 | 91.78 |
| G-54 - 12 | 0 | 66.6 | 288 | 0.26 | 1.1400 | 0.0700 | 6.14 | 0.1246 | 0.0066 | 5.30 | 0.0665 | 0.0019 | 2.86 | 0.89 | 772 | 38 | 757 | 39 | 816 | 59 | 92.77 |
| G-54 - 36 | 0 | 151.5 | 149 | 1.13 | 3.7700 | 0.1700 | 4.51 | 0.2685 | 0.0085 | 3.17 | 0.1016 | 0.0026 | 2.56 | 0.83 | 1584 | 39 | 1533 | 44 | 1651 | 48 | 92.85 |
| G-54 - 72 | 0 | 32.2 | 2500 | 0.01 | 0.2612 | 0.0082 | 3.14 | 0.0370 | 0.0009 | 2.35 | 0.0513 | 0.0011 | 2.14 | 0.73 | 235.6 | 6.7 | 234.1 | 5.4 | 252 | 48 | 92.90 |
| G-54 - 8 | 0 | 610 | 1275 | 0.52 | 0.5977 | 0.0180 | 3.01 | 0.0757 | 0.0017 | 2.25 | 0.0573 | 0.0012 | 2.09 | 0.72 | 475.6 | 11 | 470.4 | 10 | 503 | 45 | 93.52 |
| G-54 - 19 | 1 | 5.25 | 531 | 0.01 | 0.2387 | 0.0100 | 4.19 | 0.0340 | 0.0008 | 2.44 | 0.0509 | 0.0017 | 3.34 | 0.60 | 217.2 | 8.2 | 215.6 | 5.2 | 230 | 73 | 93.74 |
| G-54 - 83 | 0 | 544 | 654 | 0.93 | 0.2984 | 0.0110 | 3.69 | 0.0416 | 0.0009 | 2.21 | 0.0521 | 0.0016 | 3.07 | 0.55 | 264.9 | 9 | 262.9 | 5.7 | 280 | 71 | 93.89 |
| G-54 - 22 | 1 | 5.56 | 239 | 0.03 | 0.2350 | 0.0330 | 14.04 | 0.0321 | 0.0020 | 6.23 | 0.0532 | 0.0041 | 7.71 | 0.66 | 214 | 25 | 203.4 | 12 | 320 | 150 | 95.05 |
| G-54 - 15 | 0 | 448 | 566 | 0.87 | 0.7110 | 0.0230 | 3.23 | 0.0873 | 0.0020 | 2.29 | 0.0591 | 0.0013 | 2.20 | 0.73 | 544.8 | 14 | 539.6 | 12 | 567 | 50 | 95.17 |
| G-54 - 61 | 1 | 8.83 | 862 | 0.01 | 0.2457 | 0.0084 | 3.42 | 0.0352 | 0.0008 | 2.27 | 0.0510 | 0.0014 | 2.75 | 0.60 | 223 | 6.9 | 223.1 | 5 | 234 | 62 | 95.34 |
| G-54 - 68 | 0 | 39.5 | 131 | 0.34 | 1.6990 | 0.0690 | 4.06 | 0.1662 | 0.0049 | 2.95 | 0.0738 | 0.0021 | 2.85 | 0.71 | 1006 | 26 | 991 | 27 | 1027 | 58 | 96.49 |
| G-54 - 53 | 0 | 332 | 616 | 0.57 | 0.3574 | 0.0140 | 3.92 | 0.0489 | 0.0011 | 2.25 | 0.0530 | 0.0017 | 3.21 | 0.57 | 310 | 10 | 307.5 | 6.5 | 318 | 70 | 96.70 |
| G-54 - 39 | 1 | 11.24 | 665 | 0.02 | 0.2553 | 0.0094 | 3.68 | 0.0363 | 0.0008 | 2.23 | 0.0511 | 0.0016 | 3.13 | 0.53 | 230.7 | 7.6 | 229.8 | 5 | 237 | 68 | 96.96 |
| G-54 - 34 | 0 | 55.4 | 715 | 0.09 | 0.2543 | 0.0099 | 3.89 | 0.0362 | 0.0009 | 2.46 | 0.0511 | 0.0016 | 3.13 | 0.60 | 229.9 | 8 | 228.9 | 5.5 | 236 | 69 | 96.99 |
| G-54 - 10 | 1 | Below LOD | 446 | 0.01 | 0.1907 | 0.0090 | 4.72 | 0.0270 | 0.0007 | 2.66 | 0.0515 | 0.0022 | 4.27 | 0.44 | 177 | 7.6 | 172 | 4.5 | 251 | 90 | 97.18 |
| G-54 - 56 | 0 | 117.3 | 322 | 0.41 | 0.8440 | 0.0320 | 3.79 | 0.1009 | 0.0023 | 2.28 | 0.0610 | 0.0016 | 2.62 | 0.73 | 620 | 18 | 619.5 | 14 | 634 | 57 | 97.71 |
| G-54 - 54 | 0 | 140.2 | 377 | 0.43 | 2.2370 | 0.0720 | 3.22 | 0.2016 | 0.0049 | 2.43 | 0.0804 | 0.0018 | 2.24 | 0.72 | 1192 | 23 | 1184 | 27 | 1206 | 43 | 98.18 |
| G-54 - 41 | 0 | 11.29 | 332 | 0.04 | 0.2475 | 0.0097 | 3.92 | 0.0354 | 0.0009 | 2.52 | 0.0508 | 0.0015 | 2.95 | 0.66 | 224.4 | 7.9 | 224 | 5.5 | 227 | 68 | 98.68 |
| G-54 - 51 | 1 | 131.4 | 248 | 0.58 | 0.7420 | 0.0350 | 4.72 | 0.0916 | 0.0037 | 4.04 | 0.0588 | 0.0017 | 2.89 | 0.79 | 563 | 21 | 565 | 22 | 568 | 55 | 99.47 |
| G-54 - 7 | 1 | 9.69 | 536 | 0.02 | 0.2494 | 0.0110 | 4.41 | 0.0357 | 0.0012 | 3.37 | 0.0509 | 0.0018 | 3.54 | 0.62 | 225.8 | 9 | 225.9 | 7.3 | 227 | 78 | 99.52 |
| G-54 - 4 | 1 | 5.05 | 223.5 | 0.02 | 0.2367 | 0.0110 | 4.65 | 0.0341 | 0.0008 | 2.40 | 0.0507 | 0.0022 | 4.34 | 0.38 | 215.4 | 9 | 216.3 | 5.1 | 214 | 92 | 101.07 |
| G-54 - 30 | 0 | 44.3 | 97 | 0.50 | 1.4710 | 0.0650 | 4.42 | 0.1531 | 0.0038 | 2.48 | 0.0698 | 0.0027 | 3.87 | 0.49 | 916 | 26 | 918 | 21 | 907 | 78 | 101.21 |
| G-54 - 59 | 1 | 10.3 | 840 | 0.01 | 0.2590 | 0.0150 | 5.79 | 0.0371 | 0.0014 | 3.78 | 0.0508 | 0.0015 | 2.95 | 0.89 | 234.1 | 12 | 234.7 | 8.7 | 226 | 67 | 103.85 |
| G-54 - 50 | 0 | 184.1 | 318 | 0.65 | 0.7740 | 0.0300 | 3.88 | 0.0950 | 0.0023 | 2.42 | 0.0591 | 0.0016 | 2.71 | 0.72 | 581 | 17 | 584.9 | 14 | 562 | 58 | 104.07 |
| G-54 - 48 | 0 | 18.62 | 756 | 0.03 | 0.2446 | 0.0086 | 3.52 | 0.0353 | 0.0008 | 2.24 | 0.0503 | 0.0013 | 2.58 | 0.68 | 222.1 | 7 | 223.6 | 4.9 | 206 | 60 | 108.54 |

| | | | | | | | | | | | | | | | | | | | | | |
|------------|---|-----------|-------|------|--------|--------|-------|--------|--------|------|--------|--------|-------|------|-------|-----|-------|-----|-----|-----|--------|
| G-52d - 71 | 0 | 7.21 | 250 | 0.03 | 0.2700 | 0.0140 | 5.19 | 0.0357 | 0.0010 | 2.78 | 0.0549 | 0.0027 | 4.92 | 0.36 | 242 | 11 | 225.9 | 6.1 | 390 | 110 | 57.92 |
| G-52d - 74 | 1 | 7.97 | 210 | 0.04 | 0.2820 | 0.0140 | 4.96 | 0.0372 | 0.0009 | 2.34 | 0.0550 | 0.0026 | 4.73 | 0.33 | 252 | 11 | 235.7 | 5.4 | 390 | 100 | 60.44 |
| G-52d - 69 | 0 | 1.91 | 96.7 | 0.02 | 0.2660 | 0.0190 | 7.14 | 0.0352 | 0.0011 | 3.13 | 0.0550 | 0.0038 | 6.91 | 0.29 | 238 | 15 | 222.9 | 6.6 | 360 | 140 | 61.92 |
| G-52d - 9 | 1 | 2.57 | 123.9 | 0.02 | 0.2650 | 0.0180 | 6.79 | 0.0356 | 0.0009 | 2.62 | 0.0542 | 0.0033 | 6.09 | 0.45 | 238 | 14 | 225.2 | 5.8 | 350 | 130 | 64.34 |
| G-52d - 63 | 0 | 4.04 | 658 | 0.01 | 0.2660 | 0.0170 | 6.39 | 0.0357 | 0.0010 | 2.81 | 0.0543 | 0.0028 | 5.16 | 0.62 | 239 | 14 | 225.8 | 6.3 | 350 | 110 | 64.51 |
| G-52d - 54 | 0 | 19.9 | 310 | 0.07 | 0.2560 | 0.0130 | 5.08 | 0.0347 | 0.0009 | 2.65 | 0.0537 | 0.0025 | 4.66 | 0.41 | 230.9 | 10 | 220.1 | 5.8 | 337 | 100 | 65.31 |
| G-52d - 26 | 0 | 1.85 | 217.2 | 0.01 | 0.2599 | 0.0100 | 3.85 | 0.0356 | 0.0008 | 2.27 | 0.0536 | 0.0017 | 3.17 | 0.57 | 234.5 | 8.9 | 225.8 | 5 | 342 | 72 | 66.02 |
| G-52d - 44 | 1 | 6.43 | 179 | 0.04 | 0.2550 | 0.0410 | 16.08 | 0.0345 | 0.0012 | 3.48 | 0.0537 | 0.0067 | 12.48 | 1.03 | 230 | 29 | 218.7 | 7.3 | 330 | 180 | 66.27 |
| G-52d - 33 | 1 | 2.82 | 140 | 0.02 | 0.2490 | 0.0150 | 6.02 | 0.0337 | 0.0009 | 2.79 | 0.0536 | 0.0028 | 5.22 | 0.50 | 225 | 12 | 213.8 | 5.9 | 320 | 110 | 66.81 |
| G-52d - 6 | 0 | 204 | 444 | 0.53 | 0.5110 | 0.0290 | 5.68 | 0.0626 | 0.0029 | 4.63 | 0.0593 | 0.0016 | 2.70 | 0.88 | 419 | 19 | 391.4 | 17 | 576 | 62 | 67.95 |
| G-52d - 17 | 1 | 0.18 | 123.6 | 0.00 | 0.2600 | 0.0240 | 9.23 | 0.0353 | 0.0010 | 2.83 | 0.0536 | 0.0043 | 8.02 | 0.55 | 234 | 19 | 223.8 | 6.4 | 310 | 170 | 72.19 |
| G-52d - 13 | 1 | 12.73 | 307 | 0.05 | 0.2690 | 0.0120 | 4.46 | 0.0369 | 0.0009 | 2.55 | 0.0531 | 0.0020 | 3.77 | 0.54 | 241.8 | 9.7 | 233.3 | 5.8 | 318 | 81 | 73.36 |
| G-52d - 11 | 0 | 2.92 | 207 | 0.01 | 0.2790 | 0.0170 | 6.09 | 0.0380 | 0.0010 | 2.58 | 0.0535 | 0.0030 | 5.61 | 0.39 | 250 | 13 | 240.6 | 6.1 | 320 | 120 | 75.19 |
| G-52d - 21 | 0 | 5.01 | 173 | 0.03 | 0.2700 | 0.0150 | 5.56 | 0.0370 | 0.0010 | 2.59 | 0.0532 | 0.0028 | 5.26 | 0.34 | 242 | 12 | 234.3 | 6 | 310 | 110 | 75.58 |
| G-52d - 73 | 1 | 3.79 | 293 | 0.01 | 0.2670 | 0.0140 | 5.24 | 0.0369 | 0.0011 | 2.98 | 0.0528 | 0.0024 | 4.55 | 0.50 | 240.2 | 11 | 233.3 | 6.6 | 306 | 97 | 76.24 |
| G-52d - 15 | 1 | 7.57 | 324 | 0.03 | 0.2560 | 0.0130 | 5.08 | 0.0355 | 0.0009 | 2.53 | 0.0524 | 0.0023 | 4.39 | 0.50 | 231.3 | 11 | 225 | 5.6 | 294 | 95 | 76.53 |
| G-52d - 29 | 0 | 6.16 | 178 | 0.04 | 0.2650 | 0.0150 | 5.66 | 0.0366 | 0.0009 | 2.57 | 0.0527 | 0.0029 | 5.50 | 0.29 | 238 | 12 | 231.5 | 5.9 | 300 | 120 | 77.17 |
| G-52d - 53 | 1 | 12.92 | 285 | 0.05 | 0.2590 | 0.0130 | 5.02 | 0.0360 | 0.0010 | 2.70 | 0.0524 | 0.0022 | 4.20 | 0.55 | 233.4 | 10 | 227.7 | 6 | 292 | 93 | 77.98 |
| G-52d - 55 | 0 | 7.79 | 219 | 0.04 | 0.2580 | 0.0170 | 6.59 | 0.0358 | 0.0009 | 2.54 | 0.0530 | 0.0032 | 6.04 | 0.40 | 232 | 14 | 226.6 | 5.6 | 290 | 120 | 78.14 |
| G-52d - 49 | 1 | 8 | 364 | 0.02 | 0.2590 | 0.0140 | 5.41 | 0.0358 | 0.0009 | 2.54 | 0.0523 | 0.0024 | 4.59 | 0.53 | 233.5 | 11 | 226.7 | 5.7 | 287 | 95 | 78.99 |
| G-52d - 50 | 0 | 7.6 | 278 | 0.02 | 0.2660 | 0.0130 | 4.89 | 0.0368 | 0.0010 | 2.72 | 0.0526 | 0.0024 | 4.56 | 0.39 | 239 | 11 | 232.7 | 6.5 | 290 | 98 | 80.24 |
| G-52d - 67 | 0 | Below LOD | 284 | 0.04 | 0.2680 | 0.0140 | 5.22 | 0.0373 | 0.0010 | 2.58 | 0.0522 | 0.0022 | 4.21 | 0.60 | 241 | 12 | 235.8 | 6 | 282 | 89 | 83.62 |
| G-52d - 30 | 1 | 0.31 | 115.9 | 0.00 | 0.2650 | 0.0250 | 9.43 | 0.0322 | 0.0010 | 3.01 | 0.0598 | 0.0050 | 8.36 | 0.50 | 238 | 19 | 204.5 | 6 | 560 | 160 | 85.92 |
| G-52d - 36 | 1 | 7.59 | 390 | 0.02 | 0.2543 | 0.0110 | 4.33 | 0.0358 | 0.0009 | 2.40 | 0.0516 | 0.0017 | 3.29 | 0.66 | 229.9 | 8.7 | 227 | 5.4 | 261 | 73 | 86.97 |
| G-52d - 72 | 1 | 9.66 | 304 | 0.04 | 0.2550 | 0.0140 | 5.49 | 0.0360 | 0.0009 | 2.56 | 0.0518 | 0.0023 | 4.44 | 0.60 | 230.3 | 11 | 227.9 | 5.7 | 261 | 94 | 87.32 |
| G-52d - 2 | 1 | 9.02 | 231.9 | 0.04 | 0.2640 | 0.0140 | 5.30 | 0.0369 | 0.0010 | 2.58 | 0.0520 | 0.0023 | 4.42 | 0.56 | 237.3 | 11 | 233.5 | 5.9 | 267 | 95 | 87.45 |
| G-52d - 42 | 1 | 14.07 | 291 | 0.05 | 0.2530 | 0.0130 | 5.14 | 0.0355 | 0.0008 | 2.34 | 0.0516 | 0.0022 | 4.26 | 0.57 | 228.2 | 11 | 225 | 5.1 | 257 | 93 | 87.55 |
| G-52d - 34 | 1 | 14.38 | 260 | 0.06 | 0.2620 | 0.0140 | 5.34 | 0.0369 | 0.0009 | 2.49 | 0.0517 | 0.0025 | 4.84 | 0.43 | 238.4 | 10 | 233.5 | 5.7 | 262 | 110 | 89.12 |
| G-52d - 25 | 1 | 5.57 | 606 | 0.01 | 0.2490 | 0.0110 | 4.42 | 0.0351 | 0.0009 | 2.51 | 0.0515 | 0.0019 | 3.69 | 0.55 | 225.2 | 9 | 222.5 | 5.5 | 248 | 80 | 89.72 |
| G-52d - 43 | 0 | 23.29 | 373 | 0.07 | 0.2514 | 0.0100 | 3.98 | 0.0356 | 0.0009 | 2.50 | 0.0515 | 0.0020 | 3.88 | 0.35 | 227.5 | 8.3 | 225.4 | 5.5 | 251 | 82 | 89.80 |
| G-52d - 57 | 1 | 19.5 | 306 | 0.01 | 0.2588 | 0.0110 | 4.25 | 0.0365 | 0.0008 | 2.28 | 0.0516 | 0.0020 | 3.88 | 0.43 | 233.4 | 9.1 | 230.8 | 5.2 | 256 | 84 | 90.16 |
| G-52d - 64 | 0 | 15.35 | 313 | 0.06 | 0.2580 | 0.0130 | 5.04 | 0.0368 | 0.0009 | 2.56 | 0.0511 | 0.0023 | 4.50 | 0.45 | 234.9 | 11 | 232.8 | 5.8 | 256 | 100 | 90.94 |
| G-52d - 46 | 1 | 5.43 | 367 | 0.02 | 0.2516 | 0.0120 | 4.77 | 0.0356 | 0.0009 | 2.64 | 0.0515 | 0.0022 | 4.27 | 0.46 | 227.6 | 9.3 | 225.6 | 5.8 | 247 | 90 | 91.34 |
| G-52d - 23 | 0 | 13.28 | 300 | 0.05 | 0.2530 | 0.0130 | 5.14 | 0.0357 | 0.0009 | 2.44 | 0.0514 | 0.0021 | 4.09 | 0.62 | 228.9 | 10 | 226.1 | 5.4 | 245 | 89 | 92.29 |
| G-52d - 70 | 1 | 7.96 | 252.8 | 0.03 | 0.2490 | 0.0130 | 5.22 | 0.0353 | 0.0009 | 2.61 | 0.0514 | 0.0026 | 5.06 | 0.31 | 225.5 | 11 | 223.6 | 5.7 | 240 | 110 | 93.17 |
| G-52d - 8 | 0 | 7.01 | 560 | 0.01 | 0.2501 | 0.0100 | 4.00 | 0.0355 | 0.0008 | 2.22 | 0.0512 | 0.0018 | 3.52 | 0.48 | 226.5 | 8.3 | 225.1 | 4.9 | 240 | 78 | 93.79 |
| G-52d - 7 | 1 | 7.74 | 521 | 0.02 | 0.1960 | 0.0089 | 4.54 | 0.0269 | 0.0007 | 2.64 | 0.0530 | 0.0022 | 4.15 | 0.43 | 181.2 | 7.6 | 170.8 | 4.5 | 310 | 90 | 94.26 |
| G-52d - 75 | 0 | 12.09 | 229 | 0.06 | 0.2550 | 0.0120 | 4.71 | 0.0362 | 0.0010 | 2.71 | 0.0513 | 0.0024 | 4.68 | 0.30 | 229.9 | 9.9 | 228.9 | 6.1 | 242 | 98 | 94.59 |
| G-52d - 5 | 0 | 3.93 | 602 | 0.01 | 0.2634 | 0.0095 | 3.61 | 0.0373 | 0.0008 | 2.20 | 0.0513 | 0.0016 | 3.12 | 0.51 | 237.3 | 7.7 | 236.1 | 5.1 | 247 | 68 | 95.59 |
| G-52d - 51 | 1 | 10 | 338 | 0.03 | 0.2490 | 0.0130 | 5.22 | 0.0355 | 0.0009 | 2.59 | 0.0511 | 0.0022 | 4.31 | 0.57 | 225.7 | 10 | 225.1 | 5.8 | 230 | 92 | 97.87 |
| G-52d - 39 | 1 | 9.6 | 261 | 0.04 | 0.2510 | 0.0120 | 4.78 | 0.0362 | 0.0009 | 2.46 | 0.0506 | 0.0022 | 4.35 | 0.43 | 227.3 | 10 | 229.3 | 5.5 | 232 | 100 | 98.84 |
| G-52d - 38 | 0 | 12.43 | 287 | 0.05 | 0.2570 | 0.0130 | 5.06 | 0.0366 | 0.0009 | 2.51 | 0.0511 | 0.0023 | 4.50 | 0.46 | 231.7 | 11 | 231.9 | 5.7 | 230 | 98 | 100.83 |
| G-52d - 1 | 0 | 21 | 389 | 0.06 | 0.2584 | 0.0110 | 4.26 | 0.0368 | 0.0009 | 2.50 | 0.0510 | 0.0018 | 3.53 | 0.56 | 233.1 | 8.8 | 233.2 | 5.7 | 230 | 77 | 101.39 |
| G-52d - 14 | 0 | 5.58 | 167.2 | 0.01 | 0.2580 | 0.0140 | 5.43 | 0.0369 | 0.0011 | 2.98 | 0.0510 | 0.0025 | 4.90 | 0.44 | 233 | 12 | 233.4 | 6.5 | 230 | 110 | 101.48 |
| G-52d - 37 | 0 | 8.48 | 363 | 0.03 | 0.2510 | 0.0110 | 4.38 | 0.0359 | 0.0009 | 2.48 | 0.0509 | 0.0020 | 3.93 | 0.46 | 227.1 | 8.5 | 227.6 | 5.5 | 224 | 87 | 101.61 |
| G-52d - 3 | 0 | 17.85 | 299 | 0.07 | 0.2530 | 0.0130 | 5.14 | 0.0361 | 0.0009 | 2.41 | 0.0509 | 0.0024 | 4.72 | 0.40 | 228.6 | 11 | 228.8 | 5.4 | 225 | 96 | 101.69 |
| G-52d - 45 | 0 | 6.45 | 169 | 0.04 | 0.2620 | 0.0150 | 5.73 | 0.0370 | 0.0009 | 2.54 | 0.0512 | 0.0029 | 5.66 | 0.25 | 236 | 12 | 234.3 | 5.9 | 230 | 120 | 101.87 |
| G-52d - 59 | 0 | 48.4 | 385 | 0.14 | 0.2628 | 0.0120 | 4.57 | 0.0374 | 0.0009 | 2.43 | 0.0510 | 0.0019 | 3.73 | 0.58 | 236.6 | 9.6 | 237 | 5.7 | 232 | 82 | 102.16 |
| G-52d - 48 | 0 | 11.5 | 261 | 0.04 | 0.2550 | 0.0140 | 5.49 | 0.0365 | 0.0010 | 2.74 | 0.0509 | 0.0023 | 4.52 | 0.57 | 230.5 | 11 | 230.9 | 6.4 | 226 | 95 | 102.17 |
| G-52d - 28 | 0 | 7 | 197 | 0.04 | 0.2620 | 0.0170 | 6.49 | 0.0372 | 0.0010 | 2.61 | 0.0505 | 0.0028 | 5.54 | 0.54 | 236 | 14 | 235.5 | 6 | 230 | 120 | 102.39 |
| G-52d - 4 | 1 | 12.68 | 320 | 0.04 | 0.2610 | 0.0110 | 4.21 | 0.0373 | 0.0009 | 2.36 | 0.0510 | 0.0020 | 3.92 | 0.40 | 235.2 | 9 | 235.9 | 5.5 | 229 | 85 | 103.01 |
| G-52d - 41 | 1 | 13.87 | 305.7 | 0.05 | 0.2550 | 0.0130 | 5.10 | 0.0365 | 0.0009 | 2.44 | 0.0508 | 0.0024 | 4.72 | 0.39 | 230.2 | 11 | 231.1 | 5.5 | 222 | 99 | 104.10 |
| G-52d - 20 | 1 | 9.71 | 295 | 0.04 | 0.2490 | 0.0130 | 5.22 | 0.0357 | 0.0008 | 2.32 | 0.0506 | 0.0023 | 4.55 | 0.49 | 225 | 10 | 226.3 | 5.2 | 210 | 95 | 107.76 |
| G-52d - 10 | 0 | 25.3 | 497 | 0.06 | 0.2522 | 0.0100 | 3.97 | 0.0363 | 0.0008 | 2.31 | 0.0505 | 0.0016 | 3.17 | 0.60 | 228.1 | 8.2 | 229.8 | 5.2 | 213 | 71 | 107.89 |
| G-52d - 62 | 0 | 4.62 | 234 | 0.02 | 0.2520 | 0.0170 | 6.75 | 0.0360 | 0.0010 | 2.64 | 0.0507 | 0.0029 | 5.72 | 0.55 | 228 | 14 | 228.1 | 5.9 | 210 | 110 | 108.62 |
| G-52d - 35 | 0 | 5.92 | 510 | 0.07 | 0.2526 | 0.0110 | 4.35 | 0.0365 | 0.0009 | 2.39 | 0.0504 | 0.0020 | 3.97 | 0.43 | 228.4 | 9.3 | 230.8 | 5.4 | 206 | 83 | 112.04 |
| G-52d - 12 | 0 | 12.54 | 327 | 0.04 | 0.2530 | 0.0120 | 4.74 | 0.0367 | 0.0010 | 2.64 | 0.0500 | 0.0023 | 4.60 | 0.33 | 228.3 | 9.9 | 232.5 | 6.1 | 207 | 94 | 112.32 |
| G-52d - 24 | 0 | 4.12 | 605 | 0.01 | 0.2571 | 0.0110 | 4.28 | 0.0371 | 0.0009 | 2.35 | 0.0504 | 0.0019 | 3.77 | 0.48 | 232 | 9 | 234.7 | 5.4 | 208 | 79 | 112.84 |
| G-52d - 31 | 0 | | | | | | | | | | | | | | | | | | | | |

| | | | | | | | | | | | | | | | | | | | | | |
|-------------|---|----|----|------|--------|--------|-------|----------|--------|-------|--------|--------|------|------|------|----|------|-----|------|-----|--------|
| M2_GC061_50 | 0 | 56 | 87 | 0.64 | 0.7740 | 0.0290 | 3.75 | 0.0772 | 0.0025 | 3.24 | 0.0698 | 0.0010 | 1.43 | 0.93 | 581 | 14 | 479 | 14 | 916 | 29 | 52.29 |
| M2_GC061_25 | 1 | 19 | 19 | 1.00 | 0.7980 | 0.0520 | 6.52 | 0.0791 | 0.0039 | 4.93 | 0.0705 | 0.0020 | 2.84 | 0.91 | 594 | 22 | 491 | 22 | 902 | 60 | 54.43 |
| M3_GC061_6 | 1 | 24 | 27 | 0.89 | 0.7550 | 0.0500 | 6.62 | 0.0769 | 0.0036 | 4.68 | 0.0682 | 0.0019 | 2.79 | 0.94 | 568 | 21 | 478 | 20 | 865 | 55 | 55.26 |
| M2_GC061_26 | 0 | 22 | 18 | 1.22 | 0.8240 | 0.0600 | 7.28 | 0.0810 | 0.0041 | 5.06 | 0.0709 | 0.0022 | 3.10 | 0.94 | 606 | 25 | 502 | 23 | 899 | 67 | 55.84 |
| M2_GC061_13 | 0 | 11 | 35 | 0.31 | 1.3400 | 0.1400 | 10.45 | 0.1139 | 0.0078 | 6.85 | 0.0825 | 0.0022 | 2.67 | 0.90 | 861 | 42 | 695 | 42 | 1243 | 48 | 55.91 |
| M2_GC061_59 | 1 | 19 | 17 | 1.12 | 0.8090 | 0.0540 | 6.67 | 0.0816 | 0.0037 | 4.53 | 0.0696 | 0.0021 | 3.02 | 0.93 | 602 | 23 | 505 | 21 | 887 | 64 | 56.93 |
| M2_GC061_28 | 0 | 18 | 16 | 1.13 | 1.1810 | 0.0780 | 6.60 | 0.1053 | 0.0055 | 5.22 | 0.0782 | 0.0022 | 2.81 | 0.91 | 787 | 26 | 645 | 30 | 1128 | 55 | 57.18 |
| M2_GC061_22 | 1 | 22 | 22 | 1.00 | 0.7870 | 0.0480 | 6.10 | 0.0803 | 0.0037 | 4.61 | 0.0684 | 0.0017 | 2.49 | 0.93 | 586 | 20 | 498 | 21 | 858 | 51 | 58.04 |
| M2_GC061_60 | 0 | 25 | 27 | 0.93 | 0.9390 | 0.0660 | 7.03 | 0.0911 | 0.0046 | 5.05 | 0.0719 | 0.0016 | 2.23 | 0.99 | 668 | 27 | 562 | 26 | 968 | 40 | 58.06 |
| M2_GC061_30 | 1 | 24 | 23 | 1.04 | 0.7930 | 0.0510 | 6.43 | 0.0808 | 0.0038 | 4.70 | 0.0689 | 0.0019 | 2.76 | 0.92 | 590 | 22 | 501 | 22 | 860 | 56 | 58.26 |
| M2_GC061_3 | 1 | 22 | 23 | 0.96 | 0.8240 | 0.0460 | 5.58 | 0.0837 | 0.0036 | 4.30 | 0.0695 | 0.0017 | 2.45 | 0.91 | 610 | 20 | 518 | 20 | 888 | 51 | 58.33 |
| M2_GC061_27 | 0 | 15 | 14 | 1.07 | 0.9340 | 0.0640 | 6.85 | 0.0900 | 0.0043 | 4.78 | 0.0722 | 0.0022 | 3.05 | 0.92 | 664 | 26 | 555 | 24 | 951 | 66 | 58.36 |
| M2_GC061_40 | 0 | 24 | 22 | 1.09 | 0.8860 | 0.0530 | 5.98 | 0.0878 | 0.0039 | 4.44 | 0.0704 | 0.0016 | 2.27 | 0.95 | 641 | 21 | 542 | 22 | 922 | 47 | 58.79 |
| M2_GC061_49 | 1 | 23 | 22 | 1.05 | 0.7660 | 0.0520 | 6.79 | 0.0788 | 0.0037 | 4.70 | 0.0678 | 0.0018 | 2.65 | 0.96 | 574 | 23 | 489 | 21 | 831 | 57 | 58.84 |
| M2_GC061_35 | 1 | 24 | 24 | 1.00 | 0.7760 | 0.0490 | 6.31 | 0.0802 | 0.0037 | 4.61 | 0.0683 | 0.0018 | 2.64 | 0.93 | 581 | 21 | 497 | 21 | 844 | 55 | 58.89 |
| M2_GC061_38 | 1 | 18 | 17 | 1.06 | 0.8010 | 0.0510 | 6.37 | 0.0817 | 0.0037 | 4.53 | 0.0689 | 0.0020 | 2.90 | 0.91 | 596 | 23 | 506 | 21 | 850 | 62 | 59.53 |
| M3_GC061_7 | 0 | 24 | 26 | 0.92 | 0.7980 | 0.0490 | 6.14 | 0.0815 | 0.0039 | 4.79 | 0.0680 | 0.0017 | 2.50 | 0.92 | 593 | 21 | 505 | 22 | 847 | 51 | 59.62 |
| M2_GC061_39 | 0 | 16 | 15 | 1.07 | 0.9150 | 0.0550 | 6.01 | 0.0897 | 0.0041 | 4.57 | 0.0712 | 0.0019 | 2.67 | 0.91 | 655 | 23 | 554 | 23 | 928 | 58 | 59.70 |
| M2_GC061_23 | 0 | 22 | 27 | 0.81 | 0.8040 | 0.0550 | 6.84 | 0.0821 | 0.0041 | 4.99 | 0.0682 | 0.0018 | 2.64 | 0.95 | 596 | 23 | 509 | 23 | 849 | 55 | 59.95 |
| M2_GC061_32 | 1 | 22 | 21 | 1.05 | 0.7770 | 0.0520 | 6.69 | 0.0803 | 0.0037 | 4.61 | 0.0680 | 0.0020 | 2.94 | 0.93 | 583 | 22 | 498 | 21 | 823 | 60 | 60.51 |
| M2_GC061_21 | 0 | 2 | 4 | 0.50 | 1.0100 | 0.1500 | 14.85 | 0.0962 | 0.0092 | 9.56 | 0.0753 | 0.0044 | 5.84 | 0.98 | 709 | 51 | 591 | 48 | 970 | 120 | 60.93 |
| M2_GC061_2 | 0 | 5 | 11 | 0.45 | 1.2500 | 0.2000 | 16.00 | 0.1130 | 0.0120 | 10.62 | 0.0775 | 0.0026 | 3.35 | 0.90 | 816 | 52 | 688 | 61 | 1116 | 61 | 61.65 |
| M2_GC061_42 | 1 | 17 | 16 | 1.06 | 0.7740 | 0.0550 | 7.11 | 0.0799 | 0.0037 | 4.63 | 0.0674 | 0.0020 | 2.97 | 0.96 | 578 | 24 | 496 | 21 | 801 | 66 | 61.92 |
| M2_GC061_9 | 1 | 22 | 22 | 1.00 | 0.7790 | 0.0480 | 6.16 | 0.0811 | 0.0037 | 4.56 | 0.0670 | 0.0018 | 2.69 | 0.92 | 582 | 21 | 502 | 21 | 810 | 54 | 61.98 |
| M2_GC061_19 | 0 | 21 | 19 | 1.11 | 0.9160 | 0.0540 | 5.90 | 0.0917 | 0.0039 | 4.25 | 0.0703 | 0.0018 | 2.56 | 0.92 | 659 | 21 | 566 | 22 | 911 | 53 | 62.13 |
| M2_GC061_31 | 0 | 7 | 8 | 0.88 | 0.7930 | 0.0760 | 9.58 | 0.0807 | 0.0043 | 5.33 | 0.0692 | 0.0033 | 4.77 | 0.95 | 587 | 32 | 500 | 24 | 803 | 97 | 62.27 |
| M2_GC061_8 | 0 | 13 | 23 | 0.57 | 0.9500 | 0.0640 | 6.74 | 0.0934 | 0.0044 | 4.71 | 0.0711 | 0.0021 | 2.95 | 0.93 | 674 | 26 | 575 | 24 | 921 | 62 | 62.43 |
| M2_GC061_14 | 1 | 18 | 18 | 1.00 | 0.8050 | 0.0490 | 6.09 | 0.0835 | 0.0037 | 4.43 | 0.0673 | 0.0018 | 2.67 | 0.92 | 599 | 21 | 517 | 21 | 820 | 55 | 63.05 |
| M2_GC061_24 | 0 | 7 | 10 | 0.70 | 0.7820 | 0.0680 | 8.70 | 0.0808 | 0.0042 | 5.20 | 0.0683 | 0.0029 | 4.25 | 0.94 | 583 | 29 | 501 | 24 | 791 | 92 | 63.34 |
| M2_GC061_58 | 0 | 10 | 19 | 0.53 | 1.3130 | 0.0750 | 5.71 | 0.1179 | 0.0055 | 4.66 | 0.0783 | 0.0017 | 2.17 | 0.93 | 847 | 24 | 718 | 29 | 1130 | 44 | 63.54 |
| M2_GC061_18 | 0 | 19 | 19 | 1.00 | 0.9100 | 0.0540 | 5.93 | 0.0928 | 0.0038 | 4.09 | 0.0691 | 0.0019 | 2.75 | 0.91 | 653 | 23 | 572 | 21 | 871 | 56 | 65.67 |
| M2_GC061_34 | 0 | 22 | 20 | 1.10 | 0.9320 | 0.0560 | 6.01 | 0.0949 | 0.0040 | 4.21 | 0.0700 | 0.0019 | 2.71 | 0.92 | 667 | 24 | 584 | 22 | 887 | 60 | 65.84 |
| M2_GC061_47 | 0 | 12 | 19 | 0.63 | 0.9000 | 0.0530 | 5.89 | 0.0922 | 0.0039 | 4.23 | 0.0690 | 0.0019 | 2.75 | 0.90 | 648 | 23 | 568 | 22 | 862 | 57 | 65.89 |
| M2_GC061_48 | 0 | 11 | 11 | 1.00 | 0.8690 | 0.0620 | 7.13 | 0.0895 | 0.0040 | 4.47 | 0.0686 | 0.0023 | 3.35 | 0.94 | 632 | 27 | 552 | 22 | 827 | 74 | 66.75 |
| M2_GC061_55 | 0 | 10 | 19 | 0.53 | 1.3350 | 0.0740 | 5.54 | 0.1213 | 0.0049 | 4.04 | 0.0775 | 0.0020 | 2.58 | 0.90 | 857 | 25 | 738 | 27 | 1103 | 51 | 66.91 |
| M2_GC061_20 | 0 | 6 | 9 | 0.67 | 0.9020 | 0.0850 | 9.42 | 0.0895 | 0.0058 | 6.48 | 0.0689 | 0.0030 | 4.35 | 0.92 | 645 | 35 | 556 | 32 | 825 | 94 | 67.39 |
| M3_GC061_4 | 1 | 19 | 18 | 1.06 | 0.9520 | 0.0540 | 5.67 | 0.0976 | 0.0039 | 4.00 | 0.0687 | 0.0018 | 2.62 | 0.91 | 677 | 22 | 600 | 22 | 861 | 55 | 69.69 |
| M2_GC061_12 | 1 | 22 | 21 | 1.05 | 0.8890 | 0.0520 | 5.85 | 0.0927 | 0.0038 | 4.10 | 0.0677 | 0.0018 | 2.66 | 0.92 | 642 | 22 | 571 | 21 | 817 | 58 | 69.89 |
| M2_GC061_15 | 0 | 14 | 13 | 1.08 | 0.9670 | 0.0670 | 6.93 | 0.0983 | 0.0047 | 4.78 | 0.0693 | 0.0022 | 3.17 | 0.92 | 685 | 27 | 604 | 27 | 857 | 69 | 70.48 |
| M2_GC061_37 | 0 | 7 | 10 | 0.70 | 0.7770 | 0.0730 | 9.40 | 0.0833 | 0.0044 | 5.28 | 0.0654 | 0.0028 | 4.28 | 0.99 | 577 | 30 | 518 | 25 | 727 | 89 | 71.25 |
| M3_GC061_3 | 0 | 16 | 15 | 1.07 | 0.9740 | 0.0560 | 5.75 | 0.0994 | 0.0038 | 3.82 | 0.0692 | 0.0022 | 3.18 | 0.85 | 685 | 24 | 611 | 21 | 844 | 68 | 72.39 |
| M3_GC061_5 | 0 | 6 | 9 | 0.67 | 1.0420 | 0.0840 | 8.06 | 0.1032 | 0.0049 | 4.75 | 0.0703 | 0.0027 | 3.84 | 0.95 | 717 | 31 | 633 | 27 | 870 | 82 | 72.76 |
| M2_GC061_7 | 0 | 21 | 20 | 1.05 | 0.9400 | 0.0510 | 5.43 | 0.0975 | 0.0039 | 4.00 | 0.0678 | 0.0018 | 2.65 | 0.88 | 669 | 22 | 600 | 22 | 824 | 58 | 72.82 |
| M2_GC061_44 | 1 | 26 | 27 | 0.96 | 0.9320 | 0.0480 | 5.15 | 0.0990 | 0.0035 | 3.54 | 0.0672 | 0.0019 | 2.83 | 0.85 | 666 | 21 | 609 | 20 | 821 | 59 | 74.18 |
| M2_GC061_6 | 0 | 25 | 24 | 1.04 | 1.0420 | 0.0520 | 4.99 | 0.1071 | 0.0038 | 3.55 | 0.0694 | 0.0018 | 2.59 | 0.87 | 721 | 22 | 656 | 21 | 876 | 56 | 74.89 |
| M3_GC061_9 | 1 | 19 | 18 | 1.06 | 1.0730 | 0.0560 | 5.22 | 0.1095 | 0.0039 | 3.56 | 0.0697 | 0.0021 | 3.01 | 0.83 | 738 | 23 | 669 | 22 | 887 | 62 | 75.42 |
| M2_GC061_36 | 0 | 1 | 4 | 0.25 | 0.8000 | 0.1100 | 13.75 | 0.0851 | 0.0056 | 6.58 | 0.0679 | 0.0049 | 7.22 | 0.90 | 591 | 47 | 526 | 32 | 690 | 150 | 76.23 |
| M2_GC061_65 | 1 | 23 | 22 | 1.05 | 1.0490 | 0.0500 | 4.77 | 0.1097 | 0.0039 | 3.56 | 0.0682 | 0.0017 | 2.49 | 0.86 | 727 | 21 | 671 | 22 | 856 | 52 | 78.39 |
| M3_GC061_2 | 1 | 20 | 18 | 1.11 | 1.1230 | 0.0560 | 4.99 | 0.1151 | 0.0040 | 3.48 | 0.0695 | 0.0019 | 2.73 | 0.85 | 760 | 23 | 702 | 23 | 887 | 59 | 79.14 |
| M2_GC061_17 | 0 | 23 | 19 | 1.21 | 1.2500 | 0.0610 | 4.88 | 0.1246 | 0.0047 | 3.77 | 0.0719 | 0.0018 | 2.50 | 0.86 | 818 | 24 | 757 | 26 | 954 | 50 | 79.35 |
| M2_GC061_46 | 1 | 20 | 18 | 1.11 | 1.0040 | 0.0520 | 5.18 | 0.1058 | 0.0037 | 3.50 | 0.0677 | 0.0021 | 3.10 | 0.81 | 701 | 22 | 648 | 21 | 808 | 65 | 80.20 |
| M2_GC061_57 | 1 | 22 | 20 | 1.10 | 1.0000 | 0.0510 | 5.10 | 0.1057 | 0.0038 | 3.60 | 0.0676 | 0.0020 | 2.96 | 0.82 | 699 | 22 | 648 | 21 | 807 | 62 | 80.30 |
| M2_GC061_54 | 1 | 22 | 21 | 1.05 | 0.9980 | 0.0510 | 5.11 | 0.1067 | 0.0037 | 3.47 | 0.0671 | 0.0019 | 2.83 | 0.85 | 701 | 22 | 654 | 21 | 806 | 58 | 81.14 |
| M2_GC061_61 | 1 | 20 | 19 | 1.05 | 0.9830 | 0.0510 | 5.19 | 0.1052 | 0.0037 | 3.52 | 0.0665 | 0.0019 | 2.86 | 0.85 | 691 | 22 | 644 | 21 | 787 | 64 | 81.83 |
| M2_GC061_1 | 0 | 16 | 20 | 0.80 | 1.0490 | 0.0560 | 5.34 | 0.1104 | 0.0040 | 3.62 | 0.0676 | 0.0020 | 2.96 | 0.85 | 726 | 24 | 675 | 22 | 822 | 63 | 82.12 |
| M2_GC061_62 | 0 | 0 | 4 | 0.00 | 2.4200 | 0.6100 | 25.21 | 0.1970 | 0.0380 | 19.29 | 0.0867 | 0.0041 | 4.73 | 0.80 | 1223 | 88 | 1150 | 170 | 1245 | 91 | 92.37 |
| M2_GC061_45 | 0 | 51 | 41 | 1.24 | 1.4130 | 0.0450 | 3.18 | 0.1481 | 0.0036 | 2.43 | 0.0696 | 0.0014 | 2.01 | 0.78 | 892 | 19 | 890 | 20 | 897 | 41 | 99.22 |
| M3_GC061_13 | 0 | 52 | 45 | 1.16 | 1.5990 | 0.0490 | 3.06 | 0.1610 | 0.0039 | 2.42 | 0.0718 | 0.0013 | 1.81 | 0.81 | 967 | 19 | 962 | 22 | 969 | 36 | 99.28 |
| M2_GC061_53 | 0 | 27 | 25 | 1.08 | 1.3750 | 0.0610 | 4.44 | 0.1441 | 0.0046 | 3.19 | 0.0693 | 0.0017 | 2.45 | 0.84 | 874 | 24 | 867 | 26 | 873 | 51 | 99.31 |
| M3_GC061_11 | 0 | 60 | 71 | 0.85 | 1.6050 | 0.0450 | 2.80 | 0.1625 | 0.0039 | 2.40 | 0.0716 | 0.0010 | 1.37 | 0.87 | 971 | 17 | 970 | 22 | 969 | 29 | 100.10 |
| M2_GC061_4 | 0 | 21 | 52 | 0.40 | 1.8060 | 0.0610 | 3.38 | 0.1759</ | | | | | | | | | | | | | |

| | | | | | | | | | | | | | | | | | | | | | |
|-------------|---|-------|-------|------|--------|--------|-------|--------|--------|-------|--------|--------|-------|------|-------|----|--------|-----|------|-----|--------|
| M2_GC061_11 | 0 | 3 | 14 | 0.21 | 3.1700 | 0.1800 | 5.68 | 0.2650 | 0.0120 | 4.53 | 0.0851 | 0.0016 | 1.88 | 0.96 | 1445 | 39 | 1515 | 60 | 1301 | 37 | 116.45 |
| M2_GC061_51 | 0 | 1 | 1 | 1.00 | 1.0300 | 0.3200 | 31.07 | 0.1000 | 0.0200 | 20.00 | 0.0676 | 0.0082 | 12.13 | 0.98 | 630 | 99 | 610 | 100 | 510 | 230 | 119.61 |
| M2_GC061_16 | 0 | 10 | 9 | 1.11 | 1.3120 | 0.0920 | 7.01 | 0.1458 | 0.0049 | 3.36 | 0.0647 | 0.0038 | 5.87 | 0.55 | 826 | 38 | 877 | 27 | 660 | 120 | 132.88 |
| M1_GC021_12 | 1 | 43 | 32 | 1.34 | 0.2130 | 0.0150 | 7.04 | 0.0286 | 0.0010 | 3.50 | 0.0534 | 0.0026 | 4.87 | 0.77 | 195 | 12 | 181.6 | 6.3 | 288 | 97 | 93.13 |
| M1_GC021_9 | 1 | 74 | 47 | 1.57 | 0.3200 | 0.0160 | 5.00 | 0.0431 | 0.0011 | 2.55 | 0.0547 | 0.0025 | 4.57 | 0.42 | 280 | 13 | 271.8 | 6.9 | 345 | 90 | 97.07 |
| M1_GC021_1 | 0 | 60 | 42 | 1.43 | 0.3140 | 0.0140 | 4.46 | 0.0434 | 0.0011 | 2.53 | 0.0525 | 0.0020 | 3.81 | 0.52 | 275 | 11 | 273.9 | 6.9 | 280 | 77 | 97.82 |
| M1_GC021_2 | 1 | 82 | 57 | 1.44 | 0.3110 | 0.0140 | 4.50 | 0.0427 | 0.0011 | 2.58 | 0.0530 | 0.0021 | 3.96 | 0.48 | 274 | 11 | 269.8 | 6.5 | 304 | 81 | 98.47 |
| M1_GC021_10 | 1 | 26 | 29 | 0.90 | 0.2180 | 0.0170 | 7.80 | 0.0311 | 0.0012 | 3.86 | 0.0503 | 0.0026 | 5.17 | 0.81 | 199 | 13 | 197.3 | 7.1 | 180 | 100 | 99.15 |
| M1_GC021_4 | 1 | 47 | 56 | 0.84 | 0.2980 | 0.0130 | 4.36 | 0.0423 | 0.0010 | 2.36 | 0.0513 | 0.0020 | 3.90 | 0.46 | 263 | 11 | 267.1 | 6.4 | 232 | 78 | 101.56 |
| M1_GC021_5 | 1 | 34 | 35 | 0.97 | 0.3050 | 0.0180 | 5.90 | 0.0432 | 0.0011 | 2.55 | 0.0516 | 0.0028 | 5.43 | 0.39 | 268 | 14 | 272.4 | 6.8 | 230 | 100 | 101.64 |
| M1_GC021_8 | 1 | 17 | 19 | 0.89 | 0.2140 | 0.0180 | 8.41 | 0.0313 | 0.0012 | 3.83 | 0.0490 | 0.0029 | 5.92 | 0.78 | 195 | 15 | 198.8 | 7.1 | 130 | 110 | 101.95 |
| M1_GC021_11 | 1 | 29 | 36 | 0.81 | 0.3000 | 0.0140 | 4.67 | 0.0429 | 0.0011 | 2.56 | 0.0510 | 0.0021 | 4.12 | 0.48 | 264 | 11 | 270.9 | 6.9 | 224 | 85 | 102.61 |
| M1_GC021_7 | 1 | 24 | 30 | 0.80 | 0.3040 | 0.0170 | 5.59 | 0.0435 | 0.0012 | 2.76 | 0.0506 | 0.0025 | 4.94 | 0.47 | 267 | 13 | 274.4 | 7.1 | 201 | 95 | 102.77 |
| M1_GC021_3 | 0 | 68 | 44 | 1.55 | 0.3010 | 0.0150 | 4.98 | 0.0437 | 0.0011 | 2.52 | 0.0502 | 0.0022 | 4.38 | 0.48 | 265 | 11 | 275.7 | 6.7 | 185 | 83 | 104.04 |
| M1_GC021_6 | 0 | 63 | 38 | 1.66 | 0.2980 | 0.0170 | 5.70 | 0.0434 | 0.0011 | 2.53 | 0.0499 | 0.0025 | 5.01 | 0.48 | 262 | 13 | 273.6 | 6.9 | 179 | 97 | 104.43 |
| M1_GC021_13 | 1 | 47 | 39 | 1.21 | 0.2820 | 0.0160 | 5.67 | 0.0434 | 0.0011 | 2.53 | 0.0475 | 0.0025 | 5.26 | 0.38 | 250 | 13 | 273.6 | 6.9 | 78 | 97 | 109.44 |
| B_235_11 | 0 | 35.1 | 134 | 0.26 | 2.5400 | 0.1700 | 6.69 | 0.1903 | 0.0049 | 2.57 | 0.0968 | 0.0056 | 5.79 | 0.88 | 1276 | 47 | 1122 | 26 | 1540 | 100 | 72.86 |
| B_235_79 | 0 | 562 | 2337 | 0.24 | 1.2960 | 0.0380 | 2.93 | 0.1294 | 0.0033 | 2.55 | 0.0735 | 0.0014 | 1.91 | 0.79 | 843 | 17 | 784 | 19 | 1030 | 37 | 76.12 |
| B_235_30 | 1 | 9.01 | 82.9 | 0.11 | 2.1010 | 0.0990 | 4.71 | 0.1797 | 0.0034 | 1.89 | 0.0844 | 0.0037 | 4.38 | 0.73 | 1146 | 31 | 1065 | 19 | 1287 | 79 | 82.75 |
| B_235_75 | 1 | 10.65 | 94.1 | 0.11 | 1.9320 | 0.0840 | 4.35 | 0.1721 | 0.0033 | 1.92 | 0.0817 | 0.0032 | 3.92 | 0.92 | 1090 | 28 | 1023.7 | 18 | 1228 | 73 | 83.36 |
| B_235_21 | 1 | 94.4 | 1239 | 0.08 | 1.8490 | 0.0550 | 2.97 | 0.1692 | 0.0043 | 2.54 | 0.0789 | 0.0015 | 1.90 | 0.87 | 1062 | 20 | 1008 | 24 | 1168 | 37 | 86.30 |
| B_235_61 | 0 | 763 | 3580 | 0.21 | 1.8850 | 0.0660 | 3.50 | 0.1749 | 0.0044 | 2.52 | 0.0783 | 0.0014 | 1.79 | 0.81 | 1078 | 24 | 1039 | 24 | 1157 | 33 | 89.80 |
| B_235_22 | 0 | 37.6 | 206.8 | 0.18 | 1.9680 | 0.0680 | 3.46 | 0.1823 | 0.0061 | 3.35 | 0.0786 | 0.0014 | 1.78 | 0.86 | 1107 | 24 | 1079 | 34 | 1162 | 35 | 92.86 |
| B_235_16 | 1 | 8.04 | 58.6 | 0.14 | 1.9990 | 0.0780 | 3.90 | 0.1819 | 0.0042 | 2.31 | 0.0785 | 0.0019 | 2.42 | 0.77 | 1114 | 26 | 1077 | 23 | 1155 | 49 | 93.25 |
| B_235_74 | 0 | 51 | 223 | 0.23 | 2.4280 | 0.0640 | 2.64 | 0.2081 | 0.0060 | 2.88 | 0.0847 | 0.0019 | 2.24 | 0.78 | 1254 | 21 | 1218 | 32 | 1305 | 42 | 93.33 |
| B_235_34 | 1 | 109.6 | 381 | 0.29 | 2.4920 | 0.0700 | 2.81 | 0.2109 | 0.0055 | 2.61 | 0.0853 | 0.0019 | 2.23 | 0.65 | 1269 | 20 | 1233 | 29 | 1320 | 42 | 93.41 |
| B_235_90 | 0 | 62.6 | 307 | 0.20 | 2.0510 | 0.0570 | 2.78 | 0.1877 | 0.0042 | 2.24 | 0.0791 | 0.0014 | 1.77 | 0.86 | 1132 | 19 | 1109 | 23 | 1179 | 32 | 94.06 |
| B_235_32 | 1 | 12.46 | 100.9 | 0.12 | 1.7670 | 0.0530 | 3.00 | 0.1698 | 0.0040 | 2.36 | 0.0752 | 0.0017 | 2.26 | 0.66 | 1033 | 21 | 1011 | 22 | 1072 | 47 | 94.31 |
| B_235_69 | 1 | 25.45 | 454 | 0.06 | 2.0410 | 0.0660 | 3.23 | 0.1887 | 0.0050 | 2.65 | 0.0794 | 0.0015 | 1.89 | 0.85 | 1128 | 22 | 1114 | 27 | 1181 | 38 | 94.33 |
| B_235_4 | 0 | 32.4 | 128.8 | 0.25 | 2.2010 | 0.0640 | 2.91 | 0.1958 | 0.0050 | 2.55 | 0.0810 | 0.0016 | 1.98 | 0.79 | 1181 | 20 | 1152 | 27 | 1220 | 38 | 94.43 |
| B_235_86 | 1 | 83 | 350 | 0.24 | 2.3650 | 0.0690 | 2.92 | 0.2065 | 0.0049 | 2.37 | 0.0836 | 0.0015 | 1.79 | 0.84 | 1231 | 21 | 1210 | 26 | 1281 | 35 | 94.46 |
| B_235_43 | 0 | 241.3 | 462 | 0.52 | 2.3850 | 0.0700 | 2.94 | 0.2080 | 0.0053 | 2.55 | 0.0837 | 0.0016 | 1.91 | 0.81 | 1237 | 21 | 1218 | 28 | 1284 | 37 | 94.86 |
| B_235_1 | 0 | 90.9 | 325 | 0.28 | 1.7290 | 0.0490 | 2.83 | 0.1689 | 0.0039 | 2.31 | 0.0747 | 0.0014 | 1.87 | 0.81 | 1019 | 18 | 1006 | 21 | 1060 | 37 | 94.91 |
| B_235_7 | 0 | 10.32 | 98.2 | 0.11 | 1.7430 | 0.0520 | 2.98 | 0.1681 | 0.0040 | 2.38 | 0.0746 | 0.0017 | 2.28 | 0.64 | 1024 | 19 | 1002 | 22 | 1055 | 45 | 94.98 |
| B_235_56 | 1 | 117.1 | 436 | 0.27 | 2.4350 | 0.0770 | 3.16 | 0.2123 | 0.0059 | 2.78 | 0.0846 | 0.0017 | 2.01 | 0.81 | 1252 | 23 | 1241 | 31 | 1304 | 38 | 95.17 |
| B_235_77 | 0 | 55.5 | 218.5 | 0.25 | 2.2700 | 0.0660 | 2.91 | 0.2017 | 0.0045 | 2.23 | 0.0817 | 0.0018 | 2.20 | 0.64 | 1202 | 21 | 1184 | 24 | 1242 | 44 | 95.33 |
| B_235_84 | 1 | 45.5 | 187 | 0.24 | 1.7870 | 0.0560 | 3.13 | 0.1725 | 0.0047 | 2.72 | 0.0755 | 0.0014 | 1.86 | 0.85 | 1040 | 20 | 1030 | 26 | 1080 | 37 | 95.37 |
| B_235_35 | 1 | 26.7 | 90.1 | 0.30 | 2.1800 | 0.1100 | 5.05 | 0.1940 | 0.0053 | 2.73 | 0.0802 | 0.0025 | 3.12 | 0.91 | 1172 | 35 | 1143 | 29 | 1195 | 61 | 95.65 |
| B_235_88 | 0 | 81.8 | 380 | 0.22 | 2.3090 | 0.0730 | 3.16 | 0.2040 | 0.0056 | 2.75 | 0.0820 | 0.0016 | 1.95 | 0.85 | 1214 | 22 | 1197 | 30 | 1249 | 36 | 95.84 |
| B_235_15 | 1 | 14.24 | 113.3 | 0.13 | 1.6960 | 0.0520 | 3.07 | 0.1659 | 0.0035 | 2.11 | 0.0738 | 0.0019 | 2.57 | 0.35 | 1006 | 19 | 989 | 20 | 1031 | 49 | 95.93 |
| B_235_52 | 1 | 148.8 | 600 | 0.25 | 2.3990 | 0.0660 | 2.75 | 0.2097 | 0.0048 | 2.29 | 0.0834 | 0.0015 | 1.80 | 0.78 | 1242 | 20 | 1227 | 26 | 1278 | 36 | 96.01 |
| B_235_26 | 0 | 69.1 | 354 | 0.20 | 2.1750 | 0.0710 | 3.26 | 0.1973 | 0.0057 | 2.89 | 0.0804 | 0.0016 | 1.99 | 0.85 | 1172 | 23 | 1161 | 31 | 1209 | 37 | 96.03 |
| B_235_6 | 0 | 9.27 | 84.6 | 0.11 | 1.6720 | 0.0430 | 2.57 | 0.1649 | 0.0033 | 2.00 | 0.0735 | 0.0016 | 2.18 | 0.49 | 997.8 | 16 | 984 | 18 | 1024 | 44 | 96.09 |
| B_235_55 | 0 | 225 | 605 | 0.37 | 1.9420 | 0.0560 | 2.88 | 0.1832 | 0.0047 | 2.57 | 0.0771 | 0.0016 | 2.08 | 0.73 | 1095 | 20 | 1084 | 25 | 1128 | 39 | 96.10 |
| B_235_38 | 1 | 20.93 | 152.6 | 0.14 | 1.6640 | 0.0440 | 2.64 | 0.1642 | 0.0029 | 1.77 | 0.0733 | 0.0015 | 2.05 | 0.35 | 994.6 | 16 | 980.2 | 16 | 1019 | 39 | 96.19 |
| B_235_60 | 1 | 193.1 | 531 | 0.36 | 2.4320 | 0.0660 | 2.71 | 0.2128 | 0.0048 | 2.26 | 0.0836 | 0.0018 | 2.15 | 0.55 | 1252 | 20 | 1244 | 26 | 1293 | 41 | 96.21 |
| B_235_53 | 0 | 150.7 | 429 | 0.35 | 2.4030 | 0.0640 | 2.66 | 0.2098 | 0.0057 | 2.72 | 0.0834 | 0.0017 | 2.04 | 0.82 | 1243 | 19 | 1228 | 30 | 1276 | 40 | 96.24 |
| B_235_19 | 1 | 43.4 | 203.1 | 0.21 | 2.6690 | 0.0760 | 2.85 | 0.2237 | 0.0050 | 2.24 | 0.0866 | 0.0019 | 2.19 | 0.60 | 1322 | 20 | 1301 | 26 | 1349 | 42 | 96.44 |
| B_235_59 | 1 | 128.4 | 1029 | 0.12 | 2.2100 | 0.0620 | 2.81 | 0.1996 | 0.0049 | 2.45 | 0.0808 | 0.0015 | 1.86 | 0.82 | 1184 | 20 | 1173 | 27 | 1216 | 37 | 96.46 |
| B_235_28 | 0 | 34 | 245.2 | 0.14 | 2.2420 | 0.0830 | 3.70 | 0.1963 | 0.0059 | 3.01 | 0.0803 | 0.0015 | 1.87 | 0.92 | 1193 | 26 | 1161 | 32 | 1203 | 38 | 96.51 |
| B_235_71 | 0 | 77.3 | 265.9 | 0.29 | 1.7370 | 0.0500 | 2.88 | 0.1710 | 0.0049 | 2.87 | 0.0742 | 0.0014 | 1.89 | 0.74 | 1022 | 19 | 1018 | 27 | 1051 | 41 | 96.86 |
| B_235_78 | 1 | 79.5 | 297 | 0.27 | 2.5800 | 0.0690 | 2.67 | 0.2192 | 0.0053 | 2.42 | 0.0848 | 0.0017 | 2.00 | 0.60 | 1294 | 20 | 1278 | 28 | 1316 | 35 | 97.11 |
| B_235_37 | 0 | 32.6 | 90.9 | 0.36 | 2.2290 | 0.0690 | 3.10 | 0.2003 | 0.0046 | 2.30 | 0.0804 | 0.0018 | 2.24 | 0.70 | 1189 | 22 | 1177 | 25 | 1211 | 42 | 97.19 |
| B_235_29 | 1 | 55.8 | 276.6 | 0.20 | 2.6310 | 0.0730 | 2.77 | 0.2219 | 0.0056 | 2.52 | 0.0856 | 0.0016 | 1.87 | 0.75 | 1309 | 20 | 1292 | 29 | 1326 | 37 | 97.44 |
| B_235_80 | 1 | 59.1 | 280 | 0.21 | 1.6790 | 0.0580 | 3.45 | 0.1676 | 0.0046 | 2.74 | 0.0730 | 0.0015 | 2.05 | 0.81 | 1003 | 23 | 999 | 25 | 1025 | 41 | 97.46 |
| B_235_44 | 0 | 121 | 1011 | 0.12 | 2.1310 | 0.0730 | 3.43 | 0.1960 | 0.0060 | 3.06 | 0.0795 | 0.0014 | 1.76 | 0.85 | 1158 | 24 | 1153 | 32 | 1183 | 36 | 97.46 |
| B_235_20 | 1 | 71.4 | 328 | 0.22 | 2.4400 | 0.0670 | 2.75 | 0.2121 | 0.0058 | 2.73 | 0.0832 | 0.0018 | 2.16 | 0.77 | 1257 | 22 | 1240 | 31 | 1272 | 41 | 97.48 |
| B_235_72 | 1 | 75.7 | 232 | 0.33 | 2.0560 | 0.0640 | 3.11 | 0.1929 | 0.0053 | 2.75 | 0.0788 | 0.0015 | 1.90 | 0.78 | 1137 | 21 | 1137 | 29 | 1165 | 39 | 97.60 |
| B_235_50 | 0 | 59 | 171.5 | 0.34 | 2.5710 | 0.0810 | 3.15 | 0.2204 | 0.0050 | 2.27 | 0.0850 | 0.0019 | 2.24 | 0.82 | 1292 | 23 | 1284 | 27 | 1313 | | |

| | | | | | | | | | | | | | | | | | | | | | |
|----------|---|-------|-------|------|--------|--------|------|--------|--------|------|--------|--------|------|------|--------|----|--------|----|------|----|--------|
| B_235_40 | 0 | 76 | 290 | 0.26 | 2.4540 | 0.0830 | 3.38 | 0.2139 | 0.0054 | 2.52 | 0.0828 | 0.0020 | 2.42 | 0.72 | 1257 | 24 | 1249 | 29 | 1260 | 48 | 99.13 |
| B_235_17 | 1 | 17.2 | 116.5 | 0.15 | 1.7630 | 0.0590 | 3.35 | 0.1728 | 0.0043 | 2.49 | 0.0740 | 0.0019 | 2.57 | 0.77 | 1031 | 21 | 1027 | 23 | 1036 | 50 | 99.13 |
| B_235_76 | 0 | 40.8 | 176.9 | 0.23 | 2.4910 | 0.0670 | 2.69 | 0.2173 | 0.0042 | 1.93 | 0.0833 | 0.0016 | 1.92 | 0.68 | 1269 | 19 | 1267 | 22 | 1275 | 38 | 99.37 |
| B_235_49 | 0 | 22.89 | 170.6 | 0.13 | 1.6270 | 0.0450 | 2.77 | 0.1639 | 0.0034 | 2.07 | 0.0719 | 0.0015 | 2.09 | 0.62 | 980 | 18 | 978 | 19 | 980 | 44 | 99.80 |
| B_235_5 | 1 | 22.19 | 101.4 | 0.22 | 2.3720 | 0.0640 | 2.70 | 0.2095 | 0.0042 | 2.00 | 0.0813 | 0.0015 | 1.85 | 0.79 | 1234 | 19 | 1226 | 23 | 1228 | 36 | 99.84 |
| B_235_9 | 0 | 148 | 482 | 0.31 | 2.5000 | 0.0790 | 3.16 | 0.2165 | 0.0055 | 2.54 | 0.0826 | 0.0021 | 2.54 | 0.64 | 1271 | 23 | 1263 | 29 | 1264 | 51 | 99.92 |
| B_235_25 | 1 | 5.15 | 83.4 | 0.06 | 1.6870 | 0.0480 | 2.85 | 0.1683 | 0.0036 | 2.14 | 0.0727 | 0.0016 | 2.20 | 0.55 | 1003 | 18 | 1003 | 20 | 1003 | 45 | 100.00 |
| B_235_82 | 0 | 8.4 | 112.4 | 0.07 | 1.7190 | 0.0490 | 2.85 | 0.1713 | 0.0038 | 2.22 | 0.0730 | 0.0017 | 2.33 | 0.55 | 1018 | 19 | 1019 | 21 | 1019 | 44 | 100.00 |
| B_235_58 | 1 | 16.93 | 140.8 | 0.12 | 1.8030 | 0.0520 | 2.88 | 0.1772 | 0.0037 | 2.09 | 0.0745 | 0.0018 | 2.42 | 0.55 | 1046 | 18 | 1051 | 21 | 1051 | 48 | 100.00 |
| B_235_70 | 0 | 90.9 | 370.1 | 0.25 | 2.5260 | 0.0770 | 3.05 | 0.2191 | 0.0055 | 2.51 | 0.0834 | 0.0015 | 1.80 | 0.79 | 1279 | 22 | 1277 | 29 | 1277 | 35 | 100.00 |
| B_235_62 | 0 | 159 | 530 | 0.30 | 2.3890 | 0.0690 | 2.89 | 0.2130 | 0.0057 | 2.68 | 0.0817 | 0.0017 | 2.08 | 0.79 | 1242 | 22 | 1245 | 30 | 1237 | 40 | 100.65 |
| B_235_45 | 1 | 34.6 | 184.2 | 0.19 | 1.7070 | 0.0530 | 3.10 | 0.1696 | 0.0036 | 2.12 | 0.0727 | 0.0018 | 2.48 | 0.91 | 1011 | 20 | 1010 | 20 | 1003 | 49 | 100.70 |
| B_235_68 | 0 | 87.3 | 277.6 | 0.31 | 2.4470 | 0.0690 | 2.82 | 0.2174 | 0.0053 | 2.44 | 0.0824 | 0.0016 | 1.94 | 0.75 | 1256 | 21 | 1268 | 28 | 1258 | 38 | 100.79 |
| B_235_65 | 0 | 62 | 154.5 | 0.40 | 2.6810 | 0.0690 | 2.57 | 0.2290 | 0.0046 | 2.01 | 0.0852 | 0.0017 | 2.00 | 0.32 | 1323 | 19 | 1329 | 24 | 1318 | 38 | 100.83 |
| B_235_2 | 0 | 20.1 | 184.1 | 0.11 | 1.7040 | 0.0420 | 2.46 | 0.1692 | 0.0033 | 1.95 | 0.0725 | 0.0013 | 1.79 | 0.69 | 1009.9 | 16 | 1007 | 18 | 998 | 37 | 100.90 |
| B_235_46 | 1 | 19.5 | 156.3 | 0.12 | 1.7220 | 0.0480 | 2.79 | 0.1702 | 0.0039 | 2.29 | 0.0727 | 0.0017 | 2.34 | 0.54 | 1016 | 18 | 1013 | 22 | 1002 | 48 | 101.10 |
| B_235_48 | 0 | 80.3 | 294 | 0.27 | 2.5190 | 0.0780 | 3.10 | 0.2207 | 0.0051 | 2.31 | 0.0829 | 0.0016 | 1.93 | 0.78 | 1277 | 23 | 1285 | 27 | 1270 | 34 | 101.18 |
| B_235_67 | 1 | 18.7 | 263.2 | 0.07 | 1.6990 | 0.0450 | 2.65 | 0.1700 | 0.0043 | 2.53 | 0.0726 | 0.0014 | 1.93 | 0.80 | 1007.9 | 17 | 1012 | 24 | 1000 | 39 | 101.20 |
| B_235_85 | 1 | 17.52 | 146 | 0.12 | 1.7030 | 0.0430 | 2.52 | 0.1718 | 0.0036 | 2.10 | 0.0724 | 0.0016 | 2.21 | 0.32 | 1009.3 | 16 | 1022 | 20 | 1008 | 43 | 101.39 |
| B_235_64 | 1 | 25.5 | 177.9 | 0.14 | 1.7870 | 0.0490 | 2.74 | 0.1765 | 0.0045 | 2.55 | 0.0737 | 0.0014 | 1.90 | 0.70 | 1040 | 18 | 1048 | 25 | 1032 | 37 | 101.55 |
| B_235_3 | 1 | 9.89 | 104.5 | 0.09 | 1.7210 | 0.0490 | 2.85 | 0.1705 | 0.0032 | 1.88 | 0.0725 | 0.0015 | 2.07 | 0.83 | 1016 | 18 | 1014.7 | 18 | 998 | 42 | 101.67 |
| B_235_31 | 0 | 20.3 | 109.2 | 0.19 | 2.1880 | 0.0660 | 3.02 | 0.2023 | 0.0050 | 2.47 | 0.0788 | 0.0016 | 2.03 | 0.73 | 1176 | 21 | 1187 | 27 | 1165 | 40 | 101.89 |
| B_235_47 | 0 | 22.15 | 118.2 | 0.19 | 2.2800 | 0.0690 | 3.03 | 0.2075 | 0.0052 | 2.51 | 0.0798 | 0.0016 | 2.01 | 0.74 | 1205 | 21 | 1215 | 28 | 1191 | 40 | 102.02 |
| B_235_8 | 1 | 21.1 | 176.2 | 0.12 | 1.7070 | 0.0500 | 2.93 | 0.1696 | 0.0035 | 2.06 | 0.0722 | 0.0014 | 1.94 | 0.82 | 1011 | 19 | 1010 | 19 | 990 | 40 | 102.02 |
| B_235_66 | 1 | 70.5 | 262.5 | 0.27 | 2.7060 | 0.0690 | 2.55 | 0.2328 | 0.0049 | 2.10 | 0.0852 | 0.0017 | 2.00 | 0.64 | 1330 | 19 | 1349 | 26 | 1318 | 39 | 102.35 |
| B_235_18 | 0 | 56.8 | 580 | 0.10 | 2.6010 | 0.0980 | 3.77 | 0.2275 | 0.0091 | 4.00 | 0.0838 | 0.0017 | 2.03 | 0.94 | 1309 | 28 | 1320 | 48 | 1285 | 39 | 102.72 |
| B_235_36 | 1 | 84.7 | 224.8 | 0.38 | 2.7080 | 0.0740 | 2.73 | 0.2301 | 0.0063 | 2.74 | 0.0843 | 0.0015 | 1.78 | 0.82 | 1330 | 20 | 1335 | 33 | 1298 | 35 | 102.85 |
| B_235_13 | 1 | 82.9 | 195.4 | 0.42 | 2.3960 | 0.0720 | 3.01 | 0.2147 | 0.0053 | 2.47 | 0.0809 | 0.0016 | 1.98 | 0.73 | 1247 | 22 | 1253 | 28 | 1217 | 39 | 102.96 |
| B_235_14 | 0 | 29.5 | 107.7 | 0.27 | 2.3850 | 0.0640 | 2.68 | 0.2136 | 0.0043 | 2.01 | 0.0805 | 0.0016 | 1.99 | 0.55 | 1238 | 19 | 1248 | 23 | 1206 | 39 | 103.48 |
| B_235_10 | 1 | 68.4 | 220 | 0.31 | 1.8480 | 0.0550 | 2.98 | 0.1800 | 0.0034 | 1.89 | 0.0737 | 0.0018 | 2.44 | 0.66 | 1062 | 19 | 1067 | 19 | 1031 | 48 | 103.49 |
| B_235_73 | 1 | 67.8 | 180 | 0.38 | 2.7590 | 0.0750 | 2.72 | 0.2347 | 0.0060 | 2.56 | 0.0847 | 0.0016 | 1.89 | 0.81 | 1347 | 21 | 1359 | 31 | 1312 | 39 | 103.58 |
| B_235_39 | 0 | 25 | 181.4 | 0.14 | 1.6440 | 0.0430 | 2.62 | 0.1655 | 0.0042 | 2.54 | 0.0708 | 0.0014 | 1.98 | 0.65 | 987.1 | 16 | 987 | 23 | 950 | 42 | 103.89 |
| B_235_23 | 0 | 23.1 | 115.8 | 0.20 | 2.9830 | 0.0790 | 2.65 | 0.2466 | 0.0056 | 2.27 | 0.0868 | 0.0019 | 2.19 | 0.69 | 1403 | 20 | 1421 | 29 | 1360 | 39 | 104.49 |
| B_235_81 | 0 | 87.5 | 276 | 0.32 | 2.0460 | 0.0590 | 2.88 | 0.1953 | 0.0044 | 2.25 | 0.0761 | 0.0014 | 1.84 | 0.85 | 1130 | 20 | 1150 | 23 | 1097 | 37 | 104.83 |
| B_235_41 | 0 | 28.5 | 147 | 0.19 | 1.6890 | 0.0540 | 3.20 | 0.1717 | 0.0040 | 2.33 | 0.0710 | 0.0015 | 2.11 | 0.62 | 1003 | 20 | 1021 | 23 | 962 | 47 | 106.13 |
| B_235_87 | 1 | 10.47 | 154.3 | 0.07 | 1.6310 | 0.0430 | 2.64 | 0.1702 | 0.0041 | 2.41 | 0.0701 | 0.0015 | 2.14 | 0.67 | 982 | 17 | 1013 | 22 | 927 | 45 | 109.28 |
| B_245_15 | 1 | 47.24 | 112.3 | 0.42 | 2.1550 | 0.0920 | 4.27 | 0.1674 | 0.0039 | 2.33 | 0.0925 | 0.0035 | 3.78 | 0.25 | 1165 | 30 | 998 | 22 | 1482 | 71 | 67.34 |
| B_245_32 | 0 | 110.9 | 1148 | 0.10 | 2.4180 | 0.0660 | 2.73 | 0.1932 | 0.0049 | 2.54 | 0.0898 | 0.0014 | 1.56 | 0.93 | 1247 | 20 | 1139 | 26 | 1422 | 31 | 80.10 |
| B_245_28 | 1 | 51.8 | 792 | 0.07 | 2.4500 | 0.0710 | 2.90 | 0.2043 | 0.0058 | 2.84 | 0.0892 | 0.0029 | 3.25 | 0.74 | 1257 | 21 | 1198 | 31 | 1402 | 54 | 85.45 |
| B_245_37 | 1 | 110.6 | 2153 | 0.05 | 2.1690 | 0.1100 | 5.07 | 0.1851 | 0.0055 | 2.97 | 0.0837 | 0.0023 | 2.75 | 0.85 | 1168 | 34 | 1095 | 30 | 1281 | 53 | 85.48 |
| B_245_43 | 1 | 126.2 | 929 | 0.14 | 2.2640 | 0.0710 | 3.14 | 0.1923 | 0.0050 | 2.60 | 0.0849 | 0.0017 | 2.00 | 0.80 | 1200 | 22 | 1134 | 27 | 1319 | 44 | 85.97 |
| B_245_41 | 1 | 95.8 | 469 | 0.20 | 1.9280 | 0.0590 | 3.06 | 0.1744 | 0.0042 | 2.41 | 0.0798 | 0.0017 | 2.13 | 0.77 | 1090 | 21 | 1036 | 23 | 1197 | 38 | 86.55 |
| B_245_29 | 0 | 39.6 | 598 | 0.07 | 2.5890 | 0.0880 | 3.40 | 0.2093 | 0.0062 | 2.96 | 0.0890 | 0.0017 | 1.91 | 0.91 | 1296 | 25 | 1225 | 33 | 1408 | 38 | 87.00 |
| B_245_30 | 1 | 104 | 550 | 0.19 | 3.1350 | 0.0840 | 2.68 | 0.2376 | 0.0064 | 2.69 | 0.0973 | 0.0027 | 2.77 | 0.69 | 1441 | 21 | 1374 | 33 | 1568 | 47 | 87.63 |
| B_245_14 | 0 | 122.5 | 168.9 | 0.73 | 3.4510 | 0.0910 | 2.64 | 0.2501 | 0.0062 | 2.48 | 0.1003 | 0.0018 | 1.79 | 0.82 | 1516 | 21 | 1439 | 32 | 1628 | 33 | 88.39 |
| B_245_38 | 1 | 59 | 517 | 0.11 | 2.8660 | 0.0810 | 2.83 | 0.2263 | 0.0059 | 2.61 | 0.0926 | 0.0020 | 2.16 | 0.69 | 1375 | 20 | 1315 | 31 | 1477 | 40 | 89.03 |
| B_245_20 | 1 | 37 | 228.3 | 0.16 | 2.9370 | 0.0930 | 3.17 | 0.2308 | 0.0057 | 2.47 | 0.0921 | 0.0017 | 1.85 | 0.89 | 1391 | 24 | 1339 | 30 | 1474 | 33 | 90.84 |
| B_245_33 | 1 | 137 | 430 | 0.32 | 2.9950 | 0.1000 | 3.34 | 0.2343 | 0.0065 | 2.77 | 0.0925 | 0.0024 | 2.59 | 0.55 | 1405 | 27 | 1356 | 34 | 1484 | 43 | 91.37 |
| B_245_40 | 1 | 58.2 | 1293 | 0.05 | 1.7050 | 0.0430 | 2.52 | 0.1648 | 0.0035 | 2.12 | 0.0749 | 0.0014 | 1.87 | 0.84 | 1010.3 | 16 | 983 | 19 | 1071 | 35 | 91.78 |
| B_245_27 | 1 | 42.8 | 610 | 0.07 | 1.9970 | 0.0650 | 3.25 | 0.1816 | 0.0052 | 2.86 | 0.0787 | 0.0015 | 1.91 | 0.87 | 1113 | 22 | 1075 | 28 | 1162 | 38 | 92.51 |
| B_245_45 | 1 | 70.6 | 1163 | 0.06 | 2.3470 | 0.0810 | 3.45 | 0.2032 | 0.0050 | 2.46 | 0.0837 | 0.0019 | 2.27 | 0.75 | 1225 | 25 | 1192 | 27 | 1284 | 44 | 92.83 |
| B_245_24 | 1 | 34.6 | 562 | 0.06 | 2.9650 | 0.0830 | 2.80 | 0.2350 | 0.0056 | 2.38 | 0.0918 | 0.0015 | 1.63 | 0.88 | 1398 | 21 | 1360 | 29 | 1462 | 31 | 93.02 |
| B_245_34 | 0 | 80.3 | 781 | 0.10 | 2.4010 | 0.0850 | 3.54 | 0.2063 | 0.0060 | 2.91 | 0.0843 | 0.0021 | 2.49 | 0.78 | 1242 | 25 | 1209 | 32 | 1296 | 49 | 93.29 |
| B_245_7 | 0 | 26.7 | 686 | 0.04 | 1.9410 | 0.0560 | 2.89 | 0.1813 | 0.0042 | 2.32 | 0.0782 | 0.0014 | 1.79 | 0.86 | 1095 | 19 | 1074 | 23 | 1151 | 37 | 93.31 |
| B_245_4 | 0 | 58.6 | 632 | 0.09 | 2.2800 | 0.1600 | 7.02 | 0.1975 | 0.0088 | 4.46 | 0.0821 | 0.0024 | 2.92 | 0.99 | 1200 | 50 | 1161 | 47 | 1243 | 56 | 93.40 |
| B_245_8 | 1 | 107.1 | 655 | 0.16 | 2.0150 | 0.0500 | 2.48 | 0.1842 | 0.0043 | 2.33 | 0.0786 | 0.0014 | 1.78 | 0.78 | 1120.3 | 17 | 1089 | 23 | 1165 | 36 | 93.48 |
| B_245_19 | 0 | 35.1 | 199.5 | 0.18 | 3.7220 | 0.1200 | 3.22 | 0.2680 | 0.0080 | 2.99 | 0.1007 | 0.0019 | 1.89 | 0.93 | 1575 | 27 | 1530 | 41 | 1636 | 35 | 93.52 |
| B_245_36 | 0 | 748 | 810 | 0.92 | 4.1060 | 0.1000 | 2.44 | 0.2826 | 0.0061 | 2.16 | 0.1045 | 0.0020 | 1.91 | 0.72 | 1655 | 20 | 1604 | 31 | 1705 | 35 | 94.08 |
| B_245_6 | 0 | 53.6 | 483 | 0.11 | 2.0150 | 0.0670 | 3.33 | 0.1850 | 0.0046 | 2.49 | 0 | | | | | | | | | | |

| | | | | | | | | | | | | | | | | | | | | | |
|----------|---|-------|-------|------|--------|--------|-------|--------|--------|-------|--------|--------|-------|------|--------|-----|-------------|-----------|------|-----|--------|
| B_245_10 | 0 | 59.9 | 308.6 | 0.19 | 2.1090 | 0.0600 | 2.84 | 0.1940 | 0.0048 | 2.47 | 0.0787 | 0.0013 | 1.65 | 0.92 | 1151 | 20 | 1143 | 26 | 1165 | 34 | 98.11 |
| B_245_9 | 0 | 170.7 | 740 | 0.23 | 2.6400 | 0.0670 | 2.54 | 0.2226 | 0.0046 | 2.07 | 0.0852 | 0.0015 | 1.76 | 0.77 | 1314 | 20 | 1296 | 24 | 1320 | 35 | 98.18 |
| B_245_31 | 0 | 59.3 | 152.9 | 0.39 | 4.4200 | 0.1600 | 3.62 | 0.3034 | 0.0100 | 3.30 | 0.1056 | 0.0022 | 2.08 | 0.88 | 1715 | 30 | 1707 | 51 | 1722 | 39 | 99.13 |
| B_245_42 | 0 | 176.7 | 176.4 | 1.00 | 4.5090 | 0.1200 | 2.66 | 0.3055 | 0.0073 | 2.39 | 0.1060 | 0.0020 | 1.89 | 0.67 | 1732 | 21 | 1718 | 36 | 1731 | 35 | 99.25 |
| B_245_5 | 1 | 92.7 | 131 | 0.71 | 3.0440 | 0.0880 | 2.89 | 0.2447 | 0.0057 | 2.33 | 0.0893 | 0.0016 | 1.79 | 0.79 | 1418 | 22 | 1411 | 29 | 1409 | 34 | 100.14 |
| B_245_1 | 1 | 21.64 | 714 | 0.03 | 2.1780 | 0.0620 | 2.85 | 0.2001 | 0.0051 | 2.55 | 0.0789 | 0.0013 | 1.65 | 0.89 | 1173 | 20 | 1175 | 27 | 1170 | 31 | 100.43 |
| B_245_22 | 1 | 43.3 | 248.7 | 0.17 | 2.0850 | 0.0660 | 3.17 | 0.1943 | 0.0054 | 2.78 | 0.0775 | 0.0014 | 1.81 | 0.87 | 1143 | 22 | 1144 | 29 | 1138 | 37 | 100.53 |
| B_245_39 | 0 | 60.9 | 680 | 0.09 | 1.9860 | 0.0540 | 2.72 | 0.1881 | 0.0039 | 2.07 | 0.0764 | 0.0015 | 1.96 | 0.70 | 1110 | 18 | 1111 | 21 | 1103 | 39 | 100.73 |
| B_245_2 | 0 | 52.2 | 309 | 0.17 | 2.1370 | 0.0620 | 2.90 | 0.1988 | 0.0044 | 2.21 | 0.0775 | 0.0013 | 1.68 | 0.82 | 1160 | 20 | 1169 | 24 | 1134 | 34 | 103.09 |
| B_245_46 | 0 | 28.1 | 551 | 0.05 | 1.7220 | 0.0420 | 2.44 | 0.1718 | 0.0033 | 1.92 | 0.0721 | 0.0011 | 1.53 | 0.79 | 1016.7 | 16 | 1022 | 18 | 989 | 32 | 103.34 |
| B_245_13 | 1 | 61.7 | 270 | 0.23 | 2.3150 | 0.0740 | 3.20 | 0.2123 | 0.0060 | 2.83 | 0.0781 | 0.0013 | 1.67 | 0.92 | 1216 | 23 | 1241 | 32 | 1148 | 33 | 108.10 |
| C_172_3 | 0 | 0.002 | 1.242 | 0.01 | 1.1500 | 0.6100 | 53.04 | 0.0335 | 0.0054 | 16.12 | 0.1800 | 0.0600 | 33.33 | 0.98 | 610 | 200 | 212 | 33 | 2540 | 610 | 8.35 |
| C_172_5 | 0 | 8.51 | 170 | 0.01 | 2.7300 | 0.8000 | 29.30 | 0.0570 | 0.0120 | 21.05 | 0.3680 | 0.0880 | 23.91 | 0.71 | 1230 | 210 | 357 | 71 | 3750 | 400 | 9.52 |
| C_172_4 | 1 | 0.016 | 0.817 | 0.00 | 2.7000 | 1.1000 | 40.74 | 0.0594 | 0.0096 | 16.16 | 0.2670 | 0.0570 | 21.35 | 0.97 | 1060 | 210 | 370 | 58 | 3180 | 350 | 11.64 |
| C_172_6 | 1 | 53.5 | 287 | 0.02 | 8.6000 | 2.5000 | 29.07 | 0.1030 | 0.0160 | 15.53 | 0.5350 | 0.0530 | 9.91 | 0.95 | 2120 | 220 | 627 | 91 | 4290 | 160 | 14.62 |
| C_172_9 | 1 | 88.5 | 229.6 | 0.39 | 2.1830 | 0.0590 | 2.70 | 0.1955 | 0.0046 | 2.35 | 0.0812 | 0.0016 | 1.97 | 0.81 | 1175 | 19 | 1151 | 25 | 1224 | 37 | 94.04 |
| C_172_7 | 0 | 10.89 | 131.7 | 0.19 | 1.7170 | 0.0560 | 3.26 | 0.1691 | 0.0050 | 2.96 | 0.0745 | 0.0017 | 2.28 | 0.78 | 1014 | 21 | 1007 | 28 | 1052 | 47 | 95.72 |
| C_172_8 | 1 | 20.5 | 75.6 | 0.27 | 1.8430 | 0.0650 | 3.53 | 0.1766 | 0.0043 | 2.43 | 0.0757 | 0.0022 | 2.91 | 0.81 | 1060 | 23 | 1048 | 24 | 1092 | 54 | 95.97 |
| C_172_1 | 0 | 0.014 | 1.471 | 0.05 | 1.7120 | 0.0660 | 3.86 | 0.1671 | 0.0055 | 3.29 | 0.0737 | 0.0019 | 2.58 | 0.81 | 1012 | 25 | 995 | 30 | 1030 | 52 | 96.60 |
| C_172_2 | 1 | 0.008 | 0.597 | 0.08 | 1.7350 | 0.0520 | 3.00 | 0.1727 | 0.0042 | 2.43 | 0.0729 | 0.0016 | 2.19 | 0.83 | 1021 | 19 | 1027 | 23 | 1015 | 48 | 101.18 |

U and Pb content and Th/U ratio were calculated according to the nominal concentrations of Plesovice and GJ-1 reference zircons for the SGC and ETH Laboratories respectively

Decay constants of Jaffey et al. (1971) used

Measurements in italic are not plotted in figures and used in geochronological interpretations

Corrected isotope ratios: background extracted, drift and fractionation from (the nominal ID-TIMS) value of Plesovice GJ-1 reference zircons for the SGC and ETH Laboratories respectively

The $^{207}\text{Pb}/^{235}\text{U}$ ratio is calculated by the corrected 7/6 and 6/8 ratios as $^{207}\text{Pb}/^{206}\text{Pb} / (^{238}\text{U}/^{206}\text{Pb} * 1/137.88)$.

$\text{Rho} = ^{206}\text{Pb}/^{238}\text{U} / ^{207}\text{Pb}/^{235}\text{U}$ error correlation coefficient.

All Isotopic ratios are reported with propagated uncertainties at $2\sigma_{\text{sys}}$ level, as data from different facilities (SGC-ETH) is presented as recommended by Horstwood et al., 2016

$2\sigma_{\text{sys}}$ = Reproducibility of reference material uncertainty is propagated. Ages are quoted at 2 SE absolute, propagation is by quadratic addition.

Concordance = Concordance is calculated as $100 * ((^{206}\text{Pb}/^{238}\text{U} \text{ age}) / (^{207}\text{Pb}/^{206}\text{Pb} \text{ age}))$ for grains older than 250 Ma and $100 * ((^{206}\text{Pb}/^{238}\text{U} \text{ age}) / (207\text{Pb}/235\text{U} \text{ age}))$ for grains younger than 250 Ma

TABLE A2. Trace elements in Zircon [ppm], and Ti-in Zr Thermometry

| Sample | Target | Age U ²⁰⁶ /Pb ²³⁸ | error 2s | Al | P | Ti | Y | Nb | Ba | La | Ce | Pr | Nd | Sm | Eu | Gd | Tb | Dy | Ho | Er | Tm | Yb | Lu | Hf | Pb | Th | U | Log Ti | T ° C |
|------------|--------|---|----------|-----------|-----------|-------------|--------|-----------|-----------|-----------|-----------|-----------|-----------|-----------|-----------|-----------|------|-------|-------|-------|-------|-------|-------|-------|-------|-------|-------|--------|-------|
| G-52d - 7 | rim | 170.8 | 4.5 | Below LOD | Below LOD | Below LOD | 459.00 | 1.05 | 0.27 | Below LOD | 1.69 | Below LOD | 0.33 | 0.89 | 0.17 | 6.50 | 3.58 | 44.20 | 16.20 | 60.20 | 10.60 | 88.70 | 18.20 | 13440 | 53.3 | 7.74 | 521 | N/A | N/A |
| G-52d - 30 | rim | 204.5 | 6 | Below LOD | Below LOD | Below LOD | 36.40 | 0.43 | Below LOD | 0.18 | Below LOD | Below LOD | Below LOD | Below LOD | Below LOD | Below LOD | 0.24 | 2.79 | 1.19 | 5.84 | 1.34 | 17.30 | 3.30 | 12420 | 15.5 | 0.31 | 115.9 | N/A | N/A |
| G-52d - 33 | rim | 213.8 | 5.9 | Below LOD | Below LOD | Below LOD | 26.30 | 0.39 | 0.09 | Below LOD | Below LOD | Below LOD | Below LOD | Below LOD | Below LOD | Below LOD | 0.37 | 3.10 | 0.78 | 3.47 | 0.69 | 6.30 | 1.16 | 11600 | 20.24 | 2.82 | 140 | N/A | N/A |
| G-52d - 44 | rim | 218.7 | 7.3 | Below LOD | Below LOD | Below LOD | 54.10 | 0.53 | 0.14 | Below LOD | 0.68 | Below LOD | 0.27 | 0.37 | 0.29 | 1.87 | 0.76 | 6.07 | 1.57 | 5.47 | 1.02 | 7.09 | 1.01 | 9940 | 26.4 | 6.43 | 179 | N/A | N/A |
| G-52d - 58 | rim | 219.9 | 6.1 | 290 | Below LOD | Below LOD | 106.70 | 0.34 | 0.27 | Below LOD | 0.99 | 0.05 | 0.52 | 0.82 | 0.62 | 4.60 | 1.30 | 11.80 | 3.29 | 11.20 | 1.90 | 14.90 | 2.84 | 9910 | 38.6 | 20.3 | 266 | N/A | N/A |
| G-52d - 54 | core | 220.1 | 5.8 | Below LOD | 119 | Below LOD | 88.90 | 0.70 | 1.89 | Below LOD | 1.12 | Below LOD | 0.60 | 1.98 | 0.74 | 9.90 | 2.12 | 14.20 | 2.81 | 8.62 | 1.21 | 9.80 | 1.58 | 10980 | 43.5 | 19.9 | 310 | N/A | N/A |
| G-52d - 25 | rim | 222.5 | 5.5 | Below LOD | Below LOD | Below LOD | 199.00 | 1.96 | 0.12 | Below LOD | 0.43 | Below LOD | Below LOD | 0.47 | 0.29 | 3.81 | 1.68 | 18.30 | 6.40 | 27.10 | 5.51 | 54.00 | 10.15 | 10840 | 85.9 | 5.57 | 606 | N/A | N/A |
| G-52d - 69 | core | 222.9 | 6.6 | Below LOD | Below LOD | Below LOD | 66.80 | 0.44 | Below LOD | Below LOD | 0.21 | Below LOD | Below LOD | 0.42 | 0.19 | 1.95 | 0.58 | 6.40 | 2.08 | 8.10 | 1.57 | 16.00 | 3.46 | 9770 | 14.1 | 1.91 | 96.7 | N/A | N/A |
| G-52d - 70 | rim | 223.6 | 5.7 | Below LOD | 102 | Below LOD | 36.60 | 0.53 | Below LOD | Below LOD | 0.78 | Below LOD | Below LOD | 0.12 | 0.14 | 1.48 | 0.47 | 3.96 | 1.22 | 4.74 | 0.94 | 10.00 | 1.58 | 11120 | 36 | 7.96 | 252.8 | N/A | N/A |
| G-52d - 17 | rim | 223.8 | 6.4 | Below LOD | Below LOD | Below LOD | 73.50 | 0.51 | Below LOD | Below LOD | Below LOD | Below LOD | Below LOD | Below LOD | 0.14 | 1.40 | 0.58 | 7.32 | 2.06 | 8.33 | 1.55 | 11.90 | 2.24 | 10050 | 17.68 | 0.18 | 123.6 | N/A | N/A |
| G-52d - 15 | rim | 225 | 5.6 | Below LOD | Below LOD | Below LOD | 106.40 | 0.49 | 1.13 | Below LOD | 0.63 | Below LOD | Below LOD | 0.38 | 0.20 | 3.00 | 0.98 | 10.60 | 3.62 | 14.20 | 3.17 | 28.10 | 6.12 | 11330 | 46.9 | 7.57 | 324 | N/A | N/A |
| G-52d - 42 | rim | 225 | 5.1 | Below LOD | Below LOD | Below LOD | 49.00 | 1.28 | Below LOD | Below LOD | 1.05 | Below LOD | 0.35 | 0.79 | 0.41 | 5.01 | 1.45 | 8.01 | 1.63 | 5.02 | 0.79 | 4.17 | 0.65 | 10520 | 42.7 | 14.07 | 291 | N/A | N/A |
| G-52d - 8 | core | 225.1 | 4.9 | Below LOD | Below LOD | Below LOD | 217.60 | 2.15 | Below LOD | Below LOD | 0.71 | Below LOD | Below LOD | 0.64 | 0.44 | 4.25 | 1.83 | 20.40 | 7.16 | 28.80 | 5.83 | 53.90 | 11.42 | 10280 | 81.7 | 7.01 | 560 | N/A | N/A |
| G-52d - 51 | rim | 225.1 | 5.8 | Below LOD | Below LOD | Below LOD | 105.90 | 0.41 | Below LOD | Below LOD | 0.69 | Below LOD | Below LOD | 0.37 | 0.27 | 3.90 | 1.06 | 9.20 | 3.18 | 13.40 | 2.97 | 24.20 | 4.49 | 10960 | 48.2 | 10 | 338 | N/A | N/A |
| G-52d - 9 | rim | 225.2 | 5.8 | Below LOD | 80 | Below LOD | 35.70 | 0.33 | 0.19 | Below LOD | 0.30 | Below LOD | Below LOD | Below LOD | 0.07 | 0.84 | 0.42 | 3.35 | 1.15 | 5.02 | 1.04 | 10.00 | 2.39 | 11860 | 17.56 | 2.57 | 123.9 | N/A | N/A |
| G-52d - 43 | core | 225.4 | 5.5 | Below LOD | Below LOD | Below LOD | 101.70 | 0.93 | 0.16 | 0.12 | 1.49 | 0.06 | 0.95 | 2.77 | 0.98 | 12.70 | 2.55 | 15.80 | 3.21 | 9.20 | 1.43 | 10.50 | 1.75 | 10400 | 55.3 | 23.29 | 373 | N/A | N/A |
| G-52d - 46 | rim | 225.6 | 5.8 | Below LOD | Below LOD | Below LOD | 40.90 | 0.49 | Below LOD | Below LOD | 0.41 | Below LOD | Below LOD | 0.17 | 0.21 | 1.63 | 0.48 | 4.39 | 0.95 | 3.58 | 0.56 | 3.92 | 0.82 | 10990 | 54 | 5.43 | 367 | N/A | N/A |
| G-52d - 26 | core | 225.8 | 5 | Below LOD | Below LOD | Below LOD | 254.00 | 1.98 | 0.25 | Below LOD | 0.24 | Below LOD | Below LOD | 0.55 | 0.45 | 4.90 | 1.77 | 20.00 | 8.45 | 36.40 | 7.83 | 68.80 | 14.30 | 10650 | 92.4 | 4.04 | 658 | N/A | N/A |
| G-52d - 63 | core | 225.8 | 6.3 | Below LOD | Below LOD | Below LOD | 82.90 | Below LOD | Below LOD | Below LOD | 0.36 | Below LOD | Below LOD | 0.30 | 0.25 | 1.90 | 0.86 | 7.68 | 2.73 | 10.00 | 2.44 | 19.50 | 4.35 | 10450 | 32.6 | 1.85 | 217.2 | N/A | N/A |
| G-52d - 71 | core | 225.9 | 6.1 | Below LOD | Below LOD | Below LOD | 97.70 | 0.73 | Below LOD | Below LOD | 1.27 | Below LOD | 0.44 | 0.48 | 0.33 | 3.50 | 1.17 | 11.50 | 3.00 | 8.57 | 1.64 | 11.30 | 1.67 | 10100 | 35.4 | 7.21 | 250 | N/A | N/A |
| G-52d - 23 | core | 226.1 | 5.4 | Below LOD | Below LOD | Below LOD | 91.80 | 0.63 | Below LOD | Below LOD | 0.83 | Below LOD | Below LOD | 0.94 | 0.47 | 5.42 | 1.65 | 12.50 | 3.22 | 10.35 | 1.63 | 15.20 | 3.17 | 10590 | 43.1 | 13.28 | 300 | N/A | N/A |
| G-52d - 20 | rim | 226.3 | 5.2 | Below LOD | Below LOD | Below LOD | 47.30 | 0.81 | Below LOD | Below LOD | 0.57 | Below LOD | Below LOD | 0.34 | 0.22 | 3.13 | 0.92 | 6.00 | 1.44 | 4.16 | 0.73 | 4.91 | 0.65 | 10270 | 43.2 | 9.71 | 295 | N/A | N/A |
| G-52d - 55 | core | 226.6 | 5.6 | Below LOD | Below LOD | Below LOD | 59.20 | 0.53 | Below LOD | Below LOD | 0.60 | Below LOD | 0.19 | 0.73 | 0.58 | 4.00 | 1.17 | 7.76 | 1.85 | 5.34 | 0.70 | 6.60 | 1.23 | 10490 | 31.6 | 7.79 | 219 | N/A | N/A |
| G-52d - 49 | rim | 226.7 | 5.7 | Below LOD | Below LOD | Below LOD | 175.00 | 0.88 | Below LOD | Below LOD | 0.73 | Below LOD | 0.32 | 0.49 | 0.31 | 4.60 | 1.58 | 17.00 | 5.47 | 22.50 | 4.64 | 41.40 | 8.40 | 10790 | 54.2 | 8 | 364 | N/A | N/A |
| G-52d - 36 | rim | 227 | 5.4 | Below LOD | Below LOD | Below LOD | 72.80 | 0.47 | Below LOD | 0.16 | 0.51 | Below LOD | 0.30 | 0.20 | 0.18 | 1.29 | 0.81 | 6.60 | 2.35 | 10.51 | 2.20 | 19.50 | 4.01 | 11070 | 57.3 | 7.59 | 390 | N/A | N/A |
| G-52d - 68 | rim | 227.1 | 6.3 | Below LOD | Below LOD | 22 | 53.10 | 0.54 | 0.26 | Below LOD | 0.69 | Below LOD | Below LOD | 0.57 | 0.53 | 4.40 | 0.98 | 8.70 | 1.54 | 4.49 | 0.60 | 5.40 | 0.94 | 12550 | 34.5 | 11 | 241 | 1.3 | 815.2 |
| G-52d - 65 | core | 227.2 | 5.3 | Below LOD | Below LOD | Below LOD | 95.90 | 0.78 | Below LOD | 0.15 | 0.53 | Below LOD | 0.19 | 0.56 | 0.41 | 2.72 | 1.29 | 9.30 | 2.72 | 10.50 | 2.30 | 22.10 | 5.85 | 11150 | 52.5 | 8.57 | 358 | N/A | N/A |
| G-52d - 37 | core | 227.6 | 5.5 | Below LOD | Below LOD | Below LOD | 160.90 | 0.91 | 0.16 | Below LOD | 0.45 | Below LOD | Below LOD | 0.37 | 0.34 | 3.80 | 1.41 | 15.10 | 5.11 | 21.10 | 4.43 | 39.20 | 8.04 | 11090 | 52.2 | 8.48 | 363 | N/A | N/A |
| G-52d - 53 | rim | 227.7 | 6 | Below LOD | Below LOD | Below LOD | 76.00 | 0.82 | 0.20 | Below LOD | 1.11 | Below LOD | 0.40 | 1.35 | 0.62 | 7.26 | 1.76 | 11.39 | 2.44 | 5.76 | 1.04 | 6.74 | 1.16 | 10930 | 41.8 | 12.92 | 285 | N/A | N/A |
| G-52d - 72 | rim | 227.9 | 5.7 | Below LOD | Below LOD | Below LOD | 60.20 | 0.66 | Below LOD | Below LOD | 0.66 | Below LOD | Below LOD | 0.72 | 0.28 | 3.32 | 1.00 | 7.89 | 1.76 | 5.35 | 0.94 | 6.80 | 1.10 | 10680 | 43.5 | 9.66 | 304 | N/A | N/A |
| G-52d - 62 | core | 228.1 | 5.9 | Below LOD | Below LOD | Below LOD | 102.20 | 0.69 | 2.10 | Below LOD | 0.67 | Below LOD | Below LOD | 0.29 | 0.21 | 2.61 | 0.98 | 10.80 | 3.49 | 13.50 | 3.13 | 33.90 | 7.65 | 11340 | 34 | 4.62 | 234 | N/A | N/A |
| G-52d - 31 | core | 228.4 | 6.3 | Below LOD | Below LOD | Below LOD | 46.30 | Below LOD | Below LOD | Below LOD | 0.50 | Below LOD | Below LOD | 0.24 | 0.27 | 1.64 | 0.42 | 4.55 | 1.33 | 6.96 | 1.47 | 15.00 | 3.68 | 10330 | 19.2 | 5.84 | 132.7 | N/A | N/A |
| G-52d - 3 | core | 228.8 | 5.4 | Below LOD | Below LOD | Below LOD | 50.50 | 0.62 | Below LOD | Below LOD | 0.80 | Below LOD | 0.23 | 0.73 | 0.52 | 3.88 | 0.98 | 6.73 | 1.59 | 4.38 | 0.81 | 5.69 | 1.22 | 11280 | 43.9 | 17.85 | 299 | N/A | N/A |
| G-52d - 75 | core | 228.9 | 6.1 | Below LOD | Below LOD | Below LOD | 32.70 | 0.87 | 0.12 | Below LOD | 0.83 | Below LOD | 0.35 | 0.34 | 0.29 | 2.31 | 0.60 | 4.57 | 1.11 | 2.79 | 0.51 | 4.35 | 0.72 | 11230 | 33.5 | 12.09 | 229 | N/A | N/A |
| G-52d - 39 | rim | 229.3 | 5.5 | Below LOD | Below LOD | Below LOD | 23.50 | 0.46 | Below LOD | Below LOD | 0.59 | Below LOD | Below LOD | 0.40 | 0.18 | 1.46 | 0.49 | 3.52 | 0.79 | 2.07 | 0.30 | 2.41 | 0.36 | 11340 | 38.2 | 9.6 | 261 | N/A | N/A |
| G-52d - 22 | rim | 229.7 | 5.7 | Below LOD | Below LOD | Below LOD | 33.10 | 0.70 | Below LOD | Below LOD | 0.78 | Below LOD | Below LOD | 0.43 | 0.29 | 3.02 | 0.70 | 4.62 | 1.19 | 3.54 | 0.59 | 4.43 | 0.80 | 10940 | 42.6 | 10.86 | 292 | N/A | N/A |
| G-52d - 10 | core | 229.8 | 5.2 | Below LOD | Below LOD | Below LOD | 206.00 | 0.70 | Below LOD | 0.13 | 0.64 | Below LOD | 0.45 | 1.56 | 0.79 | 9.80 | 2.64 | 25.00 | 7.04 | 23.90 | 4.50 | 37.50 | 6.78 | 10970 | 70.9 | 25.3 | 497 | N/A | N/A |
| G-52d - 35 | core | 230.8 | 5.4 | Below LOD | Below LOD | Below LOD | 46.50 | 0.64 | 0.13 | Below LOD | 0.76 | Below LOD | 0.26 | 0.49 | 0.44 | 3.82 | 0.90 | 5.94 | 1.33 | 3.91 | 0.57 | 6.02 | 0.94 | 13050 | 45.3 | 19.5 | 306 | N/A | N/A |
| G-52d - 57 | rim | 230.8 | 5.2 | Below LOD | Below LOD | Below LOD | 149.40 | 2.17 | Below LOD | Below LOD | 0.64 | Below LOD | Below LOD | 0.27 | 0.23 | 3.32 | 1.28 | 13.60 | 5.04 | 18.70 | 4.19 | 35.90 | 7.28 | 11230 | 75.4 | 5.92 | 510 | N/A | N/A |
| G-52d - 48 | core | 230.9 | 6.4 | Below LOD | Below LOD | Below LOD | 112.80 | 0.81 | Below LOD | Below LOD | 0.74 | Below LOD | 0.37 | 0.55 | 0.30 | 3.26 | 1.26 | 11.20 | 3.71 | 13.60 | 3.24 | 26.60 | 5.35 | 10920 | 39 | 11.5 | 261 | N/A | N/A |
| G-52d - 41 | rim | 231.1 | 5.5 | Below LOD | Below LOD | Below LOD | 18.71 | 0.84 | Below LOD | Below LOD | 0.72 | Below LOD | Below LOD | 0.23 | 0.15 | 1.26 | 0.39 | 3.39 | 0.66 | 1.56 | 0.26 | 1.89 | 0.29 | 11690 | 46 | 13.87 | 305.7 | N/A | N/A |
| G-52d - 29 | core | 231.5 | 5.9 | Below LOD | Below LOD | Below LOD | 41.50 | Below LOD | Below LOD | Below LOD | 0.55 | Below LOD | 0.31 | 0.27 | 0.25 | 2.45 | 0.78 | 5.14 | 1.20 | 3.72 | 0.60 | 3.43 | 0.68 | 11080 | 26.4 | 6.16 | 178 | N/A | N/A |
| G-52d - 66 | rim | 231.6 | 7.1 | Below LOD | Below LOD | Below LOD | 37.10 | Below LOD | Below LOD | Below LOD | 0.36 | Below LOD | Below LOD | 0.39 | 0.22 | 2.11 | 0.50 | 5.27 | 1.44 | 3.92 | 0.63 | 4.47 | 0.81 | 9870 | 11.69 | 4.74 | 80.2 | N/A | N/A |
| G-52d - 18 | core | 231.8 | 7.1 | Below LOD | Below LOD | Below LOD | 61.80 | 0.66 | Below LOD | 0.14 | Below LOD | Below LOD | Below LOD | Below LOD | 0.09 | 1.12 | 0.40 | 5.75 | 1.93 | 6.80 | 1.17 | 9.20 | 1.89 | 9550 | 20 | 0.157 | 129.4 | N/A | N/A |
| G-52d - 38 | core | 231.9 | 5.7 | Below LOD | Below LOD | Below LOD | 102.50 | 0.48 | Below LOD | Below LOD | 0.76 | Below LOD | 0.33 | 1.17 | 0.66 | 6.06 | 1.74 | 13.70 | 3.41 | 8.79 | 1.57 | 9.25 | 1.69 | 10080 | 42.5 | 12.43 | 287 | N/A | N/A |
| G-52d - 47 | core | 232.2 | 5.7 | Below LOD | Below LOD | Below LOD | 32.50 | 0.67 | Below LOD | Below LOD | 0.42 | 0.03 | Below LOD | 0.23 | 0.18 | 1.54 | 0.50 | 3.73 | 0.91 | 2.69 | 0.48 | 3.55 | 0.56 | 11110 | 53 | 4.83 | 355 | N/A | N/A |
| G-52d - 12 | core | 232.5 | 6.1 | Below LOD | Below LOD | Below LOD</ | | | | | | | | | | | | | | | | | | | | | | | |

| | | | | | | | | | | | | | | | | | | | | | | | | | | | | | | |
|-----------|------|-------|-----|-----------|-----------|-----------|---------|-----------|-----------|-----------|-----------|-----------|-----------|-----------|-----------|-----------|-----------|--------|-----------|--------|-----------|-----------|-----------|-----------|-------|-------|-----------|---------|---------|-----|
| G-54 - 39 | rim | 229.8 | 5 | Below LOD | Below LOD | Below LOD | 261.00 | 0.46 | Below LOD | Below LOD | 0.47 | Below LOD | 0.33 | 0.87 | 0.31 | 6.64 | 2.82 | 28.60 | 9.20 | 31.30 | 5.80 | 43.40 | 8.01 | 12280 | 99.6 | 11.24 | 665 | N/A | N/A | |
| G-54 - 44 | core | 230.2 | 5 | Below LOD | 115 | Below LOD | 204.00 | 1.30 | Below LOD | Below LOD | 1.30 | Below LOD | 0.06 | 0.62 | 2.40 | 0.46 | 15.20 | 4.53 | 32.60 | 6.89 | 19.90 | 3.17 | 24.00 | 4.25 | 11230 | 60.5 | 19.3 | 412 | N/A | N/A |
| G-54 - 45 | core | 231 | 5.3 | Below LOD | 180 | Below LOD | 170.70 | 0.62 | Below LOD | Below LOD | 0.80 | Below LOD | 0.06 | 0.62 | 2.38 | 0.39 | 19.10 | 4.68 | 31.80 | 5.87 | 13.25 | 2.21 | 13.80 | 2.52 | 11880 | 51.8 | 13.6 | 351 | N/A | N/A |
| G-54 - 72 | core | 234.1 | 5.4 | Below LOD | 158 | Below LOD | 336.00 | 1.11 | Below LOD | Below LOD | 1.20 | Below LOD | 0.78 | 5.07 | 0.64 | 36.90 | 11.31 | 73.40 | 11.79 | 23.70 | 2.45 | 11.40 | 1.03 | 14560 | 37.2 | 32.2 | 2500 | N/A | N/A | |
| G-54 - 33 | rim | 234.1 | 6.5 | Below LOD | Below LOD | Below LOD | 156.00 | 0.68 | Below LOD | Below LOD | 0.57 | Below LOD | 0.04 | 0.47 | 1.86 | 0.27 | 12.30 | 3.89 | 26.40 | 5.25 | 13.12 | 1.81 | 14.10 | 1.53 | 11990 | 59.8 | 11.62 | 401 | N/A | N/A |
| G-54 - 33 | core | 234.4 | 4.9 | Below LOD | 145 | Below LOD | 240.00 | 0.84 | Below LOD | Below LOD | 0.61 | Below LOD | 0.19 | 1.03 | 0.26 | 8.80 | 3.25 | 31.10 | 7.51 | 27.50 | 5.03 | 44.60 | 9.63 | 12710 | 183 | 12.18 | 1200 | N/A | N/A | |
| G-54 - 59 | rim | 234.7 | 8.7 | Below LOD | 270 | Below LOD | 261.00 | 4.70 | 1.15 | Below LOD | 0.32 | Below LOD | 0.03 | 0.24 | 0.62 | 0.21 | 5.50 | 2.67 | 28.10 | 8.50 | 35.00 | 8.30 | 85.00 | 17.30 | 12380 | 122.2 | 10.3 | 840 | N/A | N/A |
| G-54 - 49 | rim | 235.8 | 5.5 | Below LOD | 173 | Below LOD | 233.20 | 0.66 | Below LOD | Below LOD | 0.89 | Below LOD | 0.64 | 0.66 | 2.12 | 0.33 | 12.80 | 4.26 | 33.10 | 8.26 | 26.40 | 4.87 | 40.40 | 6.96 | 12690 | 104.1 | 11.27 | 686 | N/A | N/A |
| G-54 - 73 | rim | 235.9 | 6.5 | Below LOD | 230 | Below LOD | 252.80 | 0.95 | 3.53 | 0.29 | 1.28 | 0.07 | 0.65 | 1.44 | 0.43 | 10.60 | 3.89 | 33.30 | 8.23 | 28.20 | 4.62 | 40.40 | 7.81 | 12590 | 65.2 | 11.83 | 412 | N/A | N/A | |
| G-54 - 62 | rim | 237.4 | 5.3 | Below LOD | 155 | Below LOD | 608.00 | 3.66 | 0.66 | 0.44 | 9.00 | 0.18 | 1.41 | 2.01 | 0.40 | 10.90 | 4.06 | 48.30 | 19.60 | 97.00 | 23.40 | 249.00 | 55.40 | 12120 | 87.9 | 69 | 585 | N/A | N/A | |
| G-54 - 25 | core | 239.6 | 6.1 | Below LOD | 254 | Below LOD | 533.00 | 2.34 | 1.98 | 1.36 | 10.70 | 2.05 | 14.70 | 13.80 | 2.01 | 38.50 | 10.59 | 79.50 | 18.20 | 50.70 | 7.98 | 57.80 | 9.34 | 11900 | 131 | 55.5 | 820 | N/A | N/A | |
| G-54 - 37 | rim | 240.4 | 8.3 | Below LOD | Below LOD | Below LOD | 244.00 | 8.30 | 0.12 | Below LOD | 0.56 | Below LOD | 0.19 | 0.43 | 0.13 | 3.66 | 1.56 | 19.40 | 7.73 | 44.70 | 15.40 | 192.00 | 40.60 | 12550 | 73.5 | 6.98 | 496 | N/A | N/A | |
| G-54 - 90 | rim | 241.2 | 44 | 828 | Below LOD | 86 | 197.00 | 1.69 | 19.80 | Below LOD | 0.77 | 0.07 | 0.45 | 2.68 | 0.38 | 16.50 | 4.96 | 32.40 | 6.56 | 16.10 | 2.69 | 19.60 | 3.70 | 12370 | 56.3 | 12.43 | 387 | 1.9 | 973.3 | |
| G-54 - 16 | core | 246.8 | 5.9 | Below LOD | 530 | 7.3 | 2084.00 | 4.25 | 0.61 | Below LOD | 16.50 | 0.21 | 3.76 | 9.60 | 0.55 | 53.80 | 18.39 | 209.00 | 74.60 | 308.00 | 62.40 | 520.00 | 95.50 | 9750 | 88.5 | 413 | 553 | 0.9 | 713.9 | |
| G-54 - 55 | rim | 248.7 | 14 | Below LOD | 230 | 11.5 | 422.00 | 1.58 | 0.80 | Below LOD | 0.78 | Below LOD | 0.52 | 1.31 | 0.24 | 10.10 | 3.70 | 31.30 | 12.37 | 69.10 | 19.10 | 214.00 | 51.60 | 12590 | 100.2 | 19.4 | 674 | 1.1 | 753.3 | |
| G-54 - 13 | rim | 249.4 | 6.3 | Below LOD | 380 | Below LOD | 853.00 | 3.57 | 3.70 | 6.10 | 20.00 | 1.50 | 6.90 | 2.50 | 0.28 | 11.80 | 4.95 | 67.00 | 27.30 | 144.00 | 35.40 | 360.00 | 78.70 | 12690 | 69.9 | 153 | 431 | N/A | N/A | |
| G-54 - 38 | core | 253.8 | 65 | Below LOD | Below LOD | Below LOD | 225.00 | Below LOD | Below LOD | Below LOD | Below LOD | Below LOD | Below LOD | Below LOD | Below LOD | Below LOD | 24.60 | 29.70 | 29.70 | 29.70 | 63.00 | Below LOD | 63.00 | Below LOD | 12910 | 82.2 | Below LOD | 561 | N/A | N/A |
| G-54 - 79 | rim | 258.8 | 7 | 522 | 360 | Below LOD | 684.00 | 2.56 | 3.20 | 4.11 | 30.90 | 4.50 | 27.90 | 23.20 | 3.74 | 44.00 | 13.40 | 103.70 | 25.80 | 82.80 | 13.08 | 99.70 | 18.30 | 13650 | 595 | 150 | 3500 | N/A | N/A | |
| G-54 - 83 | core | 262.9 | 5.7 | Below LOD | Below LOD | Below LOD | 1135.00 | 1.89 | 0.45 | Below LOD | 25.50 | 0.16 | 3.16 | 5.71 | 1.64 | 25.00 | 8.24 | 92.60 | 37.60 | 174.30 | 40.90 | 426.00 | 91.10 | 11090 | 110.5 | 544 | 654 | #VALUE! | #VALUE! | |
| G-54 - 14 | core | 263.5 | 6.4 | 119 | 1290 | Below LOD | 3180.00 | 5.47 | 1.83 | 41.00 | 134.00 | 15.50 | 71.00 | 21.60 | 1.95 | 60.50 | 19.90 | 261.00 | 110.40 | 549.00 | 125.00 | 1169.00 | 240.00 | 8840 | 65.7 | 260 | 397 | N/A | N/A | |
| G-54 - 6 | core | 265.5 | 6.3 | Below LOD | 310 | 12.2 | 544.00 | 2.91 | 0.86 | Below LOD | 16.60 | 0.07 | 0.80 | 2.11 | 0.76 | 10.20 | 3.90 | 47.70 | 18.80 | 84.20 | 18.70 | 173.00 | 34.00 | 10410 | 99.5 | 28.1 | 571 | 1.1 | 758.6 | |
| G-54 - 31 | core | 267.9 | 7.5 | 268 | 520 | 12.2 | 628.00 | 7.70 | 7.40 | 0.17 | 1.48 | 0.10 | 0.97 | 1.47 | 0.40 | 6.20 | 3.57 | 42.60 | 19.10 | 108.80 | 30.50 | 325.00 | 60.00 | 12050 | 155.4 | 23.7 | 849 | 1.1 | 758.6 | |
| G-54 - 2 | core | 274 | 8.1 | Below LOD | 460 | Below LOD | 836.00 | 0.80 | 0.28 | 0.38 | 13.70 | 0.36 | 4.09 | 4.08 | 1.39 | 18.40 | 5.83 | 70.20 | 26.60 | 131.00 | 31.10 | 314.00 | 68.10 | 10490 | 18.1 | 79.8 | 105.3 | N/A | N/A | |
| G-54 - 63 | core | 276.9 | 6.5 | Below LOD | 178 | Below LOD | 930.00 | 3.04 | 0.08 | Below LOD | 23.10 | 0.06 | 0.82 | 2.29 | 0.30 | 13.60 | 5.43 | 69.60 | 31.00 | 156.50 | 36.30 | 365.00 | 75.00 | 13030 | 68.3 | 225 | 384 | N/A | N/A | |
| G-54 - 66 | rim | 280.1 | 25 | Below LOD | Below LOD | Below LOD | 258.00 | 0.38 | 0.13 | Below LOD | 0.93 | Below LOD | 0.24 | 0.84 | 0.16 | 7.40 | 2.48 | 28.90 | 9.20 | 33.30 | 6.41 | 56.90 | 10.30 | 13240 | 165.3 | 24.2 | 1030 | N/A | N/A | |
| G-54 - 1 | core | 296.2 | 11 | Below LOD | 370 | Below LOD | 965.00 | 8.34 | 0.39 | Below LOD | 22.80 | 0.05 | 0.68 | 2.01 | 0.54 | 14.10 | 5.55 | 72.90 | 31.50 | 172.00 | 43.80 | 409.00 | 74.10 | 11360 | 106.2 | 53 | 542 | N/A | N/A | |
| G-54 - 70 | rim | 300.1 | 8.9 | Below LOD | 265 | Below LOD | 505.00 | 8.70 | 1.08 | Below LOD | 0.33 | Below LOD | 0.28 | 0.37 | 0.11 | 2.39 | 1.41 | 23.20 | 14.40 | 103.60 | 34.20 | 384.00 | 75.10 | 12050 | 115.8 | 24.2 | 574 | N/A | N/A | |
| G-54 - 18 | core | 301 | 89 | Below LOD | 290 | 10.3 | 842.00 | 4.75 | 0.61 | Below LOD | 6.40 | 0.02 | 0.87 | 1.21 | 0.20 | 9.30 | 3.57 | 50.50 | 25.70 | 154.00 | 44.50 | 438.00 | 86.20 | 12370 | 210 | 56.4 | 1146 | 1.0 | 743.4 | |
| G-54 - 42 | core | 302.2 | 9.7 | Below LOD | 228 | Below LOD | 348.00 | 1.40 | 0.13 | Below LOD | 3.90 | 0.09 | 0.78 | 1.91 | 0.08 | 9.40 | 3.38 | 33.20 | 11.68 | 48.10 | 9.97 | 79.90 | 16.37 | 10840 | 52.9 | 71.3 | 262 | N/A | N/A | |
| G-54 - 57 | core | 302.5 | 21 | Below LOD | 430 | Below LOD | 1423.00 | 11.00 | 0.71 | Below LOD | 8.30 | 0.07 | 1.41 | 2.78 | 0.65 | 17.00 | 7.77 | 104.70 | 46.80 | 257.00 | 70.50 | 717.00 | 135.40 | 12220 | 105.1 | 84.8 | 568 | N/A | N/A | |
| G-54 - 53 | core | 307.5 | 6.5 | 129 | 470 | 36 | 1640.00 | 4.29 | 2.18 | Below LOD | 19.30 | 0.17 | 2.72 | 5.55 | 1.18 | 30.40 | 10.90 | 131.00 | 53.30 | 262.00 | 59.70 | 605.00 | 127.50 | 12750 | 121.3 | 332 | 616 | 1.6 | 867.5 | |
| G-54 - 69 | rim | 311.3 | 11 | Below LOD | 132 | Below LOD | 343.00 | 1.76 | 0.35 | Below LOD | 2.60 | Below LOD | 0.48 | 0.96 | 0.19 | 7.40 | 2.50 | 29.80 | 10.96 | 50.60 | 10.87 | 105.10 | 22.20 | 11910 | 113.2 | 25.3 | 592 | N/A | N/A | |
| G-54 - 24 | rim | 312.6 | 6.6 | Below LOD | 143 | Below LOD | 544.00 | 3.08 | 0.17 | Below LOD | 7.83 | 0.03 | 0.30 | 0.90 | 0.14 | 7.11 | 2.96 | 40.10 | 17.12 | 84.80 | 21.10 | 212.00 | 46.80 | 11440 | 113.7 | 113.9 | 547 | N/A | N/A | |
| G-54 - 20 | core | 337.8 | 9.5 | 690 | 155 | 60 | 588.00 | 5.49 | 10.50 | Below LOD | 3.40 | 0.07 | 0.93 | 1.88 | 0.35 | 9.84 | 3.77 | 44.80 | 18.60 | 109.80 | 32.60 | 362.00 | 76.30 | 10090 | 47.3 | 35.9 | 228 | 1.8 | 927.3 | |
| G-54 - 86 | rim | 342 | 7.4 | Below LOD | 240 | Below LOD | 408.00 | 2.39 | 0.19 | 0.11 | 2.43 | Below LOD | 0.29 | 0.95 | 0.21 | 7.50 | 3.08 | 34.70 | 13.30 | 66.30 | 15.70 | 160.70 | 33.20 | 12420 | 169.4 | 30 | 780 | N/A | N/A | |
| G-54 - 67 | core | 372.9 | 8.1 | Below LOD | 330 | Below LOD | 540.00 | 2.84 | Below LOD | 0.15 | 1.61 | 0.05 | 0.65 | 1.30 | 0.12 | 8.00 | 3.22 | 41.90 | 18.20 | 90.50 | 20.20 | 201.00 | 38.20 | 14020 | 165 | 66.5 | 673 | N/A | N/A | |
| G-54 - 81 | core | 377.9 | 16 | 250 | 330 | 29 | 1155.00 | 3.49 | 7.80 | Below LOD | 7.45 | 0.08 | 0.87 | 3.49 | 1.10 | 19.10 | 7.39 | 96.30 | 41.20 | 192.00 | 40.80 | 395.00 | 81.40 | 9610 | 80.5 | 111.4 | 312 | 1.5 | 843.9 | |
| G-54 - 75 | core | 395.8 | 9.1 | Below LOD | 204 | Below LOD | 547.00 | 19.30 | 0.60 | Below LOD | 7.12 | 0.06 | 0.60 | 1.41 | 0.19 | 10.00 | 3.19 | 43.90 | 18.20 | 98.60 | 24.10 | 261.00 | 55.90 | 11880 | 104.9 | 34.6 | 412 | N/A | N/A | |
| G-54 - 64 | core | 399 | 9.8 | Below LOD | 450 | Below LOD | 1306.00 | 1.75 | 1.07 | Below LOD | 2.63 | 0.09 | 1.27 | 2.96 | 0.10 | 20.60 | 8.54 | 109.20 | 44.40 | 206.00 | 45.70 | 418.00 | 82.30 | 11760 | 75.4 | 70.3 | 288 | N/A | N/A | |
| G-54 - 88 | rim | 441.3 | 12 | 1340 | 154 | 109 | 283.00 | Below LOD | 25.60 | Below LOD | Below LOD | Below LOD | Below LOD | Below LOD | Below LOD | 27.30 | Below LOD | 41.10 | Below LOD | 89.00 | Below LOD | 89.00 | Below LOD | 11680 | 107.7 | 43.1 | 369 | 2.0 | 1005.6 | |
| G-54 - 60 | core | 443.8 | 14 | Below LOD | 200 | Below LOD | 303.00 | 0.78 | 0.18 | Below LOD | 3.51 | 0.14 | 1.38 | 4.22 | 0.08 | 25.50 | 6.98 | 53.70 | 10.38 | 23.30 | 2.67 | 15.40 | 1.98 | 13520 | 138.1 | 56 | 452 | N/A | N/A | |
| G-54 - 8 | core | 470.4 | 10 | Below LOD | Below LOD | Below LOD | 1360.00 | 1.80 | 0.22 | Below LOD | 19.97 | 0.18 | 2.13 | 4.27 | 0.41 | 23.30 | 8.90 | 108.30 | 44.40 | 221.30 | 52.10 | 484.00 | 89.10 | 6520 | 395 | 610 | 1275 | N/A | N/A | |
| G-54 - 5 | core | 477 | 27 | Below LOD | 260 | Below LOD | 597.00 | 11.90 | 0.52 | Below LOD | 3.06 | Below LOD | 0.39 | 0.78 | 0.19 | 7.43 | 3.05 | 43.20 | 19.20 | 112.00 | 33.40 | 375.00 | 84.30 | 12580 | 133.1 | 38.1 | 395 | N/A | N/A | |
| G-54 - 23 | core | 514.9 | 12 | 170 | 370 | Below LOD | 1399.00 | 4.49 | 1.34 | 0.33 | 35.70 | 0.31 | 3.29 | 6.05 | 1.85 | 33.00 | 10.86 | 126.80 | 48.10 | 219.00 | 47.50 | 440.00 | 87.10 | 8780 | 105.6 | 205 | 302 | N/A | N/A | |
| G-54 - 85 | core | 518 | 12 | 742 | 3480 | 48.1 | 1060.00 | 2.85 | 2.52 | 28.00 | 102.00 | 13.20 | 70.00 | 22.50 | 1.78 | 39.40 | 10.10 | 104.00 | 39.00 | 170.00 | 35.80 | 325.00 | 64.20 | 11290 | 78.9 | 126.1 | 241 | 1.7 | 900.6 | |
| G-54 - 15 | | | | | | | | | | | | | | | | | | | | | | | | | | | | | | |

| | | | | | | | | | | | | | | | | | | | | | | | | | | | | | | |
|----------|------|-------|----|-----------|----------|-----------|---------|-------|-----------|-----------|-----------|-----------|-----------|--------|-------|--------|--------|---------|--------|--------|--------|---------|--------|----------|-------|----------|-------|-------|--------|-------|
| G-52a-33 | rim | 178.3 | 13 | 1100 | 1850 | 77 | 6040.00 | 18.10 | 31.10 | 43.40 | 282.00 | 37.90 | 232.00 | 191.00 | 52.60 | 442.00 | 141.00 | 1160.00 | 220.00 | 537.00 | 86.30 | 608.00 | 74.90 | 3.36E+04 | 585 | 230 | 5300 | 1.9 | 958.8 | |
| G-52a-22 | rim | 178.4 | 14 | 3070 | 1330 | 47.6 | 4080.00 | 9.11 | 30.70 | 43.60 | 257.00 | 32.80 | 189.70 | 145.10 | 37.60 | 324.00 | 96.20 | 757.00 | 143.70 | 363.00 | 56.20 | 389.00 | 48.40 | 2.96E+04 | 464 | 631 | 4100 | 1.7 | 899.4 | |
| G-52a-34 | rim | 180.7 | 14 | 800 | 1200 | 13.9 | 2650.00 | 6.61 | 19.30 | 43.00 | 123.00 | 21.70 | 110.00 | 74.00 | 16.80 | 173.00 | 51.90 | 414.00 | 88.00 | 250.00 | 49.30 | 433.00 | 72.10 | 2.32E+04 | 464 | 428 | 3220 | 1.1 | 770.6 | |
| G-52a-21 | rim | 182.1 | 14 | 1070 | 1410 | 20.8 | 4000.00 | 8.13 | 13.00 | 33.80 | 136.00 | 21.30 | 120.00 | 98.30 | 22.60 | 247.00 | 78.70 | 624.00 | 120.30 | 328.00 | 56.60 | 436.00 | 62.10 | 22380 | 376 | 206 | 4000 | 1.3 | 809.6 | |
| G-52a-44 | core | 182.4 | 14 | 483 | 920 | 10.3 | 2100.00 | 6.06 | 14.30 | 18.20 | 75.60 | 12.98 | 77.30 | 60.60 | 14.80 | 144.00 | 46.40 | 371.00 | 78.50 | 218.00 | 39.10 | 317.00 | 44.10 | 26580 | 331 | 417 | 2840 | 1.0 | 743.4 | |
| G-52a-26 | rim | 183.8 | 14 | 490 | 730 | 7.70 | 1443.00 | 4.53 | 10.30 | 1.13 | 8.70 | 0.68 | 4.26 | 4.20 | 1.19 | 19.80 | 9.73 | 126.40 | 43.70 | 200.60 | 50.90 | 540.00 | 109.50 | 16750 | 271.6 | 51.4 | 2320 | 1.1 | 753.3 | |
| G-52a-43 | core | 184.2 | 14 | 6390 | 1330 | 67.8 | 2480.00 | 5.63 | 55.30 | 15.70 | 93.00 | 14.50 | 89.20 | 66.50 | 17.00 | 141.00 | 45.30 | 408.00 | 92.10 | 278.00 | 52.40 | 439.00 | 72.80 | 1.92E+04 | 401 | 407 | 3380 | 1.8 | 942.5 | |
| G-52a-49 | core | 187.4 | 14 | 65 | 990 | Below LOD | 2475.00 | 7.89 | 0.56 | 0.78 | 3.54 | 0.55 | 3.40 | 4.98 | 1.20 | 34.70 | 17.86 | 222.80 | 67.80 | 235.10 | 44.40 | 376.00 | 57.60 | 22500 | 691 | 54.4 | 5650 | N/A | N/A | |
| G-52a-47 | core | 188 | 15 | 1380 | 1600 | 29.8 | 4160.00 | 8.00 | 33.00 | 50.70 | 195.00 | 31.50 | 173.00 | 136.80 | 31.90 | 292.00 | 95.10 | 776.00 | 157.20 | 464.00 | 82.90 | 679.00 | 106.40 | 21930 | 530 | 342 | 4290 | 1.5 | 846.8 | |
| G-52a-8 | core | 189.1 | 15 | 1670 | 2070 | 52.9 | 5110.00 | 13.35 | 35.10 | 38.60 | 249.00 | 39.80 | 235.00 | 187.00 | 48.00 | 359.00 | 117.80 | 967.00 | 188.00 | 509.00 | 84.50 | 639.00 | 85.90 | 22140 | 656 | 506 | 5340 | 1.7 | 912.0 | |
| G-52a-40 | core | 189.1 | 16 | 1350 | 1680 | 53.5 | 2800.00 | 7.58 | 87.00 | 56.40 | 131.00 | 20.20 | 93.00 | 47.80 | 13.07 | 121.40 | 39.50 | 375.00 | 93.70 | 353.00 | 85.10 | 958.00 | 185.50 | 18480 | 559 | 349 | 4590 | 2.7 | 913.3 | |
| G-52a-11 | core | 189.7 | 15 | 10190 | 1800 | 557 | 4190.00 | 19.00 | 148.60 | 46.00 | 225.00 | 32.80 | 182.50 | 148.60 | 39.30 | 297.00 | 92.30 | 756.00 | 150.50 | 406.00 | 66.40 | 484.00 | 62.70 | 21720 | 548 | 446 | 4630 | 2.7 | 1283.2 | |
| G-52a-56 | rim | 191.3 | 16 | 3010 | 1620 | 39.5 | 4330.00 | 18.70 | 40.50 | 54.80 | 216.00 | 32.10 | 180.00 | 142.10 | 35.60 | 329.00 | 101.40 | 804.00 | 169.10 | 488.00 | 86.10 | 741.00 | 126.00 | 3.04E+04 | 473 | 519 | 3910 | 1.6 | 877.9 | |
| G-52a-42 | rim | 191.8 | 15 | 1480 | 1740 | 54 | 3950.00 | 13.20 | 18.40 | 31.20 | 171.00 | 26.50 | 157.10 | 121.80 | 34.00 | 290.00 | 92.00 | 747.00 | 143.70 | 386.00 | 55.90 | 391.00 | 53.20 | 3.07E+04 | 477 | 266 | 3810 | 1.7 | 914.4 | |
| G-52a-30 | core | 192.2 | 14 | 1440 | 2260 | 87.9 | 6600.00 | 12.80 | 31.90 | 88.40 | 314.00 | 49.70 | 283.00 | 221.00 | 54.40 | 528.00 | 157.40 | 1214.00 | 233.00 | 569.00 | 87.90 | 595.00 | 75.20 | 24110 | 573 | 2770 | 4570 | 1.9 | 976.2 | |
| G-52a-38 | rim | 192.6 | 14 | 345 | 820 | 100 | 1342.00 | 1.91 | 7.00 | 2.59 | 8.30 | 1.85 | 11.80 | 11.60 | 2.83 | 34.70 | 13.36 | 152.90 | 50.00 | 225.40 | 58.60 | 644.00 | 132.70 | 14240 | 191.8 | 77.2 | 1513 | 2.0 | 993.7 | |
| G-52a-13 | core | 194.6 | 15 | 541 | 1160 | 15.2 | 2490.00 | 5.05 | 9.60 | 14.60 | 61.00 | 9.60 | 61.00 | 46.30 | 13.50 | 127.00 | 40.40 | 359.00 | 83.80 | 265.00 | 55.50 | 550.00 | 100.00 | 27860 | 395 | 134 | 3060 | 1.2 | 779.0 | |
| G-52a-41 | rim | 208.9 | 17 | 1940 | 1720 | 47.1 | 4290.00 | 11.80 | 22.50 | 93.00 | 241.00 | 37.20 | 196.00 | 122.80 | 35.80 | 293.40 | 90.50 | 742.00 | 151.10 | 409.00 | 64.00 | 468.00 | 70.40 | 2.76E+04 | 469 | 233 | 3470 | 1.7 | 898.2 | |
| G-52a-6 | core | 217 | 18 | 3630 | 1630 | 53.9 | 3570.00 | 13.90 | 25.90 | 39.90 | 211.00 | 32.20 | 201.00 | 157.00 | 40.00 | 370.00 | 99.00 | 770.00 | 141.00 | 425.00 | 68.20 | 543.00 | 86.40 | 2.77E+04 | 505 | 3.10E+03 | 3590 | 1.7 | 914.2 | |
| G-52a-55 | core | 218.1 | 18 | 770 | 500 | 11.3 | 1036.00 | 3.88 | 12.90 | 2.55 | 4.69 | 1.10 | 7.30 | 8.40 | 1.57 | 30.30 | 11.32 | 116.90 | 31.10 | 115.50 | 25.60 | 262.00 | 49.70 | 21780 | 327 | 33.5 | 2330 | 1.1 | 751.7 | |
| G-52a-48 | rim | 260 | 22 | 1940 | 1490 | 190 | 2890.00 | 19.50 | 55.00 | 28.30 | 158.00 | 24.80 | 143.00 | 121.00 | 31.00 | 239.00 | 77.50 | 614.00 | 117.00 | 357.00 | 70.30 | 628.00 | 104.00 | 26840 | 596 | 681 | 3610 | 2.3 | 1088.3 | |
| G-55a-14 | rim | 150.3 | 11 | Below LOD | 124 | Below LOD | 672.00 | 1.36 | Below LOD | Below LOD | 11.65 | Below LOD | 0.38 | 1.51 | 0.29 | 9.82 | 3.75 | 50.80 | 21.30 | 106.90 | 25.70 | 273.00 | 57.00 | 13340 | 23.5 | 137 | 253 | N/A | N/A | |
| G-55a-13 | core | 161.1 | 12 | Below LOD | 1.22E+04 | 7.5 | 642.00 | 0.65 | 5.00 | 122.00 | 280.00 | 35.70 | 167.00 | 36.80 | 3.14 | 43.70 | 7.73 | 66.90 | 21.60 | 91.00 | 19.33 | 186.70 | 36.20 | 10180 | 9.88 | 74.4 | 96.8 | 0.9 | 716.2 | |
| G-55a-77 | rim | 163.8 | 12 | Below LOD | 260 | Below LOD | 595.00 | 0.87 | Below LOD | Below LOD | Below LOD | Below LOD | Below LOD | 0.38 | 0.17 | 6.26 | 3.85 | 54.10 | 20.61 | 86.50 | 16.22 | 139.80 | 26.80 | 13220 | 148.7 | 16.77 | 1439 | N/A | N/A | |
| G-55a-26 | rim | 177.5 | 14 | Below LOD | 308 | 12.9 | 2920.00 | 2.92 | 0.39 | 0.17 | 24.70 | 0.39 | 1.13 | 17.40 | 24.70 | 96.50 | 26.90 | 287.00 | 98.20 | 415.00 | 89.50 | 851.00 | 172.30 | 7320 | 89.50 | 11.42 | 177.2 | 100.4 | 1.1 | 763.7 |
| G-55a-27 | core | 179.5 | 15 | Below LOD | 138 | 7.7 | 1317.00 | 1.32 | 0.27 | Below LOD | 26.90 | 0.38 | 6.57 | 9.60 | 4.46 | 40.70 | 11.90 | 132.00 | 46.40 | 201.00 | 43.80 | 422.00 | 84.50 | 7610 | 5.2 | 71.8 | 46.8 | 0.9 | 718.4 | |
| G-55a-32 | rim | 187.8 | 14 | 960 | 401 | 59.5 | 1912.00 | 9.24 | 2.87 | 33.40 | 110.10 | 16.80 | 89.90 | 50.30 | 25.50 | 95.80 | 24.80 | 231.00 | 68.80 | 283.00 | 57.60 | 521.00 | 88.80 | 19190 | 322.8 | 325 | 2696 | 1.8 | 926.2 | |
| G-55a-54 | rim | 199.3 | 15 | 700 | 1160 | 69 | 2640.00 | 3.54 | 6.40 | 24.30 | 98.00 | 12.30 | 69.00 | 36.20 | 19.70 | 70.00 | 22.20 | 250.00 | 88.50 | 396.00 | 88.50 | 835.00 | 158.00 | 13390 | 255 | 84 | 1970 | 1.8 | 944.7 | |
| G-55a-68 | rim | 226.6 | 17 | Below LOD | 770 | 6.7 | 3410.00 | 9.86 | 0.60 | 5.25 | 55.60 | 3.14 | 16.90 | 11.40 | 5.10 | 50.30 | 21.60 | 293.00 | 113.60 | 547.00 | 118.20 | 1079.00 | 194.20 | 14810 | 442 | 177 | 3040 | 0.8 | 706.8 | |
| G-55a-41 | rim | 231.6 | 17 | Below LOD | 142 | 7.1 | 875.00 | 2.57 | Below LOD | Below LOD | 17.57 | 0.06 | 1.12 | 3.63 | 2.11 | 24.90 | 7.79 | 87.80 | 30.80 | 128.40 | 26.40 | 232.40 | 44.20 | 10900 | 135.1 | 281 | 918 | 0.9 | 711.6 | |
| G-55a-12 | rim | 237.1 | 18 | Below LOD | 246 | Below LOD | 2430.00 | 6.92 | Below LOD | Below LOD | 21.10 | Below LOD | 0.92 | 4.03 | 1.82 | 39.10 | 15.96 | 208.90 | 86.40 | 381.00 | 81.50 | 734.00 | 135.00 | 10640 | 130.8 | 185 | 838 | N/A | N/A | |
| G-55a-18 | rim | 238.7 | 18 | 176 | 840 | Below LOD | 2203.00 | 4.12 | 1.56 | 0.35 | 4.19 | 0.18 | 1.14 | 3.33 | 0.79 | 29.50 | 13.44 | 189.00 | 75.40 | 352.00 | 77.70 | 720.00 | 136.80 | 12550 | 273.8 | 192.7 | 1739 | N/A | N/A | |
| G-55a-35 | rim | 241.2 | 18 | Below LOD | 146 | Below LOD | 1223.00 | 2.26 | Below LOD | Below LOD | 13.35 | 0.06 | 1.08 | 3.99 | 2.12 | 26.80 | 9.34 | 113.20 | 41.50 | 177.00 | 38.20 | 349.00 | 67.10 | 10030 | 88.2 | 111 | 559 | N/A | N/A | |
| G-55a-49 | rim | 243.5 | 19 | 600 | 360 | 18.4 | 2360.00 | 9.70 | 0.74 | 5.10 | 10.53 | 1.36 | 6.20 | 6.60 | 2.29 | 42.90 | 17.70 | 216.00 | 82.00 | 361.00 | 76.00 | 670.00 | 118.00 | 11290 | 290 | 183 | 1920 | 1.3 | 797.4 | |
| G-55a-66 | rim | 248.6 | 19 | Below LOD | 329 | 18 | 2020.00 | 4.43 | 0.17 | Below LOD | 47.90 | 0.14 | 2.44 | 5.55 | 2.37 | 33.70 | 13.00 | 169.00 | 69.60 | 320.00 | 68.80 | 655.00 | 129.00 | 8040 | 65.00 | 129.00 | 124.9 | 1.3 | 795.3 | |
| G-55a-58 | rim | 249.7 | 19 | 3910 | 263 | 208 | 690.00 | 3.60 | 57.00 | 13.90 | 11.10 | 3.20 | 10.90 | 3.84 | 1.67 | 13.90 | 5.01 | 55.50 | 21.10 | 117.20 | 33.10 | 364.00 | 72.70 | 11770 | 298 | 23.5 | 1800 | 2.3 | 1102.8 | |
| G-55a-65 | core | 251.7 | 19 | Below LOD | 510 | Below LOD | 1528.00 | 2.74 | Below LOD | Below LOD | 34.30 | 0.12 | 2.02 | 4.84 | 1.71 | 30.90 | 10.87 | 135.20 | 53.20 | 251.00 | 53.00 | 497.00 | 97.60 | 9440 | 18.45 | 85.3 | 114.5 | N/A | N/A | |
| G-55a-36 | core | 251.8 | 19 | 81 | 407 | Below LOD | 2119.00 | 3.50 | 0.54 | 0.33 | 7.18 | 0.19 | 1.53 | 3.73 | 2.08 | 33.20 | 13.65 | 185.50 | 72.50 | 334.00 | 72.80 | 658.00 | 122.40 | 12270 | 250 | 146.6 | 1523 | N/A | N/A | |
| G-55a-82 | rim | 254.7 | 19 | 168 | 350 | 34 | 679.00 | 2.54 | 1.96 | 0.11 | 4.33 | 0.12 | 1.25 | 2.40 | 0.83 | 13.40 | 4.73 | 58.40 | 22.90 | 114.00 | 26.80 | 289.00 | 56.30 | 12420 | 163.4 | 101.7 | 1001 | 1.5 | 861.2 | |
| G-55a-83 | core | 255.8 | 19 | 98 | 164 | 27 | 527.00 | 2.06 | 1.43 | Below LOD | 2.47 | 0.12 | 0.87 | 2.02 | 0.63 | 10.59 | 3.78 | 47.70 | 17.50 | 89.40 | 21.90 | 239.00 | 46.90 | 11320 | 121.1 | 32.8 | 738 | 1.4 | 836.4 | |
| G-55a-23 | rim | 261.5 | 21 | 520 | 403 | 244 | 1280.00 | 3.68 | 5.50 | Below LOD | 7.40 | 0.15 | 1.53 | 3.13 | 0.92 | 19.60 | 7.37 | 97.10 | 39.80 | 233.00 | 67.50 | 770.00 | 161.00 | 12300 | 166 | 61.8 | 1050 | 2.4 | 1129.2 | |
| G-55a-19 | core | 265.8 | 20 | Below LOD | 149 | 8.6 | 428.00 | 0.89 | Below LOD | Below LOD | 4.15 | 0.03 | 0.76 | 1.63 | 0.41 | 8.20 | 2.94 | 35.50 | 13.98 | 66.30 | 15.98 | 158.50 | 34.20 | 11150 | 22.1 | 37.4 | 128 | 0.9 | 727.7 | |
| G-55a-75 | core | 266.5 | 20 | 93 | 580 | 251 | 1089.00 | 3.10 | 3.66 | Below LOD | 4.08 | 0.05 | 0.35 | 1.56 | 0.5 | | | | | | | | | | | | | | | |

| | | | | | | | | | | | | | | | | | | | | | | | | | | | | | |
|-----------|------|-------|-----|-----------|----------|------|-----------|-------|-----------|------------|------------|------------|------------|------------|---------|-----------|-----------|------------|-----------|-----------|---------|-----------|---------|-------|----------|----------|----------|-----|--------|
| G-55b - 4 | core | 3221 | 200 | Below LOD | 467 | 23.1 | 3630.00 | 9.71 | 0.19 | 1.90 | 37.60 | 1.80 | 19.00 | 24.70 | 3.31 | 114.00 | 32.70 | 372.00 | 130.00 | 538.00 | 108.60 | 958.00 | 178.70 | 8660 | 772 | 231 | 299 | 1.4 | 820.2 |
| G_95_30 | core | 435 | 33 | 187 | 1940 | 19.8 | 4070.00 | 55.30 | 3.31 | 6.90 | 32.20 | 4.87 | 30.20 | 23.00 | 2.50 | 77.80 | 27.30 | 324.00 | 126.60 | 582.00 | 130.00 | 1226.00 | 235.10 | 11970 | 1201 | 533 | 4130 | 1.3 | 804.6 |
| G_95_29 | rim | 629 | 46 | 426 | 2860 | 13.1 | 5320.00 | 33.90 | 3.10 | 34.00 | 96.00 | 9.70 | 49.00 | 23.30 | 0.97 | 86.20 | 33.10 | 424.00 | 168.50 | 780.00 | 170.50 | 1492.00 | 279.30 | 10160 | 1476 | 846 | 3400 | 1.1 | 765.1 |
| G_95_3 | core | 664 | 50 | 93 | 1460 | 13.5 | 3950.00 | 43.70 | 5.85 | 7.30 | 32.80 | 4.06 | 26.40 | 20.90 | 2.58 | 77.70 | 27.50 | 328.00 | 122.90 | 550.00 | 122.00 | 1134.00 | 217.60 | 11080 | 1835 | 694 | 4160 | 1.1 | 767.9 |
| G_95_33 | core | 673 | 49 | 1780 | 1.14E+04 | 12 | 4050.00 | 47.30 | 6.93 | 59.00 | 196.00 | 32.80 | 187.00 | 85.00 | 5.40 | 155.00 | 38.50 | 368.00 | 123.20 | 537.00 | 121.40 | 1155.00 | 221.10 | 12490 | 1249 | 398 | 2843 | 1.1 | 757.1 |
| G_95_15 | rim | 681 | 53 | 72 | 1290 | 12.6 | 2760.00 | 57.60 | 3.41 | 1.60 | 21.50 | 1.14 | 6.90 | 5.08 | 0.70 | 30.00 | 14.03 | 204.00 | 82.50 | 392.00 | 86.20 | 782.00 | 145.70 | 12220 | 1393 | 307 | 3060 | 1.1 | 761.6 |
| G_95_24 | core | 730 | 58 | 203 | 2640 | 49.1 | 3870.00 | 54.20 | 3.31 | 36.00 | 88.00 | 17.60 | 99.00 | 56.20 | 7.21 | 123.20 | 34.00 | 340.00 | 109.70 | 503.00 | 114.20 | 1165.00 | 236.50 | 11430 | 1382 | 284 | 2740 | 1.7 | 903.1 |
| G_95_6 | core | 737 | 53 | 1.24E+04 | 1.91E+06 | 316 | 399000.00 | 13.60 | 16000.00 | 2010000.00 | 4240000.00 | 520000.00 | 2060000.00 | 3870000.00 | 2970.00 | 276000.00 | 290000.00 | 1069000.00 | 140000.00 | 236000.00 | 2020.00 | 8950.00 | 986.00 | 8.7 | 2.75E+04 | 1.21E+06 | 5.65E+04 | 2.5 | 1174.0 |
| G_95_21 | rim | 743 | 53 | Below LOD | 1580 | 9.7 | 3590.00 | 45.10 | 2.18 | 12.50 | 17.70 | 7.62 | 49.30 | 30.60 | 4.17 | 86.80 | 25.80 | 287.00 | 102.30 | 466.00 | 105.20 | 1032.00 | 198.10 | 12200 | 1218 | 292.4 | 2514 | 1.0 | 738.2 |
| G_95_28 | rim | 785.4 | 56 | 66 | 1830 | 9.4 | 4310.00 | 53.60 | 2.15 | 5.33 | 40.90 | 3.64 | 23.90 | 19.20 | 2.59 | 80.60 | 29.00 | 357.00 | 136.30 | 617.00 | 134.10 | 1222.00 | 221.80 | 11320 | 1420 | 674 | 2702 | 1.0 | 735.4 |
| G_95_35 | core | 805 | 59 | 111 | 1490 | 11.1 | 2960.00 | 45.10 | 2.72 | 14.00 | 17.30 | 8.70 | 55.40 | 30.60 | 4.58 | 77.00 | 21.60 | 237.00 | 84.30 | 400.00 | 98.70 | 1004.00 | 208.80 | 12770 | 1371 | 150 | 2490 | 1.0 | 750.1 |
| G_95_17 | core | 815 | 60 | 119 | 2500 | 12.3 | 2830.00 | 38.30 | 1.42 | 31.00 | 75.00 | 10.20 | 50.00 | 20.40 | 1.85 | 48.10 | 16.80 | 207.00 | 84.80 | 427.00 | 107.60 | 1110.00 | 228.00 | 13970 | 1362 | 287 | 2590 | 1.1 | 759.4 |
| G_95_5 | rim | 857 | 61 | 360 | 1.92E+06 | 83 | 673000.00 | 15.90 | 14010.00 | 1800000.00 | 3860000.00 | 4740000.00 | 1890000.00 | 3640000.00 | 1454.00 | 272000.00 | 342000.00 | 1540000.00 | 231000.00 | 417000.00 | 3570.00 | 131300.00 | 1193.00 | 10.6 | 3.22E+04 | 1.29E+06 | 5.68E+04 | 1.9 | 968.6 |
| G_95_34 | core | 900 | 69 | Below LOD | 1630 | 13.8 | 4420.00 | 67.50 | 1.56 | 17.50 | 63.50 | 10.99 | 68.60 | 44.20 | 5.88 | 117.30 | 33.50 | 351.00 | 121.30 | 531.00 | 121.60 | 1143.00 | 216.00 | 16450 | 1638 | 148 | 2950 | 1.1 | 769.9 |
| G_95_40 | rim | 909 | 65 | Below LOD | 1030 | 8.3 | 2120.00 | 38.70 | 0.78 | 3.40 | 14.57 | 2.35 | 15.40 | 9.90 | 1.40 | 36.50 | 13.53 | 174.10 | 67.50 | 338.00 | 82.80 | 845.00 | 171.30 | 13900 | 1259 | 240 | 1976 | 0.9 | 724.7 |
| G_95_8 | rim | 923 | 66 | Below LOD | 2170 | 9.6 | 5090.00 | 63.20 | 1.74 | 3.60 | 34.60 | 1.97 | 13.30 | 12.90 | 1.28 | 72.40 | 29.60 | 392.00 | 158.20 | 733.00 | 159.50 | 1436.00 | 271.80 | 11310 | 2149 | 745 | 3325 | 1.0 | 737.2 |
| G_95_2 | rim | 931 | 67 | 89 | 1770 | 11.2 | 2820.00 | 31.60 | 0.96 | 3.32 | 98.00 | 2.21 | 13.40 | 11.70 | 1.16 | 50.50 | 18.49 | 227.60 | 90.10 | 410.00 | 96.90 | 977.00 | 193.70 | 11310 | 1313 | 571 | 2124 | 1.0 | 750.9 |
| G_95_9 | rim | 944 | 67 | 30 | 1790 | 11.4 | 4920.00 | 43.10 | 2.76 | 14.40 | 57.80 | 9.62 | 61.20 | 40.80 | 6.12 | 124.70 | 37.20 | 396.00 | 143.30 | 613.00 | 127.30 | 1139.00 | 213.00 | 11010 | 1555 | 685 | 2410 | 1.1 | 752.5 |
| G_95_14 | rim | 955 | 72 | 37 | 920 | 13 | 2710.00 | 44.80 | 0.85 | 6.36 | 19.40 | 5.82 | 37.70 | 23.30 | 3.67 | 63.40 | 19.80 | 218.00 | 79.80 | 352.00 | 81.10 | 758.00 | 140.40 | 13790 | 1543 | 245 | 2478 | 1.1 | 764.4 |
| G_95_18 | rim | 968 | 69 | Below LOD | 578 | 12.7 | 1392.00 | 18.40 | 0.30 | 1.08 | 22.50 | 0.81 | 6.69 | 9.51 | 0.53 | 48.30 | 16.48 | 154.40 | 43.60 | 154.20 | 27.20 | 215.30 | 34.90 | 13680 | 659 | 119.4 | 1042 | 1.1 | 762.3 |
| G_95_36 | rim | 973.5 | 68 | Below LOD | 771 | 9.8 | 1436.00 | 20.45 | Below LOD | Below LOD | 18.77 | 0.08 | 1.71 | 6.11 | 0.09 | 41.50 | 15.75 | 164.60 | 46.80 | 157.20 | 26.30 | 193.80 | 30.76 | 14100 | 486 | 92.6 | 715 | 1.0 | 739.0 |
| G_95_20 | rim | 985 | 69 | Below LOD | 588 | 11.9 | 1306.00 | 15.99 | 0.09 | 0.68 | 23.71 | 0.53 | 5.40 | 8.25 | 0.37 | 47.70 | 16.29 | 151.40 | 41.20 | 137.30 | 21.96 | 164.80 | 26.00 | 13730 | 541 | 107.4 | 827 | 1.1 | 756.3 |
| G_95_39 | rim | 996 | 73 | 508 | 660 | 11.9 | 1380.00 | 23.10 | 1.73 | 2.37 | 12.60 | 1.74 | 11.30 | 7.83 | 1.01 | 26.90 | 9.11 | 112.00 | 42.90 | 210.00 | 53.20 | 562.00 | 120.80 | 13050 | 1135 | 152 | 1690 | 1.1 | 756.3 |
| G_95_22 | core | 1000 | 70 | Below LOD | 481 | 10.1 | 1311.00 | 16.71 | Below LOD | 0.45 | 25.21 | 0.30 | 3.33 | 6.83 | 0.23 | 35.80 | 12.79 | 131.80 | 40.90 | 153.30 | 28.70 | 242.00 | 41.20 | 14000 | 850 | 99.7 | 1265 | 1.0 | 741.7 |
| G_95_32 | core | 1003 | 71 | Below LOD | 1320 | 8.7 | 3330.00 | 24.70 | 1.11 | 14.30 | 32.30 | 8.43 | 56.40 | 37.40 | 5.21 | 112.30 | 29.90 | 280.00 | 85.00 | 319.60 | 60.00 | 468.70 | 74.90 | 13170 | 1030 | 109.4 | 1474 | 0.9 | 728.7 |
| G_95_12 | core | 1012 | 71 | 214 | 1030 | 14.2 | 2360.00 | 37.70 | 1.17 | 1.72 | 11.16 | 1.29 | 8.40 | 7.39 | 0.79 | 31.80 | 13.36 | 177.50 | 68.10 | 309.00 | 67.80 | 628.00 | 118.00 | 13030 | 1272 | 100.7 | 1785 | 1.2 | 772.6 |
| G_95_4 | core | 1019 | 71 | 114 | 1100 | 9.7 | 2530.00 | 46.60 | 1.17 | 4.05 | 20.80 | 2.67 | 18.40 | 13.60 | 1.90 | 49.90 | 17.90 | 215.00 | 78.50 | 354.00 | 80.10 | 738.00 | 141.90 | 13270 | 1664 | 298 | 2399 | 1.0 | 738.2 |
| G_95_1 | core | 1028 | 72 | 104 | 984 | 12.1 | 2388.00 | 50.70 | 0.67 | 2.52 | 17.30 | 1.49 | 9.50 | 7.50 | 0.89 | 29.40 | 12.20 | 170.90 | 70.30 | 351.30 | 84.30 | 820.00 | 161.70 | 14160 | 1476 | 83.3 | 2091 | 1.1 | 757.9 |
| G_95_10 | core | 1035 | 75 | 133 | 536 | 13.3 | 1312.00 | 17.17 | 0.98 | 0.21 | 20.91 | 0.13 | 2.07 | 6.55 | 0.15 | 43.70 | 15.37 | 148.30 | 41.60 | 139.50 | 23.83 | 180.20 | 29.00 | 13670 | 564 | 99.4 | 800 | 1.1 | 766.5 |
| G_95_25 | core | 1037 | 72 | 43 | 1150 | 14.7 | 2900.00 | 82.20 | 1.13 | 11.10 | 18.92 | 6.72 | 41.90 | 26.80 | 3.75 | 69.90 | 20.80 | 220.60 | 78.50 | 345.00 | 72.20 | 638.00 | 114.40 | 14150 | 1950 | 127.1 | 2794 | 1.2 | 775.9 |
| G_95_27 | rim | 1038 | 73 | 65 | 1230 | 10.1 | 2680.00 | 48.90 | 0.72 | 7.70 | 28.90 | 4.91 | 31.10 | 19.50 | 2.67 | 61.40 | 19.50 | 219.00 | 79.20 | 339.00 | 72.50 | 647.00 | 120.00 | 13660 | 1629 | 213 | 2296 | 1.0 | 741.7 |
| G_95_13 | rim | 1061 | 74 | Below LOD | 329 | 11.1 | 957.00 | 39.90 | 0.10 | 0.63 | 4.66 | 0.46 | 3.22 | 2.30 | 0.31 | 11.90 | 5.09 | 69.10 | 26.50 | 119.90 | 27.90 | 276.00 | 54.90 | 14230 | 1813 | 51.4 | 2528 | 1.0 | 750.1 |
| G_95_26 | core | 1063 | 74 | Below LOD | 920 | 11.9 | 2120.00 | 56.10 | 0.26 | 0.30 | 15.12 | 0.17 | 1.62 | 3.74 | 0.16 | 26.00 | 11.49 | 154.50 | 66.00 | 335.00 | 85.80 | 880.00 | 172.10 | 13420 | 1027 | 89 | 1387 | 1.1 | 756.3 |
| G_95_23 | rim | 1101 | 77 | Below LOD | 671 | 10.3 | 1391.00 | 32.50 | Below LOD | Below LOD | 9.30 | Below LOD | Below LOD | 17.10 | 7.49 | 102.70 | 43.00 | 226.20 | 61.10 | 701.00 | 147.60 | 15370 | 1314 | 63.8 | 1758 | 1.0 | 743.4 | | |
| G_95_16 | core | 1103 | 77 | 46 | 715 | 15.1 | 1739.00 | 28.10 | 0.62 | 4.40 | 15.60 | 2.55 | 15.20 | 10.60 | 1.39 | 32.90 | 11.40 | 139.90 | 55.30 | 264.60 | 64.30 | 661.00 | 128.50 | 14400 | 1364 | 252 | 1854 | 1.2 | 778.4 |
| G_95_37 | core | 1110 | 81 | Below LOD | 851 | 9.3 | 2010.00 | 26.10 | 0.11 | 0.68 | 22.30 | 0.44 | 4.23 | 6.10 | 0.62 | 34.30 | 12.90 | 169.00 | 68.30 | 325.00 | 77.60 | 754.00 | 145.10 | 12610 | 1213 | 286 | 1610 | 1.0 | 734.5 |
| G_95_11 | core | 1119 | 77 | Below LOD | 675 | 10.1 | 1895.00 | 8.89 | 0.29 | Below LOD | 22.20 | 0.30 | 5.54 | 11.10 | 2.82 | 52.80 | 16.83 | 180.60 | 62.70 | 265.60 | 54.10 | 470.00 | 88.30 | 9780 | 435 | 304 | 551 | 1.0 | 741.7 |
| G_95_31 | core | 1145 | 81 | Below LOD | 1620 | 11.2 | 3840.00 | 58.00 | 0.21 | 2.63 | 10.74 | 1.47 | 9.30 | 8.44 | 0.86 | 41.40 | 17.97 | 256.20 | 111.70 | 572.00 | 136.60 | 1293.00 | 241.60 | 13290 | 1152 | 78.6 | 1456 | 1.0 | 750.9 |
| G_95_7 | rim | 1148 | 82 | Below LOD | 1600 | 18.2 | 5210.00 | 53.90 | 0.75 | 2.66 | 66.20 | 1.88 | 13.70 | 15.70 | 1.52 | 92.10 | 35.00 | 427.00 | 160.50 | 713.00 | 147.20 | 1298.00 | 233.20 | 10710 | 2496 | 1321 | 3066 | 1.3 | 796.3 |
| G_95_38 | core | 1226 | 89 | Below LOD | 1940 | 11.8 | 4410.00 | 32.60 | 0.28 | 1.32 | 57.20 | 0.82 | 7.20 | 13.29 | 1.25 | 77.90 | 29.50 | 361.00 | 141.00 | 637.00 | 139.50 | 1244.00 | 229.80 | 12380 | 1916 | 875 | 2274 | 1.1 | 755.6 |
| G_95_19 | core | 1278 | 88 | Below LOD | 930 | 9.7 | 1880.00 | 29.70 | 0.22 | 2.50 | 21.90 | 1.99 | 14.10 | 8.40 | 1.43 | 34.40 | 12.40 | 149.00 | 58.10 | 288.00 | 63.90 | 617.00 | 121.90 | 12030 | 1131 | 183 | 1220 | 1.0 | 738.2 |

TABLE A3. Lu, Hf and Yb ISOTOPIC DATA OBTAINED USING THE LA-ICP-MS METHOD

| Spot | Session # | Duration (s) | N ratios | Total Hf beam (V) | Age (Ma) 206/238 | 2 σ | Conc (%) | ¹⁷⁶ Hf/ ¹⁷⁷ Hf f | 2 σ | ¹⁷⁶ Lu/ ¹⁷⁷ Hf f | 2 σ | ¹⁷⁶ Yb/ ¹⁷⁷ Hf f | 2 σ | ¹⁷⁶ Hf/ ¹⁷⁷ Hf f | 2 σ | Hf Fract (β _{Hf}) | 2 σ | Yb Fract (β _{Yb}) | 2 σ | ¹⁷⁶ Lu/ ¹⁷⁷ Hf CORR | εHf (t) | ¹⁷⁶ Hf/ ¹⁷⁷ Hf (t) | 2 σ | ¹⁷⁶ Hf/ ¹⁷⁷ Hf εHf (CHUR T=t) | 2 σ | ¹⁷⁶ Hf/ ¹⁷⁷ Hf f _{CC-T=0} | T _{DM1} (y) | T _{DM1} (y) 176Hf/177Hf | (Ma) | T _{DM2} (y) 176Hf/177Hf | (Ma) | T _{DM2} (Griffith et al.2000) | (Ma) | U-S (Ga) | f _(sample) | |
|---------|-----------|--------------|----------|-------------------|------------------|-----|----------|--|----------|--|-----------|--|---------|--|----------|-----------------------------|--------|-----------------------------|--------|---|--------------|--|----------|---|------|--|----------------------|----------------------------------|-----------|----------------------------------|-------------|--|-------------|----------|-----------------------|--------------|
| G52a-1 | 2 | 36.072 | 72 | 32.4 | 168.4 | 13 | 56.5 | 0.282759861 | 0.000026 | 0.001071 | 0.000024 | 0.053 | 0.0015 | 1.46721 | 0.000027 | -1.5318 | 0.0025 | -1.261 | 0.01 | 0.000149134 | -0.88968651 | 0.282759392 | 0.000032 | 0.282679194 | 2.8 | 1.1 | 0.282806626 | 674957150.3 | 610924074 | 610.9240738 | 988631453.4 | 988.6 | 992132020.5 | 992.1 | 3.5005671 | -0.995561492 |
| G52a-2 | 2 | 36.254 | 73 | 37.9 | 172.7 | 13 | 86.1 | 0.282770861 | 0.000014 | 0.0002881 | 0.0000098 | 0.01291 | 0.00039 | 1.467193 | 0.000031 | -1.5405 | 0.0021 | -1.208 | 0.018 | 4.01172E-05 | -0.5 | 0.282770731 | 0.000023 | 0.282676488 | 3.3 | 0.8 | 0.282819174 | 658058319 | 592069525 | 592.0695248 | 960902433.9 | 960.9 | 964224488.9 | 964.2 | 3.322055001 | -0.998806037 |
| G52a-3 | 2 | 14.501 | 29 | 46.8 | 65.5 | 7.6 | 62.0 | 0.282735863 | 0.000033 | 0.0004532 | 0.0000079 | 0.01706 | 0.00067 | 1.46723 | 0.000052 | -1.5465 | 0.0041 | -1.282 | 0.021 | 6.31069E-05 | -1.737627526 | 0.282735785 | 0.000038 | 0.282743886 | -0.3 | 1.3 | 0.28275414 | 706226309.6 | 681279373 | 681.2793734 | 1104466739 | 1104.5 | 1108850643 | 1108.9 | 4.38390378 | -0.998212819 |
| G52a-4 | 2 | 36.072 | 72 | 38.7 | 164.7 | 12 | 100.0 | 0.282774861 | 0.000014 | 0.000332 | 0.00001 | 0.01272 | 0.00047 | 1.467199 | 0.000024 | -1.5358 | 0.0023 | -1.257 | 0.022 | 4.62301E-05 | -0.358556854 | 0.282774718 | 0.000023 | 0.282681523 | 3.3 | 0.8 | 0.282820913 | 652700567.8 | 589784564 | 589.784564 | 957057120 | 957.1 | 960351831.6 | 960.4 | 3.294711655 | -0.998624104 |
| G52a-5 | 2 | 36.072 | 72 | 42.9 | 217 | 18 | 7.1 | 0.282762861 | 0.000016 | 0.0004078 | 0.0000064 | 0.01763 | 0.00023 | 1.467217 | 0.000025 | -1.5384 | 0.0025 | -1.271 | 0.015 | 5.67851E-05 | -0.782886292 | 0.282762631 | 0.000024 | 0.282648597 | 4.0 | 0.9 | 0.282823525 | 669262795.2 | 586375662 | 586.375662 | 951284058.4 | 951.3 | 954357713.5 | 954.5 | 3.253658745 | -0.998309969 |
| G52a-6 | 2 | 36.216 | 72 | 32.3 | 133.6 | 10 | 30.2 | 0.282734863 | 0.000022 | 0.000158 | 0.000019 | 0.07911 | 0.00073 | 1.467184 | 0.000027 | -1.5317 | 0.0032 | -1.267 | 0.0071 | 0.000220011 | -1.772988313 | 0.282734313 | 0.000029 | 0.282701087 | 1.2 | 1.0 | 0.282771774 | 710449574.7 | 659854901 | 659.8549011 | 1065575748 | 1065.6 | 10696290959 | 1069.6 | 4.054210256 | -0.994520661 |
| G52a-7 | 2 | 36.19 | 72 | 37.7 | 189.1 | 15 | 36.2 | 0.282814859 | 0.000018 | 0.0000744 | 0.0000054 | 0.0385 | 0.0028 | 1.467208 | 0.000026 | -1.541 | 0.0022 | -1.216 | 0.0094 | 0.0001036 | -1.055874604 | 0.282814492 | 0.000026 | 0.282668417 | 5.2 | 0.9 | 0.282867543 | 598942476.8 | 526781022 | 526.7810218 | 853875966.8 | 853.9 | 856492702.3 | 856.5 | 4.062173535 | -0.996916667 |
| G52a-8 | 2 | 36.151 | 72 | 38.1 | 189.7 | 15 | 44.7 | 0.28278086 | 0.000018 | 0.0004355 | 0.000009 | 0.0228 | 0.00067 | 1.467183 | 0.000022 | -1.5401 | 0.0023 | -1.2 | 0.011 | 6.06422E-05 | -0.146392135 | 0.282780645 | 0.000026 | 0.282665788 | 4.1 | 0.9 | 0.282833865 | 644764485.3 | 572289197 | 572.2891973 | 928418613.2 | 928.4 | 931517358.9 | 931.5 | 3.098745672 | -0.998195172 |
| G52a-10 | 2 | 36.084 | 72 | 37.4 | 171 | 13 | 97.2 | 0.282701864 | 0.000016 | 0.000814 | 0.000002 | 0.0298 | 0.00011 | 1.467174 | 0.000024 | -1.5475 | 0.0021 | -1.272 | 0.012 | 0.000113347 | -2.939894266 | 0.282701502 | 0.000024 | 0.282677558 | 0.8 | 0.9 | 0.282749467 | 753570749.9 | 688545971 | 688.5459707 | 1114767578 | 1114.8 | 1119224214 | 1119.2 | 4.456635875 | -0.996262568 |
| G52a-11 | 2 | 36.175 | 72 | 37.1 | 170.9 | 13 | 79.1 | 0.282759861 | 0.000016 | 0.000658 | 0.000011 | 0.02579 | 0.00041 | 1.467196 | 0.000023 | -1.5482 | 0.0022 | -1.259 | 0.012 | 9.16247E-05 | -0.88968651 | 0.282759568 | 0.000024 | 0.282677621 | 2.9 | 0.9 | 0.282807505 | 673960647.2 | 608818828 | 608.8188285 | 986689074.9 | 986.7 | 990184249.4 | 990.2 | 3.495174493 | -0.997273073 |
| G52a-12 | 2 | 36.174 | 72 | 45.3 | 129.5 | 10 | 37.6 | 0.282697864 | 0.000018 | 0.000759 | 0.0000056 | 0.0434 | 0.0034 | 1.467188 | 0.000023 | -1.5434 | 0.0024 | -1.2488 | 0.0099 | 0.000105689 | -3.081337412 | 0.282697609 | 0.000026 | 0.282703665 | -0.2 | 0.9 | 0.282733919 | 758881676.2 | 709653411 | 709.6534112 | 1149026456 | 1149.0 | 1153762524 | 1153.8 | 4.736067926 | -0.996854503 |
| G52a-13 | 2 | 36.17 | 72 | 29.81 | 160.1 | 12 | 65.1 | 0.282673866 | 0.000018 | 0.0007242 | 0.0000096 | 0.0244 | 0.00027 | 1.467207 | 0.000029 | -1.5286 | 0.0023 | -1.26 | 0.015 | 0.000100843 | -3.929966287 | 0.282673564 | 0.000026 | 0.282684417 | -0.4 | 0.9 | 0.282718467 | 791525800.9 | 730666136 | 730.6661364 | 1183052535 | 1183.1 | 1188074001 | 1188.1 | 5.021465112 | -0.996998723 |
| G52a-14 | 2 | 36.17 | 72 | 26.3 | 158.5 | 12 | 87.7 | 0.282754862 | 0.000027 | 0.001758 | 0.000017 | 0.07043 | 0.00089 | 1.467225 | 0.000025 | -1.5356 | 0.0025 | -1.257 | 0.01 | 0.000244797 | -1.065772583 | 0.282754136 | 0.000033 | 0.282685424 | 2.4 | 1.2 | 0.28279859 | 683479465.2 | 623467806 | 623.4678057 | 1006384038 | 1006.4 | 1009998675 | 1010.0 | 3.612836448 | -0.992714382 |
| G52a-16 | 2 | 36.206 | 72 | 45.2 | 178.4 | 14 | 49.7 | 0.282747862 | 0.000018 | 0.0002422 | 0.0000039 | 0.0123 | 0.0034 | 1.467218 | 0.000025 | -1.5504 | 0.0025 | -1.198 | 0.02 | 3.37257E-05 | -1.312970829 | 0.282747749 | 0.000026 | 0.282685421 | 2.6 | 0.9 | 0.282797794 | 689239962.4 | 621180109 | 621.180109 | 1008142381 | 1008.1 | 1011799825 | 1011.0 | 3.657443637 | -0.998996259 |
| G52a-17 | 2 | 36.172 | 72 | 26.5 | 169.8 | 12 | 93.4 | 0.282673866 | 0.000021 | 0.001644 | 0.0000044 | 0.0549 | 0.0018 | 1.467223 | 0.000026 | -1.5468 | 0.0022 | -1.2925 | 0.0092 | 0.000228923 | -5.2029846 | 0.282673719 | 0.000028 | 0.282678313 | -1.5 | 1.0 | 0.282684768 | 843365466.1 | 779215199 | 779.2151986 | 1257182546 | 1257.2 | 1268221152 | 1262.8 | 5.639607412 | -0.993168828 |
| G52a-18 | 2 | 36.152 | 72 | 30.9 | 164.2 | 12 | 81.6 | 0.282739862 | 0.000012 | 0.0003112 | 0.0000066 | 0.01172 | 0.00024 | 1.467218 | 0.000024 | -1.5521 | 0.0021 | -1.212 | 0.019 | 4.33338E-05 | -1.59218438 | 0.282739729 | 0.000022 | 0.282681837 | 2.0 | 0.8 | 0.282785784 | 700412719.1 | 637735666 | 637.7356663 | 1034659399 | 1034.7 | 1038710317 | 1038.5 | 3.850717481 | -0.997910305 |
| G52a-19 | 2 | 26.465 | 53 | 19.1 | 170.2 | 13 | 81.7 | 0.282645867 | 0.000023 | 0.00101 | 0.0000033 | 0.0325 | 0.0013 | 1.467259 | 0.000043 | -1.5708 | 0.0056 | -1.29 | 0.023 | 0.00014064 | -4.920098308 | 0.282645419 | 0.000029 | 0.282678062 | -1.2 | 1.1 | 0.28269316 | 830542940.7 | 765989022 | 765.9890218 | 1238732988 | 1238.7 | 1244228697 | 1244.2 | 5.495708703 | -0.995814292 |
| G52a-20 | 2 | 36.058 | 72 | 39.5 | 173.1 | 14 | 37.4 | 0.282736862 | 0.000016 | 0.0004879 | 0.0000046 | 0.02195 | 0.00023 | 1.467176 | 0.000024 | -1.5517 | 0.0024 | -1.251 | 0.015 | 6.79388E-05 | -1.70226674 | 0.282736643 | 0.000024 | 0.282676237 | 2.1 | 0.9 | 0.282785198 | 704949119.2 | 638940623 | 638.9406232 | 1035953859 | 1036.0 | 1039810284 | 1039.8 | 3.856424593 | -0.997978013 |
| G52a-21 | 2 | 34.985 | 70 | 35.7 | 192.2 | 14 | 30.6 | 0.282754862 | 0.000017 | 0.000462 | 0.000012 | 0.02365 | 0.00086 | 1.4672 | 0.000027 | -1.5463 | 0.0021 | -1.233 | 0.011 | 6.43323E-05 | -1.065772583 | 0.28275463 | 0.000025 | 0.282664214 | 3.2 | 0.9 | 0.282808553 | 680315358.6 | 606960719 | 606.9607189 | 984375497.7 | 984.4 | 984758229.7 | 984.7 | 3.82720344 | -0.998083549 |
| G52a-22 | 2 | 36.797 | 74 | 37.7 | 173.7 | 13 | 90.0 | 0.282733863 | 0.000017 | 0.000539 | 0.00001 | 0.02136 | 0.00036 | 1.467183 | 0.000029 | -1.5391 | 0.0026 | -1.255 | 0.013 | 7.50543E-05 | -1.808349089 | 0.282733619 | 0.000025 | 0.282675859 | 2.0 | 0.9 | 0.282782342 | 709172584.2 | 642959412 | 642.959412 | 1042555920 | 1042.3 | 1046158223 | 1046.2 | 3.902303531 | -0.997766241 |
| G52a-23 | 2 | 36.072 | 72 | 32.04 | 175.7 | 13 | 80.1 | 0.282716863 | 0.000018 | 0.000589 | 0.0000026 | 0.02019 | 0.00088 | 1.46719 | 0.000028 | -1.5399 | 0.0022 | -1.288 | 0.018 | 8.20167E-05 | -2.409482769 | 0.282716591 | 0.000026 | 0.282673467 | 1.5 | 0.9 | 0.282766383 | 732501240.6 | 664885108 | 664.8851078 | 1074769950 | 1074.7 | 1081638987 | 1081.6 | 4.169036658 | -0.997559028 |
| G52a-24 | 2 | 36.058 | 72 | 32.04 | 175.1 | 13 | 84.5 | 0.282709864 | 0.000016 | 0.000907 | 0.000011 | 0.02051 | 0.00045 | 1.467173 | 0.00003 | -1.5409 | 0.0024 | -1.267 | 0.014 | 0.000126297 | -2.65700294 | 0.282709545 | 0.000024 | 0.282674978 | 1.2 | 0.9 | 0.282758567 | 742895843.5 | 676330866 | 676.330866 | 1094705207 | 1094.7 | 1099000608 | 1099.0 | 4.296479555 | -0.998441151 |
| G52a-25 | 2 | 36.152 | 72 | 24.73 | 192.6 | 14 | 50.8 | 0.282673866 | 0.000019 | 0.001335 | 0.0000022 | 0.0445 | 0.00094 | 1.467176 | 0.000029 | -1.5372 | 0.0025 | -1.291 | 0.011 | 0.000185895 | -5.2029846 | 0.282673198 | 0.000026 | 0.282663962 | -0.9 | 1.0 | 0.282691232 | 842433061.7 | 769515575 | 769.5155754 | 1242970911 | 1243.0 | 1248493912 | 1248.5 | 5.52280515 | -0.994647046 |
| G52a-26 | 2 | 36.164 | 72 | 38.7 | 173.3 | 13 | 69.7 | 0.282760861 | 0.000013 | 0.0003643 | 0.0000067 | 0.01546 | 0.00014 | 1.467172 | 0.000023 | -1.5434 | 0.0021 | -1. | | | | | | | | | | | | | | | | | | |

| | | | | | | | | | | | | | | | | | | | | | | | | | | | | | | | | | | | | |
|---------|---|--------|----|-------|-------|-----|-------|-------------|----------|------------|------------|----------|----------|----------|----------|---------|--------|--------|-------|-------------|--------------|--------------------|-----------------|-------------|-------------|------------|--------------|-------------|-------------|-------------|-------------|------------|---------------|---------------|-------------|--------------|
| G55b-52 | 2 | 36.193 | 72 | 22.29 | 254.7 | 19 | 97.7 | 0.28258987 | 0.000017 | 0.000761 | 0.000024 | 0.0265 | 0.0011 | 1.467165 | 0.000036 | -1.5326 | 0.0023 | -1.29 | 0.016 | 0.000105967 | -6.90030235 | 0.28258987 | 0.000025 | 0.282624843 | -1.3 | 0.9 | 0.282660863 | 906072120.6 | 809361184 | 809.3611839 | 1309707306 | 1309.7 | 1315899008 | 1315.9 | 6.151702209 | -0.996846214 |
| G55b-53 | 2 | 34.523 | 69 | 16.69 | 255.8 | 19 | 98.0 | 0.282480875 | 0.000025 | 0.000083 | 0.000014 | 0.02968 | 0.00064 | 1.46717 | 0.000004 | -1.5272 | 0.0036 | -1.282 | 0.021 | 0.000115575 | -10.75462807 | 0.282480322 | 0.000031 | 0.28262415 | -5.1 | 1.1 | 0.28255213 | 1054470280 | 957.6477449 | 1547969503 | 1549.0 | 1565656651 | 1556.6 | 8.587148562 | -0.99656026 | |
| G55b-54 | 2 | 36.175 | 72 | 14.37 | 2015 | 22 | 94.4 | 0.281533923 | 0.000025 | 0.0007588 | 0.0000086 | 0.02772 | 0.00025 | 1.467208 | 0.000038 | -1.5276 | 0.0033 | -1.303 | 0.024 | 0.000105661 | -44.24129285 | 0.281529872 | 0.000031 | 0.281496889 | 1.2 | 1.2 | 0.282104922 | 2324278147 | 1562051425 | 1562.051425 | 2516923712 | 2516.9 | 2539601578 | 2539.6 | 22.67786632 | -0.996855332 |
| G52d-1 | 2 | 36.183 | 72 | 16.01 | 233.2 | 5.7 | 100.0 | 0.28259187 | 0.00002 | 0.0000528 | 0.0000011 | 0.001954 | 0.00003 | 1.467189 | 0.000039 | -1.5246 | 0.0036 | -1.29 | 0.021 | 7.35226E-06 | -6.829580777 | 0.282591838 | 0.000027 | 0.282638392 | -1.6 | 1.0 | 0.282657288 | 901072942.7 | 812182022 | 812.1820219 | 1317559325 | 1317.6 | 1323810403 | 1323.8 | 6.251078012 | -0.999781183 |
| G52d-2 | 2 | 33.047 | 66 | 18.12 | 228.8 | 5.4 | 100.1 | 0.282619868 | 0.000016 | 0.0000116 | 0.0000029 | 0.00046 | 0.0001 | 1.467185 | 0.000033 | -1.5317 | 0.0028 | -1.46 | 0.95 | 0.28261164 | -5.83928756 | 0.282619832 | 0.000024 | 0.28261164 | -0.8 | 0.9 | 0.2826284074 | 862919479.2 | 775628004 | 775.6280037 | 1258709445 | 1258.7 | 1264416398 | 1264.4 | 5.37774194 | -0.99953117 |
| G52d-3 | 2 | 30.152 | 60 | 16.02 | 235.9 | 5.5 | 100.3 | 0.28258187 | 0.000027 | 0.00001723 | 0.0000043 | 0.000665 | 0.000017 | 1.467188 | 0.000044 | -1.533 | 0.0031 | -1.38 | 0.82 | 2.39923E-06 | -7.138318642 | 0.282581836 | 0.000033 | 0.282636691 | -1.9 | 1.2 | 0.282648069 | 914531652 | 824612791 | 824.6127908 | 1337797737 | 1337.8 | 1344243458 | 1344.3 | 6.445721063 | -0.999928594 |
| G52d-4 | 2 | 29.298 | 39 | 17.69 | 236.1 | 5.1 | 99.5 | 0.282604869 | 0.000003 | 0.0001208 | 0.0000059 | 0.0043 | 0.00022 | 1.467172 | 0.000043 | -1.5268 | 0.004 | -1.44 | 0.13 | 1.68211E-05 | -6.369890587 | 0.282604795 | 0.000035 | 0.282636565 | -1.1 | 1.2 | 0.282671067 | 883634883.2 | 793640756 | 793.640756 | 1023730827 | 1023.7 | 1293273457 | 1293.2 | 5.965249937 | -0.99949373 |
| G52d-5 | 2 | 11.541 | 23 | 18.22 | 391.4 | 17 | 93.4 | 0.282164891 | 0.000032 | 0.000717 | 0.000025 | 0.0264 | 0.00097 | 1.467191 | 0.000058 | -1.5291 | 0.0044 | -1.271 | 0.037 | 9.98403E-05 | -21.9286366 | 0.282164519 | 0.000037 | 0.282538571 | -1.3 | 1.3 | 0.282721712 | 1481145299 | 133821014 | 1338.21014 | 2152272432 | 2152.3 | 2168868924 | 2168.9 | 16.59649166 | -0.997028562 |
| G52d-6 | 2 | 17.778 | 32 | 19.29 | 170.8 | 4.5 | 94.3 | 0.28254877 | 0.000024 | 0.0001776 | 0.0000029 | 0.00607 | 0.00012 | 1.467186 | 0.000045 | -1.5213 | 0.0052 | -1.237 | 0.08 | 2.47303E-05 | -11.67400852 | 0.282547988 | 0.000030 | 0.282677684 | -7.9 | 1.1 | 0.282507026 | 1087226908 | 1022445946 | 1022.445946 | 1659199363 | 1659.0 | 16659129878 | 1665.8 | 9.862198931 | -0.999263978 |
| G52d-1 | 3 | 36.161 | 72 | 14.11 | 225.1 | 4.9 | 99.4 | 0.282597652 | 0.000026 | 0.00013177 | 0.0000059 | 0.004683 | 0.000038 | 1.467216 | 0.000046 | -1.4998 | 0.0032 | -1.23 | 0.16 | 1.83486E-05 | -6.625109536 | 0.282597575 | 0.000032 | 0.282643495 | -1.6 | 1.1 | 0.282660746 | 893473191.2 | 807705261 | 807.705261 | 1309963870 | 1309.9 | 1316140356 | 1316.1 | 6.176485982 | -0.99945391 |
| G52d-2 | 3 | 36.179 | 72 | 13.2 | 225.2 | 5.8 | 94.6 | 0.282639653 | 0.000026 | 0.0000787 | 0.0000023 | 0.002367 | 0.000052 | 1.467239 | 0.000037 | -1.4799 | 0.0039 | -1.41 | 0.34 | 1.09588E-05 | -5.139852538 | 0.282639607 | 0.000032 | 0.282643432 | -0.1 | 1.1 | 0.282702807 | 836236365.1 | 750312388 | 750.3123878 | 1217514947 | 1217.5 | 1222852722 | 1222.0 | 5.37774194 | -0.999673846 |
| G52d-3 | 3 | 36.192 | 73 | 14.18 | 229.8 | 5.2 | 100.7 | 0.282648653 | 0.000026 | 0.0000811 | 0.0000021 | 0.002874 | 0.000075 | 1.467239 | 0.000037 | -1.4942 | 0.0037 | -1.26 | 0.26 | 1.1293E-05 | -4.821583182 | 0.282648604 | 0.000032 | 0.282640534 | -0.3 | 1.1 | 0.282713098 | 824006634.3 | 736303502 | 736.3035021 | 1194869666 | 1194.9 | 1200010815 | 1200.9 | 5.141149358 | -0.9996639 |
| G52d-4 | 3 | 36.056 | 72 | 13.48 | 240.6 | 6.1 | 96.2 | 0.282717654 | 0.000028 | 0.0000299 | 0.0000036 | 0.000914 | 0.000082 | 1.467226 | 0.000039 | -1.4978 | 0.0035 | -1.5 | 1.1 | 4.16349E-06 | -2.381518114 | 0.282717635 | 0.000033 | 0.282633729 | 3.0 | 1.2 | 0.282785167 | 729964304.1 | 637938151 | 637.9381505 | 1036021221 | 1036.0 | 1039888260 | 1039.9 | 3.867039012 | -0.999876086 |
| G52d-5 | 3 | 36.058 | 72 | 14.05 | 232.5 | 6.1 | 101.8 | 0.282651653 | 0.000028 | 0.0000944 | 0.0000061 | 0.00312 | 0.00016 | 1.467228 | 0.000044 | -1.5022 | 0.0034 | -1.23 | 0.31 | 1.31449E-05 | -4.715493396 | 0.282651596 | 0.000033 | 0.282638833 | 0.5 | 1.2 | 0.282716849 | 819965904.7 | 731229258 | 731.2292576 | 1186614001 | 1186.6 | 1191684023 | 1191.7 | 3.807021913 | -0.999608781 |
| G52d-6 | 3 | 36.054 | 72 | 14.33 | 233.3 | 5.8 | 96.5 | 0.282594652 | 0.000025 | 0.00001164 | 0.0000044 | 0.000443 | 0.000017 | 1.467227 | 0.000045 | -1.4973 | 0.0037 | -0.1 | 1.5 | 1.62084E-06 | -6.731199321 | 0.282594645 | 0.000031 | 0.282638329 | -1.5 | 1.1 | 0.282660123 | 897164164.3 | 808207642 | 808.2076424 | 1311333363 | 1311.3 | 1317527019 | 1317.5 | 6.193655792 | -0.999951761 |
| G52d-7 | 3 | 36.182 | 72 | 13.11 | 233.4 | 6.5 | 100.2 | 0.282885658 | 0.000028 | 0.0000148 | 0.0000042 | 0.000495 | 0.000056 | 1.467204 | 0.000044 | -1.5029 | 0.0036 | -1.08 | 0.19 | 2.06086E-05 | -3.559098275 | 0.282885568 | 0.000033 | 0.282638266 | -8.7 | 1.2 | 0.282951074 | 500878275.2 | 411291790 | 411.2917904 | 668543065.1 | 668.5 | 6701557019 | 6701.2 | 1.609952593 | -0.999386649 |
| G52d-8 | 3 | 36.186 | 73 | 16 | 225 | 5.6 | 97.3 | 0.282675653 | 0.000022 | 0.0000577 | 0.0000018 | 0.002007 | 0.000063 | 1.467188 | 0.000038 | -1.4902 | 0.0033 | -1.33 | 0.3 | 8.03457E-06 | -3.866775112 | 0.28267562 | 0.000029 | 0.282643558 | 1.1 | 1.0 | 0.2827338763 | 787213567.4 | 701277156 | 701.277156 | 1138354362 | 1138.4 | 1143021674 | 1143.0 | 4.667311973 | -0.999760876 |
| G52d-9 | 3 | 36.159 | 71 | 14.12 | 245.8 | 7.2 | 101.2 | 0.282724654 | 0.000028 | 0.00012141 | 0.0000089 | 0.003746 | 0.000025 | 1.467248 | 0.000039 | -1.4992 | 0.0035 | -1.3 | 0.2 | 1.6906E-06 | -2.133975282 | 0.282724577 | 0.000033 | 0.282630452 | 3.3 | 1.2 | 0.282793571 | 720664938.4 | 626676279 | 626.6762793 | 1017467109 | 1017.5 | 1021195015 | 1021.2 | 3.727906186 | -0.999496845 |
| G52d-10 | 3 | 36.155 | 72 | 12.98 | 231.8 | 7.1 | 102.1 | 0.282800656 | 0.000022 | 0.0000323 | 0.0000041 | 0.001009 | 0.00008 | 1.467203 | 0.000048 | -1.4987 | 0.0041 | -1.3 | 0.84 | 4.49769E-06 | -0.553632618 | 0.282800636 | 0.000029 | 0.282639274 | 5.7 | 1.0 | 0.282865693 | 616808456.7 | 527971840 | 527.9718399 | 85794578.3 | 858.0 | 860627279.9 | 860.2 | 6.252701532 | -0.99986614 |
| G52d-11 | 3 | 36.158 | 72 | 12.43 | 254.1 | 6.7 | 92.1 | 0.282691654 | 0.000025 | 0.0000282 | 0.0000011 | 0.001109 | 0.00004 | 1.46722 | 0.00004 | -1.4988 | 0.0041 | -1.85 | 0.78 | 3.92677E-06 | -3.900962922 | 0.282691636 | 0.000031 | 0.282652221 | 2.3 | 1.1 | 0.282762965 | 765358612.6 | 668215270 | 668.215270 | 108501082.1 | 1085.0 | 10842126205 | 1084.6 | 4.24126205 | -0.999833132 |
| G52d-12 | 3 | 36.192 | 72 | 13.22 | 234.3 | 6 | 96.8 | 0.282650653 | 0.000024 | 0.00001349 | 0.0000039 | 0.000601 | 0.000019 | 1.467253 | 0.000043 | -1.5028 | 0.0037 | -2.1 | 1.3 | 1.87845E-06 | -4.750856658 | 0.282650645 | 0.000030 | 0.28263699 | 0.5 | 1.1 | 0.282716404 | 821089179.4 | 731624065 | 731.6240646 | 1187593038 | 1187.6 | 1192673776 | 1192.7 | 5.800738728 | -0.999944094 |
| G52d-13 | 3 | 36.151 | 72 | 14.02 | 229.7 | 5.7 | 100.0 | 0.282611652 | 0.000019 | 0.00002532 | 0.00000075 | 0.000942 | 0.000031 | 1.467214 | 0.000042 | -1.5018 | 0.0037 | -1.61 | 0.67 | 1.85254E-06 | -6.13002387 | 0.282611637 | 0.000026 | 0.282640597 | -1.0 | 0.9 | 0.282762063 | 874122320.4 | 786511654 | 786.5116545 | 1276229297 | 1276.2 | 1282095616 | 1282.1 | 5.080721461 | -0.999895067 |
| G52d-14 | 3 | 36.174 | 72 | 14.56 | 226.1 | 5.4 | 98.8 | 0.282657653 | 0.000024 | 0.00001038 | 0.0000074 | 0.0032 | 0.00017 | 1.467244 | 0.00004 | -1.5073 | 0.0035 | -1.26 | 0.27 | 1.46539E-05 | -4.503313825 | 0.282657592 | 0.000030 | 0.282642865 | 0.5 | 1.1 | 0.282721045 | 811832616.3 | 725537259 | 725.5372589 | 117376683 | 1173.4 | 1182367876 | 1182.4 | 4.99192337 | -0.999569825 |
| G52d-15 | 3 | 36.068 | 73 | 13.84 | 234.7 | 5.4 | 101.2 | 0.282671653 | 0.000028 | 0.00002199 | 0.0000037 | 0.00706 | 0.00011 | 1.467224 | 0.00004 | -1.5006 | 0.0038 | -1.317 | 0.088 | 2.00520E-05 | -4.008228159 | 0.282671519 | 0.000030 | 0.28264477 | 1.2 | 1.2 | 0.282737091 | 793114182 | 703554583 | 703.5545834 | 1143178262 | 1143.4 | 1146066014 | 1146.4 | 6.87752238 | -0.999808676 |
| G52d-16 | 3 | 36.062 | 72 | 13.91 | 233 | 6.8 | 89.6 | 0.28263653 | 0.000025 | 0.00002176 | 0.0000073 | 0.000817 | 0.000035 | 1.467193 | 0.000038 | -1.4979 | 0.0033 | -2.3 | 1.1 | 3.03002E-06 | -4.291134254 | 0.28263634 | 0.000031 | 0.282638518 | 0.9 | 1.1 | 0.282729034 | 803435746.5 | 714443361 | 714.443361 | 1159786129 | 1159.8 | 1164631686 | 1164.6 | 4.845557029 | -0.999909821 |
| G52d-17 | 3 | 36.196 | 73 | 13.88 | 235.5 | 6 | 99.8 | 0.28266653 | 0.000028 | 0.0000311 | 0.0000019 | 0.001168 | 0.000038 | 1.467225 | 0.000044 | -1.4992 | 0.0034 | -1.43 | 0.66 | 4.33059E-06 | -4.185044667 | 0.28266634 | | | | | | | | | | | | | | |

Table with multiple columns containing numerical data, likely representing a dataset or simulation results. The table is organized into several vertical sections, each starting with a label (e.g., G54-40, G54-41, MT-1, MT-2, etc.) and containing rows of numerical values. The data is presented in a structured, grid-like format.

| | | | | | | | | | | | | | | | | | | | | | | | | | | | | | | | | | | | | |
|----------------|---|--------|----|-------|-----|---|-----|-------------|----------|------------|------------|----------|----------|----------|----------|---------|--------|--------|-------|-------------|--------------|--------------------|-----------------|-------------|-------------|------------|-------------|------------|-------------|-------------|------------|--------|------------|---------------|--------------|--------------|
| MT - 27 | 3 | 36.085 | 72 | 15.17 | 570 | 2 | 100 | 0.28251165 | 0.000023 | 0.00003623 | 0.00000017 | 0.001593 | 0.000015 | 1.467215 | 0.000044 | -1.5037 | 0.0037 | -1.68 | 0.4 | 5.04493E-06 | -9.666350054 | 0.282511596 | 0.000029 | 0.282425523 | 3.0 | 1.0 | 0.282672077 | 1009816054 | 792018754 | 792.0187539 | 1285074732 | 1285.1 | 1291021993 | 1291.0 | -7.418499479 | -0.999849853 |
| MT - 28 | 3 | 36.152 | 72 | 15.54 | 570 | 2 | 100 | 0.28251765 | 0.000024 | 0.00001798 | 0.00000021 | 0.000752 | 0.000015 | 1.467226 | 0.000038 | -1.5045 | 0.0039 | -1.14 | 0.96 | 2.50367E-06 | -9.454170483 | 0.282517623 | 0.000030 | 0.282425523 | 3.3 | 1.1 | 0.282678104 | 1001621148 | 783767762 | 783.7677622 | 1271830216 | 1271.8 | 127656232 | 1277.7 | 36.86276661 | -0.999925486 |
| MT - 29 | 3 | 36.184 | 72 | 15.29 | 570 | 2 | 100 | 0.28250365 | 0.000025 | 0.00001564 | 0.00000018 | 0.000651 | 0.000014 | 1.467226 | 0.000043 | -1.5023 | 0.0038 | -1.1 | 1.1 | 2.17783E-06 | -9.949256149 | 0.282503627 | 0.000031 | 0.282425523 | 2.8 | 1.1 | 0.282664108 | 1020579297 | 802800255 | 802.8002552 | 1302581997 | 1302.6 | 1308692983 | 1308.7 | 8.313023028 | -0.999935184 |
| MT - 30 | 3 | 36.151 | 73 | 15.37 | 570 | 2 | 100 | 0.28250265 | 0.000025 | 0.00001105 | 0.00000019 | 0.000474 | 0.000014 | 1.467244 | 0.000045 | -1.5033 | 0.0037 | -1.9 | 1.4 | 1.53868E-06 | -9.984619411 | 0.282502633 | 0.000031 | 0.282425523 | 2.7 | 1.1 | 0.282663114 | 1021917114 | 804137818 | 804.1378177 | 1304763405 | 1304.8 | 1310895020 | 1310.9 | -1304.763405 | -0.999954206 |
| Plesovice - 1 | 1 | 36.135 | 72 | 22.06 | 338 | 1 | 100 | 0.282484 | 0.000015 | 0.00013581 | 0.00000033 | 0.006869 | 0.000063 | 1.46714 | 0.00003 | -1.5183 | 0.0029 | -1.253 | 0.046 | 1.89112E-05 | -10.64412893 | 0.28248388 | 0.000024 | 0.282572298 | -3.1 | 0.8 | 0.282578836 | 1047635654 | 919036582 | 919.0365819 | 1489547111 | 1489.5 | 1497530851 | 1497.5 | 7.983739744 | -0.999437167 |
| Plesovice - 2 | 1 | 22.109 | 44 | 21.5 | 338 | 1 | 100 | 0.282482 | 0.000023 | 0.00010276 | 0.00000017 | 0.005186 | 0.000018 | 1.467213 | 0.000041 | -1.5164 | 0.0035 | -1.2 | 0.084 | 1.43091E-05 | -10.71485404 | 0.282481909 | 0.000029 | 0.282572298 | -3.2 | 1.0 | 0.282576866 | 1050220934 | 921603807 | 921.6038072 | 1493860721 | 1493.9 | 1501892243 | 1501.9 | 8.031522597 | -0.999574135 |
| Plesovice - 3 | 1 | 36.177 | 72 | 22.29 | 338 | 1 | 100 | 0.282486 | 0.000018 | 0.000186 | 0.00000027 | 0.009362 | 0.000095 | 1.467193 | 0.000028 | -1.5124 | 0.0021 | -1.279 | 0.043 | 0.0000259 | -10.57340382 | 0.282485836 | 0.000026 | 0.282572298 | -3.1 | 0.9 | 0.282580792 | 1045113338 | 916.5450732 | 916.5450732 | 1485266227 | 1485.3 | 1493201902 | 1493.2 | 7.935674974 | -0.999291637 |
| Plesovice - 4 | 1 | 27.59 | 55 | 23.07 | 338 | 1 | 100 | 0.282479 | 0.000016 | 0.0001279 | 0.00000046 | 0.00632 | 0.000026 | 1.467186 | 0.000032 | -1.5169 | 0.0032 | -1.212 | 0.08 | 1.78097E-05 | -10.8209417 | 0.282478887 | 0.000024 | 0.282572298 | -3.3 | 0.9 | 0.282573843 | 1054377482 | 925788807 | 925.7888071 | 1500474608 | 1500.5 | 1508576166 | 1508.6 | 8.101551271 | -0.999469948 |
| Plesovice - 5 | 1 | 23.1 | 46 | 19.9 | 338 | 1 | 100 | 0.282474 | 0.00002 | 0.00017139 | 0.00000024 | 0.00894 | 0.000023 | 1.467185 | 0.000046 | -1.5162 | 0.0032 | -1.246 | 0.053 | 2.38656E-05 | -10.99775448 | 0.282473849 | 0.000027 | 0.282572298 | -3.5 | 1.0 | 0.282568805 | 1061312013 | 932771941 | 932.7719412 | 1511499007 | 1511.5 | 1519717861 | 1519.7 | 7.261854266 | -0.999289714 |
| Plesovice - 6 | 1 | 26.224 | 52 | 21.42 | 338 | 1 | 100 | 0.282483 | 0.000021 | 0.00010512 | 0.00000017 | 0.005255 | 0.000018 | 1.467188 | 0.000038 | -1.5133 | 0.0033 | -1.2 | 0.081 | 1.46377E-05 | -10.67949149 | 0.282482907 | 0.000028 | 0.282572298 | -3.2 | 1.0 | 0.282577864 | 1048875562 | 920256933 | 920.2569333 | 1491676631 | 1491.7 | 1499684602 | 1499.7 | 8.007971163 | -0.999564355 |
| Plesovice - 7 | 1 | 31.269 | 63 | 21.81 | 338 | 1 | 100 | 0.282479 | 0.000019 | 0.00010734 | 0.00000041 | 0.005416 | 0.000011 | 1.467173 | 0.000031 | -1.5014 | 0.0031 | -1.19 | 0.07 | 1.49468E-05 | -10.8209417 | 0.282478905 | 0.000026 | 0.282572298 | -3.0 | 0.9 | 0.282573862 | 1054300414 | 925696457 | 925.6964575 | 1500434948 | 1500.4 | 1508537029 | 1508.5 | 8.102080208 | -0.999555155 |
| Plesovice - 8 | 1 | 23.083 | 46 | 20.51 | 338 | 1 | 100 | 0.282487 | 0.000021 | 0.00012917 | 0.00000023 | 0.006635 | 0.000029 | 1.467187 | 0.000034 | -1.4977 | 0.0032 | -1.279 | 0.081 | 1.79866E-05 | -10.53804127 | 0.282486886 | 0.000028 | 0.282572298 | -3.0 | 1.0 | 0.282581842 | 1043547715 | 914939399 | 914.9393988 | 1482967572 | 1483.0 | 1490881312 | 1490.9 | 7.913740618 | -0.999464685 |
| Plesovice - 9 | 1 | 27.274 | 55 | 21.73 | 338 | 1 | 100 | 0.282478 | 0.000016 | 0.00020141 | 0.00000016 | 0.010468 | 0.000043 | 1.467188 | 0.000042 | -1.5018 | 0.0032 | -1.254 | 0.04 | 2.80458E-05 | -10.85630426 | 0.282477822 | 0.000024 | 0.282572298 | -3.3 | 0.9 | 0.282572779 | 1056007629 | 927476864 | 927.4768641 | 1502804687 | 1502.8 | 1510927959 | 1510.9 | 8.123272875 | -0.999165304 |
| Plesovice - 10 | 1 | 36.212 | 72 | 21.74 | 338 | 1 | 100 | 0.282485 | 0.000018 | 0.00007153 | 0.00000035 | 0.00363 | 0.000035 | 1.467222 | 0.000031 | -1.4922 | 0.0022 | -1.15 | 0.11 | 9.96036E-06 | -10.60876638 | 0.282484937 | 0.000026 | 0.282572298 | -3.1 | 0.9 | 0.282579893 | 1046042167 | 917392064 | 917.392064 | 1487234265 | 1487.2 | 1495196196 | 1495.2 | 7.961930547 | -0.999703561 |
| Plesovice - 16 | 2 | 36.153 | 72 | 18.85 | 338 | 1 | 100 | 0.282482875 | 0.000016 | 0.00012797 | 0.00000028 | 0.006348 | 0.000047 | 1.467165 | 0.000028 | -1.5448 | 0.0026 | -1.361 | 0.057 | 1.78195E-05 | -10.6839065 | 0.282482762 | 0.000024 | 0.282572298 | -3.2 | 0.9 | 0.282577719 | 1049129863 | 920528625 | 920.5286249 | 1491993972 | 1492.0 | 1500004296 | 1500.0 | 8.010332827 | -0.999469658 |
| Plesovice - 17 | 2 | 18.811 | 38 | 20.19 | 338 | 1 | 100 | 0.282473876 | 0.000026 | 0.0000892 | 0.00000021 | 0.004823 | 0.000083 | 1.467116 | 0.000045 | -1.5412 | 0.0036 | -1.358 | 0.084 | 1.24209E-05 | -11.00215358 | 0.282473797 | 0.000032 | 0.282572298 | -3.5 | 1.1 | 0.282568753 | 1050336347 | 932569598 | 932.5695975 | 1511612667 | 1511.6 | 1519836639 | 1519.8 | 8.223971406 | -0.999630332 |
| Plesovice - 18 | 2 | 36.161 | 72 | 19.49 | 338 | 1 | 100 | 0.282478875 | 0.000015 | 0.00010085 | 0.00000033 | 0.005174 | 0.000018 | 1.46718 | 0.000036 | -1.5381 | 0.003 | -1.298 | 0.064 | 1.40431E-05 | -10.82534965 | 0.282478786 | 0.000024 | 0.282572298 | -3.3 | 0.8 | 0.282573743 | 1054444870 | 925836496 | 925.836496 | 1506095204 | 1506.7 | 1508800394 | 1508.8 | 8.10519021 | -0.999582051 |
| Plesovice - 19 | 2 | 31.241 | 62 | 20.14 | 338 | 1 | 100 | 0.282481875 | 0.000019 | 0.00008841 | 0.00000012 | 0.004568 | 0.00003 | 1.467147 | 0.00003 | -1.5456 | 0.0023 | -1.323 | 0.089 | 1.23109E-05 | -10.71923647 | 0.282481797 | 0.000026 | 0.282572298 | -3.2 | 0.9 | 0.282576753 | 1050336347 | 921708963 | 921.7089625 | 1494106173 | 1494.1 | 1502140994 | 1502.1 | 8.034821323 | -0.999633606 |
| Plesovice - 20 | 2 | 35.25 | 71 | 18.72 | 338 | 1 | 100 | 0.282481875 | 0.000017 | 0.00013039 | 0.00000022 | 0.006904 | 0.000039 | 1.467148 | 0.000037 | -1.544 | 0.0026 | -1.199 | 0.073 | 1.81565E-05 | -10.71927629 | 0.28248176 | 0.000025 | 0.282572298 | -3.2 | 0.9 | 0.282576716 | 1050493123 | 921896939 | 921.8969392 | 1494187161 | 1494.2 | 150220916 | 1502.2 | 8.033754552 | -0.999459629 |
| Plesovice - 6 | 3 | 36.056 | 72 | 15.89 | 338 | 1 | 100 | 0.282479649 | 0.000024 | 0.00009563 | 0.00000027 | 0.004984 | 0.000047 | 1.46724 | 0.000036 | -1.5066 | 0.0034 | -1.2 | 0.14 | 1.33162E-05 | -10.79797443 | 0.282479565 | 0.000030 | 0.282572298 | -3.3 | 1.1 | 0.282576216 | 1053377109 | 924762336 | 924.7623357 | 1498991064 | 1499.0 | 1507078118 | 1507.1 | 8.204574651 | -0.999484619 |
| Plesovice - 7 | 3 | 29.499 | 59 | 15.92 | 338 | 1 | 100 | 0.282474649 | 0.000028 | 0.00012436 | 0.00000021 | 0.006617 | 0.000062 | 1.467241 | 0.000045 | -1.5074 | 0.0038 | -1.26 | 0.11 | 1.73168E-05 | -10.97479074 | 0.28247454 | 0.000033 | 0.282572298 | -3.5 | 1.2 | 0.282569496 | 1060255307 | 916787161 | 916.787161 | 1509987520 | 1510.0 | 1518192179 | 1518.2 | 8.204659536 | -0.999484619 |
| Plesovice - 8 | 3 | 36.154 | 72 | 15.51 | 338 | 1 | 100 | 0.28248565 | 0.000023 | 0.00012971 | 0.00000059 | 0.006579 | 0.000027 | 1.467196 | 0.000037 | -1.507 | 0.0036 | -1.29 | 0.1 | 1.80618E-05 | -10.5879486 | 0.282485535 | 0.000029 | 0.282572298 | -3.1 | 1.0 | 0.282580941 | 1045378744 | 916767667 | 916.767667 | 1485924617 | 1485.9 | 1493869891 | 1493.9 | 7.945274197 | -0.999462447 |
| Plesovice - 9 | 3 | 35.194 | 71 | 15.81 | 338 | 1 | 100 | 0.28249065 | 0.000027 | 0.00017185 | 0.00000032 | 0.009004 | 0.00005 | 1.467226 | 0.000033 | -1.5136 | 0.0052 | -1.263 | 0.078 | 2.39297E-05 | -10.40897855 | 0.282490498 | 0.000033 | 0.282572298 | -2.9 | 1.2 | 0.282585454 | 1038761789 | 910167861 | 910.1678613 | 1475059992 | 1475.1 | 1482887728 | 1482.9 | 7.82773726 | -0.999287808 |
| Plesovice - 10 | 3 | 36.19 | 73 | 15.51 | 338 | 1 | 100 | 0.28248965 | 0.000021 | 0.00012445 | 0.00000044 | 0.006635 | 0.000068 | 1.467223 | 0.000041 | -1.508 | 0.0033 | -1.37 | 0.1 | 1.73293E-05 | -10.44434181 | 0.28248954 | 0.000028 | 0.282572298 | -2.9 | 1.0 | 0.282584496 | 1039941273 | 911315360 | 911.3153599 | 1477 | | | | | |

Mafic magmatism during Middle Permian at ca. 272 Ma possibly related to a continuous Permian arc.

230 Ma anatexis and metamorphism of the Guajira Arch, during back-arc extension, updoming and migmatization of the lower crust.

223 Ma crustal attenuation and development of a mylonitic detachment during core-complex emplacement.

Triassic ϵHf_i spectrum is dominated by juvenile compositions with the mixing of older crustal unradiogenic sources, whose T_{DM} model ages are indistinguishable from the Proterozoic Gondwanan basement.

190-150 Ma Early-Middle Jurassic Rifting, granitoid emplacement, and collateral arc volcanoclastic deposits and marine sediments.

Jurassic Trends of near CHUR to positive ϵHf_i values indicate mixing of primitive sources and slightly depleted compositions in the setting of a low-lying magmatic arc.

Declaration of interests

The authors declare that they have no known competing financial interests or personal relationships that could have appeared to influence the work reported in this paper.

The authors declare the following financial interests/personal relationships which may be considered as potential competing interests:

Journal Pre-proof